UNIVERSIDADE FEDERAL DO RIO GRANDE DO SUL
INSTITUTO DE QUÍMICA
PROGRAMA DE PÓS-GRADUAÇÃO EM QUÍMICA

COMPLEXOS METÁLICOS EM LÍQUIDOS IÔNICOS: APLICAÇÕES NA SÍNTESE DE NANOPARTÍCULAS E EM SISTEMAS HOMOGÊNEOS

Jackson Damiani Scholten

Porto Alegre, 2011.

UNIVERSIDADE FEDERAL DO RIO GRANDE DO SUL

INSTITUTO DE QUÍMICA

PROGRAMA DE PÓS-GRADUAÇÃO EM QUÍMICA

JACKSON DAMIANI SCHOLTEN

Tese elaborada sob orientação do Prof. Dr. Jaïrton Dupont, apresentada ao Instituto de Química da UFRGS como requisito final à obtenção do título de Doutor em Química.

Prof. Dr. Jaïrton Dupont

Orientador

Porto Alegre, julho de 2011.

Na presente Tese serão introduzidos os trabalhos publicados durante o período de doutoramento no Instituto de Química da Universidade Federal do Rio Grande do Sul sob orientação do Professor Dr. Jaïrton Dupont. A Tese foi julgada adequada para a obtenção do título de Doutor em Química pela seguinte banca examinadora:

Comissão Examinadora:

Prof. Dr. Mario Roberto Meneghetti
IQ-UFAL

Prof^a. Dr^a. Liane Marcia Rossi
IQ-USP

Prof. Dr. Daniel Eduardo Weibel
IQ-UFRGS

Prof. Dr. Ricardo Gomes da Rosa
IQ-UFRGS

Prof^o. Dr. Jaïrton Dupont
Orientador

Jackson Damiani Scholten

Dedico esta Tese aos meus familiares.

AGRADECIMENTOS

À minha família por todo o carinho, força e motivação que me proporcionaram sempre, em todos os momentos;

À um dos maiores e mais premiados pesquisadores na área de Química, Prof º. Dr. Jaïrton Dupont, pela oportunidade de poder trabalhar em seu grupo de pesquisa e também por acreditar no meu trabalho;

Ao Prof º. Dr. Günter Ebeling pelo auxílio na preparação e caracterização dos líquidos iônicos;

Ao colega Martin H. G. Prechtl pelas colaborações e aprendizado ao longo de seu Pós-Doutorado;

À minha namorada Virgínia pelo apoio e carinho sempre presentes;

Aos meus colegas do laboratório pelas discussões sempre bastante proveitosas e pelas brincadeiras que ajudavam a descontrair;

E ao CNPq pela bolsa de doutorado concedida.

Artigos Publicados Durante o Período de Doutoramento Integrados na Tese

Dupont, J; SCHOLTEN, J. D. "On the Structural and Surface Properties of Transition-Metal Nanoparticles in Ionic Liquids" *Chem. Soc. Rev.* **2010**, *39*, 1780-1804.
DOI: 10.1039/b822551f

SCHOLTEN, J. D.; Prechtl, M. H. G.; Dupont, J. "Decomposition of Formic Acid Catalyzed by a Phosphine-Free Ruthenium Complex in a Task-Specific Ionic Liquid" *ChemCatChem* **2010**, *2*, 1265-1270.
DOI: 10.1002/cctc.201000119

Prechtl, M. G. H.; Campbell, P. S.; SCHOLTEN, J. D.; Fraser, G. B.; Machado, G.; Santini, C. C.; Dupont, J.; Chauvin, Y. "Imidazolium Ionic Liquids as Promoters and Stabilising Agents for the Preparation of Metal(0) Nanoparticles by Reduction and Decomposition of Organometallic Complexes" *Nanoscale* **2010**, *2*, 2601-2606.
DOI: 10.1039/c0nr00574f

Prechtl, M. H. G.; SCHOLTEN, J. D.; Dupont, J. "Tuning the Selectivity of Ruthenium Nanoscale Catalysts with Functionalised Ionic Liquids: Hydrogenation of Nitriles" *J. Mol. Cat. A: Chem.* **2009**, *313*, 74-78.
DOI: 10.1016/j.molcata.2009.08.004

Bernardi, F.; SCHOLTEN, J. D.; Fecher, G. H.; Dupont, J.; Morais, J. "Probing the Chemical Interaction Between Iridium Nanoparticles and Ionic Liquid by XPS Analysis" *Chem. Phys. Lett.* **2009**, *479*, 113-116.
DOI: 10.1016/j.cplett.2009.07.110

SCHOLTEN, J. D.; Dupont, J. "Alkene Hydroformylation Catalyzed by Rhodium Complexes in Ionic Liquids: Detection of Transient Carbene Species" *Organometallics* **2008**, *27*, 4439-4442.
DOI: 10.1021/om8003948

Capítulos de Livro Publicados

SCHOLTEN, J. D.; Dupont, J. "Catalytic Properties of Soluble Iridium Nanoparticles" in: *Iridium Complexes in Organic Synthesis*, Luis A. Oro; Carmen Claver. (Org.), Weinheim, Wiley-VCH, **2009**, p. 369-389.

Prechtl, M. H. G.; SCHOLTEN, J. D.; Dupont, J. "Palladium Nanoscale Catalysts in Ionic Liquids: Coupling and Hydrogenation Reactions" in: *Ionic Liquids: Applications and Perspectives*, Alexander Kokorin (Ed.), Rijeka, InTech, **2011**, p. 393-414.

SCHOLTEN, J. D.; Prechtl, M. H. G.; Dupont, J. "Formation of Nanoparticles Assisted by Ionic Liquids" in: *Handbook of Green Chemistry - Green Processes*, Anastas (Ed.), Wiley-VCH, **2011**, submetido.

SCHOLTEN, J. D.; Dupont, J. "Hydrogenation with Nanoparticles Using Supported Ionic Liquids" in: *Supported Ionic Liquids. Fundamentals and Applications*, Fehrmann et al. (Eds.), Wiley-VCH, **2011**, submetido.

ÍNDICE GERAL

RESUMO

A referida Tese apresentará os principais trabalhos publicados durante o período de doutoramento, no que se refere à síntese de nanopartículas metálicas em líquidos iônicos a partir de precursores metálicos, bem como as evidências da interação do líquido iônico com as nanopartículas. Posteriormente serão abordadas as aplicações de complexos metálicos em líquidos iônicos em catálise homogênea, principalmente reações de hidroformilação e produção de hidrogênio a partir de ácido fórmico.

ABSTRACT

The present Thesis will show the main articles published during the PhD period referred to the synthesis of metal nanoparticles in ionic liquids from their correspondent metallic precursors as well as the evidences of the interaction between the ionic liquid and the metal NPs. Further, it will be present the applications of metal complexes dissolved in ionic liquids in homogeneus catalysis, focusing on hydroformylation reactions and hydrogen gas production from formic acid.

OBJETIVOS

O objetivo geral desta Tese realizada por integração de artigos é abordar os principais trabalhos desenvolvidos referentes à síntese de nanopartículas metálicas em líquidos iônicos e também a utilização de precursores metálicos em reações de hidroformilação bifásicas e catálise em meio homogêneo visando à produção de hidrogênio molecular.

Na primeira abordagem serão mostrados estudos para um melhor entendimento das espécies envolvidas durante a preparação de nanopartículas metálicas em líquidos iônicos, uma vez que estas podem auxiliar na estabilização das nanopartículas bem como influenciar na atividade e seletividade destes nanomateriais em reações catalíticas. Para finalizar, pretende-se apresentar as investigações a respeito das possíveis espécies formadas em processos de hidroformilação bem como a otimização da decomposição de ácido fórmico em líquido iônico para a produção de hidrogênio molecular.

LISTA DE ABREVIATURAS

acac: acetilacetonato

AF: ácido fórmico

(BCN)MI: 1-butironitrila-3-metilimidazólio

$B(CN)_4$: tetracianoborato

BF_4: tetrafluoroborato

$BnEt_3N$: benziltrietilamônio

BMEI: 1-*n*-butil-2-etil-3-metilimidazólio

BMI: 1-*n*-butil-3-metilimidazólio

B_2MI: 1,2-di-*n*-butil-3-metilimidazólio

BPy: *N*-butilpiridínio

COD: 1,5-ciclooctadieno

COE: *cis*-ciclocteno

COT: 1,3,5-ciclooctatrieno

C_6D_6: benzeno deuterado

$C_8H_{17}OSO_3$: octilsulfato

CNT: *carbon nanotubes* (nanotubos de carbono)

$Cy(CH_2)_3MI$: 1-(3-cicloexil)propil-3-metilimidazólio

$Cy_2(CH)(CH_2)MI$: 1-(2,2-dicicloexil)etil-3-metilimidazólio

diglime: *bis*(2-metoxietil)éter

DMF: dimetilformamida

DMI: 1-*n*-decil-3-metilimidazólio

DMSO: dimetilsulfóxido

dppe: 1,2-*bis*(difenilfosfino)etano

DRIFT: *diffuse-reflectance infrared Fourier transform* (infravermelho por transformada de Fourier via refletância difusa)

DRX: difração de raio-X

EDS: *energy dispersive spectroscopy* (espectroscopia de energia dispersiva)

EMI: 1-etil-3-metilimidazólio

ESI/MS: *electrospray ionization mass spectrometry* (espectrometria de massas por ionização eletrospray)

Et$_3$N: trietilamina

EtSO$_4$: etilsulfato

FID: *flame ionization detector* (detector por ionização em chama)

FWHM: *full width at half maximum* (largura máxima à meia altura)

GC: *gas chromatography* (cromatografia gasosa)

GC/MS: *gas chromatography mass spectrometry* (cromatografia gasosa com espectrometria de massas)

HDA: hexadecilamina

HexNMe$_2$: *N,N*-dimetilexilamina

HM$_2$I: 1-*n*-hexil-2,3-dimetilimidazólio

HRMS: *high resolution mass spectrometry* (espectrometria de massas de alta resolução)

IV: infravermelho

LIs: líquidos iônicos

MeOc$_3$N: metiltrioctilamônio

MET: microscopia eletrônica de transmissão

N(CN)$_2$: dicianoimida

NHC: *N-heterocyclic carbenes* (carbenos *N*-heterocíclicos)

NPs: nanopartículas

NTf$_2$: *N-bis*(trifluorometanosulfonil)imida

OAc: acetato

PEM: *polymer electrolyte membrane* (membrana de polímero eletrolítica)

PF$_6$: hexafluorofosfato

Ph(CH$_2$)$_3$MI: 1-(3-fenil)propil-3-metilimidazólio

Ph$_2$(CH)(CH$_2$)MI: 1-(2,2-difenil)etil-3-metilimidazólio

PhCN: benzonitrila

PPh$_3$: trifenilfosfina

*i*Pr$_2$NEMI: 1-(2-diisopropilaminoetil)-3-metilimidazólio

PVP: polivinilpirrolidona

RMN: ressonância magnética nuclear

SAXS: *small angle X-ray scattering* (espalhamento de raio-X em baixo ângulo)

Sulfoxantphos: 4,5-*bis*(difenilfosfino)-9,9-dimetilxanteno-2,7-disulfonada

TCD: *thermal conductivity detector* (detector por condutividade térmica)

THF: tetraidrofurano

TPPMS: *meta-sodium monosulfonated-triphenylphosphine* (trifenilfosfina mono-sulfonada)

TPPTS: *meta-sodium trisulfonated-triphenylphosphine* (trifenilfosfina tri-sulfonada)

tpy: (2,2',6',2'')terpiridina

TOF: *turnover frequency* (freqüência de rotação)

TON: *turnover number* (número de rotação)

tos: 4-toluenosulfonato

TPD/MS: *temperature-programmed-desorption mass spectrometry* (dessorção à temperatura programada com espectrometria de massas)

Xantphos: 4,5-*bis*(difenilfosfino)-9,9-dimetilxanteno

XPS: *X-ray photoelectron spectroscopy* (espectroscopia de fotoelétrons excitados por raio-X)

CAPÍTULO 1

INTRODUÇÃO

A presente Tese descreve a aplicação de complexos metálicos dispersos em líquidos iônicos (LIs) na síntese de nanopartículas (NPs) metálicas e em sistemas homogêneos. A Tese será dividida nos seguintes capítulos:

Capítulo 1: Introdução. Apresentação dos capítulos a serem discutidos na Tese.

Capítulo 2: Revisão Bibliográfica. Breve abordagem revisando os trabalhos de maior impacto publicados na literatura a respeito dos assuntos discutidos na Tese.

Capítulo 3: Nanopartículas Metálicas em Líquidos Iônicos. Neste capítulo serão apresentados três artigos publicados a respeito da síntese e aplicação catalítica de NPs metálicas em LIs.

Capítulo 4: Aplicações em Sistemas Homogêneos. Neste capítulo será introduzido um artigo publicado a respeito do uso de LIs deuterados em reações de hidroformilação de olefinas em sistema bifásico (apesar de ser um sistema bifásico, considerou-se como uma catálise homogênea, pois o sistema de Rh/fosfina é solúvel no LI). O outro trabalho se refere ao uso de LIs como meio reacional e co-catalisador na desidrogenação de ácido fórmico na presença de um precursor organometálico de Ru.

Capítulo 5: Referências

Capítulo 6: Conclusões

Os artigos publicados referentes aos trabalhos mencionados seguem em anexo ao final da Tese.

CAPÍTULO 2

REVISÃO BIBLIOGRÁFICA

2.1. Nanopartículas Metálicas em Líquidos Iônicos

Dentre os diversos tipos de estabilizantes utilizados na síntese de NPs metálicas, a classe denominada de líquidos iônicos (em particular os baseados no cátion imidazólio) apresenta papel de destaque. Além de ser um meio reacional apropriado para a geração e estabilização de NPs, estes LIs ou sais fundidos (sais líquidos à temperatura ambiente) apresentam propriedades bastante atrativas, tais como: baixa densidade e viscosidade, alta estabilidade térmica e química, baixa pressão de vapor, e suas propriedades físico-químicas podem ser moduladas através de mudanças nos grupos alquila do cátion imidazólio.[1] Estes sais fundidos se diferenciam dos sais clássicos em pelo menos um importante aspecto: eles apresentam estruturas altamente organizadas principalmente através de ligações de hidrogênio que induz direcionalidade estrutural.[2-4] A síntese de NPs metálicas em LIs pode ser realizada de diferentes formas: **i)** redução de precursores metálicos na presença de agentes redutores (H_2, $NaBH_4$), **ii)** decomposição térmica de precursores onde o metal se encontra com nox zero; **iii)** bombardeamento de metal bulk com íons gasosos ou **iv)** através de transferência de fase. A formação e estabilização de NPs metálicas em LIs ocorre, possivelmente, através da reorganização das ligações de hidrogênio intermoleculares e a geração de nanoestruturas polares e não-polares. O LI forma uma camada protetora localizada próximo à superfície metálica da NP, evitando a agregação e oxidação das partículas. Esta camada é composta, provavelmente, por agregados moleculares do tipo $\{[(C)_x(A)_{x-n}]^{n+}[(C)_{x-n}(A)_x]^{n-}\}_m$ onde C é o cátion imidazólio e A o ânion. Este argumento é suportado por estudos independentes de SAXS[5-7] e troca isotópica[8] utilizando NPs dispersas em LI. Entretanto, um recente trabalho de simulação molecular sugere que a estabilização ocorra principalmente através de uma única camada iônica onde os cátions e os ânions do LI interagem com o metal, excluindo os mecanismos de estabilização via dupla camada eletrostática e por efeitos estéreos.[9]

A revisão bibliográfica sobre NPs metálicas em LIs será baseada em um "*critical review*" publicado na revista *Chemical Society Reviews* no ano de 2010. Este review abordará a síntese de NPs, bem como os métodos de caracterização e suas aplicações em diferentes processos químicos (ver Artigo I).

2.2. Hidroformilação de Alcenos

A reação de hidroformilação se tornou um dos processos mais investigados na área de catálise.[10, 11] Descoberto por Roelen em 1938,[12] esta reação é um importante processo catalítico homogêneo aplicado na indústria, sendo um método bastante conveniente para a síntese de aldeídos a partir da ativação de ligações C=C.[13] O primeiro catalisador utilizado por Roelen foi [HCo(CO)$_4$], o qual demonstrou-se mais tarde que sua seletividade aumentava na presença de um ligante fosfina.[14] A seletividade observada para o aldeído linear ou ramificado depende de fatores eletrônicos e estéreos do precursor metálico. De forma geral, os fatores estéreos são preponderantes frente aos eletrônicos. Na etapa de inserção/migração do hidreto à ligação C=C da olefina, a adição Markovnikov (hidreto migra para o carbono com maior número de hidrogênios) gera um grande impedimento estéreo entre os ligantes na esfera de coordenação e o metal. Uma vez que a repulsão estérea se torna menor pela adição anti-Markovnikov, os catalisadores metálicos normalmente empregados oferecem uma seletividade maior para o produto linear (ver Esquema 1).

Utilizando como exemplo um complexo tipo [MHL$_4$], onde M é um metal com configuração eletrônica d^9 e L um ligante a 2 elétrons, o mecanismo aceito para o processo de hidroformilação pode ser visto em seguida (Esquema 1). A primeira etapa do mecanismo começa com o precursor metálico (M^I, 18 elétrons) perdendo um ligante L formando uma espécie de 16 elétrons (**I**) que iniciará o ciclo catalítico. A etapa seguinte corresponde à coordenação da olefina no sítio vacante do metal gerando a espécie **II** (M^I, 18 elétrons). Posteriormente, uma inserção/migração 1,2 do hidreto à ligação C=C (no esquema mostrado adição anti-Markovnikov) produz o intermediário **III** contendo uma ligação σ metal-alquila (M^I, 16 elétrons). A entrada de uma molécula de CO gera primeiramente uma espécie [ML$_3$(CO)(alquil)] (M^I, 18 elétrons; não mostrado) que, com a posterior migração da alquila na ligação σ metal-CO, forma-se um composto metal-acila **IV** contendo um sítio vacante (M^I, 16 elétrons). Em seguida ocorre uma adição oxidativa de H$_2$ ao centro metálico aumentando o *nox* do metal em duas unidades acarretando na geração do intermediário **V** (M^{III}, 18 elétrons). Para finalizar o ciclo, um hidreto participa de uma etapa de eliminação redutiva formando o aldeído linear (mostrado no esquema) e regenerando a

espécie inicial **I** (M^I, 16 elétrons). A formação do aldeído ramificado difere apenas na etapa de inserção/migração do hidreto na olefina. Neste caso, a inserção/migração ocorre tipo Markovnikov seguido por etapas idênticas às apresentadas. Esta seqüência das etapas mecanísticas pode ser extrapolada para o uso de quaisquer outros precursores metálicos.
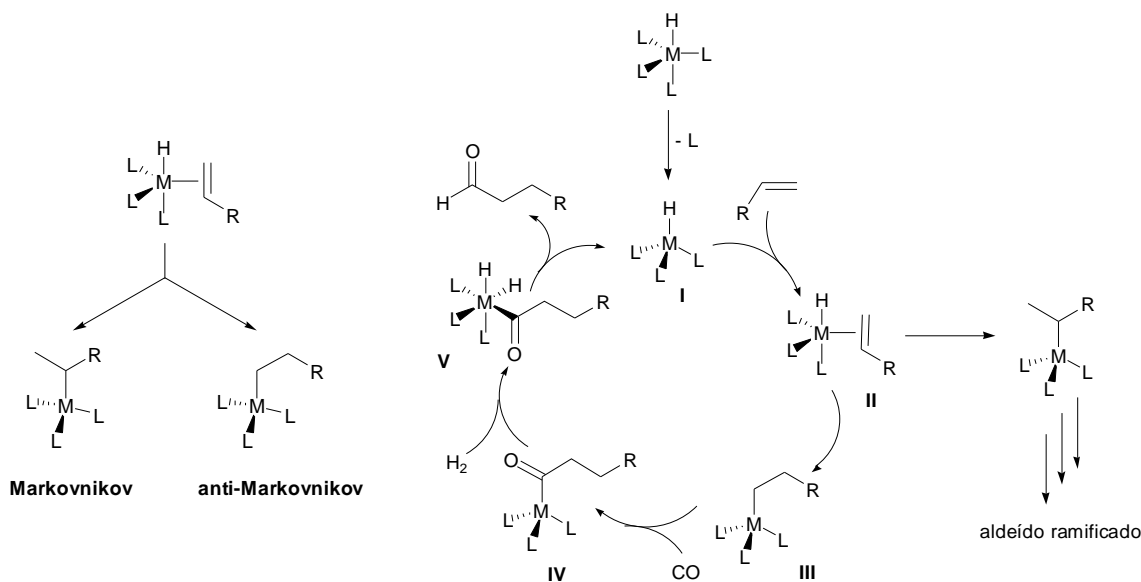

Esquema 1. Adição Markovnikov ou anti-Markovnikov do hidreto à ligação C=C (esquerda). Ciclo mecanístico aceito para a hidroformilação de alcenos (direita).

Os precursores metálicos mais comumente utilizados são baseados em Rh,[15-18] Co[19, 20] e Pt[21]. Complexos metálicos suportados também têm sido empregados em reações de hidroformilação na tentativa de combinar as vantagens de um sistema heterogêneo com a eficiência da catálise homogênea.[22, 23] Além disso, diferentes meios reacionais como solventes orgânicos,[24, 25] água,[26] CO_2 supercrítico[27] e LIs[28] foram utilizados no processo de hidroformilação. Em particular, o uso de LIs apresenta muitas vantagens como meios reacionais para reações de hidroformilação bifásicas. Dentre as vantagens pode-se destacar a estabilidade do catalisador na fase do LI com posterior reciclagem e a facilidade na separação dos produtos (decantação, destilação). A seguir serão mostrados alguns trabalhos referentes ao uso de LIs como eficientes meios reacionais para processos de hidroformilação.

### 2.2.1. Hidroformilação de Alcenos em Líquidos Iônicos

Os primeiros estudos a respeito da reação de hidroformilação em LIs catalisada por complexos de Rh/fosfina foram realizados por Chauvin e colaboradores (Esquema 2).[29] O precursor de Rh [Rh(acac)(CO)$_2$] (acac = acetilacetonato) na presença de ligantes triarilfosfinas apresentou atividade catalítica na hidroformilação bifásica de 1-penteno em BMI.PF$_6$. Ao empregar a fosfina PPh$_3$, uma considerável porção do catalisador de Rh migrou da fase iônica (LI) para a fase dos produtos. Apesar de controlar a lixiviação ao utilizar a fosfina sulfonada TPPMS (*meta*-sodium monosulfonated-triphenylphosphine), uma significativa desativação do catalisador em LI foi observada pelos valores de TOF (59 h^{-1} para TPPMS; 333 h^{-1} para PPh$_3$). Apenas seletividades moderadas entre 50-80% foram encontradas para o aldeído linear usando o referido sistema catalítico.
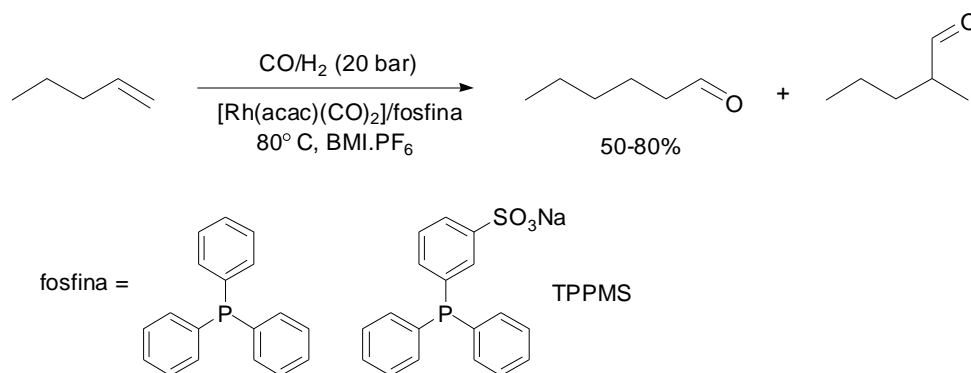
Esquema 2. Hidroformilação de 1-penteno catalisada por um complexo de Rh em LI.[29]

A hidroformilação do composto 3-pentenoato de metila catalisada por complexos de Rh em LI foi realizada por Keim e colaboradores.[30] Um importante desafio neste caso é obter alta seletividade no produto linear, uma vez que este substrato pode isomerizar e hidrogenar gerando sub-produtos. A regio-seletividade observada nas reações foi atribuída não ao solvente, mas sim ao tipo de ligante utilizado. Por exemplo, a reação com complexo de Rh [Rh(acac)(CO)$_2$] na presença de PPh$_3$ em tolueno ou BMI.PF$_6$ produz seletividades mais altas nos produtos **2** (38-39%) e **3** (37-42%). Por outro lado, a reação com o ligante fosfito (propicia alto impedimento estéreo, ver Esquema 3) acarreta em uma seletividade preferencial para o produto linear **1** (47-50%). Este fato pode estar relacionado à tendência de isomerização propiciada pelo ligante fosfito aumentando a formação do produto de

interesse. Além disso, verificou-se que na presença de PPh₃ o sistema desativa-se após o primeiro (tolueno) ou quarto (LI) ciclo, enquanto que para o ligante fosfito em LI atingiu-se valores de TON até 6640 após 10 ciclos.
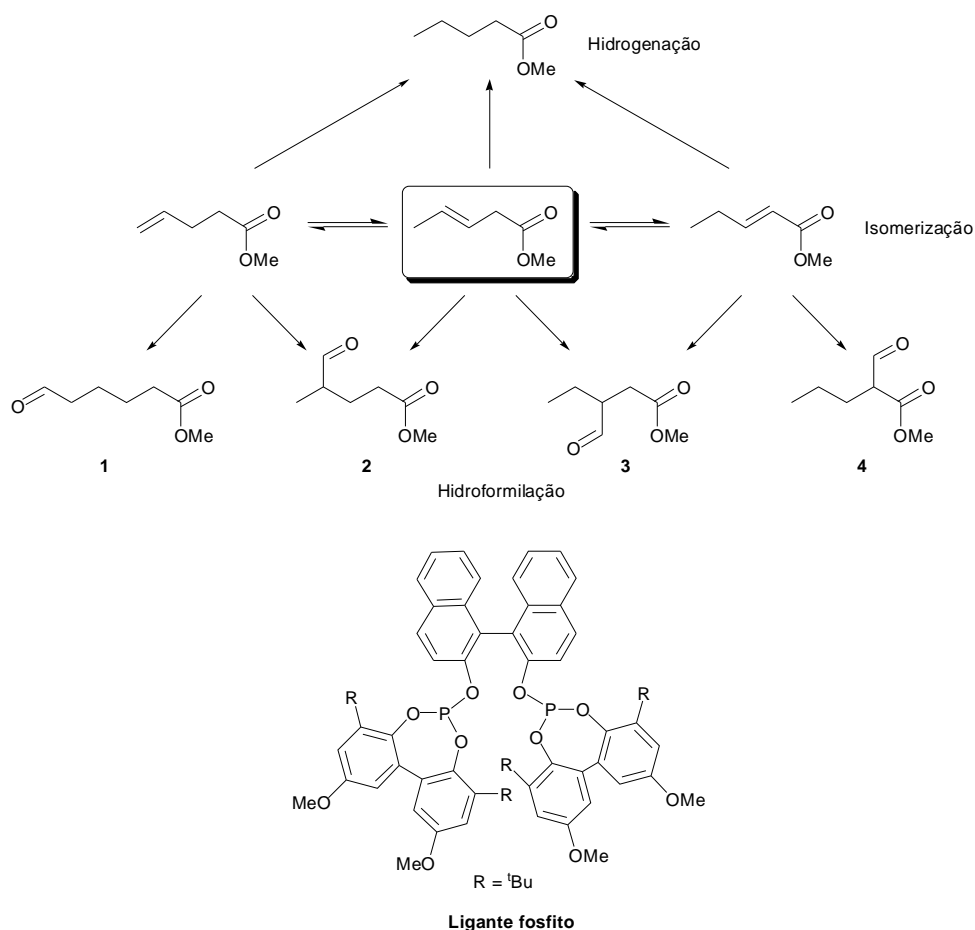

Esquema 3. Possíveis etapas de hidrogenação, isomerização e hidroformilação para o composto 3-pentenoato de metila na presença do precursor [Rh(acac)(CO)₂]/fosfina e CO/H₂ (1:1) em LI ou tolueno a 110 °C. Abaixo é mostrada a estrutura do ligante fosfito utilizado nos estudos.[30]

Convém mencionar que o complexo [PtCl₂(PPh₃)₂] dissolvido em LIs (levemente ácidos) contendo o ânion cloroestanato, demonstrou ser um catalisador ativo durante a hidroformilação do 3-pentenoato de metila e 1-octeno.[31]

O primeiro trabalho que demonstrou a influência da estrutura de diferentes LIs (cátions e ânions) em reação de hidroformilação foi publicado pelo grupo de Olivier-Bourbigou.[32] Diferentes cátions e anions foram estudados, bem como o efeito da solubilidade de 1-

hexeno/LIs na atividade catalítica do sistema. Exceto para o caso do anion NTf_2 onde apesar da boa solubilidade do substrato uma baixa atividade foi observada, constatou-se que o aumento de solubilidade do substrato no LI está diretamente ligado ao aumento da atividade do catalisador de Rh ([Rh(acac)(CO)$_2$]/TPPMS). Foi mostrado neste trabalho que é possível otimizar as atividades catalíticas e regio-seletividade das reações de hidroformilação apenas ajustando a natureza de cátions e ânions dos LIs e também os ligantes utilizados (em todos os casos obteve-se seletividades em aldeídos > 97%).

Wasserscheid e colaboradores apresentaram um método baseado na síntese de fosfinas ionofílicas contendo grupamento guanidínio, para auxiliar na imobilização do catalisador de Rh na fase do LI durante reações de hidroformilação (Esquema 4).[33] Assim como em outros exemplos, o uso de PPh$_3$ propicia uma boa atividade catalítica na hidroformilação bifásica de 1-octeno em BMI.PF$_6$ porém com alta lixiviação do catalisador para a fase orgânica. Apesar de se observar uma menor atividade, as fosfinas ionofílicas oferecem uma excelente condição de imobilização do catalisador na fase iônica. Por exemplo, a fosfina ionofílica PhP[(PhN$_3$H$_9$C$_2$)PF$_6$]$_2$ se manteve ativa até o terceiro reciclo (35% de conversão) com quase inexistente perda do catalisador para a fase orgânica. Estes resultados de atividade foram ainda superiores quando comparados ao ligante sulfonado TPPTS (*meta-sodium trisulfonated-triphenylphosphine*). Sabendo que fosfinas com um grande ângulo P-metal-P (*bite angle*) geram um sistema bastante regio-seletivo em reações de hidroformilação,[34] os autores se basearam em um tipo de ligante estudado por van Leeuwen[35-37]. A diferença consiste na síntese de um ligante derivado do Xantphos, mas contendo grupos guanidínios ionofílicos, uma vez que o ligante Xantphos tende a ser mais solúvel na fase orgânica que no LI. Como esperado, utilizando o ligante ionofílico preparado tipo-Xantphos na hidroformilação bifásica de 1-octeno em BMI.PF$_6$, a atividade aumenta com os reciclos chegando a um máximo de conversão no sétimo experimento (44%) com boas seletividades para o aldeído linear.
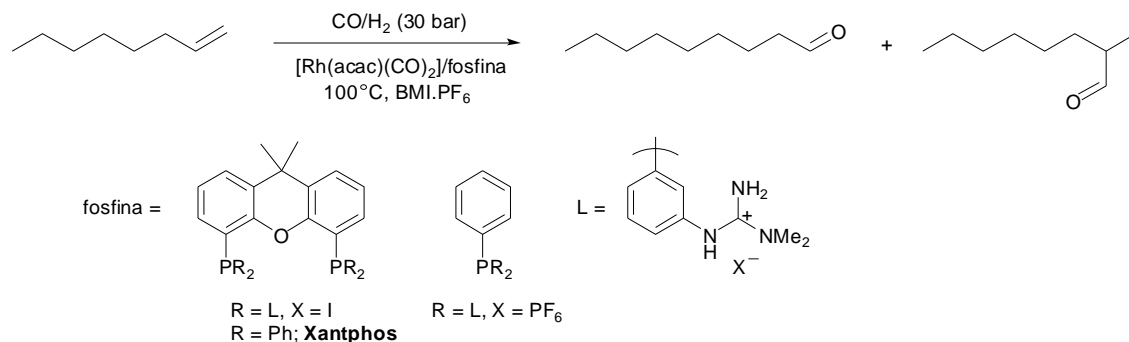
Esquema 4. Hidroformilação bifásica de 1-octeno em BMI.PF$_6$ na presença de um complexo de Rh contendo fosfinas ionofílicas.[33]

Estudos independentes feitos por Dupont e colaboradores demonstram o efeito dos parâmetros reacionais (pressão, temperatura, LI) na hidroformilação bifásica de diferentes alcenos em LIs (Esquema 5).[38] O sistema baseado no precursor [Rh(acac)(CO)$_2$]/Xantphos em BMI.PF$_6$ produz uma maior atividade catalítica comparado ao ligante Sulfoxantphos (TOF$_{Xantphos}$ = 245 h^{-1}; TOF$_{Sulfoxantphos}$ = 47 h^{-1}) durante a hidroformilação de 1-octeno. Entretanto, em testes de reciclo uma considerável lixiviação do catalisador para a fase orgânica é observada ao se empregar a fosfina Xantphos (conversão passa de 99% para 60%). A presença da fosfina sulfonada permite uma maior reciclabilidade do catalisador evitando perdas por lixiviação e mantendo altos valores de conversão. De fato, conversões quase totais e seletividade em torno de 80% podem ser obtidas aumentando o tempo reacional e ajustando a relação fosfina/Rh. A investigação da influência de parâmetros reacionais mostra que o aumento da pressão de gás diminui a conversão de 1-octeno e a seletividade em *n*-nonanal. O acréscimo de temperatura acarreta em um aumento na conversão, enquanto que a seletividade aumenta na faixa entre 60-100 °C e decresce a partir desta temperatura. Utilizando as melhores condições reacionais (15 bar de gás, 100 °C e fosfina/Rh = 4), foram testados diferentes alcenos e meios reacionais (BMI.PF$_6$, BMI.PF$_6$/H$_2$O, BMI.PF$_6$/PhMe, BMI.BF$_4$, H$_2$O, PhMe). A maior relação *n/i* (61) foi observada na reação de hidroformilação de 1-deceno com a fosfina Sulfoxantphos em BMI.PF$_6$. É esperado que as seletividades das reações de hidroformilação estejam diretamente relacionadas à natureza do LI. Nota-se que os maiores valores foram alcançados na presença de um LI hidrofóbico (BMI.PF$_6$), sem a adição de co-solventes. Ao contrário do LI puro onde existe uma estrutura supramolecular organizada com interações

fracas, a adição de outra molécula pode causar mudanças nesta organização estrutural do LI, criando nano-regiões polares e apolares. Supõe-se que estes efeitos ocasionem variações nas miscibilidades parciais dos alcenos, gás e produtos formados na fase do LI.

Posteriormente, a reação de hidroformilação de 1-octeno catalisada pelo sistema [Rh(acac)(CO)$_2$]/Sulfoxantphos em BMI.PF$_6$ foi acompanhada por análises de alta pressão de IV e RMN.[39] De forma similar como em solventes orgânicos, os isômeros [(difosfina)Rh(CO)$_2$H] *ee* (fosfina na posição bis-equatorial) e *ea* (equatorial-axial) foram detectadas em LI. Foi observado que a relação entre estas espécies é dependente da temperatura e da pressão do gás de síntese. O aumento da pressão de gás desloca o equilíbrio para a formação da espécie *ea*, a qual reduz a seletividade em aldeído, fato este comprovado previamente[38].
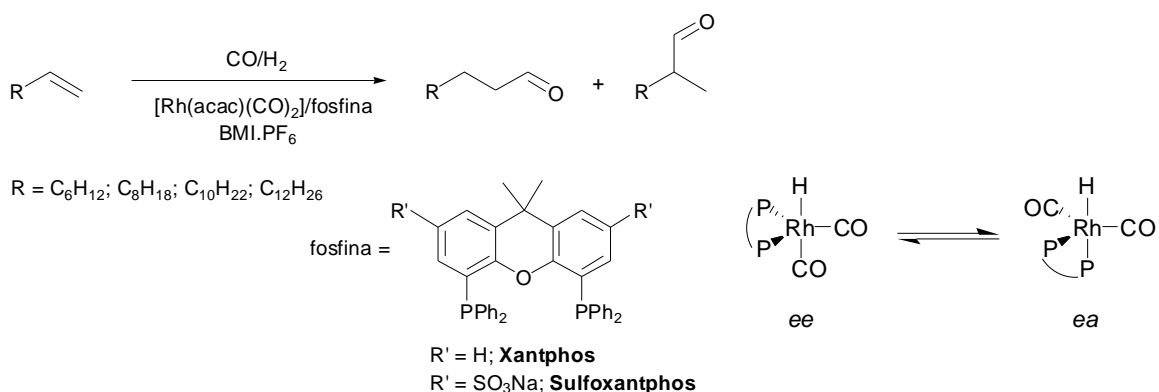
Esquema 5. Reação de hidroformilação de diferentes alcenos em LI utilizando o sistema [Rh(acac)(CO)$_2$] na presença do ligante Xantphos ou Sulfoxantphos (esquerda). Equilíbrio entre as espécies de Rh formadas *in situ* na reação de hidroformilação de 1-octeno em BMI.PF$_6$ detectadas por IV e RMN (direita).[38, 39]

Investigações do uso de um LI imidazólio contendo ânion octilsulfato (BMI.C$_8$H$_{17}$OSO$_3$) como meio reacional para a hidroformilação de 1-octeno mostraram bons resultados.[40] Este LI, ao contrário de outros clássicos como BMI.PF$_6$, proporciona um sistema monofásico na presença de 1-octeno. O sistema homogêneo constituído de BMI.C$_8$H$_{17}$OSO$_3$, 1-octeno e do catalisador de Rh/fosfina apresentou atividade catalítica e seletividade em aldeído linear superiores aos meios bifásicos (BMI.PF$_6$ e BMI.BF$_4$). Mesmo tornando um sistema bifásico pela adição de cicloexano como co-solvente, a atividade para este sistema continua sendo maior que para os outros LIs (TOF = 892 e 862

h^{-1} para BMI.$C_8H_{17}OSO_3$ e BMI.$C_8H_{17}OSO_3$ + C_6H_{12}, respectivamente; TOF = 276 e 317 h^{-1} para BMI.PF_6 e BMI.BF_4, respectivamente). Estes resultados estão provavelmente relacionados com a natureza do meio reacional, onde se espera que em meio homogêneo a reação seja mais efetiva que em condições bifásicas.

Shreeve e Omotowa propuseram o uso de LIs altamente viscosos contendo cátions perfluorados na hidroformilação de 1-octeno.[41] Um ligante piridínio contendo um grupo fosfina foi investigado para a imobilização do precursor de Rh durante a reação. Durante a hidroformilação de 1-octeno na presença dos LI perfluorados e da fosfina ionofílica (ver Esquema 6) a 80 °C e 69 bar de CO/H_2 (1:1), conversões quantitativas foram obtidas entre 14-19 h (dependendo do LI) com seletividades apenas em *n*-nonanal e 2-metiloctanal (sem hidrogenação ou isomerização do substrato). Nos experimentos de reciclo do sistema, detectou-se apenas uma pequena diminuição nas atividades e seletividades, atribuídas possivelmente pela lixiviação de Rh (0,40-26,5 ppm).

Esquema 6. Reação de hidroformilação de 1-octeno catalisada por [Rh(acac)(CO)$_2$]/fosfina em LIs perfluorados.[41]

Williams e colaboradores focaram seus estudos na hidroformilação de acetato de vinila promovida por [Rh(acac)(CO)$_2$]/ligante em diferentes LIs.[42] O objetivo foi obter o máximo de seletividade em 2-acetoxipropanal (produto *iso*), uma vez que é um importante intermediário na síntese do composto lactato de etila. Os LIs que mostraram maiores atividades foram [BnEt$_3$N]NTf$_2$ (BnEt$_3$N = benziltrietilamônio) e BPy.NTf$_2$ (BPy = *N*-butilpiridínio), os quais com valores de TOF cerca de duas vezes maior que para o tolueno. Para todos os LIs testados verificou-se altas seletividades no aldeído ramificado (produto

iso). A maior seletividade (*i*:*n* > 99:1) foi observada utilizando o LI [MeOc$_3$N]NTf$_2$ (MeOc$_3$N = metiltrioctilamônio). De forma interessante, mostrou-se que a mistura de dois LIs pode afetar positivamente a cinética da reação bem como a seletividade.

Além das clássicas reações de hidroformilação de alcenos[43-50], outros exemplos em LIs podem ser citados como sistemas em fluxo contínuo[51, 52], hidroformilações assimétricas[53] e reações alternativas empregando CO_2 ao invés de CO[54]. Informações mais detalhadas a respeito de reações de hidroformilação em LIs podem ser encontradas em um *review* publicado recentemente.[28]

2.3. H₂ como Fonte Limpa para Produção de Energia

Embora o hidrogênio seja um dos elementos mais abundantes no planeta, apenas 1% se apresenta como gás hidrogênio, sendo a grande maioria presente na composição da água e de hidrocarbonetos. Devido às suas vantajosas propriedades, o H_2 surge como uma das formas alternativas de energia mais interessantes. De fato, sua densidade de energia gravimétrica é de 33,3 kWh/kg, o qual corresponde cerca de três vezes mais o valor obtido para a gasolina (ver Tabela 1).[55] Entretanto, o H_2 gasoso apresenta densidade de energia volumétrica em torno de 0,8 kWh/L a 350 bar, valor este considerado muito inferior quando comparado ao da gasolina (9,5 kWh/L).[56] Em termos práticos, para suprir uma quantidade de energia fornecida por 4,5 L de gasolina, necessita-se um volume de aproximadamente 3430 L de H_2 em condições padrão de temperatura e pressão.[57] Por exemplo, um reservatório de aço de 50 L com uma pressão de 300 bar contém apenas 1,36 kg de H_2. Considerando a massa do reservatório de 90 kg, a densidade em massa de H_2 no sistema é de apenas 1,5%. Este valor pode chegar a 5% em massa ao utilizar hidrogênio líquido, mas neste caso com perdas diárias de até 1% devido à evaporação.[58]

Para fins de utilização do H_2 em veículos automotivos, necessita-se de reservatórios compactos, leves e seguros.[55] No caso de hidrogênio gasoso, altas pressões de gás e um alto volume são requeridos para se obter uma quantidade significativa de H_2 em porcentagem mássica. Uma alternativa visando o aumento na quantidade de H_2 *vs* volume, seria a utilização de hidrogênio líquido (d = 70,8 kg/m³). Entretanto, a necessidade de se manter o sistema a baixíssimas temperaturas (acima de -241°C o H_2 se torna gás) é um fator limitante. Além disso, a constante perda de hidrogênio por evaporação devido à própria transferência de calor pelo reservatório (presença de exaustão para evitar uma pressão excessiva de gás) é outro fator que ainda inviabiliza seu uso. Estes são os principais fatores que desafiam futuras aplicações de H_2 como fonte energética.

O estudo para descobertas de materiais alternativos que armazenem hidrogênio de forma segura e eficiente tem sido o foco de pesquisas recentes nesta área. A utilização de sólidos com grande área superficial para uma efetiva adsorção de H_2 ou materiais que contenham o hidrogênio quimicamente ligado em sua estrutura molecular, estão entre os mais pesquisados. Dentre estes últimos, a eletrólise da água, o uso de moléculas orgânicas (ácido fórmico, hidrocarbonetos), amino-boranas, metal hidretos e LIs são os sistemas mais

estudados para a geração de H$_2$. A seguir será brevemente discutida a aplicação destes materiais com alguns exemplos para facilitar a compreensão da importância de cada sistema.

Tabela 1. Propriedades físico-químicas comparativas entre hidrogênio (H$_2$), metano e petróleo[55]

Propriedades	H$_2$	Metano	Petróleo
Densidade energética (kWh/kg)	33,3	13,9	12,4
Temperatura de ignição (°C)	585	540	228-501
Temperatura de chama (°C)	2.045	1.875	2.200
Propagação da chama no ar (m/s)	2,65	0,4	0,4

2.3.1. Eletrólise da Água

A eletrólise da água representa um processo possível para a produção de H_2. Através da passagem de uma corrente elétrica, a molécula de água é decomposta via um processo de oxi-redução em H_2 (formado no cátodo) e O_2 (formado no ânodo). Uma vez que a condutividade da água pura é praticamente nula, necessita-se de uma grande quantidade de energia para realizar a eletrólise. Para contornar este problema, geralmente se adiciona algum eletrólito para aumentar a condução da corrente elétrica facilitando a eletrólise. Apesar de ser uma alternativa interessante para a produção de hidrogênio, a eletrólise da água necessita de grande quantidade energética, o que acarreta ainda em limitações para sua aplicação em células a combustível.

2.3.2. Amônia-Borana

Dentre os materiais recentemente utilizados como fonte de H_2, destacam-se os compostos denominados de amino-boranas. Em especial, amônia-borana (H_3NBH_3) tem sido muito investigada como alternativa para futuras aplicações em célula a combustível. É importante mencionar que o comportamento térmico deste composto foi primeiramente estudado no ano de 1978 por Hu, Geanangel e Wendlandt.[59] Além de apresentarem alta quantidade em massa de hidrogênio (19,6%), amônia-boranas cumprem requisitos importantes como: não-inflamáveis e não-explosivos em condições padrão, os quais a torna um bom material candidato a ser testado em células a combustível.[56] Apesar de todas estas vantagens, um grande desafio diz respeito à regeneração da amônia-borana após a desidrogenação. Ao ser liberado os 3 equivalentes molares de H_2 ocorre a formação de nitretos de boro (B-N), os quais são muito estáveis entalpicamente ($\Delta H^o_{f, 298K}$ = -59,97 ± 0,37 kcal/mol)[60] para serem transformados novamente em H_3NBH_3. Por este motivo, intensifica-se estudos a cerca de uma liberação de H_2 rápida e controlada (~13% em massa) a fim de se evitar ao máximo a formação de sub-produtos (amônia e borazina, por exemplo) de difícil regeneração e que também podem danificar a célula a combustível, restringindo seu uso em testes futuros.

A decomposição de amônia-borana pode ser resumida basicamente em três etapas (Tabela 2).

Tabela 2. Etapas da decomposição de amônia-borana com os respectivos valores calculados de entalpia de reação em fase gasosa a 298K

Etapas	ΔH de reação (kJ/mol) em fase gasosa calculados a 298K[61]
$H_3NBH_3 \longrightarrow H_2NBH_2 + H_2$ (1)	-21,3
$H_2NBH_2 \longrightarrow HNBH + H_2$ (2)	131,4
$HNBH \longrightarrow BN + H_2$ (3)	562,1

É possível verificar que a primeira etapa da decomposição é um processo exotérmico onde se conclui que a liberação de H_2 é favorecida, uma vez que a contribuição entrópica é sempre positiva. Entretanto, as etapas 2 e 3 mostram valores de entalpia significativamente

positivos, indicando que altas temperaturas devem ser empregadas no processo, principalmente na última etapa onde a liberação da molécula de H_2 ocorre a T>1200 ºC[56]. Um dos grandes desafios neste caso é a identificação dos intermediários das etapas durante a desidrogenação de amônia-borana. De forma geral, pode ocorrer a formação de compostos cíclicos e poliméricos tais como: poliaminoboranas $(H_2NBH_2)_x$, poliiminoboranas $(HNBH)_x$, borazina $(B_3N_3H_6)$, ciclotriborazona $(H_2NBH_2)_3$, poliborazilenos $(B_3N_3H_6)_x$, entre outros.

Informações mais detalhadas a respeito de aspectos estruturais, propriedades físico-químicas e reatividade destes compostos podem ser encontrados em recentes *reviews* publicados na literatura.[56, 62] A seguir serão mostrados apenas alguns trabalhos a fim de exemplificar o uso de amônia-boranas como fontes de H_2.

2.3.2.1. Amônia-Borana em LI: Melhor Desempenho na Liberação de H_2

Sneddon e colaboradores demonstraram que o desempenho na decomposição de amônia-borana na presença de LI aumenta de forma significativa.[63] Os testes catalíticos foram realizados em temperaturas de 85-95 ºC. Primeiramente testou-se a decomposição da amônia-borana em estado sólido e, posteriormente, comparou-se os resultados com os obtidos a partir de uma mistura de amônia-borana/BMI.Cl nas mesmas condições reacionais. A Figura 1 mostra os equivalentes molares de H_2 liberados em função do tempo para os dois sistemas. Para o sistema contendo apenas H_3NBH_3, em 3 h a 95 ºC uma quantidade de 0,8 equivalentes molares de H_2 foram liberados e somente após 17 h obteve-se 0,9 equivalentes molares de H_2. Além disso, percebe-se que durante 1 h praticamente não houve reação. Entretanto, quando a mistura H_3NBH_3/BMI.Cl é aquecida a 85 ºC, cerca de 0,5 equivalentes molares de gás são liberados em 1 h de reação, sem período de indução. Neste mesmo tempo reacional, a 95 ºC percebe-se a formação de 1,1 equivalentes molares H_2. Após 22 h de reação chega-se a 1,6 equivalentes molares, valor bastante superior quando comparado ao sistema contendo apenas H_3NBH_3.
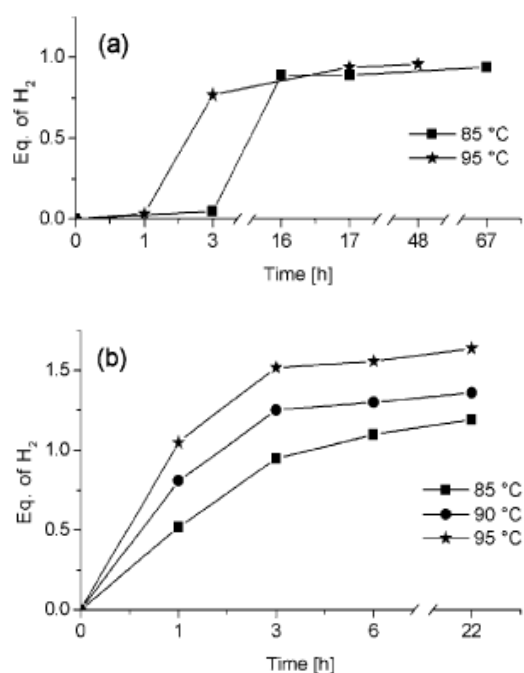
Figura 1. Decomposição de H_3NBH_3 **a)** em estado sólido e **b)** na presença de BMI.Cl a diferentes temperaturas. Reproduzido com permissão da referência [63] (American Chemical Society).

Experimentos de RMN [11]B mostram que em 1 h de reação apenas o sinal da amônia-borana é verificado em -22,4 ppm, ao contrário da reação na presença de BMI.Cl onde vários sinais foram observados (Figura 2). É interessante notar que os espectros em 19 h da reação com H₃NBH₃ e o de 3 h para a mistura H₃NBH₃/BMI.Cl são bastante similares.
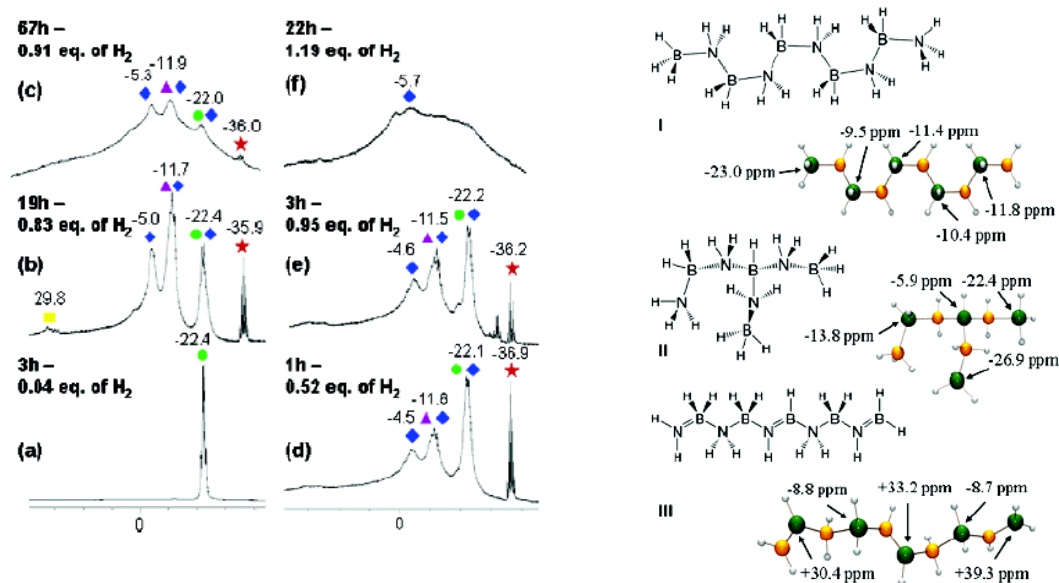

Figura 2. (Esquerda) Análises de RMN [11]B dos resíduos das reações: **(a, b, c)** em estado sólido, H₃NBH₃, e **(d, e, f)** da mistura H₃NBH₃/BMI.Cl. Em verde o sinal da amônia-borana, laranja BH₄⁻, roxo BH₂⁺, azul poliaminoborana, amarelo B=N. (Direita) Cálculos teóricos dos deslocamentos químicos no espectro de RMN [11]B dos possíveis compostos provenientes da reação de decomposição. Reproduzido com permissão da referência [63] (American Chemical Society).

Estudos prévios[64] mostraram que o composto diamoniato de diborana [(NH₃)₂BH₂]⁺BH₄⁻ apresenta sinais próximos a -38 ppm (BH₄⁻) e -14 ppm (BH₂⁺), os quais concordam relativamente bem com os indicados acima. Além disso, sinais propostos ao grupo BH₂ de poliaminoboranas (I) ou cicloborazonas (-10 a -13 ppm)[65], bem como os sinais próximos a -5 e -25 ppm relativos aos grupos N-BH-N e BH₃ terminal (II), respectivamente. O sinal em torno de 30 ppm no espectro pode ser atribuído aos grupos B=N ou B=NH₂ provenientes da desidrogenação de espécies poliaminoboranas, os quais estão de acordo pelas simulações para a espécie III. Os autores sugerem neste caso que, devido à habilidade dos LIs na estabilização de estados de transição iônicos/polares,[1] o efeito ativador do LI pode estar associado à uma possível indução na formação e

estabilização da espécie iônica $[(NH_3)_2BH_2]^+BH_4^-$ (esta espécie também pode formar poliaminoboranas sob aquecimento)[66], a qual já é formada em apenas 1 h de reação na presença do LI.

2.3.2.2. Decomposição de Amônia-Borana Catalisada por Metal de Transição

Um exemplo que demonstra uma efetiva decomposição de amônia-borana catalisada por metais de transição foi publicado por Baker e colaboradores.[67] Utilizando um complexo de Ni-NHC (NHC = *N-heterocyclic carbenes*) gerado *in situ*, quantidades bastante expressivas de H_2 (>2,5 equivalentes molares; 18% em massa) foram gerados a partir de H_3NBH_3. Este sistema catalítico é, sem dúvida, um dos mais eficientes desenvolvidos até o momento.

A mistura de uma solução de C_6D_6 contendo o complexo de Ni/ligante ([Ni(COD)$_2$], COD = 1,5-ciclooctadieno, + 2 equivalentes molares do ligante 1,3,4-trifenil-4,5-diidro-1H-1,2,4-triazol-5-ilideno) com outra contendo a amônia-borana (10 equivalentes molares) a 60 °C produz H_2 imediatamente, sendo que após 4 h de reação, cerca de 2,5 equivalentes molares de H_2 são liberados (Esquema 7).

$$[Ni(COD)_2] + 2 \text{ (carbeno de Enders)} \xrightarrow[\text{4 h, 60 °C} \atop \text{C}_6\text{D}_6 \text{ ou diglime}]{10 \text{ H}_3\text{NBH}_3} \mathbf{H_2} + \text{sub-produtos}$$
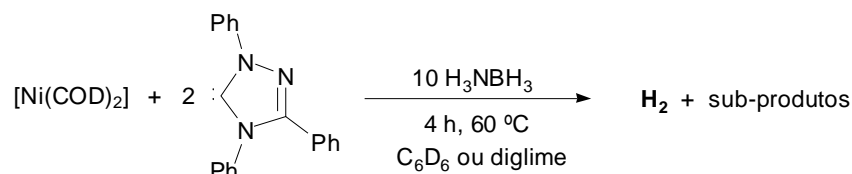
Esquema 7. Decomposição de amônia-borana catalisada pelo complexo Ni-NHC gerado *in situ*.[67]

Como sub-produtos majoritários, os sinais entre 18-40 ppm no espectro de RMN [11]B foram atribuídos às espécies B-N derivadas de unidades de borazina. Testes catalíticos empregando diferentes ligantes carbenos foram realizados, porém o carbeno de Enders (1,3,4-trifenil-4,5-diidro-1H-1,2,4-triazol-5-ilideno)[68] apresentou resultados muito superiores. Outros complexos metálicos, como [RuCl$_2$(*p*-cimeno)]$_2$ e [RhCl(COE)$_2$]$_2$ (COE = *cis*-cicloocteno) também foram testados na presença do carbeno de Enders. Entretanto, o catalisador de Ni apresentou atividade catalítica bastante superior aos catalisadores de Ru e Rh. Efeitos isotópicos foram evidenciados na decomposição de H_3NBD_3 (1,7), D_3NBH_3 (2,3) e D_3NBD_3 (3,0) catalisadas pelo complexo de Ni-NHC, sugerindo que as ligações N-H e B-H estão sendo quebradas na etapa determinante da velocidade reacional. Um mecanismo baseado nas etapas de ativação B-H seguido de eliminação-β da ligação N-H

foi proposto, implicando em constantes de velocidade similares devido aos efeitos isotópicos observados (Esquema 8).
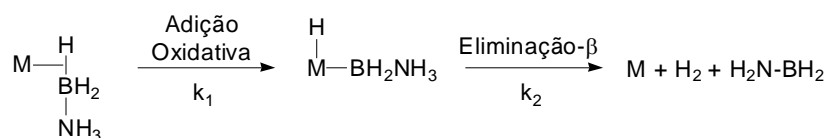
Esquema 8. Proposta mecanística para a decomposição catalítica de H_3NBH_3.[67]

Apesar de algumas etapas mecanísticas estarem ainda sendo discutidas,[69] Hall e Yang[70] propuseram um mecanismo para a reação desenvolvida por Baker. Através de estudos computacionais, primeiramente é proposto uma transferência protônica do grupo NH_3 para o ligante carbeno seguido de uma ativação C-H (carbeno) pelo metal com posterior formação e liberação de H_2 (Esquema 9). Neste estudo, os autores calcularam a energia relativa para a espécie $[H-Ni(NHC)_2(H_2BNH_3)]$ formada pela ativação da ligação B-H (proposto por Baker). Pelos cálculos, encontra-se uma entalpia em fase gasosa cerca de 6,8 kcal/mol maior comparado à etapa de transferência protônica ($2 \rightarrow$ **TS$_{23}$**, Esquema 9). Portanto, descarta-se uma primeira etapa como ativação B-H, mas sim uma transferência de próton entre NH_3 e o ligante carbeno. Este mecanismo, segundo os autores, explica a importância do ligante carbeno na reação de decomposição da amônia-borana e provem barreiras energéticas menores comparadas ao mecanismo via ativação B-H-Ni ou N-H-Ni.

Além de amino-boranas, compostos similares denominados de amido-boranas (MNH_2BH_3, M = Li, Na, K) tem sido utilizados como fontes de H_2. Mais detalhes a respeito da capacidade de armazenamento (% massa de H_2) e reatividade desta classe de compostos frente à liberação de H_2 podem ser encontrados na literatura.[71, 72]
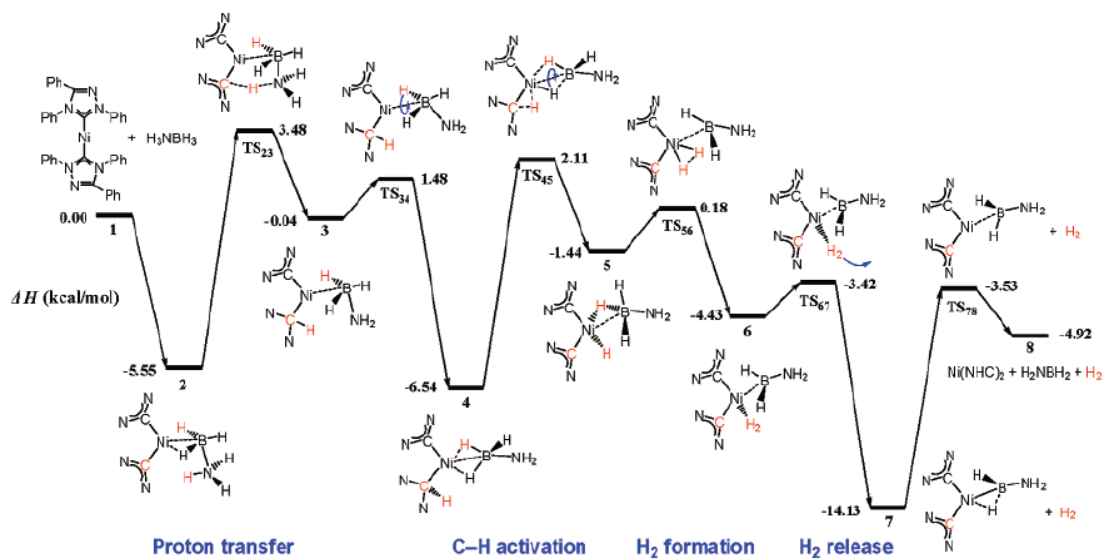
Esquema 9. Mecanismo proposto por cálculos teóricos para a decomposição da amônia-borana catalisada pelo complexo [Ni(NHC)₂] (NHC = carbeno de Enders). Reproduzido com permissão da referência [70] (American Chemical Society).

2.3.3. Hidretos Metálicos

Dentre os materiais alternativos desenvolvidos para uma segura e eficiente estocagem/liberação de H_2, a classe denominada de metal-hidreto apresenta grande potencial para futuras aplicações em células a combustível. Isto se deve, principalmente, pela alta densidade de hidrogênio armazenado (6,5 átomos de H/cm^3 para MgH_2) por estes materiais quando comparado ao gás hidrogênio (0,99 átomos H/cm^3) e até mesmo ao hidrogênio líquido (4,2 átomos de H/cm^3).[73] É importante citar que boro-hidretos metálicos também podem apresentar alta capacidade de armazenamento de hidrogênio. Para o caso de $LiBH_4$, chega-se a uma quantidade de até 18,5% em massa de hidrogênio, valor este superior ao encontrado para a gasolina (15,8% em massa). Porém para a maioria dos hidretos metálicos conhecidos, algumas limitações ainda precisam ser contornadas: condição termodinâmica não-favorável (alta temperatura para a liberação de H_2), baixas velocidades de liberação de H_2, dificuldade de regeneração a baixas temperatura e pressão e formação de sub-produtos indesejáveis.

Apesar de conter 7,6% em massa de hidrogênio, a formação de MgH_2 a partir de Mg *bulk* e gás hidrogênio é bastante lenta.[55] Portanto, formas alternativas de hidretos metálicos devem ser desenvolvidas para evitar tais limitações. Por exemplo, o uso de ligas de Mg antes da formação do hidreto seria uma opção. O composto Mg_2Ni gera o hidreto Mg_2NiH_4 que contém em torno de 3,6% em massa de hidrogênio. Apesar de sua rápida formação, este hidreto metálico necessita de 280 °C para liberar 1 bar de H_2. Para hidretos metálicos com baixa cinética de formação (ex: MgH_2), uma maneira alternativa seria a síntese a partir da reação de ligas metálicas mais reativas com gás hidrogênio formando como produto o hidreto metálico de interesse. A fins de exemplo, o composto Mg_2Cu reage facilmente com H_2 produzindo MgH_2 e $MgCu_2$.[55]

O grande atrativo recente desta classe de materiais são as misturas binárias que, quando comparado aos compostos simples que a constituem, apresentam melhoras significativas nas condições termodinâmicas, alta pureza de H_2 e, em certos casos, reversibilidade. Pode-se citar misturas como $LiNH_2/MgH_2$,[74] $LiBH_4/MgH_2$[75] e $LiNH_2/LiBH_4$[76]. Entretanto, algumas desvantagens destes sistemas ainda devem ser consideradas: a temperatura de dessorção ainda é alta para fins de aplicação, em alguns casos a reação é irreversível, para os sistemas contendo nitrogênio ocorre a liberação de NH_3 juntamente com H_2.

Neste contexto, Yang e colaboradores desenvolveram um sistema baseado em uma mistura contendo três hidretos metálicos (2LiNH$_2$/LiBH$_4$/MgH$_2$; 8,2% em massa de hidrogênio).[77] A grande vantagem deste sistema foi a existência de uma reação auto-catalítica resultando em uma cinética mais rápida e menor temperatura de liberação de H$_2$ comparado aos sistemas binários (Figura 3). Além disso, a quantidade de amônia liberada neste caso é praticamente nula.
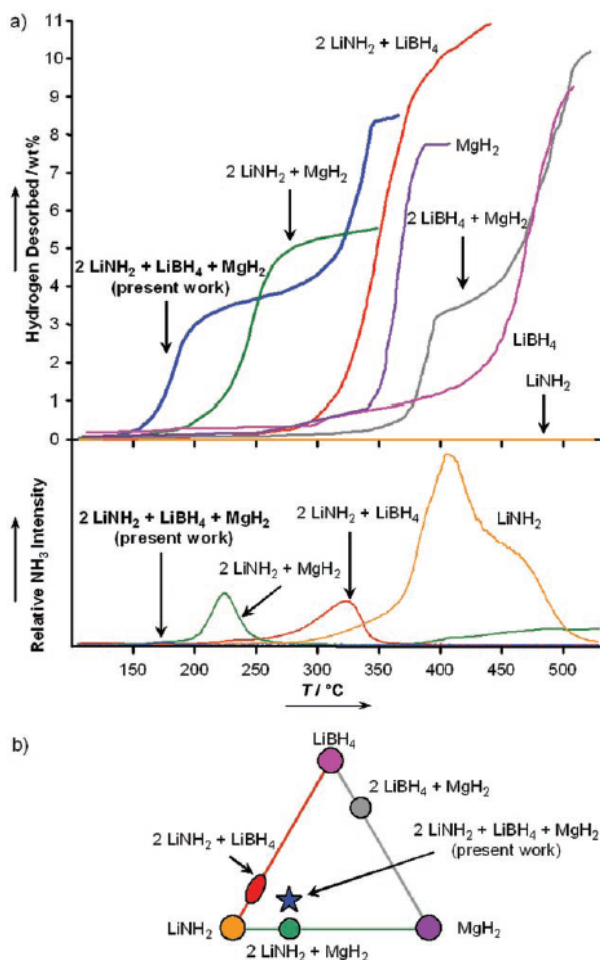

Figura 3. a) Comparação entre os perfis de liberação de H$_2$ do sistema desenvolvido pelo grupo de Yang e outras misturas; **b)** diagrama ternário mostrando a composição do presente sistema. Reproduzido com permissão da referência [77] (Wiley-VCH Verlag GmbH & Co. KGaA).

A reversibilidade do processo também foi investigada. Constatou-se que o material se mantém ativo mesmo após 5 ciclos a 160 °C, liberando cerca de 3% em massa de H$_2$ em 20 min na primeira reação (Figura 4a). Os testes a diferentes temperaturas (140-180 °C)

mostram que o sistema é capaz de liberar mais de 2,5% em tempos de 10 min a 180 °C e 2,5 h a 140 °C (Figura 4b). A quantidade restante de hidrogênio pode ser liberada a temperaturas superiores (260-320 °C) chegando ao total de 8,2% de H_2 (Figura 5).
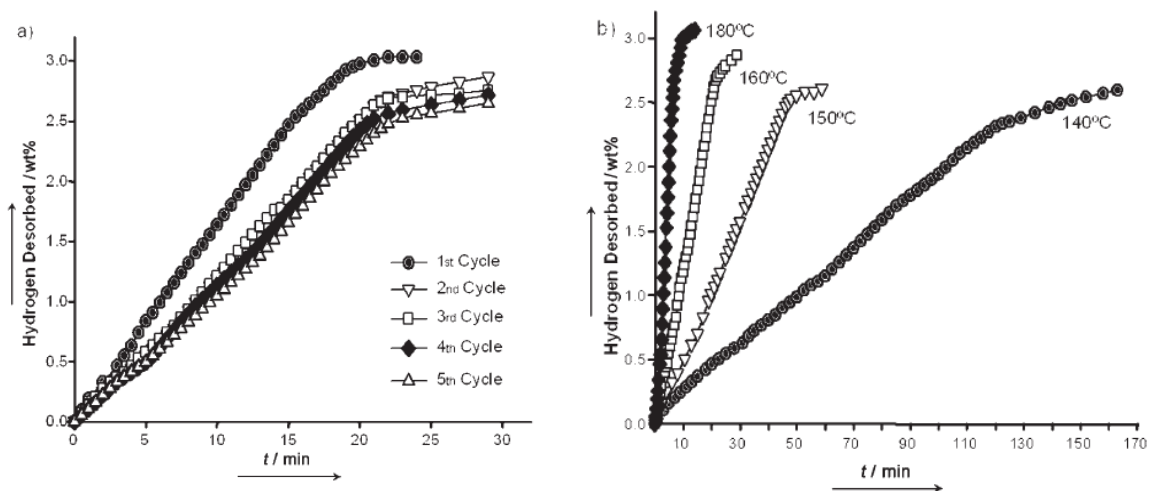

Figura 4. a) Testes de reciclos para o sistema $2LiNH_2/LiBH_4/MgH_2$ a 160 °C e 1 bar (para regeneração o sistema foi mantido a 160 °C e 100 bar de H_2); **b)** testes de desidrogenação a diferentes temperaturas (140-180 °C). Reproduzido com permissão da referência [77] (Wiley-VCH Verlag GmbH & Co. KGaA).
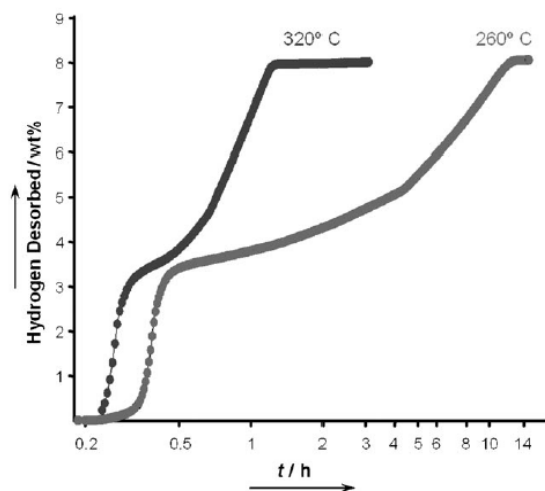
Figura 5. Testes de desidrogenação isotérmicos utilizando o sistema $2LiNH_2/LiBH_4/MgH_2$. Reproduzido com permissão da referência [77] (Wiley-VCH Verlag GmbH & Co. KGaA).

Para uma melhor compreensão da composição e as espécies responsáveis pela liberação de H_2 no sistema, realizou-se análises de TPD/MS (TPD/MS = temperature-programmed-

desorption mass spectrometry), difração de raio-X (DRX) e infravermelho (IV). Por TPD/MS verificou-se a existência de sinais em 180, 190 (sobreposto), 310 e 560 ºC. Através dos sinais de geração de H_2 (TPD/MS) bem como das composições das fases (DRX e IV), os autores sugerem várias etapas de reação envolvendo diferentes espécies as quais são formadas e consumidas durante o processo (Figura 6). Primeiramente, os hidretos $LiNH_2$ e $LiBH_4$ reagem formando a espécie $Li_4BN_3H_{10}$, a qual posteriormente interage com MgH_2 gerando $Mg(NH_2)_2$ e LiH. Portanto a composição inicial pode ser atribuída às espécies $Li_4BN_3H_{10}$, $LiBH_4$, MgH_2, $Mg(NH_2)_2$ e LiH. Após aquecimento, mas antes da liberação de H_2, ocorre a formação de mais espécie $Mg(NH_2)_2$ de acordo com a reação 1 (ver Figura 6).

A partir da temperatura de 100 ºC, ocorre a fusão do hidreto $Li_4BN_3H_{10}$ que reage com MgH_2 produzindo $Li_2Mg(NH)_2$, $LiBH_4$ e liberando H_2 (sinal em 180 ºC, TPD/MS) através da reação 2. Esta etapa 2, segundo os autores, serve para catalisar a reação reversível 3 entre $Mg(NH_2)_2$ e LiH gerando outra quantidade de H_2 (sinal sobreposto em 190-230 ºC, TPD/MS). Neste ponto convém mencionar que os autores denominam de sistema auto-catalítico uma vez que a etapa 2 pré-forma a espécie $Li_2Mg(NH)_2$ para a posterior etapa 3, aumentando as propriedades cinéticas do processo.

Aumentando ainda mais a temperatura, a reação segue pela etapa 4 onde $Li_2Mg(NH)_2$ reage com $LiBH_4$ formando Li_3BN_2, Mg_3N_2, LiH e hidrogênio (sinal em 310 ºC, TPD/MS). Para um aquecimento acima de 350 ºC, é proposto que as espécies Li_3BN_2 e Mg_3N_2 interajam com o remanescente $LiBH_4$ produzindo $LiMgBN_2$ tetragonal e a não determinada *fase X* (etapa 5) que após mais aquecimento se transforma completamente em $LiMgBN_2$ tetragonal (etapa 6). Por fim, a etapa 7 mostra a decomposição de LiH gerando uma liberação adicional de 2,1% de H_2 (sinal em 560 ºC, TPD/MS).
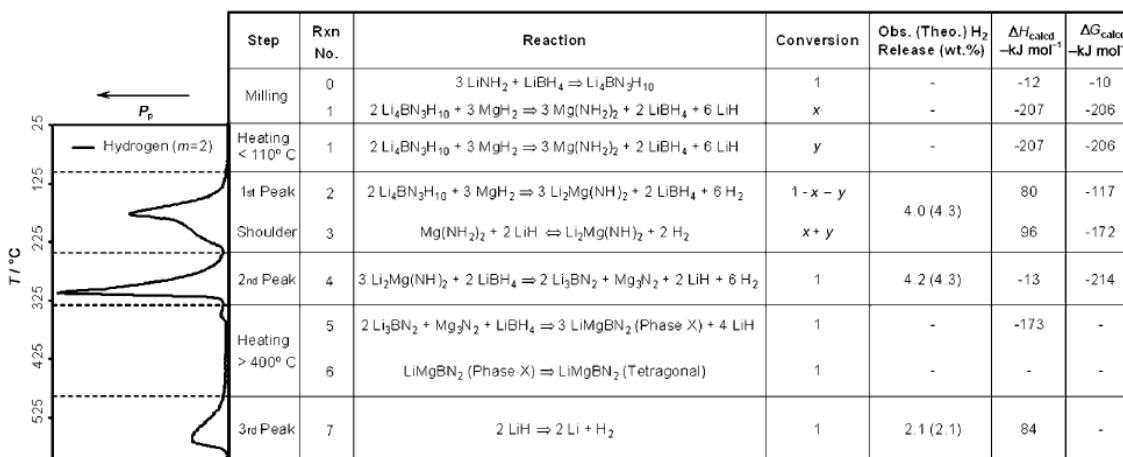
Step	Rxn No.	Reaction	Conversion	Obs. (Theo.) H$_2$ Release (wt.%)	ΔH_{calcd} $-$kJ mol^{-1}	ΔG_{calcd} $-$kJ mol^{-1}
Milling	0	$3\ LiNH_2 + LiBH_4 \Rightarrow Li_4BN_3H_{10}$	1	-	-12	-10
	1	$2\ Li_4BN_3H_{10} + 3\ MgH_2 \Rightarrow 3\ Mg(NH_2)_2 + 2\ LiBH_4 + 6\ LiH$	x	-	-207	-206
Heating < 110° C	1	$2\ Li_4BN_3H_{10} + 3\ MgH_2 \Rightarrow 3\ Mg(NH_2)_2 + 2\ LiBH_4 + 6\ LiH$	y	-	-207	-206
1st Peak	2	$2\ Li_4BN_3H_{10} + 3\ MgH_2 \Rightarrow 3\ Li_2Mg(NH)_2 + 2\ LiBH_4 + 6\ H_2$	$1 - x - y$	4.0 (4.3)	80	-117
Shoulder	3	$Mg(NH_2)_2 + 2\ LiH \Leftrightarrow Li_2Mg(NH)_2 + 2\ H_2$	$x + y$		96	-172
2nd Peak	4	$3\ Li_2Mg(NH)_2 + 2\ LiBH_4 \Rightarrow 2\ Li_3BN_2 + Mg_3N_2 + 2\ LiH + 6\ H_2$	1	4.2 (4.3)	-13	-214
Heating > 400° C	5	$2\ Li_3BN_2 + Mg_3N_2 + LiBH_4 \Rightarrow 3\ LiMgBN_2\ (Phase\ X) + 4\ LiH$	1	-	-173	-
	6	$LiMgBN_2\ (Phase\ X) \Rightarrow LiMgBN_2\ (Tetragonal)$	1	-	-	-
3rd Peak	7	$2\ LiH \Rightarrow 2\ Li + H_2$	1	2.1 (2.1)	84	-

Figura 6. Etapas reacionais propostas para a geração de H$_2$ a partir do sistema 2LiNH$_2$/LiBH$_4$/MgH$_2$. À esquerda mostra-se o gráfico obtido pela análise de TPD/MS. Reproduzido com permissão da referência [77] (Wiley-VCH Verlag GmbH & Co. KGaA).

Desta forma demonstrou-se que a liberação de H$_2$ a partir da mistura 2LiNH$_2$/LiBH$_4$/MgH$_2$ não segue pela simples superposição das etapas dos sistemas constituintes. Sugerem-se etapas via um mecanismo auto-catalítico onde a formação de uma fase iônica líquida e um núcleo gerado para uma reação reversível posterior aumenta a cinética do processo, diminui a temperatura de desidrogenação e torna nula a liberação de amônia quando comparado às respectivas misturas binárias.

Mais detalhes a respeito da síntese e propriedades de hidretos metálicos podem ser encontrados na literatura.[73]

2.3.4. Líquidos Iônicos

2.3.4.1. Líquidos Iônicos Imidazólios

A primeira aplicação utilizando LIs como materiais para o armazenamento e liberação de H_2 foi apresentada por Dupont e colaboradores.[78] Neste trabalho desenvolveu-se primeiramente a síntese de sais derivados de *N*-bis(trifluorometanosulfonil)imida de 1-alquil(aril)-3-metilimidazólio. Além de apresentarem propriedades atrativas já bem conhecidas de LIs como: baixa pressão de vapor, estabilidade térmica e não-inflamáveis, estes sais podem adicionar reversivelmente entre 6-12 átomos de hidrogênio na presença de Pd/C (5%). O procedimento de síntese destes LIs foi baseado em um método previamente descrito na literatura.[79] Este processo consiste em uma etapa de alquilação entre 1-metilimidazol e alquil-metanosulfonatos produzindo **1**. Em seguida, fez-se troca aniônica utilizando $LiNTf_2$ para gerar compostos do tipo **2** e, finalmente, um processo de hidrogenação catalítica fornece os correspondentes sais de imidazólio **3** (Esquema 10).
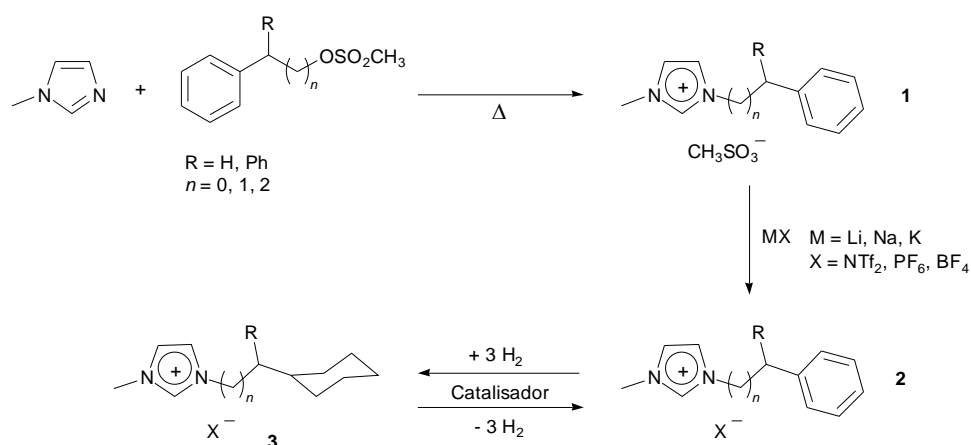
Esquema 10. Etapas reacionais da preparação dos sais de imidazólio **1**, **2** e **3**.[78]

Convém mencionar que compostos similares aos sais de imidazólio **2** já foram descritos previamente.[80-82] Os LIs contendo um grupamento cicloexila ligado ao cátion imidazólio (**3**) podem ser utilizados como materiais alternativos para o armazenamento e liberação de H_2. Além disso, devido às suas vantajosas propriedades físico-químicas, estes materiais apresentam potencial aplicação em veículos automotivos. Entretanto, a estabilidade dos LIs **2** e **3** frente às reações de hidrogenação/desidrogenação depende da natureza do cátion e

ânion do LI. Por exemplo, os LIs **2** contendo um grupo benzila (n = 0) ligado ao cátion ou ânions PF_6 e BF_4, quando submetidos à reação de hidrogenação na presença de catalisadores clássicos (Rh/C (5%), Pd/C (5%)), demonstram certa instabilidade e decompõem-se em uma mistura de produtos. Por outro lado, LIs contendo um maior espaçamento entre o grupo arila e o cátion imidazólio (n = 1, 2) e ânion NTf_2 apresentaram resultados mais satisfatórios. Apesar do requerimento de um longo tempo reacional (100 h) para total conversão nos correspondentes LIs **3**, o processo de hidrogenação catalítico foi realizado de forma efetiva na faixa de temperatura entre 70-90 ºC e pressão de gás hidrogênio 35-50 bar. Dentre os diversos catalisadores suportados testados, Pd/C (5%) mostrou os melhores resultados nesta etapa (Figura 7).
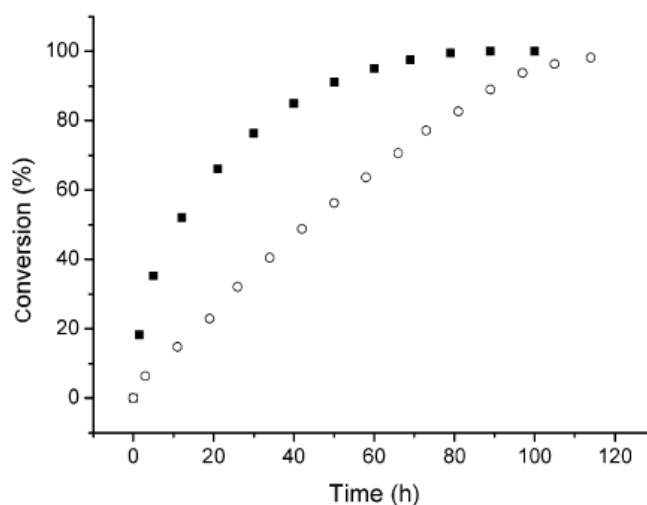
Figura 7. Hidrogenação dos LIs **2**: (○) $Ph(CH_2)_3MI.NTf_2$ a 70 ºC e (■)$Ph_2(CH)(CH_2)MI.NTf_2$ a 90 ºC na presença de 50 bar de H_2 e Pd/C (5%). LI/catalisador = 100/1 em massa. Reproduzido com permissão da referência [78] (American Chemical Society).

Posteriormente, os sistemas contendo o LI **3** (pré-formado) e o catalisador foram testados em reações de desidrogenação. Foi observado que a condução desta reação sob atmosfera inerte é de fundamental importância para evitar a decomposição do LI. A geração de hidrogênio molecular para os compostos **3** inicia-se em torno de 230 ºC, atingindo o máximo de conversão em 300 ºC (Figura 8). Acima desta temperatura, observou-se uma significativa decomposição da mistura reacional.
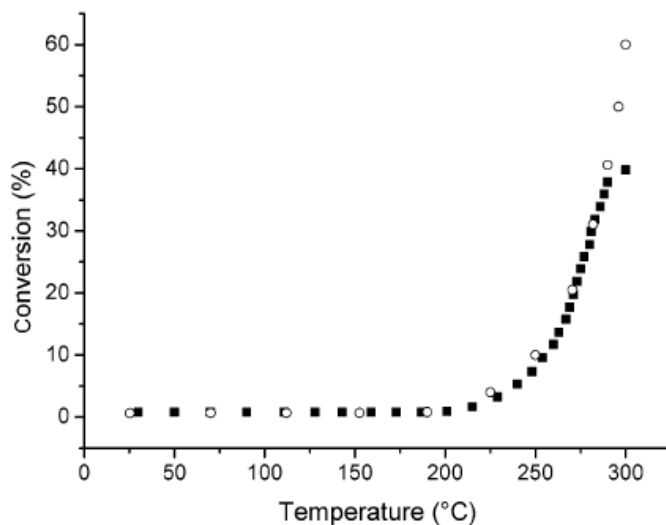
Figura 8. Desidrogenação dos LIs **3**: (○) Cy(CH₂)₃MI.NTf₂ e (■) Cy₂(CH)(CH₂)MI.NTf₂ na presença de Pd/C (5%). LI/catalisador = 100/1 em massa. Reproduzido com permissão da referência [78] (American Chemical Society).

Os LIs **2** resultantes do processo de desidrogenação podem ser facilmente hidrogenados novamente aos correspondentes **3** fechando um ciclo de hidrogenação/desidrogenação. Demonstrou-se assim que as combinações dos sais de imidazólio contendo um grupo cicloexila (**3**) com o catalisador clássico Pd/C (5%) podem adicionar reversivelmente 6-12 átomos de hidrogênio por par iônico (1,2% em massa de hidrogênio para $Cy(CH_2)_3MI.NTf_2$ e 2,2% em massa para $Cy_2(CH)(CH_2)MI.NTf_2$), constituindo-se em materiais alternativos para dispositivos de estocagem química de hidrogênio (Esquema 11). Apenas para motivos de comparação, o sal $Cy_2(CH)(CH_2)MI.NTf_2$ contém incorporados, à temperatura e à pressão ambiente, cerca de 30 $g.L^{-1}$ de hidrogênio, o qual é o dobro do que se obtém na prática industrial de compressão de hidrogênio (15 $g.L^{-1}$ a 350 bar).
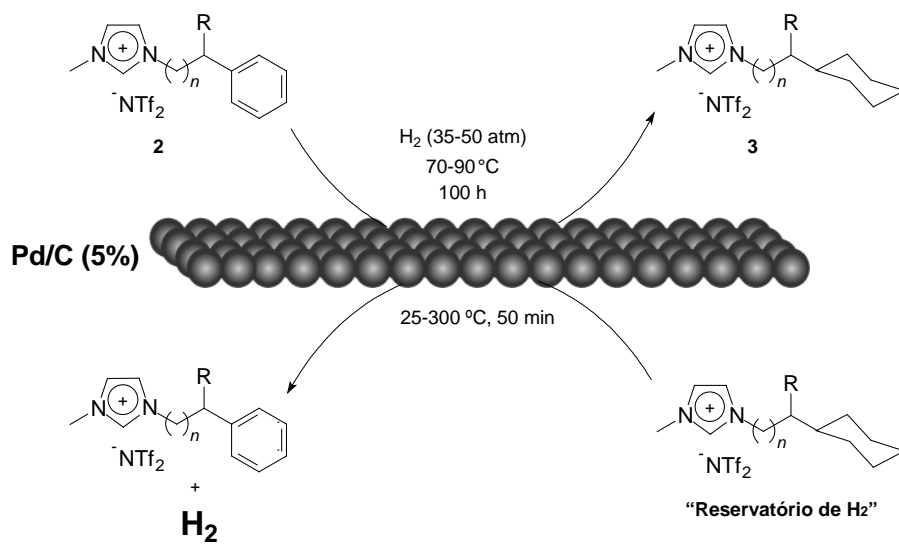
Esquema 11. Modelo mostrando as etapas de hidrogenação dos LIs **2** a **3** e desidrogenação de **3** a **2** na presença de Pd/C (5%). Sugere-se que os LIs **3** possam atuar como "reservatório de H$_2$".[78]

2.3.4.2. Líquidos Iônicos Baseados no Cátion Guanidínio

Um recente trabalho desenvolvido por Rieger e colaboradores evidencia uma potencial aplicabilidade de LIs guanidínios como agentes de estocagem/liberação de hidrogênio molecular.[83] Como exemplo, borohidreto de metilguanidínio (**1**) foi utilizado como fonte de H_2 a partir de sua decomposição térmica ou catalítica. Uma vez que este LI apresenta cerca de 9% em massa de hidrogênio capaz de ser liberado (4 equivalentes molares de H_2/molécula de LI), este se torna um sistema bastante promissor tendo em vista sua alta capacidade de armazenamento de hidrogênio. Os testes catalíticos de desidrogenação foram conduzidos utilizando diglime como solvente na presença do complexo de Wilkinson $[RhCl(PPh_3)_3]$ ou $[FeCl_2]$. Um experimento testando apenas a decomposição térmica do LI **1** também foi realizada. A Figura 9 mostra o perfil de liberação de H_2 *vs* tempo para cada reação.
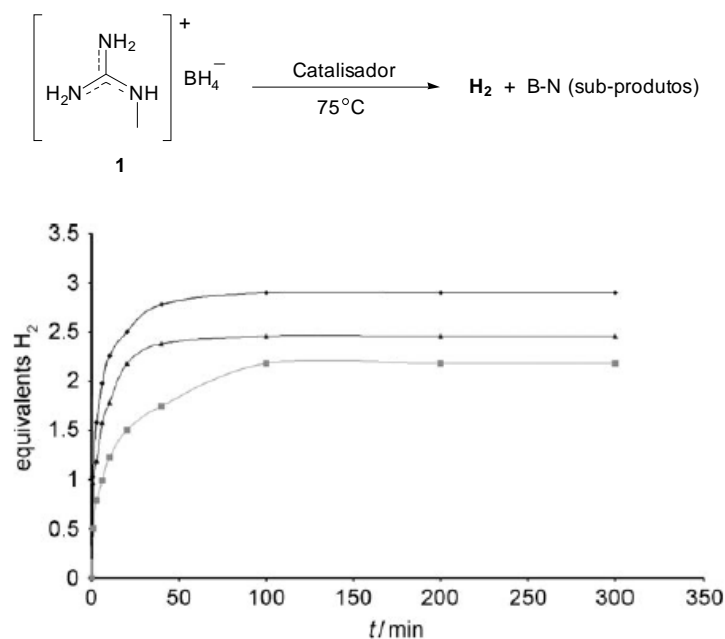
Figura 9. Decomposição catalítica do LI **1** a 75 ºC na presença de (♦) $[RhCl(PPh_3)_3]$ (1 mol%), (▲) $[FeCl_2]$ (1 mol%) ou (■) decomposição térmica. Reproduzido com permissão da referência [83] (Wiley-VCH Verlag GmbH & Co. KGaA).

Nota-se que o melhor desempenho foi obtido utilizando o complexo de Wilkinson, onde 2,9 equivalentes molares de H_2 foram liberados em apenas 50 min de reação. Resultados

muito similares foram encontrados utilizando [FeCl$_2$] ou através de decomposição térmica. Na presença de [FeCl$_2$], observou-se a liberação de 2,4 equivalentes molares de H$_2$, enquanto que via decomposição térmica obteve-se 2,3 equivalentes molares de H$_2$. Para fins comparativos, demonstrou-se também a aplicação do sal boro-hidreto de guanidínio (**2**) como fonte de H$_2$, o qual apresenta 10,7% em massa de hidrogênio com potencial a ser liberado. Neste caso, o complexo de Wilkinson mostrou uma atividade catalítica bastante superior quando comparado ao [FeCl$_2$]. De fato, quantidades de 3,9 equivalentes molares de H$_2$ (10,3% massa) foram produzidas quando da utilização de [RhCl(PPh$_3$)$_3$] e apenas 2,0 equivalentes molares (5,3% massa) com [FeCl$_2$]. Portanto, quantidades significativas de gás hidrogênio podem ser geradas a partir da decomposição catalítica do sal **2** dissolvido em diglime a 75 ºC.

Entretanto, tanto para a decomposição utilizando o LI **1** como para o sal **2**, verifica-se a formação de um precipitado ao longo da reação. Este precipitado é constituído basicamente por compostos contendo ligações B-N. Para evidenciar e sugerir as estruturas destes sub-produtos, analisou-se as amostras pela técnica de RMN ^{11}B de estado sólido. Além disso, cálculos teóricos de *Ab Initio* foram desenvolvidos para estimar os deslocamentos químicos das espécies nos espectros de RMN ^{11}B. Devido à simplicidade nos cálculos, melhor intensidade dos sinais e o mínimo efeito propiciado pelo grupo metila (LI **1**) nos deslocamentos químicos observados no RMN ^{11}B, a reação de decomposição do sal **2** foi escolhida como sistema a ser analisado, tornando-se possíveis conclusões similares à reação com o LI **1**. As análises de RMN ^{11}B do precipitado proveniente da reação de decomposição catalítica ou térmica do sal **2** indicaram dois sinais mais intensos em δ = -4 ppm (sobreposição de sinal em -8 ppm) e -39 ppm. É possível a percepção de sinais pouco intensos em δ = 9, -16 e -28 ppm (Figura 10). Deslocamentos químicos similares foram observados para a amostra proveniente da reação de decomposição do LI **1**.

Através do auxílio de cálculos teóricos, o sinal em δ = -39 ppm foi atribuído ao BH$_4^-$ residual (sal que não reagiu) e em δ = -4 ppm a um composto tetravalente de B-N (Figura 11c). De fato, os deslocamentos químicos calculados para o espectro de RMN ^{11}B mostram que os valores variam dependendo do número de átomos de N coordenados ao átomo de boro (δ = -8,5 ppm para 2N; -6,0 ppm para 3N e -3,5 ppm para 4N).

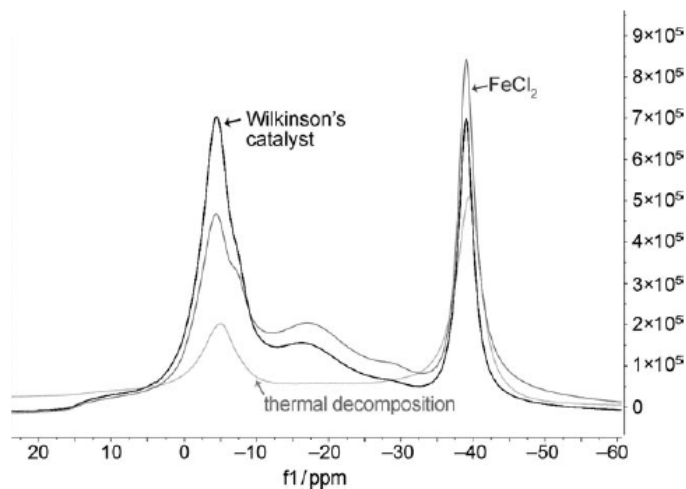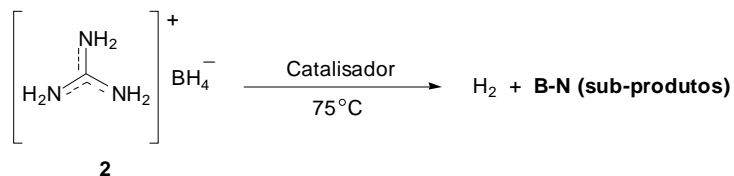**Figura 10.** Análises de RMN [11]B de estado sólido do precipitado formado durante a desidrogenação catalítica do sal **2** com [RhCl(PPh$_3$)$_3$] (0,1 mol%), [FeCl$_2$] (2 mol%) a 75 ºC ou apenas por decomposição térmica (75 ºC). Reproduzido com permissão da referência [83] (Wiley-VCH Verlag GmbH & Co. KGaA).
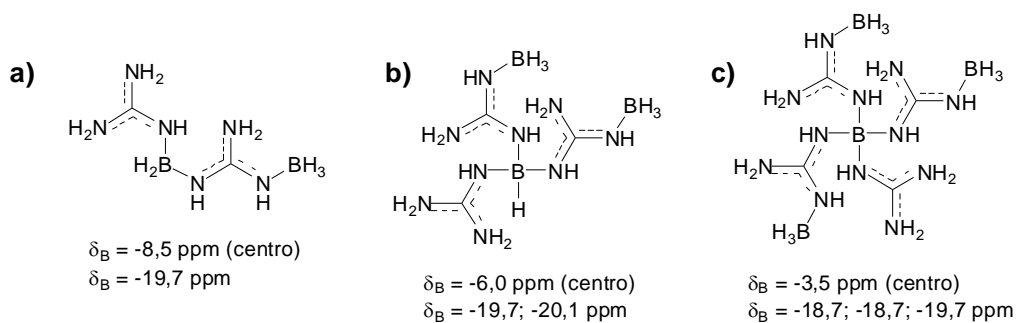

Figura 11. Espécies propostas para a composição do sólido formado após a decomposição do sal **2**. Os deslocamentos químicos calculados para o espectro de RMN [11]B são mostrados abaixo de cada estrutura.[83]

Pela grande capacidade de armazenamento em massa de hidrogênio e facilidade de liberação (condições amenas de reação), pode-se considerar que o LI **1** e o sal **2** possam ser materiais alternativos para futuras aplicações no que se refere à estocagem/liberação de H$_2$.

2.3.5. Hidrocarbonetos

A geração de hidrogênio através da decomposição de hidrocarbonetos utilizando catalisadores suportados foi demonstrada por Huffman e colaboradores.[84, 85] Por exemplo, uma eficiente decomposição de cicloexano e metil-cicloexano foi observada na presença de 0,1-1% Pt suportado em nanotubos de carbono (CNT).[84] Para a reação com cicloexano, detectou-se a formação de hidrogênio e benzeno enquanto que no caso da decomposição de metil-cicloexano, hidrogênio e tolueno foram os produtos gerados. A Figura 12 mostra o desempenho dos diferentes catalisadores testados nas reações de decomposição de cicloexano e metil-cicloexano.
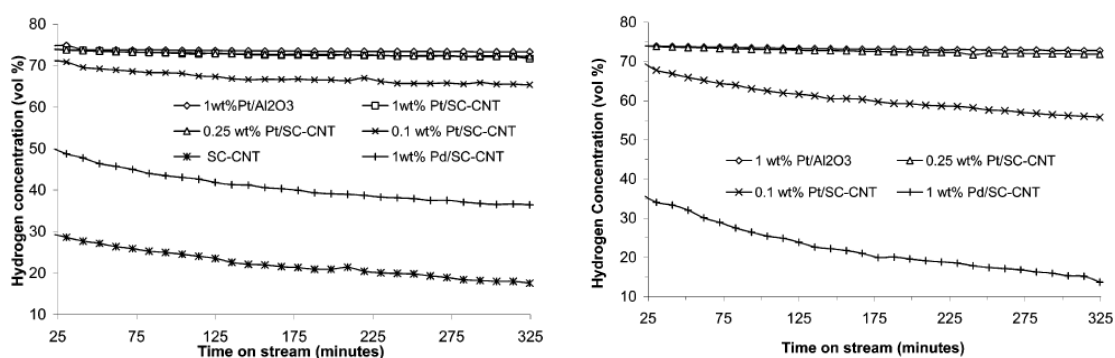
Figura 12. Concentração de H_2 durante a decomposição de cicloexano (esquerda) e metil-cicloexano (direita) a 315 ºC utilizando diferentes catalisadores suportados. Reproduzido com permissão da referência [84] (American Chemical Society).

É possível notar que, para os dois substratos, as atividades do catalisador 0,25% Pt suportado em nanotubos de carbono são similares às observadas para o catalisador comercial 1% Pt/Al_2O_3. Entretanto, observou-se que o catalisador contendo 0,1% Pt/CNT demonstrou uma maior eficiência na produção de H_2 por átomo metálico (Turnover number, TON).

Catalisadores binários de Fe-M (M = Pd, Mo, Ni) suportados em alumina apresentaram alta eficiência na desidrogenação catalítica de etano, propano e cicloexano.[85, 86] Apenas hidrogênio e metano foram detectados durante a decomposição de etano e propano na presença dos diferentes catalisadores binários.[85] Não se verificou a presença de eteno, propeno, água ou óxidos de carbono no sistema. Segundo os autores, após uma pré-redução

a 700 ºC, os três tipos de catalisadores mostraram uma diminuição na temperatura de decomposição comparada ao suporte (Al$_2$O$_3$) e ao catalisador monometálico de Fe/Al$_2$O$_3$. Além disso, observou-se via análises de microscopia eletrônica de transmissão (MET) a deposição de carbono em duas formas diferentes, as quais dependem da temperatura. Abaixo de 500 ºC o carbono é depositado na forma de nanofibras e acima de 600 ºC como nanotubos multi-camadas. A seguir é mostrada as atividades catalíticas dos diferentes catalisadores na decomposição de etano e propano (Figura 13).
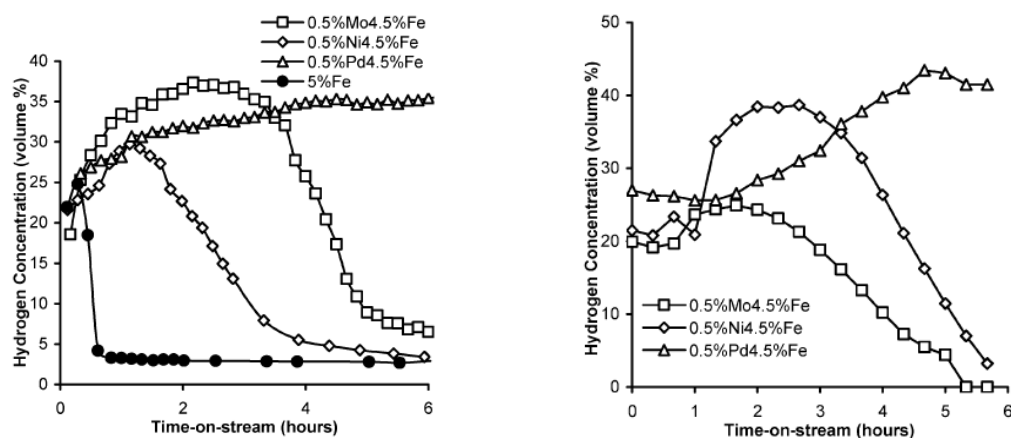
Figura 13. Decomposição catalítica de etano (esquerda) a 500 ºC e propano (direita) a 475 ºC na presença de diferentes catalisadores bimetálicos (pré-redução a 700 ºC). Reproduzido com permissão da referência [85] (American Chemical Society).

A decomposição de cicloexano também foi testada na presença de catalisadores bimetálicos.[86] Neste caso observa-se apenas a formação de H$_2$, metano e benzeno (Figura 14, esquerda). Além disso, análises de MET confirmam a presença de nanofibras de carbono proveniente da decomposição do metano (CH$_4$ → 2H$_2$ + C). A uma temperatura maior (625 ºC) sugere-se uma desativação do catalisador por volta de 1,5 h com a formação de espécies C2 e C3 proveniente da polimerização do metano (Figura 14, direita). A presença de nanotubos e nanofibras de carbono também foi verificada (MET) nesta temperatura.
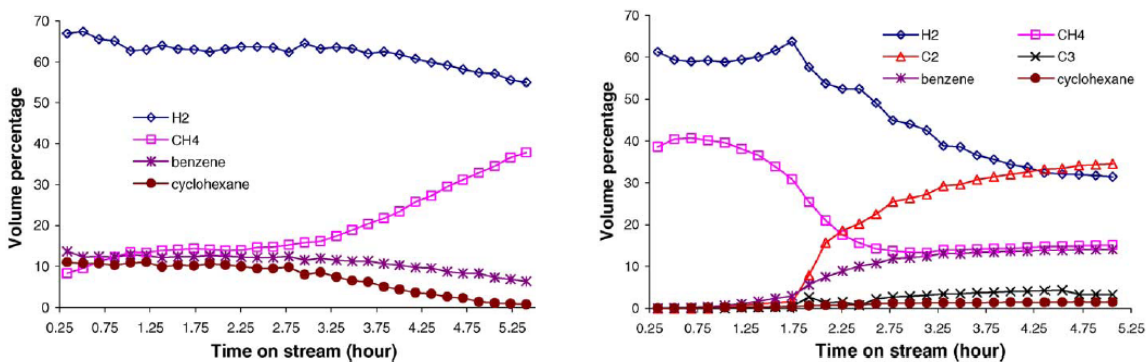
Figura 14. Distribuição dos produtos durante a decomposição de cicloexano a 475 ºC (esquerda) e 625 ºC (direita) na presença do catalisador 0,5%Pd-4,5%Fe/Al$_2$O$_3$. Reproduzido com permissão da referência [86] (Elsevier).

Outro exemplo do uso de hidrocarbonetos como fonte de H$_2$ é a desidrogenação catalítica de isopentano promovida por catalisadores de irídio.[87] Neste estudo, Böhmer e Alt utilizaram diferentes catalisadores de Ir suportados em sílica. Ao longo dos experimentos percebeu-se uma grande influência da presença de fosfinas na atividade catalítica. Ao aumentar o número de ligantes fosfinas, aumentava a conversão de isopentano (Figura 15, esquerda). De fato, a simples adição de 4 equivalentes molares de trifenilfosfina acarretou em uma considerável melhora na atividade do complexo [H$_2$IrCl$_6$] suportado em sílica (Figura 15, direita).
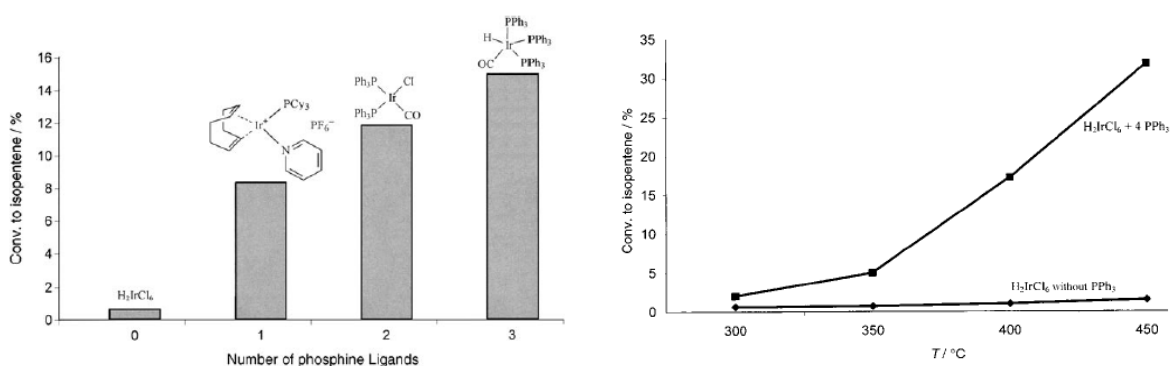

Figura 15. Efeito do número de ligantes fosfina na desidrogenação de isopentano utilizando diferentes catalisadores de Ir suportados em sílica a 400 ºC (esquerda). Aumento significativo da atividade do sistema [H$_2$IrCl$_6$]/SiO$_2$ na presença de 4 equivalentes molares de PPh$_3$ (direita). Reproduzido com permissão da referência [87] (Wiley-VCH Verlag GmbH & Co. KGaA).

Para fins comparativos, utilizou-se o complexo [Ir(COD)$_2$]BF$_4$ suportado em sílica na ausência de fosfina, com 4 e 8 equivalentes molares de PPh$_3$. Além disso, testou-se a atividade do mesmo complexo de Ir suportado em sílica funcionalizada contendo grupamento fosfina. Os resultados são mostrados na Figura 16.
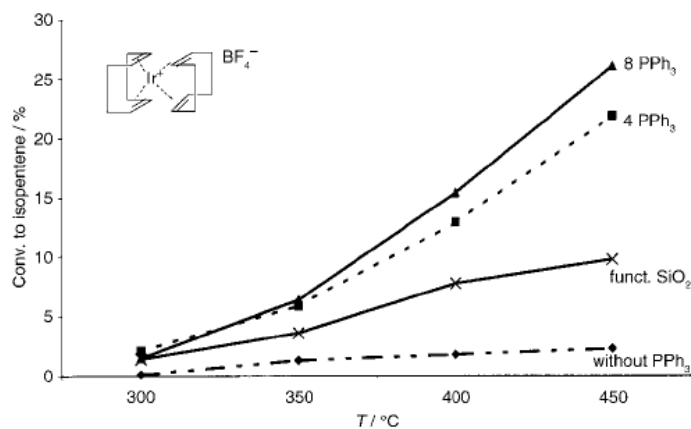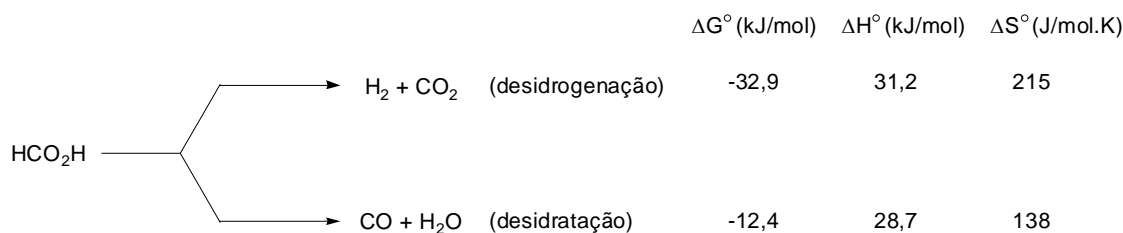

Figura 16. Desidrogenação de isopentano utilizando o sistema [Ir(COD)$_2$]BF$_4$/SiO$_2$ na presença ou não de fosfina. Reproduzido com permissão da referência [87] (Wiley-VCH Verlag GmbH & Co. KGaA).

Através da detecção de saída de grupos fenila do catalisador para os produtos da reação, os autores sugerem que a perda de grupos fenila é importante para a formação de uma espécie mais ativa. Ainda, segundo eles, é provável que espécies do tipo Ir-fosfito, Ir-P "*cage*" ou nanoclusters sejam responsáveis pela atividade catalítica observada.

Portanto, hidrocarbonetos surgem como uma possível alternativa para a estocagem e liberação de H$_2$. Por exemplo, cicloexano apresenta uma capacidade de poder gerar, reversivelmente, até seis átomos de hidrogênio (7,1% em massa). Entretanto, para hidrocarbonetos líquidos algumas desvantagens para a utilização em células a combustível seriam: volatilidade, inflamabilidade e baixa densidade (reflete em pouca quantidade de H$_2$/volume).

2.3.6. Ácido Fórmico

Nos últimos anos, a decomposição de ácido fórmico (AF) é uma das reações mais estudadas para a produção *in situ* de hidrogênio molecular. Entretanto, de forma geral sua decomposição pode seguir dois caminhos: i) um envolvendo a formação de H_2 e CO_2 e ii) o outro via formação de CO e H_2O (Esquema 12).[88, 89] Portanto, para fins de produção de hidrogênio é essencial que uma efetiva reação de desidrogenação (descarboxilação) ocorra sem a concomitante desidratação (descarbonilação) do substrato, uma vez que esta reação paralela reduz o rendimento em gás hidrogênio e gera CO, indesejável para futuras aplicações em células a combustível.[90]

			ΔG° (kJ/mol)	ΔH° (kJ/mol)	ΔS° (J/mol.K)
	$\rightarrow$ $H_2 + CO_2$	(desidrogenação)	-32,9	31,2	215
HCO$_2$H					
	$\rightarrow$ CO + H_2O	(desidratação)	-12,4	28,7	138

Esquema 12. Possíveis caminhos para a decomposição do ácido fórmico e seus valores termodinâmicos.[91]

A utilização de uma mistura azeotrópica entre ácido fórmico/trietilamina (AF:Et$_3$N 5:2) como fonte de gás hidrogênio em reações por transferência de hidrogênio foi mostrada há aproximadamente duas décadas por Leitner[92] e Noyori[93]. Leitner e colaboradores demonstraram o uso do hidrogênio produzido para a hidrogenação enantiosseletiva de ácidos carboxílicos α,β-insaturados catalisada por complexos de Rh[92] e mais recentemente alguns detalhes mecanísticos a respeito deste processo também foram investigados[94]. De forma similar, utilizando a mistura AF:Et$_3$N 5:2 como fonte de H_2, o grupo de Noyori demonstrou a hidrogenação assimétrica de cetonas a alcoóis catalisada por complexos de Ru.[93]

Visando futuras aplicações em células a combustível, o grupo de Beller tem desenvolvido sistemas catalíticos que promovam uma eficiente cinética de formação de H_2 a partir da mistura AF:Et$_3$N 5:2 (Figura 17).[91, 95-98] Um dos primeiros trabalhos desenvolvidos mostrou a atividade de diferentes catalisadores metálicos durante a decomposição de AF a partir da mistura azeotrópica a 40 °C.[95] Dentre os testados, o complexo [RuCl$_2$(*p*-cimeno)]$_2$ apresentou melhor desempenho (TON = 42 em 6 h). Em um

experimento de longa duração o sistema se manteve ativo por mais de 42 h atingindo cerca de 93% de conversão (Figura 18).
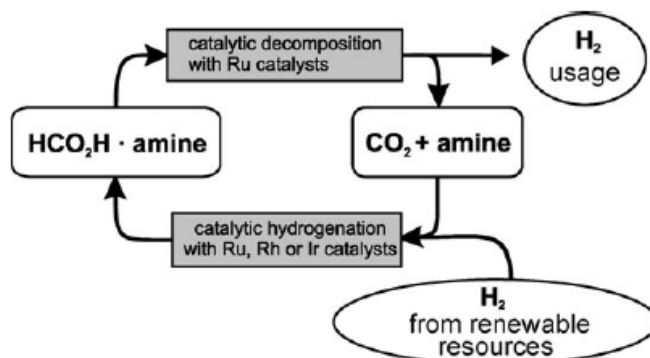

Figura 17. Ciclo da formação de H_2 a partir do sistema AF/amina. Reproduzido com permissão da referência [95] (Wiley-VCH Verlag GmbH & Co. KGaA).
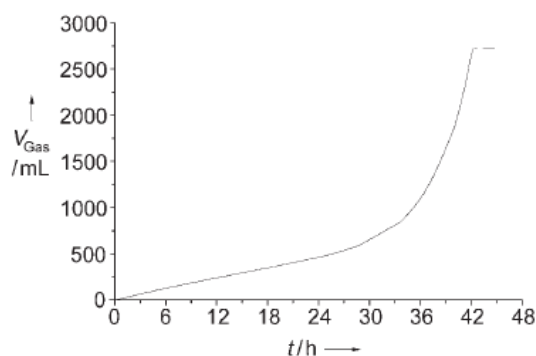

Figura 18. Decomposição de AF em H_2 e CO_2 (1:1) a partir da mistura AF:Et_3N 5:2 catalisada por [$RuCl_2$(p-cimeno)]$_2$ a 40 °C. Reproduzido com permissão da referência [95] (Wiley-VCH Verlag GmbH & Co. KGaA).

Outras bases orgânicas também foram testadas na reação nas mesmas condições reacionais. Os melhores resultados entre todas as bases investigadas foram obtidos utilizando *N,N*-dimetilexilamina e *N,N*-dimetilaminoetanol (TON = 30 em 3 h). Uma atividade significativamente maior foi observada para a reação utilizando a mistura padrão AF/Et_3N 5:2 catalisada pelo complexo [$RuCl_2$(PPh_3)$_3$] a 40 °C (90% de conversão em 3 h, TON = 905). Após um pré-tratamento do sistema com dimetilformamida (DMF) a 80 °C é possível atingir um TOF de até 2688 h^{-1} após 20 min de reação a 40 °C, sendo um dos sistemas mais eficientes já estudados para a decomposição de AF. Em todos os casos apenas H_2 e CO_2 foram detectados. A fim de testar a potencialidade do sistema, fez-se um

experimento de decomposição acoplado a uma célula a combustível H_2/O_2. De fato, o gás gerado pelo sistema AF/Et$_3$N 5:2 + [RuCl$_2$(p-cimeno)]$_2$ a 40 °C converteu em um máximo de energia elétrica de 47 mW a um potencial de 374 mV por mais de 29 h, o qual apresentou uma densidade energética similar à uma mistura comercial de H_2/CO_2 (1:1).

De forma complementar, novos catalisadores de Ru foram testados na presença de fosfinas.[96] Após realizado um pré-tratamento entre o complexo de Ru e ligante em DMF, o sistema contendo [RuBr$_3$.xH$_2$O]/3PPh$_3$ mostrou uma das melhores atividades já medidas na decomposição de AF (TOF = 3630 h^{-1} em 20 min). Entretanto, certa desativação do catalisador é verificada após algum tempo de reação. Por outro lado, o sistema baseado no complexo [RuCl$_2$(benzeno)]$_2$ e PPh$_3$ apresenta boa atividade e robustez. Utilizando este complexo, variou-se a relação metal/fosfina bem como o uso de fosfinas mono ou bidentadas. Fosfinas muito coordenantes mostraram forte inibição na atividade. Para as fosfinas bidentadas, 1,2-bis(difenilfosfino)etano (dppe) mostrou ser o melhor ligante enquanto que para as fosfinas monodentadas, PPh$_3$ demonstrou melhores resultados.

A fim de testar o sistema contendo o complexo [RuCl$_2$(benzeno)]$_2$ para geração de energia, uma mistura AF/HexNMe$_2$ (5:4) foi colocada na presença de [RuCl$_2$(benzeno)]$_2$/6PPh$_3$ a 26,5 °C. O gás gerado foi introduzido diretamente a uma unidade de célula a combustível H_2/O_2 PEM (Figura 19; PEM = Polymer Electrolyte Membrane). Após passar por um filtro purificador (Charcoal; CarboTex) para a retirada de traços de amina, o gás gerou inicialmente uma energia elétrica de 48 mW, o qual decresceu para 26 mW (medido a 370 mV) mantendo-se constante por 42 h. O valor ainda atingiu 14 mW após a total conversão de AF (Figura 19).
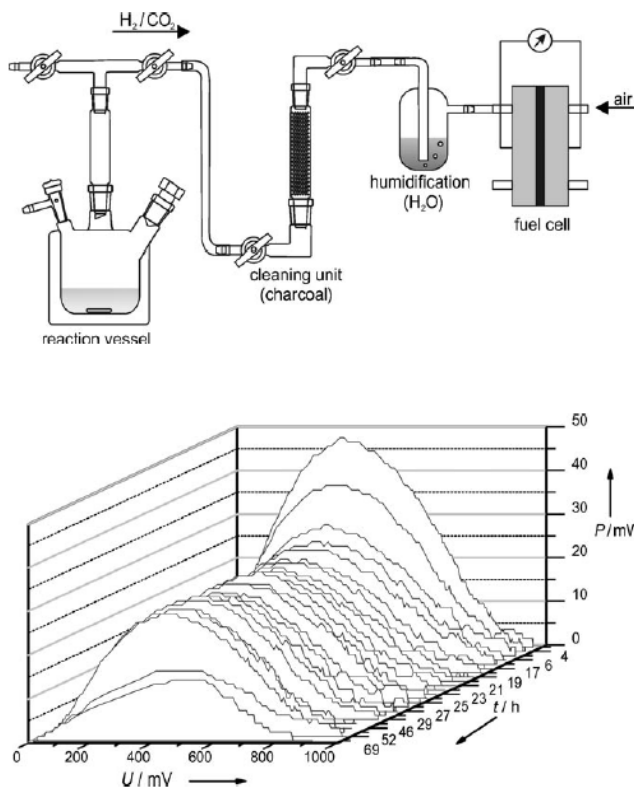
Figura 19. Modelo da unidade utilizada para a geração de H_2 e sua utilização no protótipo de célula a combustível (acima). Gráfico mostrando a energia elétrica produzida pelo H_2 gerado através do sistema AF/HexNMe$_2$ (5:4) com [RuCl$_2$(benzeno)]$_2$ (29,75 μmol)/6 equivalentes molares de PPh$_3$ a 26,5 °C (abaixo). Reproduzido com permissão da referência [96] (Wiley-VCH Verlag GmbH & Co. KGaA).

O efeito ativador da irradiação de luz (lâmpada Xe; PerkinElmer Cermax 300 W) foi investigado durante a geração de H_2 pela decomposição de AF catalisada por complexos de Ru.[97] Neste estudo foi verificado que a presença de luz acelera significativamente a produção de hidrogênio. Para os testes, a mistura AF/Et$_3$N (5:2) foi aquecida a 40 °C na presença de diferentes complexos de Ru e ligantes fosfinas. As reações também foram testadas em ambiente escuro. Experimentos de controle mostraram que a adição do ligante fosfina é de fundamental importância para a ocorrência efetiva da reação. Os resultados obtidos para os diferentes sistemas na presença de irradiação foram comparados com as reações em ambiente escuro (Figura 20).
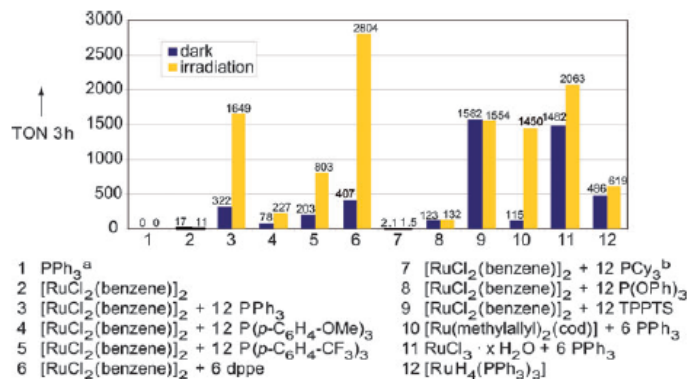
Figura 20. Efeito da irradiação de luz na reação de decomposição de AF a partir da mistura AF/Et$_3$N (5:2) catalisada por complexos de Ru. [a] Não verificou-se H$_2$; [b] neste caso não utilizou-se ambiente escuro e sim condição de luminosidade natural. Reproduzido com permissão da referência [97] (The Royal Society of Chemistry).

É facilmente notável o efeito da irradiação de luz aos sistemas catalíticos. A melhor atividade foi observada para o sistema contendo [RuCl$_2$(benzeno)]$_2$/6dppe (TON = 2804; conversão = 90% em 2 h). Estudos mostraram ainda que mesmo a baixas temperaturas ocorre uma efetiva evolução de H$_2$ na presença do sistema [RuCl$_2$(benzeno)]$_2$/12PPh$_3$ (0 °C: TON$_{escuro}$ = 26, TON$_{irradiação}$ = 195; 25 °C: TON$_{escuro}$ = 217, TON$_{irradiação}$ = 1321). Posteriormente, análises de RMN ^{1}H auxiliaram em uma proposta para o mecanismo deste processo (Esquema 13). Inicialmente, o precursor é ativado pela incidência de irradiação de luz visível formando uma espécie metal-hidreto contendo ligantes fosfina. Ocorre então a adição de AF e conseqüente formação da molécula de H$_2$ coordenada ao metal. As etapas finais seriam a saída de H$_2$ e CO$_2$, as quais são influenciadas pela presença de luz, regenerando a espécie metal-hidreto. Neste trabalho demonstrou-se que é possível controlar a formação de H$_2$ pela presença ou ausência de luz. Ainda, observa-se que os sistemas irradiados pela luz podem apresentar até duas vezes mais atividade que aqueles não-ativados pela irradiação.
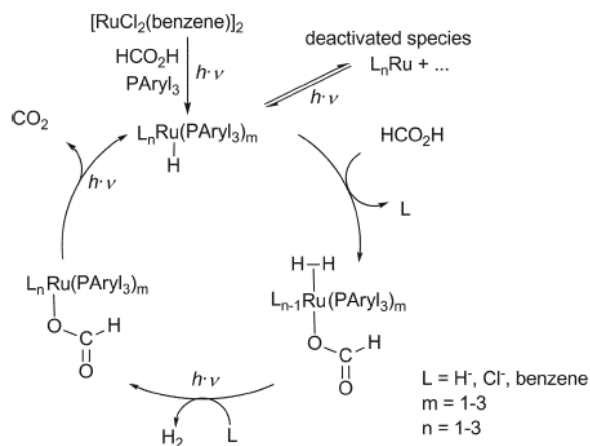
Esquema 13. Ciclo catalítico proposto para a decomposição de AF catalisada por complexos de Ru/fosfina na presença de irradiação de luz. Reproduzido com permissão da referência [97] (The Royal Society of Chemistry).

Um dos principais desafios da catálise organometálica é a substituição de catalisadores contendo metais nobres (Ru, Rh, Ir, Pd) para sistemas não-nobres (Fe, Co, Cu, Ni). Neste contexto, o grupo de Beller desenvolveu recentemente um sistema catalítico baseado em complexos de ferro-carbonila/fosfina para a decomposição de AF na presença de luz visível.[91] Apesar de baixas conversões de AF observadas (10%), este foi, sem dúvida, um grande avanço científico e econômico no que diz respeito a geração de H_2 a partir de AF. Dentre os diferentes precursores metálicos utilizados (Mo, Mn, Cr, Co e Fe) o complexo [$Fe_3(CO)_{12}$] na presença de PPh_3 e [2,2',6',2'']terpiridina (tpy) (Fe/PPh_3/tpy 1:1:1) em DMF mostrou a melhor atividade catalítica. Sem a presença de luz (ambiente escuro) houve considerável geração de H_2 em 120 °C (TON = 7,3 em 3 h). Entretanto, a seletividade é bastante baixa formando uma quantidade significativa de CO (H_2 ou CO_2/CO 1:5) indicando que a reação de desidratação (formação de CO + H_2O) é favorecida em temperaturas altas. O mesmo sistema, quando colocado sob irradiação de luz, atinge valores superiores de TON mesmo a 25 °C (8,1 em 3 h) chegando ao máximo em 60 °C e 80 °C (TON = 44 e 48, respectivamente, em 3 h). E o mais importante, sob luz a seletividade na reação de desidrogenação é predominante, onde apenas traços de CO são observados. A 40 °C verifica-se um valor de TON igual a 23 (3 h) e 44 após 24 h (Figura 21). O efeito ativador da presença de luz foi comprovado uma vez que parada a irradiação, a geração de gás é interrompida imediatamente, indicando que a irradiação não somente inicia a

formação da espécie ativa, mas também é fundamental durante o ciclo catalítico. Isto implica, segundo os autores, em uma produção de H_2 foto-assistida. Para fins de otimização do sistema, diferentes fosfinas e aminas foram testadas juntamente com o precursor $[Fe_3(CO)_{12}]$ (Figura 22). Entre as fosfinas utilizadas, PPh_3 apresentou os melhores resultados, enquanto que para as aminas, excelentes resultados foram observados para o ligante tpy e os referentes à numeração 12-16 (ver Figura 22). Apesar dos ligantes tpy e 12-14 mostrarem valores mais altos de TON, o ligante 15 apresentou melhor estabilidade chegando a um TON de 126 após 24 h. Este valor corresponde à maior atividade catalítica já encontrada para um catalisador homogêneo contendo metal não-nobre para a decomposição de AF.
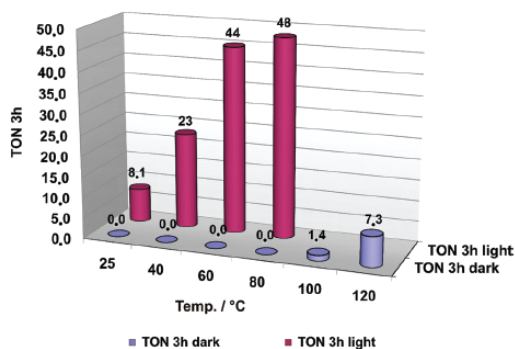

Figura 21. Comparação dos valores de TON a diferentes temperaturas para a decomposição de AF a partir da mistura AF/Et$_3$N (5:2) catalisada pelo sistema $[Fe_3(CO)_{12}]/PPh_3/tpy$ (Fe/PPh$_3$/tpy = 1:1:1) em DMF na presença ou não de irradiação. Reproduzido com permissão da referência [91] (American Chemical Society).
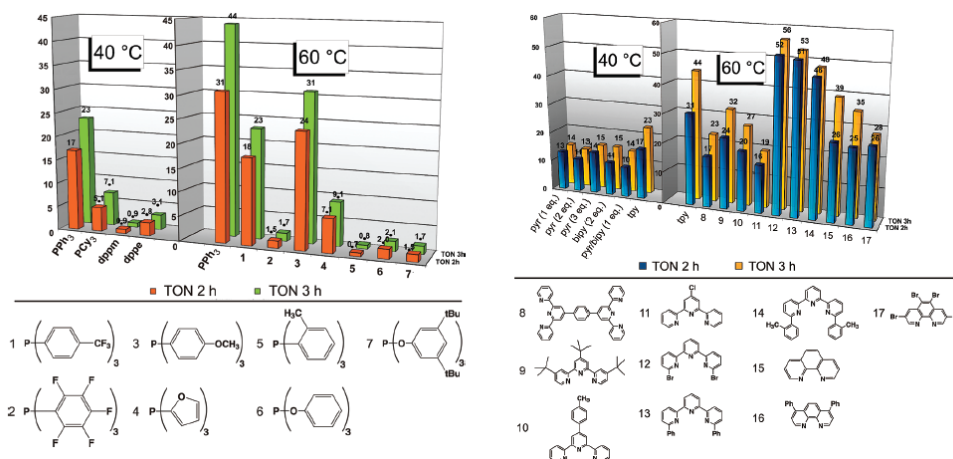

Figura 22. Valores de TON para os diferentes ligantes testados na decomposição de AF a partir da mistura AF/Et$_3$N (5:2) em DMF a 40 °C ou 60 °C sob irradiação de luz. (Esquerda) precursor: $[Fe_3(CO)_{12}]/$Ligante P/tpy (Fe/P/tpy 1:1:1); (direita) precursor: $[Fe_3(CO)_{12}]/PPh_3/$amina (Fe/PPh$_3$/amina 1:1:1). Reproduzido com permissão da referência [91] (American Chemical Society).

Finalmente, através de análises de RMN, IV, HRMS (High Resolution Mass Spectrometry) e cálculos teóricos, um mecanismo similar ao descrito anteriormente para o catalisador de Ru[97] foi proposto pelos autores considerando as espécies formadas (Esquema 14).
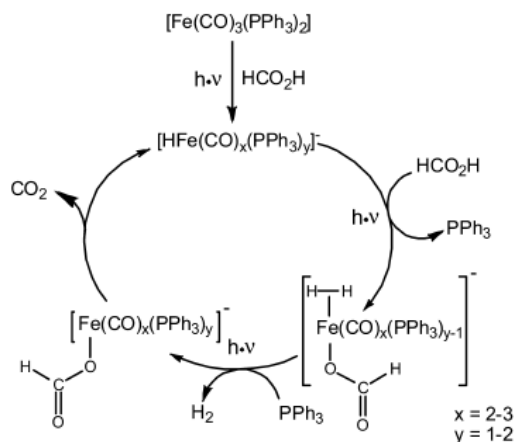
Esquema 14. Ciclo catalítico proposto para a decomposição de AF catalisada pelo sistema $[Fe_3(CO)_{12}]/PPh_3/tpy$ ($[Fe(CO)_3(PPh_3)_2]$) na presença de luz. Reproduzido com permissão da referência [91] (American Chemical Society).

Além da utilização da mistura azeotrópica AF/Et_3N (5:2) para geração de H_2, outros sistemas e meios reacionais tem sido empregados. Apesar do conhecimento prévio de que AF na presença de sua base conjugada (sal de formiato) pode ser fonte de hidrogênio,[99-103] Laurenczy e colaboradores desenvolveram um sistema catalítico para a decomposição de AF utilizando complexos de Ru na presença de formiato de sódio (HCO_2Na) em água.[104] Por exemplo, o complexo $[Ru(H_2O)_6](tos)_2$ com o ligante TPPTS dissolvido em água produz um eficiente meio para a decomposição da mistura AF/HCO_2Na (9:1) observando-se conversões até 95% (Figura 23). Mesmo para a reação a 100 °C descartou-se a presença de traços de CO na mistura gasosa por IV (limite de detecção de 3 ppm). Portanto, apenas H_2 e CO_2 estão presentes na composição do gás liberado. O catalisador se manteve estável e ativo por um longo período de tempo em solução. Além disso, este sistema catalítico também apresentou boa atividade em reações de fluxo contínuo. Os autores sugerem ainda um possível aproveitamento do CO_2, a partir de sua captura e redução à AF tornando o sistema ainda mais viável.
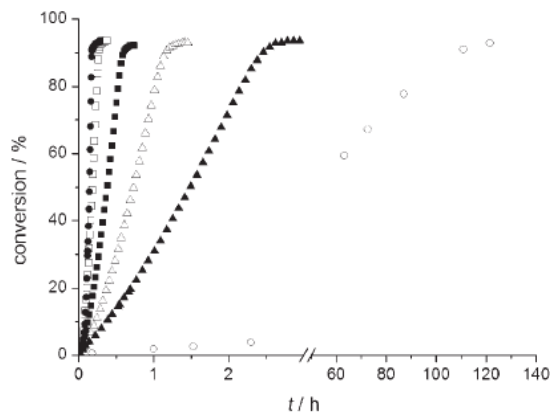
Figura 23. Decomposição de AF a partir de uma solução de AF/HCO$_2$Na (9:1) em H$_2$O/D$_2$O (1:1) catalisada pelo complexo [Ru(H$_2$O)$_6$](tos)$_2$/2TPPTS a diferentes temperaturas: (○) 25 °C, (▲) 70 °C, (Δ) 80 °C, (■) 90 °C, (□) 100 °C e (●) 120 °C. Reproduzido com permissão da referência [104] (Wiley-VCH Verlag GmbH & Co. KGaA).

Outros exemplos sobre a decomposição de AF catalisada por complexos de Rh e Ir-Ru em água na presença de HCO$_2$Na foram descritos por Fukuzumi e colaboradores.[88, 105] Detalhes a respeito do mecanismo de formação de H$_2$ e efeitos isotópicos em cada sistema podem ser verificados nos referidos trabalhos.

Deng e colaboradores demonstraram a geração de H$_2$ a partir de AF catalisada por um complexo de Ru em um LI-amino funcionalizado na presença de uma base adicional (HCO$_2$Na).[106] Valores de TON chegando a 627 em 1 h foram obtidos para o complexo [RuCl$_2$(*p*-cimeno)]$_2$ em *i*Pr$_2$NEMI.Cl (*i*Pr$_2$NEMI = 1-(2-diisopropilaminoetil)-3-metilimidazólio) e HCO$_2$Na a 60 °C. Entretanto, os autores não discutiram detalhes cinéticos e as possíveis espécies envolvidas no processo.

Em termos do emprego de catálise heterogênea para a decomposição de AF, Iglesia e Ojeda propõem um catalisador suportado baseado em pequenos clusters de Au (não-detectável por MET) em alumina.[107] Apesar de o metal Pt ser considerado o sólido mais ativo para a decomposição de AF (pelo menos nas formas de grandes clusters ou material *bulk*),[108] análises cinéticas comprovaram que o catalisador de Au/Al$_2$O$_3$ apresenta atividade superior ao análogo suportado de Pt. Verificou-se ainda a existência de efeitos isotópicos significativos ao testar HCOOD (1,6), DCOOH (2,5) e DCOOD (4,7) na decomposição promovida pelo catalisador de Au/Al$_2$O$_3$ a 353 K. Sugere-se um mecanismo via decomposição do formiato assistida por H ou via clivagens seqüenciais de ligação O-H

e C-H com posterior recombinação de átomos de H em sítios isolados do catalisador. Ainda, somente H_2 e CO_2 foram detectados no gás gerado (quantidades de CO abaixo de 10 ppm).

Os exemplos aqui brevemente apresentados demonstram a grande potencialidade de aplicação do AF (4,4% em massa de hidrogênio) como material alternativo para a produção de H_2 e sua utilização em células de combustível. Uma das grandes vantagens propiciadas pela decomposição de AF é a não-formação de sub-produtos sólidos ou líquidos, indesejáveis para aplicações em células a combustível. De fato, apenas H_2 e CO_2 (considerando desidrogenação) são gerados facilitando a purificação do gás de interesse pela simples retenção do CO_2 através de um filtro adequado. Além disso, o CO_2 produzido pode ser separado da mistura gasosa e reduzido a AF o que tornaria o processo ainda mais viável do ponto de vista econômico e ambiental.

CAPÍTULO 3

NANOPARTÍCULAS METÁLICAS EM LÍQUIDOS IÔNICOS

Artigo I

On the Structural and Surface Properties of Transition-Metal Nanoparticles in Ionic Liquids

Jairton Dupont and Jackson D. Scholten

Chemical Society Reviews **2010**, *39*, 1780-1804.

Artigo II

Tuning the Selectivity of Ruthenium Nanoscale Catalysts with Functionalised Ionic Liquids: Hydrogenation of Nitriles

Martin H. G. Prechtl, Jackson D. Scholten and Jairton Dupont

Journal of Molecular Catalysis A: Chemical **2009**, *313*, 74-78.

Artigo III

Imidazolium Ionic Liquids as Promoters and Stabilising Agents for the Preparation of Metal(0) Nanoparticles by Reduction and Decomposition of Organometallic Complexes

Martin H. G. Prechtl, Paul S. Campbell, Jackson D. Scholten, Georgina B. Fraser, Giovanna Machado, Catherine C. Santini, Jairton Dupont and Yves Chauvin

Nanoscale **2010**, *2*, 2601-2606.

Artigo IV

Probing the Chemical Interaction Between Iridium Nanoparticles and Ionic Liquid by XPS Analysis

Fabiano Bernardi, Jackson D. Scholten, Gerhard H. Fecher, Jairton Dupont and Jonder Morais

Chemical Physics Letters **2009**, *479*, 113-116.

CAPÍTULO 4

APLICAÇÕES EM SISTEMAS HOMOGÊNEOS

Artigo V

Alkene Hydroformylation Catalyzed by Rhodium Complexes in Ionic Liquids: Detection of Transient Carbene Species

Jackson D. Scholten and Jairton Dupont

Organometallics **2008**, *27*, 4439-4442.

Artigo VI

Decomposition of Formic Acid Catalyzed by a Phosphine-Free Ruthenium Complex in a Task-Specific Ionic Liquid

Jackson D. Scholten, Martin H. G. Prechtl and Jairton Dupont

ChemCatChem **2010**, *2*, 1265-1270.

CAPÍTULO 5

REFERÊNCIAS

[1] J. Dupont, R. F. de Souza, P. A. Z. Suarez, *Chem. Rev.* **2002**, *102*, 3667-3691.

[2] S. Tsuzuki, H. Tokuda, K. Hayamizu, M. Watanabe, *J. Phys. Chem. B* **2005**, *109*, 16474-16481.

[3] C. Hardacre, J. D. Holbrey, S. E. J. McMath, D. T. Bowron, A. K. Soper, *J. Chem. Phys.* **2003**, *118*, 273-278.

[4] J. Dupont, P. A. Z. Suarez, *Phys. Chem. Chem. Phys.* **2006**, *8*, 2441-2452.

[5] G. S. Fonseca, G. Machado, S. R. Teixeira, G. H. Fecher, J. Morais, M. C. M. Alves, J. Dupont, *J. Colloid Interface Sci.* **2006**, *301*, 193-204.

[6] C. W. Scheeren, G. Machado, S. R. Teixeira, J. Morais, J. B. Domingos, J. Dupont, *J. Phys. Chem. B* **2006**, *110*, 13011-13020.

[7] G. Machado, J. D. Scholten, T. de Vargas, S. R. Teixeira, L. H. Ronchi, J. Dupont, *Int. J. Nanotechn.* **2007**, *4*, 541-563.

[8] J. D. Scholten, G. Ebeling, J. Dupont, *Dalton Trans.* **2007**, 5554-5560.

[9] A. S. Pensado, A. A. H. Padua, *Angew. Chem. Int. Ed.* **2011**, DOI: 10.1002/anie.201103096.

[10] F. Ungvary, *Coord. Chem. Rev.* **2007**, *251*, 2072-2086.

[11] F. Ungvary, *Coord. Chem. Rev.* **2007**, *251*, 2087-2102.

[12] O. Roelen, *Ger. Offen. 849,548, 1938*.

[13] C. Claver, P. van Leeuwen, Eds., *Rhodium Catalyzed Hydroformylation, Vol. 1*, Kluwer Academic Publishers, Dordrecht, **2000**.

[14] B. Cornils, W. A. Herrmann, M. Rasch, *Angew. Chem. Int. Ed. Engl.* **1994**, *33*, 2144-2163.

[15] Y. J. Yan, X. W. Zhang, X. M. Zhang, *J. Am. Chem. Soc.* **2006**, *128*, 16058-16061.

[16] A. F. Peixoto, M. M. Pereira, A. M. S. Silva, C. M. Foca, J. C. Bayon, M. Moreno, A. M. Beja, J. A. Paixao, M. R. Silva, *J. Mol. Catal. A: Chem.* **2007**, *275*, 121-129.

[17] J. M. Praetorius, M. W. Kotyk, J. D. Webb, R. Y. Wang, C. M. Crudden, *Organometallics* **2007**, *26*, 1057-1061.

[18] M. Kuil, T. Soltner, P. van Leeuwen, J. N. H. Reek, *J. Am. Chem. Soc.* **2006**, *128*, 11344-11345.

[19] P. N. Bungu, S. Otto, *Dalton Trans.* **2007**, 2876-2884.

[20]   R. J. Klingler, M. J. Chen, J. W. Rathke, K. W. Kramarz, *Organometallics* **2007**, *26*, 352-357.

[21]   R. van Duren, J. I. van der Vlugt, H. Kooijman, A. L. Spek, D. Vogt, *Dalton Trans.* **2007**, 1053-1059.

[22]   Q. R. Peng, D. H. He, *Catal. Lett.* **2007**, *115*, 19-22.

[23]   S. C. Bourque, H. Alper, L. E. Manzer, P. Arya, *J. Am. Chem. Soc.* **2000**, *122*, 956-957.

[24]   M. L. Clarke, G. J. Roff, *Green Chem.* **2007**, *9*, 792-796.

[25]   H. J. V. Barros, C. C. Guimaraes, E. N. dos Santos, E. V. Gusevskaya, *Catal. Commun.* **2007**, *8*, 747-750.

[26]   S. Paganelli, M. Marchetti, M. Bianchin, C. Bertucci, *J. Mol. Catal. A: Chem.* **2007**, *269*, 234-239.

[27]   J. Ke, B. X. Han, M. W. George, H. K. Yan, M. Poliakoff, *J. Am. Chem. Soc.* **2001**, *123*, 3661-3670.

[28]   M. Haumann, A. Riisager, *Chem. Rev.* **2008**, *108*, 1474-1497.

[29]   Y. Chauvin, L. Mussmann, H. Olivier, *Angew. Chem. Int. Ed. Engl.* **1995**, *34*, 2698-2700.

[30]   W. Keim, D. Vogt, H. Waffenschmidt, P. Wasserscheid, *J. Catal.* **1999**, *186*, 481-484.

[31]   P. Wasserscheid, H. Waffenschmidt, *J. Mol. Catal. A: Chem.* **2000**, *164*, 61-67.

[32]   F. Favre, H. Olivier-Bourbigou, D. Commereuc, L. Saussine, *Chem. Commun.* **2001**, 1360-1361.

[33]   P. Wasserscheid, H. Waffenschmidt, P. Machnitzki, K. W. Kottsieper, O. Stelzer, *Chem. Commun.* **2001**, 451-452.

[34]   C. P. Casey, G. T. Whiteker, M. G. Melville, L. M. Petrovich, J. A. Gavney, D. R. Powell, *J. Am. Chem. Soc.* **1992**, *114*, 5535-5543.

[35]   M. Kranenburg, Y. E. M. Vanderburgt, P. C. J. Kamer, P. Vanleeuwen, K. Goubitz, J. Fraanje, *Organometallics* **1995**, *14*, 3081-3089.

[36]   L. A. van der Veen, M. D. K. Boele, F. R. Bregman, P. C. J. Kamer, P. van Leeuwen, K. Goubitz, J. Fraanje, H. Schenk, C. Bo, *J. Am. Chem. Soc.* **1998**, *120*, 11616-11626.

[37]   P. van Leeuwen, P. C. J. Kamer, J. N. H. Reek, P. Dierkes, *Chem. Rev.* **2000**, *100*, 2741-2769.

[38]   J. Dupont, S. M. Silva, R. F. de Souza, *Catal. Lett.* **2001**, *77*, 131-133.

[39]   S. M. Silva, R. P. J. Bronger, Z. Freixa, J. Dupont, P. van Leeuwen, *New J. Chem.* **2003**, *27*, 1294-1296.

[40]   P. Wasserscheid, R. van Hal, A. Bosmann, *Green Chem.* **2002**, *4*, 400-404.

[41]   B. A. Omotowa, J. M. Shreeve, *Organometallics* **2004**, *23*, 783-791.

[42]   D. B. G. Williams, M. Ajam, A. Ranwell, *Organometallics* **2007**, *26*, 4692-4695.

[43]   Q. Lin, W. D. Jiang, H. Y. Fu, H. Chen, X. J. Li, *Appl. Catal. A: Gen.* **2007**, *328*, 83-87.

[44]   C. C. Brasse, U. Englert, A. Salzer, H. Waffenschmidt, P. Wasserscheid, *Organometallics* **2000**, *19*, 3818-3823.

[45]   P. Illner, A. Zahl, R. Puchta, N. van Eikema Hommes, P. Wasserscheid, R. van Eldik, *J. Organomet. Chem.* **2005**, *690*, 3567-3576.

[46]   F. Z. Kong, J. Y. Jiang, Z. L. Jin, *Catal. Lett.* **2004**, *96*, 63-65.

[47]   Y. Yang, C. X. Deng, Y. Z. Yuan, *J. Catal.* **2005**, *232*, 108-116.

[48]   N. Sieffert, G. Wipff, *J. Phys. Chem. B* **2007**, *111*, 4951-4962.

[49]   C. P. Mehnert, R. A. Cook, N. C. Dispenziere, E. J. Mozeleski, *Polyhedron* **2004**, *23*, 2679-2688.

[50]   R. P. J. Bronger, S. M. Silva, P. C. J. Kamer, P. van Leeuwen, *Dalton Trans.* **2004**, 1590-1596.

[51]   P. B. Webb, M. F. Sellin, T. E. Kunene, S. Williamson, A. M. Z. Slawin, D. J. Cole-Hamilton, *J. Am. Chem. Soc.* **2003**, *125*, 15577-15588.

[52]   A. Riisager, P. Wasserscheid, R. van Hal, R. Fehrmann, *J. Catal.* **2003**, *219*, 452-455.

[53]   C. X. Deng, G. N. Ou, J. R. She, Y. Z. Yuan, *J. Mol. Catal. A: Chem.* **2007**, *270*, 76-82.

[54]   K. Tominaga, *Catal. Today* **2006**, *115*, 70-72.

[55]   L. Schlapbach, A. Zuttel, *Nature* **2001**, *414*, 353-358.

[56]   A. Staubitz, A. P. M. Robertson, I. Manners, *Chem. Rev.* **2010**, *110,* 4079-4124.

[57]   J. Graetz, *Chem. Soc. Rev.* **2009**, *38*, 73-82.

[58] C. W. Hamilton, R. T. Baker, A. Staubitz, I. Manners, *Chem. Soc. Rev.* **2009**, *38*, 279-293.

[59] M. G. Hu, R. A. Geanangel, W. W. Wendlandt, *Thermochim. Acta* **1978**, *23*, 249-255.

[60] S. S. Wise, J. L. Margrave, H. M. Feder, W. N. Hubbard, *J. Phys. Chem.* **1966**, *70*, 7-10.

[61] D. A. Dixon, M. Gutowski, *J. Phys. Chem. A* **2005**, *109*, 5129-5135.

[62] F. H. Stephens, V. Pons, R. T. Baker, *Dalton Trans.* **2007**, 2613-2626.

[63] M. E. Bluhm, M. G. Bradley, R. Butterick, U. Kusari, L. G. Sneddon, *J. Am. Chem. Soc.* **2006**, *128*, 7748-7749.

[64] T. P. Onak, I. Shapiro, *J. Chem. Phys.* **1960**, *32*, 952-952.

[65] J. S. Wang, R. A. Geanangel, *Inorg. Chim. Acta* **1988**, *148*, 185-190.

[66] E. Mayer, *Inorganic & Nuclear Chemistry Letters* **1973**, *9*, 343-346.

[67] R. J. Keaton, J. M. Blacquiere, R. T. Baker, *J. Am. Chem. Soc.* **2007**, *129*, 1844-1845.

[68] D. Enders, K. Breuer, G. Raabe, J. Runsink, J. H. Teles, J. P. Melder, K. Ebel, S. Brode, *Angew. Chem. Int. Ed. Engl.* **1995**, *34*, 1021-1023.

[69] A. Staubitz, A. P. M. Robertson, M. E. Sloan, I. Manners, *Chem. Rev.* **2010**, *110*, 4023-4078.

[70] X. Z. Yang, M. B. Hall, *J. Am. Chem. Soc.* **2008**, *130*, 1798-1799.

[71] H. V. K. Diyabalanage, T. Nakagawa, R. P. Shrestha, T. A. Semelsberger, B. L. Davis, B. L. Scott, A. K. Burrell, W. I. F. David, K. R. Ryan, M. O. Jones, P. P. Edwards, *J. Am. Chem. Soc.* **2010**, *132*, 11836-11837.

[72] Y. S. Chua, P. Chen, G. T. Wu, Z. T. Xiong, *Chem. Commun.* **2011**, *47*, 5116-5129.

[73] B. Sakintuna, F. Lamari-Darkrim, M. Hirscher, *Int. J. Hydrogen Energy* **2007**, *32*, 1121-1140.

[74] W. F. Luo, *J. Alloys Compd.* **2004**, *381*, 284-287.

[75] J. J. Vajo, S. L. Skeith, F. Mertens, *J. Phys. Chem. B* **2005**, *109*, 3719-3722.

[76] F. E. Pinkerton, G. P. Meisner, M. S. Meyer, M. P. Balogh, M. D. Kundrat, *J. Phys. Chem. B* **2005**, *109*, 6-8.

[77] J. Yang, A. Sudik, D. J. Siegel, D. Halliday, A. Drews, R. O. Carter, C. Wolverton, G. J. Lewis, J. W. A. Sachtler, J. J. Low, S. A. Faheem, D. A. Lesch, V. Ozolins, *Angew. Chem. Int. Ed.* **2008**, *47*, 882-887.

[78] M. P. Stracke, G. Ebeling, R. Cataluna, J. Dupont, *Energy Fuels* **2007**, *21*, 1695-1698.

[79] C. C. Cassol, G. Ebeling, B. Ferrera, J. Dupont, *Adv. Synth. Catal.* **2006**, *348*, 243-248.

[80] S. V. Dzyuba, R. A. Bartsch, *Chemphyschem* **2002**, *3*, 161-166.

[81] J. K. Lee, M. J. Kim, *J. Org. Chem.* **2002**, *67*, 6845-6847.

[82] M. E. Moret, A. B. Chaplin, A. K. Lawrence, R. Scopelliti, P. J. Dyson, *Organometallics* **2005**, *24*, 4039-4048.

[83] A. Doroodian, J. E. Dengler, A. Genest, N. Rosch, B. Rieger, *Angew. Chem. Int. Ed.* **2010**, *49*, 1871-1873.

[84] Y. G. Wang, N. Shah, G. P. Huffman, *Energy Fuels* **2004**, *18*, 1429-1433.

[85] N. Shah, Y. G. Wang, D. Panjala, G. P. Huffman, *Energy Fuels* **2004**, *18*, 727-735.

[86] Y. G. Wang, N. Shah, G. P. Huffman, *Catal. Today* **2005**, *99*, 359-364.

[87] H. G. Alt, I. K. Bohmer, *Angew. Chem. Int. Ed.* **2008**, *47*, 2619-2621.

[88] S. Fukuzumi, T. Kobayashi, T. Suenobu, *Chemsuschem* **2008**, *1*, 827-834.

[89] C. Fellay, N. Yan, P. J. Dyson, G. Laurenczy, *Chem.-Eur. J.* **2009**, *15*, 3752-3760.

[90] B. Sorensen, *Hydrogen and Fuel Cells, emerging technologies and applications*, Elsevier, Amsterdam, **2005**.

[91] A. Boddien, B. Loges, F. Gartner, C. Torborg, K. Fumino, H. Junge, R. Ludwig, M. Beller, *J. Am. Chem. Soc.* **2010**, *132*, 8924-8934.

[92] W. Leitner, J. M. Brown, H. Brunner, *J. Am. Chem. Soc.* **1993**, *115*, 152-159.

[93] A. Fujii, S. Hashiguchi, N. Uematsu, T. Ikariya, R. Noyori, *J. Am. Chem. Soc.* **1996**, *118*, 2521-2522.

[94] S. Lange, W. Leitner, *J. Chem. Soc.-Dalton Trans.* **2002**, 752-758.

[95] B. Loges, A. Boddien, H. Junge, M. Beller, *Angew. Chem. Int. Ed.* **2008**, *47*, 3962-3965.

[96] A. Boddien, B. Loges, H. Junge, M. Beller, *Chemsuschem* **2008**, *1*, 751-758.

[97] B. Loges, A. Boddien, H. Junge, J. R. Noyes, W. Baumann, M. Beller, *Chem. Commun.* **2009**, 4185-4187.

[98] H. Junge, A. Boddien, F. Capitta, B. Loges, J. R. Noyes, S. Gladiali, M. Beller, *Tetrahedron Lett.* **2009**, *50*, 1603-1606.

[99] R. S. Paonessa, W. C. Trogler, *J. Am. Chem. Soc.* **1982**, *104*, 3529-3530.

[100] Y. Gao, J. K. Kuncheria, H. A. Jenkins, R. J. Puddephatt, G. P. A. Yap, *J. Chem. Soc.-Dalton Trans.* **2000**, 3212-3217.

[101] S. Ogo, H. Nishida, H. Hayashi, Y. Murata, S. Fukuzumi, *Organometallics* **2005**, *24*, 4816-4823.

[102] J. R. Hyde, M. Poliakoff, *Chem. Commun.* **2004**, 1482-1483.

[103] E. Garcia-Verdugo, Z. M. Liu, E. Ramirez, J. Garcia-Serna, J. Fraga-Dubreuil, J. R. Hyde, P. A. Hamley, M. Poliakoff, *Green Chem.* **2006**, *8*, 359-364.

[104] C. Fellay, P. J. Dyson, G. Laurenczy, *Angew. Chem. Int. Ed.* **2008**, *47*, 3966-3968.

[105] S. Fukuzumi, T. Kobayashi, T. Suenobu, *J. Am. Chem. Soc.* **2010**, *132*, 1496-1497.

[106] X. L. Li, X. Y. Ma, F. Shi, Y. Q. Deng, *Chemsuschem* **2010**, *3*, 71-74.

[107] M. Ojeda, E. Iglesia, *Angew. Chem. Int. Ed.* **2009**, *48*, 4800-4803.

[108] M. A. Barteau, *Catal. Lett.* **1991**, *8*, 175-184.

CAPÍTULO 6

CONCLUSÕES

A respeito dos trabalhos sobre a síntese de NPs em LIs pode-se concluir os seguintes aspectos:

1. NPs de Ru(0) com 2,2 ± 0,5 nm em diâmetro podem ser sintetizadas a partir do precursor [Ru(COD)(2-metilalil)$_2$] em um LI contendo um grupamento nitrila ligado ao cátion imidazólio ((BCN)MI.NTf$_2$). Utilizando o LI (BCN)MI.NTf$_2$, a funcionalidade do LI controla a seletividade do catalisador, evitando a reação de hidrogenação de arenos (tolueno). Entretanto, o sistema catalítico Ru-NPs/(BCN)MI.NTf$_2$ é ativo para a hidrogenação de nitrilas (benzonitrila). Desta forma, é proposto que o grupamento funcional do LI esteja se coordenando à superfície metálica das NPs modificando a seletividade do catalisador frente a diferentes substratos.

2. NPs de Ru(0) (2,0 ± 0,3 nm) foram sintetizadas a partir da redução do precursor [Ru(COD)(2-metilalil)$_2$] utilizando o LI imidazólio HM$_2$I.NTf$_2$ (HM$_2$I = 1,2-dimetil-3-hexilimidazólio) como meio e promotor da reação. A formação das NPs foi realizada sob condições brandas de reação e mais interessante, na ausência de um agente redutor tradicional (H$_2$, NaBH$_4$). Neste caso sugere-se um ataque nucleofílico do ânion NTf$_2$ ao ligante alila do precursor metálico, gerando espécies moleculares de Ru(0) as quais coalescem formando NPs estabilizadas pelo LI. Para LIs contendo outros ânions como BF$_4$, B(CN)$_4$ e N(CN)$_2$ não observou-se a formação de NPs metálicas. Um comportamento similar de decomposição foi verificado para o precursor [Ni(COD)$_2$] produzindo NPs de Ni(0) na presença de LIs imidazólios contendo o ânion NTf$_2$.

3. A análise de XPS mostrou ser uma importante ferramenta no entendimento da interação de NPs metálicas e LIs imidazólios (no referido estudo: LIs não-funcionalizados). Para tal estudo, sintetizou-se NPs de Ir(0) (1,6 ± 0,3 nm) no LI EMI.EtSO$_4$. As análises de XPS mostraram mudanças na energia de ligação do componente C2 do LI (região C 1s) na presença das NPs de Ir(0). Este fato é uma forte indicação da interação entre as NPs metálicas e o LI. Estes resultados corroboram com análises anteriores de troca isotópica, onde se verificou que para o LI deuterado [EMI]-d_3.EtSO$_4$ ocorrem trocas D/H preferenciais na posição mais ácida C2, ao contrário de outros LIs testados. Além disso,

não se pode excluir a possibilidade de o ânion EtSO$_4$ estar atuando como base no meio reacional. Portanto, as NPs de Ir em EMI.EtSO$_4$ são provavelmente estabilizadas através da interação de agregados moleculares aniônicos do líquido com a superfície metálica e, a partir destes agregados, carbenos *N*-heterocíclicos derivados do anel imidazólio podem estar sendo formados auxiliando na estabilização das NPs.

Para complexos metálicos dissolvidos em LI e suas aplicações em catálise homogênea nas reações de hidroformilação e desidrogenação de ácido fórmico, pode-se concluir que:

1. Não se pode excluir a possibilidade da formação de carbenos *N*-heterocíclicos durante a reação de hidroformilação de 1-octeno em LIs catalisadas por complexos de ródio/fosfina. Trocas D/H foram observadas no anel imidazólio do LI sugerindo a presença de espécies carbenos transientes. Estas trocas foram mais intensas na posição mais ácida do anel imidazólio (C2) e, mais importante, a presença do ligante fosfina e metanol (solvente) foram essenciais para a ocorrência efetiva de troca D/H. Portanto, a troca isotópica no cátion imidazólio é efetivamente maior na presença de bases relativamente fracas.

2. A desidrogenação de ácido fórmico à hidrogênio molecular e dióxido de carbono é efetivamente catalisada pelo complexo {[RuCl$_2$(*p*-cymene)]$_2$} dissolvido em um LI funcionalizado com grupamento −NEt$_2$ ligado ao cátion imidazólio. O LI amino-funcionalizado estabiliza a espécie ativa e atua como co-catalisador na reação. Em poucas horas de reação altas conversões podem ser obtidas, alcançando TOFs até 1540 h^{-1}. Medidas cinéticas preliminares indicam ordens de reação de 0,7 para o catalisador de Ru, 0,8 para o LI e 2,0 para o ácido fórmico. Estes resultados sugerem que o ácido fórmico possa estar atuando em sua forma dimérica na reação. A energia de ativação do processo foi estimada em 69,1 kJ mol^{-1}, que está na faixa dos mais clássicos sistemas para a desidrogenação de ácido fórmico. Análises de ESI(+)-MS mostraram espécies diméricas de Ru como possíveis espécies ativas durante a decomposição de ácido fórmico. A estabilidade frente ao ar e humidade, robustes à reações de recargas sem perda significativa na atividade catalítica, fazem deste um potencial sistema para a produção de hidrogênio.

Artigo I

On the Structural and Surface Properties of Transition-Metal Nanoparticles in Ionic Liquids

Jairton Dupont and Jackson D. Scholten

On the structural and surface properties of transition-metal nanoparticles in ionic liquids

Jairton Dupont* and Jackson D. Scholten

Ionic liquids (ILs), in particular imidazolium-based ILs, have proven to be suitable media for the generation and stabilisation of soluble metal nanoparticles (NPs). Indeed, transition-metal NPs with small sizes, narrow size distribution and different shapes have been prepared by reduction of organometallic compounds with molecular hydrogen, decomposition of transition-metal complexes in the zero-valent state, metal bombardment or simple transfer for previously prepared water- or classical organic solvent-soluble colloids to the ILs. The formation and stabilisation of NPs in these highly hydrogen bonded organised supramolecular fluids occur with the re-organisation of the hydrogen bond network and the generation of nanostructures with polar and non-polar regions, including the NPs. The IL forms a protective layer, which is probably composed of imidazolium aggregates located immediately adjacent to the nanoparticle surface, which provides both steric and electronic protection against aggregation and/or agglomeration. These stable transition-metal NPs immobilised in the ILs have proven to be efficient green catalysts for several reactions in multiphase conditions and also novel materials for chemical sensors. In this *critical review*, the structural/surface properties of these soluble metal NPs dispersed in ILs and their application in catalysis and as chemical sensors are discussed, with particular attention paid to the stabilisation models proposed to explain the stability and properties of these metal NPs (219 references).

1. Introduction

Metal NPs with small diameters and a narrow size distribution have received intense attention in scientific research and

Laboratory of Molecular Catalysis, Institute of Chemistry, UFRGS, Avenida Bento Gonçalves, 9500 Porto Alegre 91501-970 RS, Brazil. E-mail: jairton.dupont@ufrgs.br; Fax: 55 51 33087304; Tel: 55 51 33086321

industrial applications due to their unique properties based on their inherent large surface-to-volume ratios and quantum size effects.[1,2] Modern transition-metal NPs differ from classical colloids in several important aspects, including size and stability in solution. Modern metal NPs are 1–10 nm in diameter and display a narrow size distribution, whereas classical colloids typically are > 10 nm in diameter.[3] However, it is well known that transition-metal NPs are only kinetically

Jairton Dupont received his PhD at the Université Louis Pasteur of Strasbourg (France) and after a period as a post-doc at the University of Oxford (UK), he became a Professor of Chemistry at the Institute of Chemistry, UFRGS (Brazil). He has been an invited Professor at ULP (France), Nuremberg-Erlangen (Germany) and Universidad de Alcala de Henares (Spain). He is a member of the Brazilian Academy of Sciences and has received the Humboldt Research Award. His research interests are mainly centered on ionic liquids with special emphasis in catalysis, nanomaterials and alternative energies. He has authored around 200 scientific publications and several patents and book chapters.
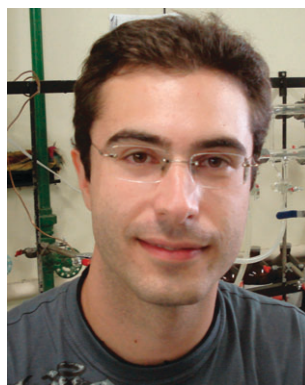
Jairton Dupont

Jackson Damiani Scholten received his Bachelor degree in chemistry from UFRGS. In 2007, he completed his MSc at UFRGS under the supervision of Prof. Dr Jairton Dupont, focusing on the stabilization of iridium nanoparticles in ionic liquids. Currently, he is a PhD student in the same University at Prof. Dupont's research group. His research interests are centered on catalysis using organometallic complexes and transition-metal nanoparticles in ionic liquids.

Jackson D. Scholten

stable. Consequently, NPs freely dissolved in solution are not stable and must be stabilised in order to prevent their agglomeration (diffusing together and coalescing), the thermo-dynamically favoured process that eventually leads to the formation of the bulk metal.[4] To prevent aggregation, the NPs must be stabilised by the use of stabilising agents, such as water-soluble polymers, quaternary ammonium salts, surfactants, or polyoxoanions,[5–10] which provide electronic and/or steric protection.

In this context, ILs have emerged as one of the most important and investigated classes of stabilising agents for the synthesis and stabilisation of metal NPs.[11–14] Herein we present and discuss the most recent contributions on the use of ILs (particularly those based on imidazolium cations) in the formation and stabilisation of transition-metal NPs, the surface and structural properties of these systems, and their applications in catalysis and chemical sensors.

2. Stabilisation of metal NPs in ILs

It is well known that ILs, in particular imidazolium-derived salts, can be used to generate in situ and stabilise metallic NPs.[15] In particular, ILs resulting from the association of the 1-n-butyl-3-methylimidazolium (BMI) cation with relatively weakly coordinating anions, such as tetrafluoroborate, hexafluorophosphate, and trifluoromethanesulfonate (Fig. 1), display unique physico-chemical properties. They are liquids over a large range of temperatures (down to −80 °C), possess high thermal and chemical stability, a large electrochemical window, high ion density, relatively low viscosity, and negligible vapour pressure.[16]

These ILs differ from the classical ammonium salts, at least in one very important aspect: they possess pre-organised structures, mainly through hydrogen bonds,[17–19] that induce structural directionality (IL effect). By contrast, aggregates of classical salts display charge-ordered structures.

The ILs act as stabilising media, but most importantly, they display high self-organisation on the nanomolecular scale. The ILs form extended hydrogen-bond networks at the liquid state and therefore ar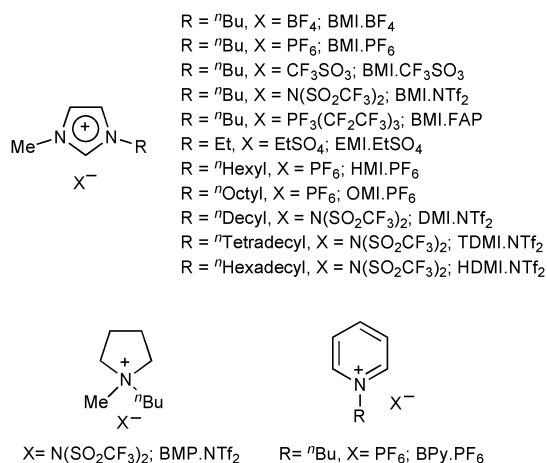e by definition "supramolecular" fluids. This structural organisation of ILs can be used as "entropic drivers" (the so-called "IL effect") for the spontaneous, well-defined and extended ordering of nanoscale structures. For example, ILs have already been used as media for the synthesis of some zeolite-related, microporous alumino-phosphates or ordered mesoporous materials in which ILs have served both as the solvent and structure-directing agents.[20–24]

It is now clear that the properties of the ILs, especially the imidazolium-based salts, are based on their formation of aggregates rather than on their isolated cations and anions.[25–27] Indeed, the structures of 1,3-dialkylimidazolium salts follow a typical trend, forming an extended network of cations and anions connected together by hydrogen bonds in the condensed phase, which is maintained to a great extent in the gas phase.[27] The monomeric unit is always composed of one imidazolium cation surrounded by at least three anions, and in turn, each anion is surrounded by at least three imidazolium cations.[28] The 3D arrangement of the imidazolium ILs is generally formed through chains of the imidazolium rings. This molecular arrangement generates channels in which the anions are generally accommodated as chains (Fig. 2).

These IL structures can adapt to or are adaptable by many species, as they provide hydrophobic or hydrophilic regions and a high directional polarisability, which can be oriented parallel or perpendicular to the included species.[19] Therefore, there is the presence of a continuous tridimensional network of ionic channels, coexisting with the non-polar domains, which in some cases form dispersed microphases and in other cases build continuous phases (Fig. 3).[29]

The segregation of polar and non-polar domains in imidazolium-based ILs affects their solvation and their ability to interact with different species. Indeed, polar substrates are preferentially dissolved in polar domains and non-polar compounds in non-polar ones.[30,31] For example, two extreme situations are those of alkane and water solutions, and the solute is concentrated either in the non-polar domain or in the charged domain.[32–34]

Therefore non-polar transition-metal precursors (organo-metallic) or salts will be dissolved preferentially in the

R = nBu, X = BF4; BMI.BF4
R = nBu, X = PF6; BMI.PF6
R = nBu, X = CF3SO3; BMI.CF3SO3
R = nBu, X = N(SO2CF3)2; BMI.NTf2
R = nBu, X = PF3(CF2CF3)3; BMI.FAP
R = Et, X = EtSO4; EMI.EtSO4
R = nHexyl, X = PF6; HMI.PF6
R = nOctyl, X = PF6; OMI.PF6
R = nDecyl, X = N(SO2CF3)2; DMI.NTf2
R = nTetradecyl, X = N(SO2CF3)2; TDMI.NTf2
R = nHexadecyl, X = N(SO2CF3)2; HDMI.NTf2

X= N(SO2CF3)2; BMP.NTf2   R= nBu, X= PF6; BPy.PF6

Fig. 1 Examples of imidazolium-, pyrrolidinium- and pyridinium-based ILs.
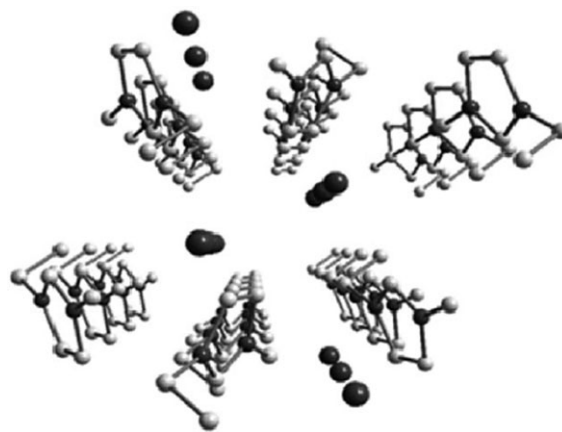

Fig. 2 Supramolecular arrangement of 1,3-dialkylimidazolium-based ILs showing the channels where the anions (spheres) are accommodated. (Copyright from ref. 19).
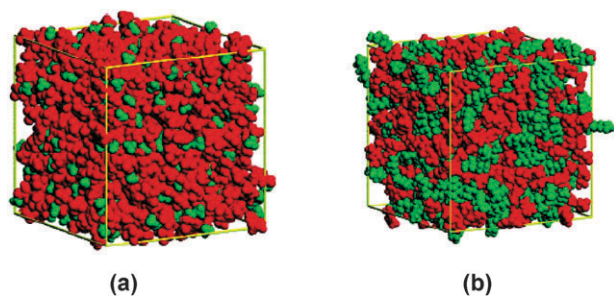
This journal is © The Royal Society of Chemistry 2010

Chem. Soc. Rev., 2010, 39, 1780–1804 | 1781

Fig. 3 Simulation study of imidazolium-based ILs (boxes contain 700 ions) showing the polar (red) and non-polar (green) domains for (a) EMI.PF$_6$ (1-ethyl-3-methylimidazolium hexafluorophosphate), and (b) OMI.PF$_6$ (1-methyl-3-*n*-octylimidazolium hexafluorophosphate), l = 54.8 Å. l is the length of the box side. As expected, increased IL side chains lead to larger non-polar domains. (Figure adapted from ref. 29).

non-polar domains of the IL whereas polar ones will favour the IL polar regions. Consequently, the size and shape of the metal NPs are modulated by the volume of these IL nanoregions (see later for details).

In parallel, the formed metal NPs in non-functionalised imidazolium ILs can be stabilised by ionic aggregates of the type $\{[(BMI)_x(X)_{x-n}]^{n+}[(BMI)_{x-n}(X)_x]^{n-}\}_m$ (where BMI is the 1-*n*-butyl-3-methylimidazolium cation and X is the anion), rather than by isolated anions and cations. Therefore, the DLVO (Derjaguin–Landau–Verwey–Overbeek) model of colloid stability cannot be used in these systems, as recently pointed out by Finke and Ott,[35] because the DLVO model was not designed to account for counter-ions with multiple charges nor was it designed to account for sterically stabilised systems.[36,37]

There are several pieces of evidence indicating that the non-functionalised ionic liquids interact relatively strongly with the surface of metal NPs either dispersed in ILs or even when isolated.

The XPS analysis of the isolated NPs (Ir, Rh, Pt, Ru and Pd) prepared in ILs containing the PF$_6$ and BF$_4$ anions revealed the IL–metal surface interaction to be M–O (metal-oxide) and M–F contributions in most cases. The contribution of the M–F component is more pronounced in the case of PF$_6$ anion than for BF$_4$ anion. The F 1s, P (in the case of PF$_6$), and B (in the case of BF$_4$) contributions are also observed in the XPS spectra.[38] These results clearly indicate that even relatively weak coordinating anions, such as PF$_6$ and BF$_4$, coordinate with the metal surface (Fig. 4).

In addition, the presence of the M–O contribution of the isolated metal NPs, as detected by these XPS experiments, indicates that the metal NP surfaces are more susceptible to oxidation in air than the bulk metal and that this oxide layer may also be a significant source of stability of the metal NPs.[39] Notably, after Ar$^+$ sputtering, almost all of these surface-bound species are removed. Indeed, XPS spectra after sputtering (Fig. 5) display mainly the M–M component at the 4f region, demonstrating that only the external surface metal atoms are bound to F and O.[38,40–42]

Interestingly, the chemical interaction between iridium NPs and EMI.EtSO$_4$ IL was also observed by *in situ* XPS
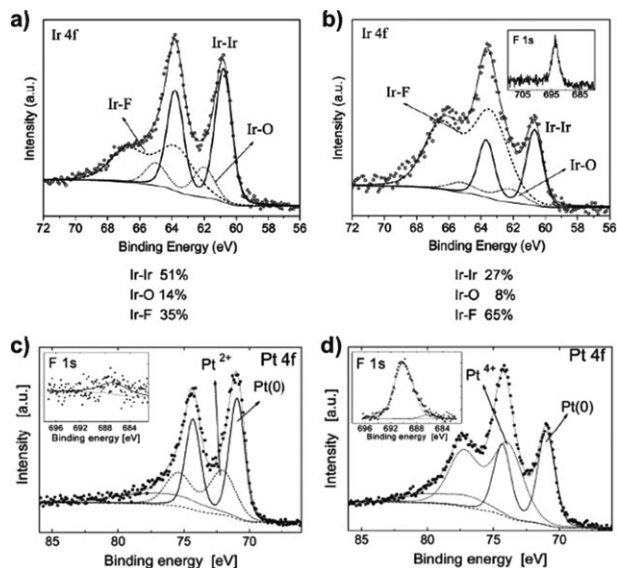

Fig. 4 (a) XPS spectrum of iridium NPs prepared in BMI.BF$_4$ and (b) BMI.PF$_6$ showing the Ir 4f region with the fitting results; the Ir 4f doublet presents up to three components corresponding to Ir–Ir (thick line), Ir–O (dotted curve), and Ir–F bonds (dashed curve); the inset of (b) shows the F 1s signal observed in that case. (c) XPS spectrum of platinum NPs prepared in BMI.BF$_4$ and (d) BMI.PF$_6$ showing the Pt 4f region with the fitting results (Shirley type background); the insets of (c) and (d) show the F 1s signal observed for each case. (Figure adapted from ref. 38 and 42).
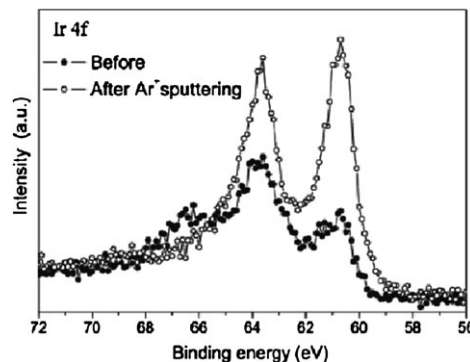

Fig. 5 XPS spectrum of the Ir 4f region for [Ir(0)]$_n$ NPs synthesized in BMI.PF$_6$ before and after Ar$^+$ sputtering. The Ar$^+$ sputtering eliminates the outmost layers of the NPs and therefore resulting in the Ir 4f region with mainly Ir–Ir bond component. (Figure adapted from ref. 38).

analysis.[43] The C2 component of the imidazolium cation was shifted to a lower binding energy in the presence of the metal NPs. Moreover, these results corroborate those obtained previously by D/H labelling experiments, where the isotope exchange occurred preferentially at the most acidic imidazolium ring position at the beginning of the reaction.[44] Therefore, metal nanoparticles are effectively surrounded by aggregates and may interact preferentially through the ionic parts ("ionic channels") and/or with non-polar domains created by the grouping of lipophilic alkyl chains (see Fig. 3). The interaction of the non-polar domains may explain the H/D exchange
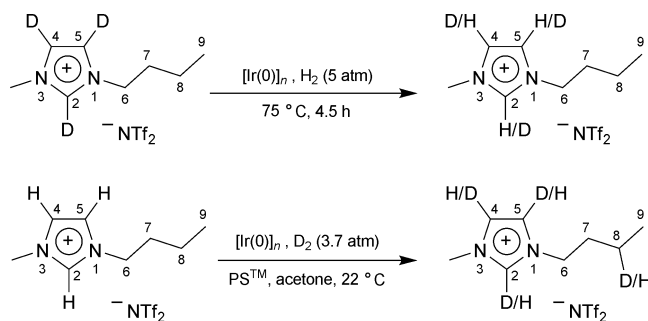
Scheme 1 D/H and H/D exchange reactions in imidazolium ILs promoted by $[Ir(0)]_n$ NPs.[44,45]

reaction observed in labelling experiments using D_2 for the generation of $[Ir(0)]_n$ NPs from the reduction of $[Ir(COD)(MeCN)_2]BF_4$ (COD = 1,5-cyclooctadiene) in $BMI.NTf_2$. In these experiments, besides the H/D of the imidazolium hydrogens, the alkyl side chains also undergo important H/D exchange reactions (Scheme 1).[45] Indeed, ^2H NMR spectroscopy showed deuterium incorporation in the 2-, 4-, 5-, and 8-positions of the imidazolium cation and a faster rate of D incorporation was observed for the 2-, 4-, and 5-positions; incorporation at the 8-position of the alkyl chain is slower (>8 h). These results are strong indications of the interaction of the imidazolium N-alkyl side chains with the metal surfaces that should contain surfaces hydrides/deuterides. Therefore, the metal NPs may also be surrounded by these non-polar pockets, similar to the "solvent-only" stabilised nanoclusters prepared from the anion-free precursor $[Ru(COD)(COT)]$ (COT = 1,3,5-cyclooctatriene) in THF/MeOH[46] in which the presence and stability of hydrogen species on the metal surface were previously demonstrated.[47,48]

The $[Rh(0)]_n$ NPs synthesised in $BMI.PF_6$ in the presence of bipyridine ligand were also characterised by XPS analysis.[49] The signal of fluorine was mainly seen, due to the residual IL and nitrogen that possibly correspond to the bipyridine ligand. However, no phosphorus signal from the IL was observed in this case. Infrared analysis of silver NPs obtained in $BMI.BF_4$ also showed the presence of IL on the NP surface.[50]

The SAXS analysis of $[Ir(0)]_n$ and $[Pt(0)]_n$ NPs dispersed in the ILs indicated the formation of a layer surrounding the metal particles. It is important to note that calculations using the Guinier Approximation Law at the small angle region gave inconsistent results, indicating that the assumption that the NPs are simply diluted in the ILs cannot be applied in these cases. By contrast, the calculations using Porod's law yielded consistent results. The Porod's region gives information about the interfaces present in the sample, with the electronic contrast only occurring at the interface between the two media (Fig. 6).

In this model, the presence of two phases, a crystalline phase (nano-crystal or NPs) and a semi-ordered phase (IL), is assumed.[18,51–53] This model can be used since ILs are not considered as statistical aggregates of anions and cations but instead as a three-dimensional network of anions and cations, *i.e.*, polymeric supramolecular structures constituted of aggregates of the type $\{[(BMI)_x(X)_{x-n}]^{n+}[(BMI)_{x-n}(X)_x]^{n-}\}_m$. In this context, the two-phase model was adopted to represent the
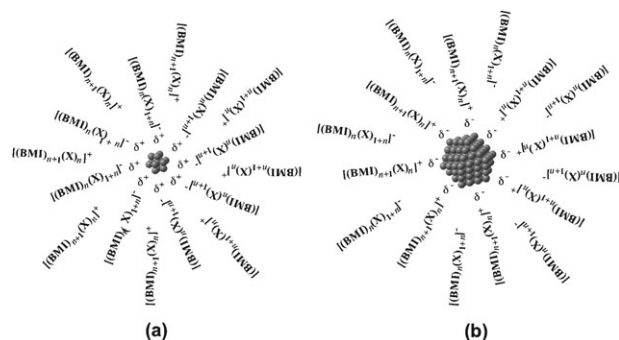

Fig. 6 Interaction of metal NPs with IL supramolecular aggregates: (a) small particles tend to interact preferentially with anionic aggregates of the ILs, whereas (b) large ones probably interact preferentially with the cationic aggregates.

nano-crystals dispersed in the IL.[54] Applying the interface distribution function in the experimental data, the extended molecular lengths of pure ILs (semi-ordered phase) were estimated to be 2.8, 4.0, and 4.0 nm for $BMI.BF_4$, $BMI.PF_6$ and $BMI.OTf$, respectively. The obtained extended molecular length of 2.8 nm for $BMI.BF_4$ is around twice that of the calculated value for a monomeric $BMI.BF_4$ unit.[55,56] Moreover, the calculated molecular length (AM1) for the $[(BMI)_2(BF_4)_3]^-$ and $[(BMI)_4(PF_6)_5]^-$ supramolecular clusters are 2.4 nm and 4.1 nm, respectively.[57] For the semi-empirical method AM1 calculations it was considered that the geometries of all species were obtained by energy minimization without restrictions of the geometric parameters. There is little doubt that the stabilisation of very small metal NPs (1–10 nm) is essentially due to the positive charge on the metal surface, which is ultimately induced by the adsorption of the anionic IL species onto the coordinatively unsaturated, electron-deficient, and initially neutral metal surface (Fig. 6). However, recent surface-enhanced Raman spectroscopy (SERS) studies using gold NPs dispersed in an ether-functionalised IL (**5**; see Fig. 8) suggest that the surface-type interaction of the relatively large metal nanoparticle occurs with the imidazolium cation of the IL (Fig. 6).[58]

Indeed, the SERS insights reveal a parallel coordination mode of the imidazolium cation on the $[Au(0)]_n$ NP surface and the ether functionality chain of IL is away from the NP surface, thus providing additional steric protection against the aggregation. Interestingly, no significant interaction between the IL anion ($MeSO_3^-$) and $[Au(0)]_n$ NPs was detected once

that the Raman signals of the anion were not surface-enhanced in the presence of the NPs. Notably, these gold NPs were prepared by hydrazine reduction from a chloroauric acid solution in the IL. Since previous zeta potential measurements of Au particles prepared by a reduction process indicated NPs with a negatively charged surface,[59] it is reasonable to suggest the cation stabilisation of gold NPs promoted by the IL.

In a similar manner, the SERS effect was analysed for silver metal NPs dispersed in BMI.BF$_4$ and compared to a silver island film coated with the same IL.[60] The results verified that a small amount of water is enough to cause an aggregation of the $[Ag(0)]_n$ NPs with further precipitation. However, without water, there are NP aggregates sufficiently dispersed in the IL to make the SERS spectra observable. Therefore, due to the water adsorption on the NP surface, the double layer of the IL is not formed around the metal particle, explaining their aggregation and precipitation. However, in the absence of water, the IL double layer is present, therefore stabilising the $[Ag(0)]_n$ NPs and avoiding precipitation. Again, the imidazolium cation interacts with the $[Ag(0)]_n$ NP surface in a flat mode to form the positive layer; the anions act only on the charge balance in a second layer but do not interact chemically with the NPs.

The H/D and D/H labelling measurements were also useful to assess the interaction between imidazolium ILs and metal NPs. The ^2H NMR studies during the iridium nano-particle formation by D$_2$ reduction of the precursor $[Ir(COD)(MeCN)_2]BF_4$ embedded in BMI.NTf$_2$/acetone with 1,8-*bis*(dimethylamino)naphthalene (PS™) at 22 °C revealed that the 2-position of the imidazolium cation mainly forms *N*-heterocyclic carbenes (NHCs) from ILs in the presence of $[Ir(0)]_n$ NPs.[45] Noteworthy, interesting results that evidence the interaction of the IL with metal NPs were collected *via* D/H labelling experiments during cyclohexene hydrogenation.[44] Using $[Ir(COD)Cl]_2$ as the catalyst precursor, and cyclohexene and molecular hydrogen in [BMI]-d_3.NTf$_2$ as the standard system, D/H exchange was detected at the imidazolium cation (Scheme 1). As commented above, the occurrence of a D/H exchange reaction at the imidazolium cation indicates the formation of NHCs in the reaction medium.

Moreover, these exchanges occurred only after the formation of the $[Ir(0)]_n$ NPs and cyclohexene conversion, suggesting that the D/H exchange process is probably catalysed by the metal NPs. Interestingly, the D/H exchange is more pronounced at the least acidic C4 and C5 imidazolium positions, indicating that the imidazolium cations react with the nanoparticle surface preferentially as aggregates of the type $\{[(DAI)_x(X)_{x-n}]^{n+}[(DAI)_{x-n}(X)_x]^{n-}\}_m$ (in which DAI is the 1,3-dialkylimidazolium cation and X is the anion) rather than as isolated cations. These NHC species attached on the metal surface may provide an enhanced stabilisation for transition-metal NPs embedded in imidazolium ILs. It is also quite probable that surface hydrogen species are also elements of the NP stabilisation for those prepared under hydrogen reduction akin to that observed for metal NPs prepared in organic solvents.[46–48] Importantly, this isotopic exchange was not observed for iridium large metal particles of around 600 nm in diameter.
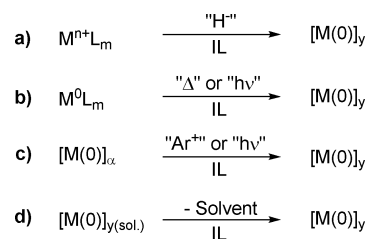
3. Synthesis of metal NPs in ILs

Soluble transition-metal NPs have been prepared in ILs mainly by the following methods: (a) simple reduction of M(I), M(II), M(III) or M(IV) compounds, (b) decomposition of the organometallic complexes in the formal zero oxidation state, (c) bombardment of bulk metal precursors with deposition onto the ILs and (d) phase transfer of pre-formed NPs in water or organic solvents to the IL (Scheme 2).

3.1 Reduction of metal precursors in ILs

The simple reduction of metal complexes or metal salts in ILs by chemical or electrochemical agents is the most investigated and used method for the generation of a plethora of "soluble" transition-metal NPs (Table 1). Indeed, this approach was the first used to prepare $[Ir(0)]_n$ NPs in ILs from the simple reduction of the organometallic precursor $[Ir(COD)Cl]_2$ by molecular hydrogen (4 atm, constant pressure) in BMI.PF$_6$[15] (entry 1, Table 1). After this first report, numerous other metal NPs (see Table 1) of different sizes and shapes (Fig. 7) were prepared similarly in various other ILs (Fig. 8).

Although it is not yet clear how the IL stabilises and may control the size and shape of the nanomaterials, particularly of NPs prepared in these media, it is clear that these aspects are intimately related to the nature of the metal precursor (section 3.1.1), type of reducing agent (section 3.1.2), type of the IL (section 3.1.3) and reaction conditions (temperature, metal precursor concentration and pressure).

3.1.1 Type of metal precursor. Notably, the nature of the metal precursor and reducing agent (see 3.1.2) is important because they generate by-products that can coordinate to the metal surface and thus act as extra-stabilisers or poisons and influence the properties (optical, magnetic and catalytic) of the metal NPs. This is particularly true in the case of halide metal precursors that generate halide anions that may strongly bind to the metal surface of the nanoparticle. There are basically two approaches for avoiding the presence of these species. First, metal precursors containing ligands that are or may be transformed in innocuous compounds can be employed. For example, Ag$_2$O in which the by-product is water (entry 47, Table 1), $[Ru(COD)(2-methylallyl)_2]$, which contains only hydrocarbon ligands that are easily reduced and transformed in innocuous saturated hydrocarbons (entries 31 and 32, Table 1), and $[Ir(COD)(MeCN)_2]BF_4$, which has a weak coordinating ligand (MeCN) and hydrocarbons associated with a non-coordinating counter-anion (entry 2, Table 1). Second, scavengers such as 1,8-*bis*(dimethylamino)naphthalene[45] and alkylimidazoles (Scheme 3) can be used.[67,68]

a) $M^{n+}L_m \xrightarrow[\text{IL}]{\text{"H"}} [M(0)]_y$

b) $M^0L_m \xrightarrow[\text{IL}]{\text{"}\Delta\text{" or "h}\nu\text{"}} [M(0)]_y$

c) $[M(0)]_\alpha \xrightarrow[\text{IL}]{\text{"Ar}^{+}\text{" or "h}\nu\text{"}} [M(0)]_y$

d) $[M(0)]_{y(sol.)} \xrightarrow[\text{IL}]{\text{- Solvent}} [M(0)]_y$

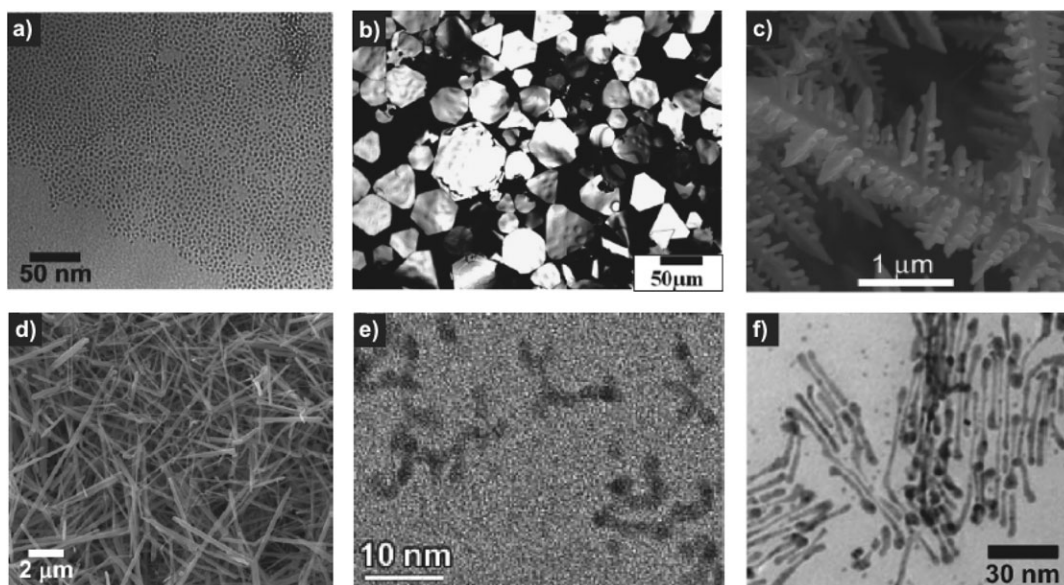**Scheme 2** General methods used to prepare metal NPs in ILs.

Fig. 7 Parts of TEM micrographs exemplifying transition-metal NPs exhibiting different shapes prepared from the reduction of metal precursors in ILs. (a) [Ru(0)]$_n$ nanospheres/[Ru(COD)(2-methylallyl)$_2$]/DMI.NTf$_2$/H$_2$;[61] (b) Au(0) prisms/[HAuCl$_4$·3H$_2$O]/BMI.NTf$_2$/imidazolium cation;[62] (c) Au(0) dendrites/[HAuCl$_4$·4H$_2$O]/BMI.PF$_6$/Zn foil;[63] (d) Ag(0) nanowires/[AgNO$_3$]/BMI.MeSO$_4$/ethyleneglycol;[64] (e) [Ir(0)]$_n$ nanoworms/[Ir(COD)$_2$]BF$_4$/DMI.BF$_4$/H$_2$;[65] (f) [Au(0)]$_n$ nanorods/[HAuCl$_4$]/ EMI.EtSO$_4$/ascorbic acid.[66]
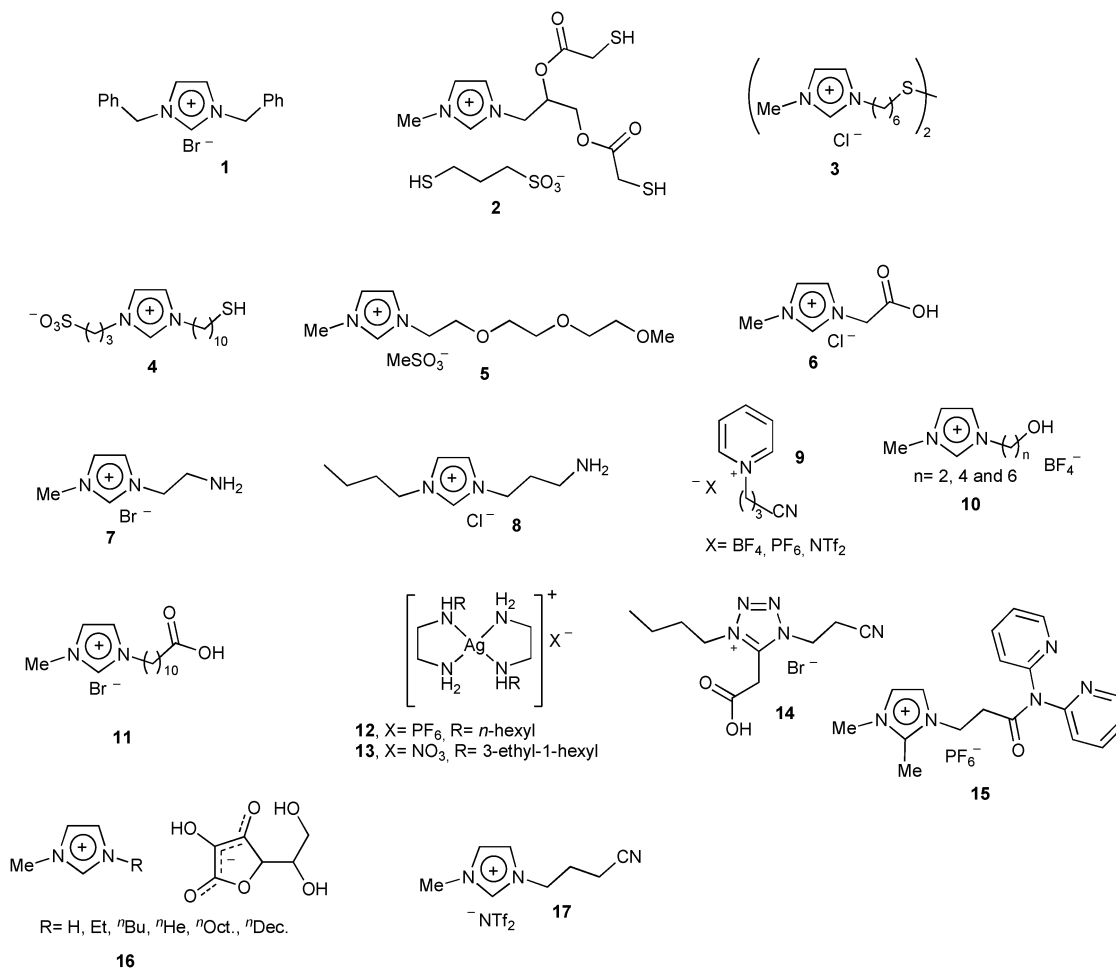
Fig. 8 ILs used in the preparation of NPs by reduction of metal compounds.

Table 1 Size of various metal NPs prepared by reduction of transition-metal compounds in ILs

Entry	IL	Metal precursor	Reducing agent	M(0) size (nm)[a]	Ref.
1	BMI.BF$_4$ BMI.PF$_6$ BMI.CF$_3$SO$_3$	[Ir(COD)Cl]$_2$	H$_2$	2.9 2.0 2.6	15,38,75,78,79
2	BMI.NTf$_2$ BMI.BF$_4$	[Ir(COD)(MeCN)$_2$]BF$_4$	H$_2$	2.1 3.6	45
3	EMI.EtSO$_4$	[Ir(COD)Cl]$_2$	H$_2$	1.6	43
4	BMI.BF$_4$	[HAuCl$_4$.4H$_2$O]	UV light	1–100 μm	80
5	BMI.NTf$_2$	[NaAuCl$_4$.2H$_2$O]	e$^-$	122 7.6[b]	81
6	BMI.NTf$_2$	[NaAuCl$_4$.2H$_2$O]	e$^-$ or γ-rays	26.4[c] 2.9[d] 10.7[e]	82
7	**1**	[AuCl$_3$]	Thiol	1.0–2.0	83
8	**2**	[HAuCl$_4$]	NaBH$_4$	2.0–3.5	84
9	**3**	[HAuCl$_4$]	NaBH$_4$	5.0	85
10	**4**	[HAuCl$_4$.4H$_2$O]	NaBH$_4$	2.4–2.7	86
11	**5**	[HAuCl$_4$.3H$_2$O]	Hydrazine	7.5[f]	58
12	**6**	[HAuCl$_4$]	NaBH$_4$	3.5	87
13	**7**	[HAuCl$_4$]	Trisodiumcitrate	23, 42, 98[g]	87
14	**8**	[HAuCl$_4$.3H$_2$O]	NaBH$_4$	33	88
15	**16**	[HAuCl$_4$.3H$_2$O]	Ascorbate	Various shapes and diameters[h]	89
16	BMI.PF$_6$ BMI.NTf$_2$	[HAuCl$_4$.3H$_2$O]	Imidazolium cation	Prismatic particles[i]	62
17	BMI.PF$_6$	[HAuCl$_4$.4H$_2$O]	Zn	Dendrites[j]	63
18	EMI.EtSO$_4$	[HAuCl$_4$]	Trisodiumcitrate NaBH$_4$[k] Ascorbic acid[l]	9.4 3.9 nanorods	66
19	BMI.PF$_6$	[HAuCl$_4$]	NaBH$_4$	3.7[m] 4.4	68
20	BMI.BF$_4$	[HAuCl$_4$.3H$_2$O]	Microwave	Nanosheets[n]	90
21	BMI.PF$_6$	[HAuCl$_4$.4H$_2$O]	Aniline	450[o]	91
22	BMI.PF$_6$	[HAuCl$_4$.4H$_2$O]	Copolymer	Large nanoplates[p]	92
23	BMI.BF$_4$	[Au(CO)Cl]	Thermal decomposition/reduction	1.8[q], 4.1[r] and 61[s]	93
24	BMI.BF$_4$	[KAuCl$_4$]	Thermal decomposition/reduction	1.1[q]	93
25	**2**	[Na$_2$Pt(OH)$_6$]	NaBH$_4$	2.0–3.2	84
26	**6**	[H$_2$PtCl$_6$]	NaBH$_4$	2.5	87
27	EMI.BF$_4$	[K$_2$PtCl$_4$]	Ascorbic acid	4.0	94
28	BMI.NTf$_2$	[Pt(acac)$_2$]	1,2-hexadecanediol	4.5[t]	95
29	BMI.BF$_4$ BMI.PF$_6$ BMI.BF$_4$	[PtO$_2$]	H$_2$	3.0 2.3 2.0	76
30	BMI.PF$_6$ BMI.CF$_3$SO$_3$ BMI.NTf$_2$	[RuO$_2$]	H$_2$	2.5 2.5 2.1	96
31	BMI.BF$_4$ DMI.NTf$_2$ DMI.BF$_4$	[Ru(COD)(2-methylallyl)$_2$]	H$_2$	2.9 2.1 2.7	61
32	**17**	[Ru(COD)(2-methylallyl)$_2$]	H$_2$	2.2	97
33	BMI.PF$_6$	[Pd(acac)$_2$]	H$_2$	4.9	40
34	BMI.PF$_6$	Palladacycle	Dimethylallene	1.7	98
35	BMI.PF$_6$	[Pd(COD)Cl$_2$]	H$_2$	6–8	99
36	BMI.PF$_6$	[PdCl$_2$]	H$_2$	7	99
37	BMI.PF$_6$	[PdCl$_2$]	H$_2$	12[f]	100
38	**9**	[12]$_2$[PdCl$_4$]	PhB(OH)$_2$	5.0	101
39	**10**	[PdCl$_2$]	**10**	150, 30 and 10[u]	102
40	**11**	[PdCl$_2$]	NaBH$_4$	10–30	103
41	**15**	[Pd(OAc)$_2$]	H$_2$	5–6	104,105
42	BMI.PF$_6$	[Pd(OAc)$_2$]	H$_2$	2–5[v]	106
43	BMP.NTf$_2$	[PdX$_4$]$^{2-}$	e$^-$	5–35[f,x]	107
44	BMI.Br or BMI.BF$_4$	[Pd(OAc)$_2$] or [PdCl$_2$]	IL/sonochemical[y]	1.0	108
45	BMI.PF$_6$ BPy.BF$_4$	[Pd(OAc)$_2$]	Probable ligand-assisted (AcO$^-$)	1.3 1.6	109
46	BMI.BF$_4$	[Ag(I)]	Chemical	20	50
47	BMI.BF$_4$ and others	[AgX] (X = BF$_4$, PF$_6$, OTf) or [Ag$_2$O]	H$_2$	2.8 to 26.1[z]	67
48	**13**	**13**	NaBH$_4$	5.7 to 8.3	110
49	**10**	[AgNO$_3$]	**10**	2.2	111
50	BMI.MeSO$_4$	[AgNO$_3$]	Ethylene glycol	15 μm nanowires	64
51	EMI.OTf	[AgOTf]	e$^-$	200[w]	112

Table 1 (*continued*)

Entry	IL	Metal precursor	Reducing agent	M(0) size (nm)[a]	Ref.
	EMI.OTf	[AgNO$_3$]			
52	BMI.OTf	[AgOTf]	e^{-aa}	20	113,114
	BMP.OTf				
53	BMI.BF$_4$	[AgBF$_4$]	e$^-$	Dendrites	115
54	BMI.NTf$_2$	[Ag(F$_3$-OAc)]	Probable ligand-assisted (F$_3$-AcO$^-$)	4.5^{bb}	95
55	BMI.BF$_4$	[AgClO$_4$.H$_2$O]	Photochemical^{cc}	8.9^{dd}	116
	OMI.BF$_4$			4.9^{dd}	
56	**14**	[InCl$_3$]	NaBH$_4$	20	117
57	BMI.PF$_6$	[RhCl$_3$.3H$_2$O]	H$_2$	2.3	78
58	BMI.PF$_6$	[RhCl$_3$.3H$_2$O]	NaBH$_4$	2.0^{ee}	49,118
	HEA.NTf$_2$			3.0^{ee}	
59	BMI.BF$_4$	[RhCl$_3$.nH$_2$O]	H$_2$	5.0	119
60	BMI.PF$_6$	[Rh(COD)Cl]$_2$	H$_2$	15^f	100
61	BMI.PF$_6$	[CuCl]	e$^-$	10	120
62	BMP.NTf$_2$	[Cu(I)] from a copper	e$^-$	26^{ff}	121
	EMI.NTf$_2$	wire		11^{ff}	
63	BMI.BF$_4$	[Cu(NO$_3$)$_2$]	Carbon^{gg}	100^{hh}	122
64	BMI.BF$_4$	[Ni(NO$_3$)$_2$]	Carbon^{gg}	100^{hh}	122
65	BMI.PF$_6$	[K$_2$PdCl$_4$] and [HAuCl$_4$] (3/1)	NaBH$_4$	3.0^{m,ii} 6.0^{ii}	68
66	BMI.OTf	[K$_2$PdCl$_4$] and [HAuCl$_4$] (3/1)	NaBH$_4$	4.9^{ii}	68
67	BMI.NTf$_2$	[Pt(acac)$_2$] and [Co(acac)$_3$] (0.5/1.5)	Probable ligand-assisted (acac$^-$)	8.0^{ii,jj}	123
		[Pt(acac)$_2$] and [Co(acac)$_3$] (10/3.3 or 3.3/3.3)		5.0^{ii,kk}	
68	EMI.BF$_4$	[Pt(acac)$_2$] and [Fe(CO)$_5$] (1/2 molar ratio)	1,2-hexadecanediol	4.3^{ii}	124
	BMP.OTf			2.4^{ii}	
69	BMI.Cl	[FeCl$_3$.6H$_2$O]	NaBH$_4$	50^{ll}	125
	BMI.Br			50^{ll}	
	BMI.PF$_6$			20^{mm}	
	OMI.BF$_4$			20^{nn}	

^{a} Determined by TEM; ^{b} Electron beam irradiation at 6 kGy; ^{c} Electron beam irradiation at 20 kGy; ^{d} γ-Ray irradiation at 6 kGy; ^{e} γ-Ray irradiation at 20 kGy; ^{f} Determined by XRD; ^{g} Depends on citrate concentration; ^{h} Various particle morphologies can form, such as quasi-spherical, raspberry-like, flakes or dendritic depending of the N-alkylimidazolium side chain; ^{i} Broad size range of 3–20 μm in diameter and 10–400 nm in thickness in BMI.PF$_6$ whereas uniform, single-crystal nano- and microprisms with a size of about 100 μm in BMI.NTf$_2$; ^{j} Dendritic gold nanostructures with a three-order hierarchy resulting from fractal growth; ^{k} In the presence of trisodium citrate and cetyltrimethylammonium bromide (CTAB); ^{l} In the presence of AgNO$_3$ and gold spherical nanoseeds; ^{m} In the presence of n-butylimidazole or methylimidazole as the scavenger and extra-stabilising ligand; ^{n} Nanosheets with a size larger than 30 μm in length and thickness of about 50 nm; ^{o} Polyaniline/Au particles were formed (biphasic medium: IL/water); ^{p} P123(45%)–IL–HAuCl$_4$(0.03 M) aqueous solution (small amounts of gold nanobelts were observed from sample P123(45%)–IL(10%)–HAuCl$_4$(0.015 M) after 45 days); ^{q} Only thermal treatment (in the presence of n-butylimidazole); ^{r} Microwave-assisted for 5 min (in the presence of n-butylimidazole); ^{s} Photocatalytic-assisted for 3 min (in the presence of n-butylimidazole); ^{t} In the presence of oleic acid and oleylamine; ^{u} Depends on IL; ^{v} Phenanthroline was used as an extra-stabiliser ligand; ^{x} Depends on the reaction temperature; ^{y} Pd-biscarbene complex was firstly formed with a subsequent sonolytic conversion to Pd metal zero-valent species; ^{z} Depends on IL, silver precursor and the presence of a scavenger; ^{w} Nanowires 3 μm in length; ^{aa} By plasma-electrochemical deposition; ^{bb} Silver trifluoroacetate/oleic acid molar ratio of 1:6; ^{cc} Benzoin was used as photoactivator for metal NPs formation; ^{dd} Silver metal NPs prepared in water-in-IL microemulsions; ^{ee} Bipy/THF was used as an extra-stabiliser ligand; ^{ff} Particles are partly oxidised leading to a CuO shell; ^{gg} Carbon from the IL due to microwave heating; ^{hh} Copper and nickel NPs are coated with an amorphous carbon layer on their surface; ^{ii} Bimetallic NPs were formed; ^{jj} Nanorods with an average atom ratio of Pt$_{39}$Co$_{61}$ (in the presence of CTAB); ^{kk} NPs with an average atom ratio of Pt$_{78}$Co$_{22}$ (Pt/Co = 10/3.3 molar ratio) and Pt$_{65}$Co$_{35}$ (Pt/Co = 1 molar ratio) (in the presence of CTAB); ^{ll} Roughly spherical or chain-like morphology particles with 50 nm in diameter and 600 nm in length (IL/[FeCl$_3$.6H$_2$O] molar ratio = 1:5); ^{mm} Spherical NPs (IL/[FeCl$_3$.6H$_2$O] molar ratio = 1:2); ^{nn} Spherical NPs organised into chain-like aggregates (IL/[FeCl$_3$.6H$_2$O] molar ratio = 1:3). BMP = 1-n-butyl-1-methylpyrrolidinium; HEA = N,N-dimethyl-N-dodecyl-N-(2-hydroxyethyl) ammonium; F$_3$-AcO$^-$ = trifluoroacetate.

Notably, metal NPs with larger diameters and size distributions as well as lower stabilities were obtained in the absence of n-butylimidazole (see for example entries 19 and 47, Table 1). These results are strong indications that the n-butylimidazole is acting also as an extra-stabilising ligand through bonding to the Ag[67] and Au[68] surfaces.[69]

Moreover, even very weak bases can easily deprotonate the imidazolium cation, thereby providing NHCs as extra ligands in the reaction medium.[70] The extra strong stabilisation of the metal NPs provided by the *in situ* formed NHCs was claimed to be responsible for the catalytic inhibition of [Ir(0)]$_n$ NPs in the hydrogenation of ketones in ILs.[71] Although the presence of NHCs was also detected in the case of [Ir(0)]$_n$ NPs in ILs, no significant influence on the olefin hydrogenation catalytic activity was observed.[44]

The solubility of the metal precursor also influences the size, shape and properties of the metal NPs. Indeed, well-defined monometallic and IL-soluble metal complexes when reduced by molecular hydrogen have a strong tendency to follow the autocatalytic mechanism developed by Finke and co-workers.[72,73]
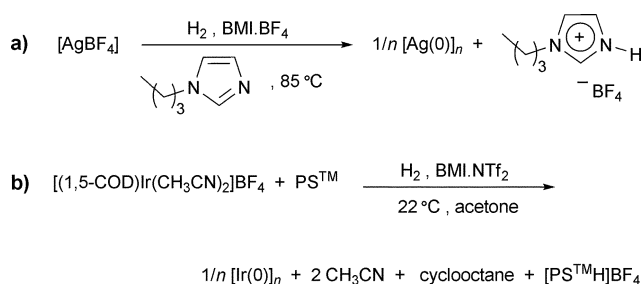
Scheme 3 Examples of NP formation in the presence of scavengers such as (a) *n*-butylimidazole and (b) 1,8-*bis*(dimethylamino)-naphthalene.

Fig. 9 Simplified representation of the polar and non-polar nano-domains of imidazolium ILs in which neutral and ionic metal NP precursors may dissolve preferentially.

This mechanism basically involves two steps: nucleation and surface growth. Furthermore, in a more recent mechanistic study of transition-metal NP formation and agglomeration,[72] two types of agglomeration were identified, namely bimolecular agglomeration of NPs and a new autocatalytic agglomeration of NPs with larger agglomerated NPs and/or bulk metal (four-step mechanism).[73,74] This four-step kinetic system can be used to check for the involvement (in ILs) of large agglomerates/bulk metal as part of the catalytic active species in hydrogenation reactions. If the curves only fit with the four-step mechanism, techniques other than transmission electron microscopy (TEM) should be used to detect the presence or absence of agglomerates/bulk metal in the system. Indeed, the direct application of the double autocatalytic mechanism could be used to explain the formation of $[Ir(0)]_n$ NPs in ILs.[38,75] However, this mechanism was not appropriate for the $[Pt(0)]_n$ NPs *via* $[PtO_2]$ reduction in imidazolium ILs because of the non-homogeneity and solubility of the metal precursor (platinum oxide has a "polymeric" structure) in the IL and mass transfer limitations associated with the substrate and hydrogen.[76] Moreover, the very low solubility of the metal precursors, such as $[PdCl_2]_n$, Ag_2O (see Table 1, entries 36, 37, 39, 40 and 47), usually led to a very broad size distribution and different shapes (usually difficult to reproduce) since the precursors are heterogeneously distributed in the media.

Interestingly, imidazolium ILs may provide hydrophobic or hydrophilic regions (polar and non-polar regions),[28–30] the nature of the metal precursor—ionic or neutral for instance—is also a key determinant of the size and shape of the prepared metal NPs since these compounds may concentrate in the polar or non-polar regions of the IL. In such cases, the nanoparticle growth process is probably controlled by the local concentration of the precursor and consequently limited to the size and shape of the IL polar or non-polar domains (see Fig. 3 and 9). In the case of imidazolium ILs associated with the same anion, the volume of the ionic nano-region is almost the same regardless of the nature of the imidazolium alkyl side chains. By contrast, the size of the non-polar region can be modulated by the length of the *N*-alkyl side chains, such as in BMI.X and DMI.X ILs (DMI = 1-*n*-decyl-3-methylimidazolium).

For example, the ionic precursor $[Ir(COD)_2]BF_4$ is preferentially solvated in the ionic nano-region (populated by aggregates of the imidazolium cations and tetrafluoroborate anions), rathe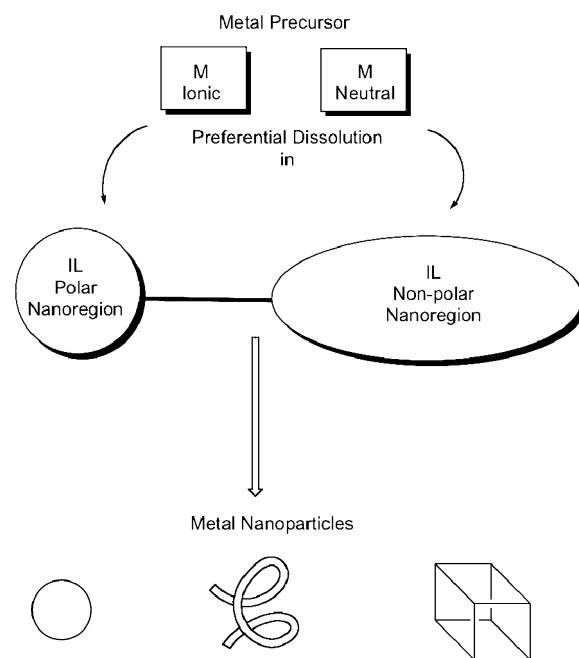r than the aliphatic side chains of the imidazolium cation (for instance, *n*-butyl or *n*-decyl), and the reduction and nanoparticle growth occurs in this "polar" nano-region.[77] Consequently, the size of the NPs is probably controlled by the space determined by this "Coulombic" region. Since this nano-region has almost the same volume in both ILs (they have the same anion), the generated NPs should have the same size using the cationic Ir(I) precursor. As expected, this was observed (see Table 2).

However, the neutral precursor $[Ir(COD)Cl]_2$ tends to be concentrated in the less polar nano-region. Therefore, larger nano-sized particles should be formed in DMI.BF$_4$, which has a higher concentration of the metal precursor. Indeed, NPs of 3.6 ± 0.9 nm were observed in DMI.BF$_4$, whereas smaller, irregular spherical NPs of 2.5 ± 0.5 nm were formed in BMI.BF$_4$ (Table 2).[126] This nano-region dissolution effect was elegantly demonstrated in the case of the decomposition of $[Ru(COD)(COT)]$ in imidazolium ILs by molecular hydrogen[127] (see section 3.2). In particular, a relationship between the size of IL non-polar domains calculated by molecular dynamics simulation and the Ru nanoparticle size measured by TEM was demonstrated. Therefore, the phenomenon of nanoparticle growth is probably controlled by the local concentration of $[Ru(COD)(COT)]$ and consequently limited to the size of the non-polar domains.[128] Similarly, the volume

Table 2 Size^a (nm) of $[Ir(0)]_n$ NPs prepared in ILs that possess different non-polar volume domains (DMI.BF$_4$, and BMI.BF$_4$) using neutral and ionic Ir(I) organometallic precursors

Entry	IL	$[Ir(COD)Cl]_2$	$[Ir(COD)_2]BF_4$
1	BMI.BF$_4$	2.5 ± 0.5	1.9 ± 0.4
2	DMI.BF$_4$	3.6 ± 0.9	1.9 ± 0.4

^{a} Determined by TEM.

of the polar domains of the imidazolium ILs may be controlled by changing the size of the anions. The silver NPs obtained by hydrogen reduction of silver salts (AgX, X = BF$_4$, PF$_6$, OTf) dissolved in ILs and in the presence of n-butylimidazole have a narrow size distribution in the diameter range of 2.8–26.1 nm (entry 47, Table 1), which increases linearly with the molecular volume of the IL anion,[67] or more likely of the anionic aggregates. In contrast, the size of Fe(0) NPs prepared by NaBH$_4$ reduction of FeCl$_3$ in BMI.X (X = Cl, Br, BF$_4$ and PF$_6$) ILs decreases linearly with the augmentation the anion volume (entry 69, Table 1).[125] Note that in this case the NPs size increases with the decrease of the anion coordination ability.

Notably, the metal precursor itself can be an IL, such as those based on Ag(I) associated with N-containing ligands that under reductive conditions produces [Ag(0)]$_n$ NPs.[110] For example, starting from the salts of the type [bis(alkylethylenediamine)silver(I)], it is possible to prepare [Ag(0)]$_n$ NPs from their own IL. The treatment of silver(I) IL [Ag(eth-hex-en)$_2$]NO$_3$ (eth-hex-en = ethylhexene-ethylenediamine) with aqueous NaBH$_4$ yielded well-dispersed NPs (entry 48 in Table 1 and Scheme 4). In contrast, the same procedure with [Ag(hex-en)$_2$]PF$_6$ did not provide soluble metal NPs, and only a silver precipitate was observed instead. These results can be explained by the stabilising ability of the ligands to avoid [Ag(0)]$_n$ NP aggregation in each silver(I) complex. This procedure for NP preparation from a silver complex where the complex is a metal provider and a particle protector was published previously by Imae and co-workers.[129]

3.1.2 Reducing agents. Irradiation or the use of chemicals such as molecular hydrogen or hydrides are the most frequently used methods for the reduction of metal compounds in ILs.

The most clean reducing methods are electrochemical- and irradiation-induced since they do not generate by-products other than those originating from the metal precursor in the medium. Radical species are involved in most irradiation-induced metal reduction methods in ILs. For example, anisotropic large gold particles were prepared by photo-induced (UV light) reduction of the [HAuCl$_4$.4H$_2$O] precursor dissolved in a solution of BMI.BF$_4$/acetone (entry 4, Table 1). Different reaction conditions, such as time and concentration of reagents, can affect the metal particle morphology and size. A mechanism involving the radical species was proposed to explain the growth of these large

Au(0) particles, which could reach 1–100 μm in size depending on the reaction conditions.[80] The reducing agent is probably a Me$_2$COH radical formed from the hydrogen atom abstraction of the imidazolium cation by acetone in its excited state, induced by UV light. It is also quite probable that radical intermediates (such as radicals of the imidazolium species) generated by the solvated electrons may be involved in the growth of [Au(0)]$_n$ NPs prepared using the electron beam irradiation technique. The reduction of an Au(III) precursor dissolved in the IL is induced by a low-energy electron beam irradiation to furnish large and well-dispersed metal gold NPs around 122 nm in size (entry 5, Table 1).[81] Radical species are also involved in a system containing thiol, organic solvent and 1,3-dibenzylimidazolium halide IL (in the absence of other common reducing agents, such as hydrogen or boron hydride) to prepare gold NPs 1–2 nm in size from the [AuCl$_3$] precursor (entry 7, Table 1). The radical pathway probably begins with the carbene formation of the IL and coordination to the gold cations.[83] The thiol further reduces the gold complex to Au(0) and releases benzylimidazole, which plays a very important role as the NP surface ligand, akin to the use of alkylimidazole as a scavenger and extra stabilising surface ligand[67,68] leading to the formation of well-dispersed and stable [Au(0)]$_n$ NPs (Scheme 5).
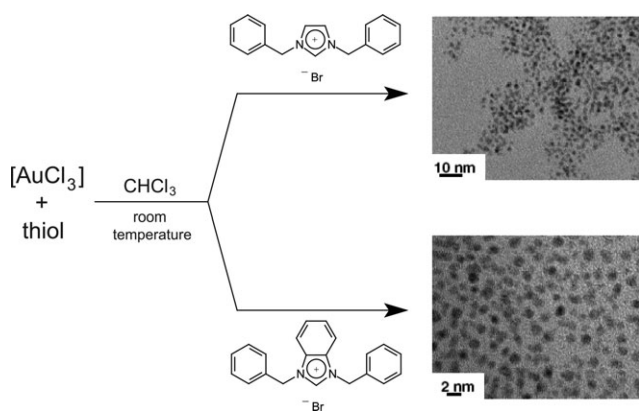
Together with molecular hydrogen, hydrides (mainly NaBH$_4$) are the most frequently used reducing agents for the generation of metal NPs (Scheme 6). However, hydride sources are not likely to be used in ILs, due their basic character, to deprotonate the imidazolium cation and generate carbenes that may bind to metal surface (akin to the classical monometallic coordination chemistry). This reducing agent produces various by-products, such as Na and B compounds, that are difficult to remove from the IL.

However, it is quite interesting to note that, except in one case with IL **8** (entry 14, Table 1), the reduction of Au(III) precursors in ILs by NaBH$_4$ (entries 8–10, 12, 18 and 19, Table 1) generates irregularly spherical-shaped gold nanoparticles with diameters of 2–5 nm, regardless of the IL. These results are probably related to the strong reducing power of NaBH$_4$, which rapidly transforms all of the Au(III) precursors into Au(0). In turn, Au(0) aggregates into thermodynamic local minima to size and shape the gold NPs.
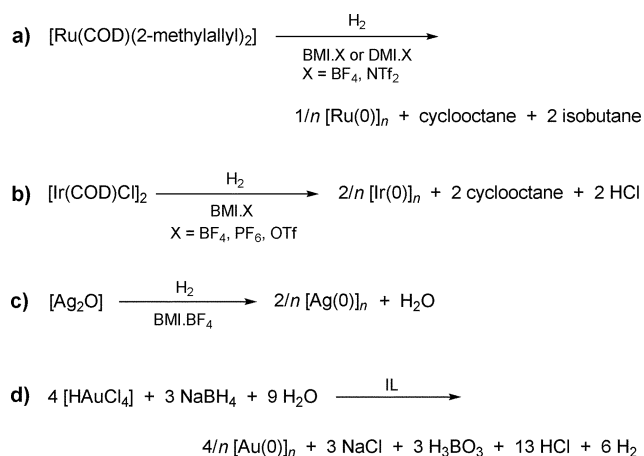
Silver NPs around 20 nm in diameter (entry 46, Table 1) were also obtained under reducing conditions in BMI.BF$_4$.[50]
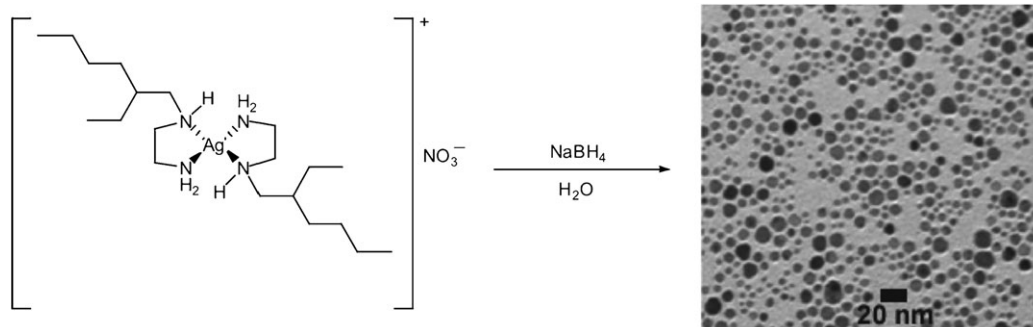
Scheme 4 Silver NPs (8.3 ± 0.3 nm in diameter) prepared from their own IL system. (Figure adapted from ref. 110).

This journal is © The Royal Society of Chemistry 2010

Chem. Soc. Rev., 2010, **39**, 1780–1804 | 1789

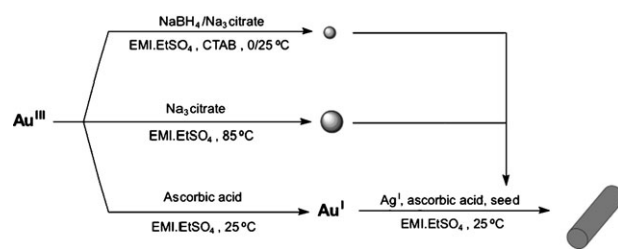**Scheme 5** ILs and thiol as the reducing agent for $[Au(0)]_n$ NP formation under mild reaction conditions. (Scheme adapted from ref. 83).

a) $[Ru(COD)(2\text{-methylallyl})_2]$ $\xrightarrow[\substack{\text{BMI.X or DMI.X} \\ X = BF_4, NTf_2}]{H_2}$

$1/n\ [Ru(0)]_n + \text{cyclooctane} + 2\ \text{isobutane}$

b) $[Ir(COD)Cl]_2$ $\xrightarrow[\substack{\text{BMI.X} \\ X = BF_4, PF_6, OTf}]{H_2}$ $2/n\ [Ir(0)]_n + 2\ \text{cyclooctane} + 2\ HCl$

c) $[Ag_2O]$ $\xrightarrow[\text{BMI.BF}_4]{H_2}$ $2/n\ [Ag(0)]_n + H_2O$

d) $4\ [HAuCl_4] + 3\ NaBH_4 + 9\ H_2O$ $\xrightarrow{IL}$

$4/n\ [Au(0)]_n + 3\ NaCl + 3\ H_3BO_3 + 13\ HCl + 6\ H_2$

Scheme 6 Examples of metal NP syntheses in ILs using molecular hydrogen and sodium borohydride as reducing agents.

Alternatively, hydrazine monohydrate has been used as the reducing agent to prepare $[Au(0)]_n$ NPs from the $[HAuCl_4 \cdot 3H_2O]$ precursor in an ether-functionalised IL (IL **5**) (entry 11, Table 1). Notably, only innocuous by-products are formed using this strong reducing agent that generate almost instantaneously the gold NPs in the IL.[58] The use of more gentle reducing agents is useful for controlling the size and shape of the metal NPs. Indeed, under conditions of decelerated particle growth (by use of weak reducing agents), the stabilisation of nanocrystals may be facilitated by the weak coordination ability of unmodified imidazolium ILs. This was nicely demonstrated by the formation of various shaped and sized gold nanostructures from the reduction of Au(III) by soft reducing agents: ascorbate and/or citrate in ILs (entries 13, 15 and 18, Table 1).[66,87,89] It was proposed that the size and shape of the NPs is dictated by the preferential binding affinity of the imidazolium cations to low-density gold crystal facets when weak reducing agents are being used for particle growth.[66] In each step, the size and shape of the prepared gold nanostructures were modulated by the nature of the reducing agent (Scheme 7).

Molecular hydrogen is a relatively mild reducing agent and may produce acid as its sole by-product, which can be then trapped with scavengers, such as alkylimidazoles (Scheme 3).[67,68] Its consumption can be used as a probe to monitor the NP formation, but mass transfer problems are usually present due to its very low solubility in ILs.[130–132] Notably, metal NPs can be prepared *in situ* in ILs with hydrogen. The resultant NPs can then be used without purification or isolation for hydrogen reactions. For example, metal ruthenium NPs were efficiently generated from the reduction of the Ru(II) precursor $[Ru(COD)(2\text{-methylallyl})_2]$ by molecular hydrogen in several imidazolium ILs under mild conditions (entry 31, Table 1).[61] Depending on the type of IL (cation and anion), the reduction time to obtain $[Ru(0)]_n$ NPs varied significantly and their separation from the IL phase could not be achieved in some cases. However, the IL/Ru NPs could be used directly for the hydrogenation of alkenes and arenes.

In some cases, the IL itself can carry the reducing agent, such as hydroxylated imidazolium salts **10**; depending on the redox potential of the metal precursor, the imidazolium cation can undergo the oxidation process (Scheme 8). For example, metal silver NPs have been prepared using hydroxylated ILs **10**, namely 1-(2-hydroxyethyl)-3-methyl-imidazolium tetrafluoroborate and 1-(2′-hydroxyethyl)-2-methyl-3-dodecylimidazolium chloride (entry 49 in Table 1 and Scheme 8).[111] In the case of Au(III), the imidazolium cation itself can act as a reducing agent to yield prismatic particles in BMI.PF$_6$ with a very broad size range of 3–20 μm in diameter and 10–400 nm in thickness (entry 16 in Table 1 and Scheme 8).

However, in BMI.NTf$_2$, single-crystal nano- and micro-prisms with larger sizes of about 100 μm in diameter were prepared.[62]

Electrochemical reductions of metal compounds in ILs are likely the cleanest methods for preparing metal NPs since only

Scheme 7 Synthesis of gold nanorods using ILs as the shape-regulating medium. (Scheme adapted from ref. 66).

a) $HAuCl_4 + $ [imidazolium-butyl PF$_6$] $\xrightarrow{H_2O}$ $1/n\ [Au(0)]_n + HCl + $ [oxidized imidazolium PF$_6$]

b) $2\ AgNO_3 + $ [hydroxyethyl imidazolium BF$_4$] $\xrightarrow{H_2O}$ $2/n\ [Ag(0)]_n + $ [aldehyde imidazolium BF$_4$] $+ 2\ HNO_3$
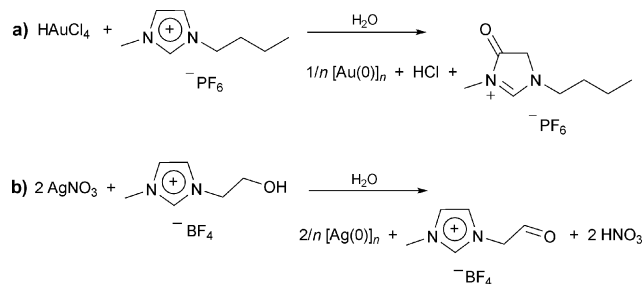
Scheme 8 Preparation of metal NPs using (a) the imidazolium cation of the IL and (b) the hydroxyl group attached on the imidazolium cation as reducing agents.
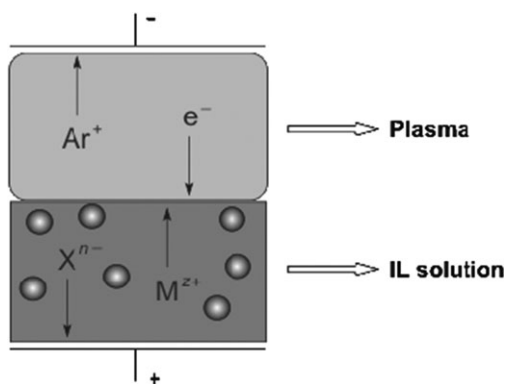
Fig. 10 Plasma-electrochemical reduction of a metal precursor in IL. (Figure adapted from ref. 113).

electrons are involved. Indeed, isolated, dispersed silver NPs with an average diameter of 20 nm can be deposited on the surface of BMI.OTf IL by electrochemical reduction of Ag(I) salts with free electrons from a low-temperature plasma (Fig. 10 and entry 52, Table 1).[113,114] Moreover, nanocrystalline silver films and nanowires in EMI.OTf have been prepared in a similar manner by electroreduction of [AgOTf] (entry 51, Table 1).[112]

Interestingly, a specifically designed electrochemical cell has been developed to observe electrochemical metal deposition from IL in real time by scanning electron microscopy (SEM).

The cell was successfully employed for the deposition of silver from BMI.NTf$_2$ containing [AgNTf$_2$]. This process yielded growth of granular and dendritic forms of Ag deposits.[133] This procedure, which is directly performed in the ultra high vacuum chamber of a SEM apparatus, has also been used for electron beam-induced Ag deposition from the BMI.BF$_4$ IL containing [AgBF$_4$] on anatase TiO$_2$ surfaces (entry 53 in Table 1 and Fig. 11).[115] Because Ag deposition occurs in anatase TiO$_2$ and not with Au and amorphous TiO$_2$, which are not photosensitive, it was proposed that the deposition mechanism is of a pseudo-photocatalytic nature.

3.1.3 Nature of the IL and extra-stabilising ligands. One of the key factors in the preparation of the metal NPs is the purity of the ILs, especially the halides and water content. Indeed, these impurities may dramatically change the physico-chemical properties of the ILs.[134,135] In addition, these impurities may act as an extra ligand and/or change the kinetics of the
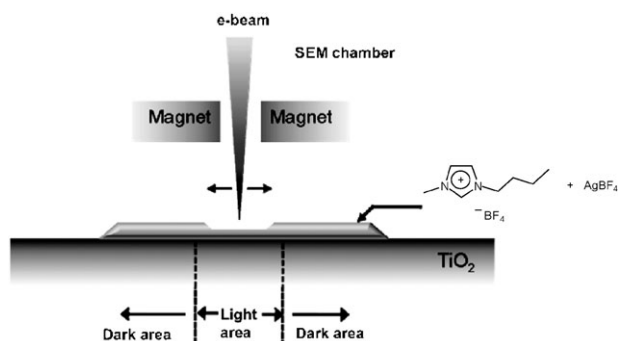
Fig. 11 Electrochemical deposition of silver from IL on anatase TiO$_2$ surface, as observed by SEM. (Figure adapted from ref. 115).

NP formation. For example, the size of [Ir(0)]$_n$ NPs depends upon the level of chloride and water contamination of the BMI.BF$_4$ IL (Table 3).

In particular, the presence of water in ILs containing hydrolysable anions, such as BF$_4$ and PF$_6$, causes the formation of several by-products that may have detrimental effects on the formation of metal NPs.[15,136]

To increase the stability of the metal NPs in ILs, extra ligands were used or ILs containing organic functions that can bind more effectively with the metal surface have been used (Fig. 12).

Indeed, transition-metal NPs have also been synthesised in several functionalised ILs *via* chemical reduction of metal precursors. Different groups, such as thiols, amines, carboxylic acids and ethers (example ILs are in Fig. 8), could be attached on the cation and/or anion of IL, thereby providing additional stabilisation of the NPs due to its coordination on the metal surface.

For example, stable metal palladium NPs with diameters of 2–5 nm were obtained from the hydrogen reduction of [Pd(OAc)$_2$] in BMI.PF$_6$ followed by addition of phenanthroline (entry 42, Table 1).[106] The phenanthroline binds to the metal surface akin to the interaction observed with classical giant Pd clusters,[137,138] giving extra stabilisation to NPs without impairing its catalytic activity for hydrogenation reactions under multiphase conditions. Using the same approach, stable bipyridine [Rh(0)]$_n$ NPs with diameters of around 2 nm in BMI.PF$_6$ were prepared and used as arene hydrogenation catalysts (entry 58, Table 1).[49,118] Recently, an imidazolium-monofunctionalised bipyridine ligand was also used as an efficient extra protective agent for [Rh(0)]$_n$ NPs synthesised in BMI.PF$_6$.[139] Similarly, stable and well-dispersed [Pd(0)]$_n$ NPs with mean diameters of 5–6 nm were prepared in 2,2′-dipyridylamine-functionalised imidazolium IL (entry 41, Table 1).[104] Notably, the arene moieties present in the media may also be an extra source of NP stabilisation, similar to that observed in classical organic solvents (Fig. 12).[140]

Not surprisingly, although thiols are one of the most frequently used stabilising agents for water- or classical organic solvent–soluble gold NPs, they are also widely employed for the stabilisation of gold NPs in ILs. In most cases, the synthesis of [Au(0)]$_n$ NPs are performed in thiol-functionalised ILs, such as **2–4** (Fig. 8). The typical reduction of [HAuCl$_4$] with NaBH$_4$ in 3,3′-[disulfanyl-*bis*-(hexane-1,6-diyl)]-*bis*(1-methyl-1*H*-imidazol-3-ium)dichloride produces metal NPs with diameters of 5 nm (entry 9, Table 1).[85] These Au NPs could be used as optical sensors of anions in water *via* a particle aggregation process. Similarly, stable [Au(0)]$_n$ NPs have been prepared in a zwitterionic imidazolium sulfonate-terminated thiol IL (zwitter IL **4**).[86]

Table 3 Influence of chloride and water impurities in BMI.BF$_4$ on the size of the [Ir(0)]$_n$ NPs prepared by hydrogen reduction of [Ir(COD)(MeCN)$_2$]BF$_4$[45]

Entry	Water (wt%)	Chloride (ppm)	Size by TEM (nm)
1	0.19896	228	2.5 ± 0.8
2	0.050387	228	2.8 ± 0.7
3	0.006854	12.6	3.6 ± 0.9

This journal is © The Royal Society of Chemistry 2010

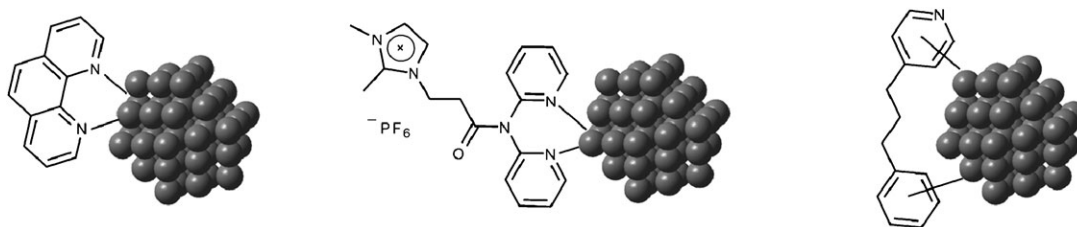*Chem. Soc. Rev.*, 2010, **39**, 1780–1804 | 1791

Fig. 12 Simplified representation of coordination of bipyridine/dipyridylamine moiety (σ interaction) or py/arene (π–π interaction) ligands onto the surface of metal NPs in ILs.

The chemical reduction of $[HAuCl_4 \cdot 4H_2O]$ by $NaBH_4$ in the presence of zwitter IL **4** in MeOH yielded well-dispersed capped zwitter-$[Au(0)]_n$ NPs (entry 10 in Table 1 and Fig. 13). These NPs were insoluble in water and common polar and non-polar organic solvents, such as MeOH, acetone, DMSO, THF, *n*-hexane, benzene and $CHCl_3$. However, they also presented good stability in aqueous solutions of different electrolytes, proteins and ILs. The mean diameters of the capped zwitter-$[Au(0)]_n$ NPs re-dispersed in some aqueous electrolytes were in the range 2.4–2.7 nm.

Aqueous thiol-functionalised ILs have been employed successfully to produce $[Au(0)]_n$ and $[Pt(0)]_n$ NPs.[84] Several ILs similar to **2**, containing a thiol moiety at different places at the cation and/or at the anion, were tested in the reduction of $[HAuCl_4]$ and $[Na_2Pt(OH)_6]$ with sodium borohydride in water (entries 8 and 25, Table 1). It was suggested that the metal NP size is dependent on the number and position of thiol group in the IL structure. The diameter of the NPs decreased as the number of thiol groups increased in the cation and the diameter also decreased when a sulfite anion with a thiol group was adopted. Moreover, these metal NPs were stable after re-dispersion in water, indicating that the IL produces a protective layer surrounding the NPs to prevent their aggregation. ^{1}H NMR analysis also revealed the interaction of the IL (through the thiol group) and the NP surface. Notably, the NPs apparently do not present significant plasmon absorption due to their very small size. However, it is possible that the thiol and imidazolium cation are strongly coordinated to the metal surface, thereby causing a negating effect on the plasmon absorption.

The nature of the IL anion, including both electronic and steric properties, is one of the key factors determining the size and shape of the nanostructures. Electronically, the coordination strength of the anionic aggregates for small NPs (<10 nm) is a key factor, whereas the coordination strength of cationic aggregates is most significant for larger NPs. For example, cubic NPs and octahedral particles were observed in BMI.Cl and BMI.Br, respectively, from $[AgNO_3]$ and ethylene glycol. However, for ILs with the $MeSO_4$ anion independent of the cation, silver nanowires of up to about 15 μm were preferentially produced, indicating a strong anion effect due to its single coordination ability in the metal surface precursor, and thus leading to different types of nanostructures (entry 50, Table 1).[64] The XRD, TEM and SAXS analyses revealed that isolated $[Ir(0)]_n$ NPs of 2–3 nm in mean diameter were formed from the hydrogen reduction of $[Ir(COD)Cl]_2$ in all cases, regardless of the type of ionic liquid anion; however, slightly larger nanoparticles were obtained in the IL containing the weaker coordinating anion (BF_4).[38]
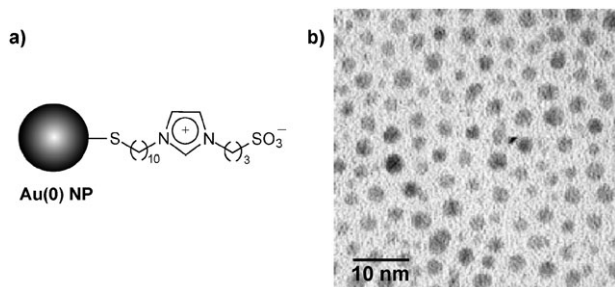
Amino-functionalised ILs, such as **7** and **8**, have also been reported to be effective stabiliser agents for $[Au(0)]_n$ NP formation (entries 13 and 14, Table 1).[87,88] In addition, NPs were efficiently synthesised in carboxyl-functionalised ILs. As expected, the IL interacts with the NP surface by coordination of the carboxyl group (entry 40, Table 1).[103] In the same context, the synthesis of $[Au(0)]_n$ and $[Pt(0)]_n$ NPs in carboxyl-functionalised ILs was also performed.[87] In this case, particularly for IL **6**, gold and platinum NPs were prepared using a typical reduction method with sodium borohydride and the precursors $[HAuCl_4]$ and $[H_2PtCl_6]$, respectively (entries 12 and 26, Table 1). Furthermore, $NaBH_4$ (methanolic solution) has also been used for the reduction of $[InCl_3]$ in IL **14** at 70 °C to generate large $[In(0)]_n$ NPs with mean diameters of around 20 nm (entry 56, Table 1).[117]

3.2 Decomposition of metal complexes in ILs

The simple decomposition of metal compounds in their formal zero oxidation states is an additional method to prepare metal NPs in ILs. For example, the controlled decomposition of the complex $[Pt_2(dba)_3]$ (dba = dibenzylideneacetone) with hydrogen (4 atm) in BMI.PF$_6$ leads to stable and isolable platinum NPs with diameters of 2.0–2.5 nm (entry 1 in Table 4 and Fig. 14).[141]

Ruthenium NPs have also been prepared in ILs[41] using a controlled decomposition method developed previously.[142,143] The treatment of $[Ru(COD)(COT)]$ in BMI.PF$_6$, BMI.BF$_4$ or BMI.CF$_3SO_3$ with molecular hydrogen (4 atm) at 75 °C efficiently produces $[Ru(0)]_n$ NPs. The TEM analysis shows the formation of spherical superstructures of Ru particles with diameters of 57 ± 8 nm. Inside these superstructures, $[Ru(0)]_n$ NPs with diameters of 2.6 ± 0.4 nm were observed (entry 2 in Table 4 and Fig. 14).
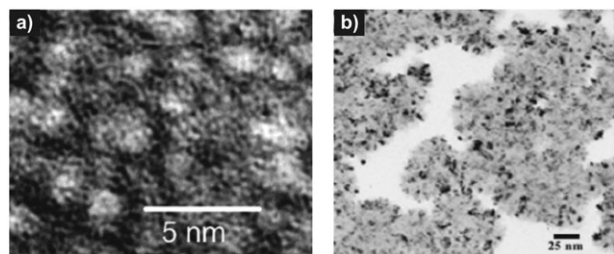

Fig. 13 (a) Zwitter-$[Au(0)]_n$ NPs synthesised in the zwitterionic IL and (b) a selected TEM micrograph of these NPs re-dispersed in an aqueous solution of NaCl. (Figure adapted from ref. 86).

Fig. 14 Selected TEM micrographs of (a) $[Pt(0)]_n$ NPs (2.0–2.5 nm) (negative image, under focus) in $BMI.PF_6$ showing the contrast density fluctuation around the metal NPs and (b) the $[Ru(0)]_n$ NPs (2.6 ± 0.4 nm) inside the Ru superstructures dispersed in $BMI.PF_6$. (Figure adapted from ref. 41,141).

Interestingly, as recently reported by Chaudret and co-workers,[127] the size of $[Ru(0)]_n$ NPs synthesised from the precursor [Ru(COD)(COT)] dissolved in ILs varies between 0–25 °C. Lower temperatures (with or without stirring) resulted in smaller particles (ca. 1 nm) and higher temperatures (25–75 °C) led to slightly larger particles (2–3 nm), which are inversed results from those prepared in organic solvents[143] (entry 3, Table 4). Notably, metal NPs prepared at 0 °C under stirring agglomerated into large clusters containing 2–3 nm in size. However, agglomeration is not verified for the NPs synthesized without stirring at the same temperature. These observations indicate that at lower temperatures (0 °C), the metal species in IL are better isolated than at high temperatures (25 °C). This effect may be directly related to the organisation type of ILs.[57] As expected, at low temperatures and without stirring, the organisation of supramolecular aggregates in IL tends to be better maintained, increasing the efficiency of the confinement of the metal species in the IL structure, and thus providing smaller particles. On the other hand, the presence of stirring, even at 0 °C, was suggested to perturb this 3D organisation and leads to partial agglomeration of the metal NPs, thereby yielding larger particles. The same research group also published the influence of the IL 3D organisation on the size of ruthenium NPs.[128] A linear relationship between the NP size and the length of the alkyl chain in IL was described (Fig. 15). In addition, the NP crystal growth could be controlled by the local concentration of the Ru precursor ([Ru(COD)(COT)]), as well as be limited to the size of the IL non-polar domain.[128]

This trend corroborates earlier observations on the formation of nickel NPs with a narrow size distribution from the decomposition of [bis(1,5-cyclooctadiene) nickel(0)] organometallic precursor in 1-alkyl-3-methylimidazolium ILs.[144,145] Indeed, the simple decomposition of $[Ni(COD)_2]$ dissolved in 1-alkyl-3-methylimidazolium N-bis(trifluoro-methanesulfonyl)imide ILs yields Ni NPs probably composed of a Ni metal core and a NiO cap. The diameter, size distribution and the metal/metal oxide ratio depend on the structural arrangement of the salt. There are slight decreases in

Table 4 Synthesis of NPs by decomposition of several transition-metal(0) organometallic compounds in ILs

Entry	IL	Decomposition	Metal precursor	M(0) size (nm)[a]	Ref.
1	$BMI.PF_6$	In the presence of H_2	$[Pt_2(dba)_3]$	2.0	141
2	$BMI.PF_6$	In the presence of H_2	[Ru(COD)(COT)]	2.6[b]	41
3	$BMI.NTf_2$	In the presence of H_2	[Ru(COD)(COT)]	2.4[c]	127
				0.9[d]	
				1.1[e]	
4	$BMI.NTf_2$	Thermal	$[Co_2(CO)_8]$	7.7	146
	$DMI.BF_4$			4.5	
5	$DMI.NTf_2$	Thermal	$[Co_2(CO)_8]$	79[f] and 11[g]	147
	DMI.FAP			53[h]	
6	$BMI.BF_4$	Thermal	$[Co_2(CO)_8]$	14	148
7	$BMI.BF_4$	Thermal	$[Cr(CO)_6]$	1.5	149
8	$BMI.BF_4$	Photolytic	$[Mo(CO)_6]$	1.5	149
	$NMe_3^nBu.NTf_2$			150	
9	$BMI.BF_4$	Thermal	$[W(CO)_6]$	1.5	149
	$BMI.CF_3SO_3$			5.7	
	$BMI.NTf_2$			33	
	$NMe_3^nBu.NTf_2$			67	
10	$BMI.BF_4$	Thermal or photolytic	$[Fe_2(CO)_9]$	5.2	150
			$[Ru_3(CO)_{12}]$	1.6	
			$[Os_3(CO)_{12}]$	2.5	
11	$BMI.BF_4$	Thermal	$[Rh_6(CO)_{16}]$	3.0	148
	$BMI.CF_3SO_3$			4.4	
	$NMe_3^nBu.NTf_2$			14	
12	$BMI.BF_4$	Thermal	$[Ir_4(CO)_{12}]$	1.7	148
	$BMI.CF_3SO_3$			3.6	
	$NMe_3^nBu.NTf_2$			81	
13	$BMI.NTf_2$	In the presence of H_2	$[Ni(COD)_2]$	5.9	144,145
	$TDMI.NTf_2$			5.1	
	$HDMI.NTf_2$			5.5	

[a] Determined by TEM; [b] These small NPs are inside the Ru superstructures, which are 57 nm in size; [c] At 25 °C; [d] At 0 °C (in this case, the NPs are agglomerated and forming clusters of 2–3 nm in size); [e] At 0 °C without stirring; [f] Co nanocubes; [g] Co irregular nanoparticles; [h] After 5 min of decomposition. BMI = 1-n-butyl-3-methylimidazolium; DMI = 1-n-decyl-3-methylimidazolium; TDMI = 1-methyl-3-n-tetradecylimidazolium; HDMI = 1-n-hexadecyl-3-methylimidazolium; NMe_3^nBu = n-butyl-tri-methylammonium; NTf_2 = N-bis(trifluoromethanesulfonyl)imide; FAP = tris(perfluoroethyl)-trifluorophosphate.

This journal is © The Royal Society of Chemistry 2010

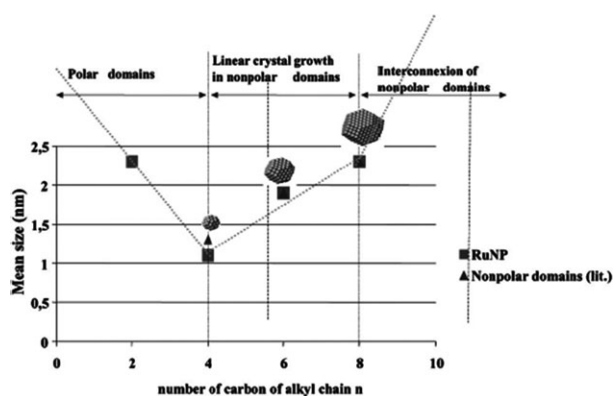*Chem. Soc. Rev.*, 2010, **39**, 1780–1804 | 1793

Fig. 15 Schematic showing the correlation between the size of the ruthenium NPs and the number of carbons on the alkyl chain of the IL. (Copyright from ref. 128).

both the nanoparticle diameter and the size distribution with increasing carbon number of the alkyl side chain of the imidazolium cation up to 14 carbons (entry 13, Table 4).

The thermal decomposition of metal carbonyls constitutes another simple and clean method for the production of NPs in ILs. Indeed, the only by-product is CO gas, which has a very low solubility in ILs and thus is rapidly expelled from the medium and having little opportunity to interact with the NP surface. However, relatively high reaction temperatures must be used to decompose the metal carbonyl compounds. For example, the thermal decomposition of the cobalt carbonyl precursor [Co$_2$(CO)$_8$] dissolved in BMI.NTf$_2$ occurs at 150 °C to yield cobalt NPs with a mean diameter of 7.7 ± 1.2 nm.[146] Moreover, cobalt NPs of 4.5 ± 0.6 nm in size are obtained from the decomposition of the same precursor in 1-*n*-decyl-3-methylimidazolium tetrafluoroborate (DMI.BF$_4$). These results suggest that the size of the Co NPs can be controlled depending on the type of the IL chosen (entry 4, Table 4).

Most remarkable, [Co(0)]$_n$ nanocubes can be prepared in imidazolium ILs without additional stabiliser.[147] The decomposition of the [Co$_2$(CO)$_8$] precursor at 150 °C using DMI.NTf$_2$ as the solvent leads to cobalt nanocubes having a size of 79 ± 17 nm together with smaller irregular NPs (11 ± 3 nm) (entry 5, Table 4). Depending on the decomposition time, different percentages of nanocubes and spheres are observed. On the other hand, employing DMI.FAP (FAP = *tris*-(perfluoroethyl)trifluorophosphate), the formation of controlled Co nanocubes depends strongly on the reaction time. For DMI.FAP, these cubic particles are observed only at the beginning of the reaction (5 min) and transforming quickly into irregular NPs. These results suggest that in both cases (DMI.NTf$_2$ and DMI.FAP) the nanocubes are transformed into small irregular NPs with long reaction times. Therefore, by properly choosing the IL type (cation and anion) and reaction conditions, it is possible to obtain selectively cubic shaped or irregular particles (Fig. 16). In addition, the formation of the metal nanocubes can be related to the intrinsic IL self-organisation. For example, these nanostructures were not observed using BMI.NTf$_2$ or an anion with a higher coordination ability, such as BF$_4^-$. Of note, the IL-dispersed cobalt NPs are much less prone to oxidation than those isolated from the media, similar to the results observed with the Ru NPs.[41] In
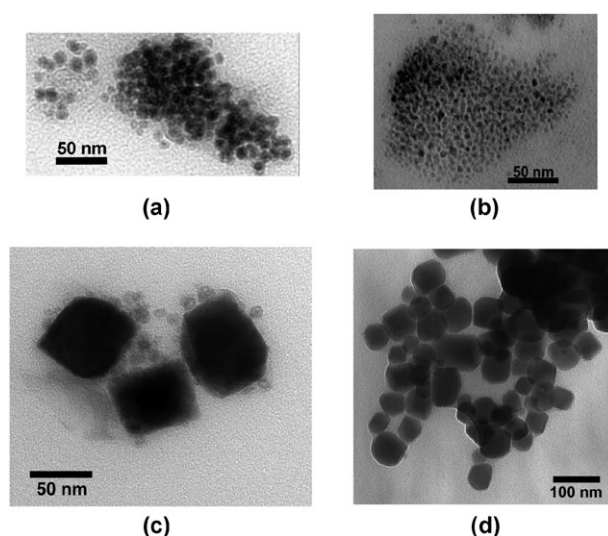
Fig. 16 TEM micrographs of the [Co(0)]$_n$ NPs dispersed in (a) BMI.NTf$_2$ (7.7 ± 1.2 nm), (b) DMI.BF$_4$ (4.5 ± 0.6 nm), (c) DMI.NTf$_2$ (79 ± 17 nm) and (d) DMI.FAP (53 ± 22 nm) (5 min of decomposition time). (Figure adapted from ref. 146 and 147.)

parallel, stable Cr, Mo and W NPs can be synthesised by thermal or photolytic decomposition of their respective mononuclear metal carbonyl precursors [M(CO)$_6$] dispersed in ILs (entries 7–9, Table 4).[149]

Using the same method, small Fe, Ru and Os metal NPs with diameters of 1.5–2.5 nm from the metal precursors [Fe$_2$(CO)$_9$], [Ru$_3$(CO)$_{12}$] and [Os$_3$(CO)$_{12}$], respectively, dissolved in BMI.BF$_4$ were prepared (entry 10, Table 4).[150] Cobalt, rhodium and iridium NPs were also prepared in IL by the same research group by thermal decomposition of the molecular clusters [Co$_2$(CO)$_8$], [Rh$_6$(CO)$_{16}$] and [Ir$_4$(CO)$_{12}$], respectively (entries 6, 11 and 12, Table 4).[148] However, the thermal decomposition of [Fe(CO)$_5$] dissolved in BMI.NTf$_2$ IL only produced iron oxide NPs.[151,152]

3.3 Formation of metal NPs by bombardment

The bombardment of metal or large-sized metal particles by laser irradiation[153] or energetic gaseous ions may cause their breakup and generate smaller particles. The irradiation of metal particles promotes the photoejection of electrons, which induces subsequent fragmentations,[154] and this constitutes an alternative and selective method for the breakup of large or irregular particles into smaller and regular ones (Fig. 17).[155,156]

The irradiation of large metal nanoclusters dissolved in ILs is an alternative method for the generation of smaller NPs with a narrow size distribution. The restructuring of those particles leads to their aggregation into larger particles after use, such as in catalysis. Indeed, the *in situ* laser radiation of relatively large [Pd(0)]$_n$ and [Rh(0)]$_n$ NPs dispersed in BMI.PF$_6$ IL induces their fragmentation into smaller particles with a narrow size distribution (entries 1 and 2, Table 5).[100]

The time-of-flight mass spectrometry studies of the ablation of several imidazolium salts of the form [R$_1$R$_2$I]X (R$_1$ = methyl; R$_2$ = methyl, ethyl, butyl, and hexyl; X = Cl$^-$, NO$_3^-$, and CH$_3$SO$_4^-$) showed that at least 99%
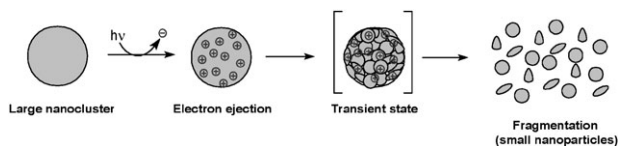
Fig. 17 Simplified representation of the fragmentation of metal clusters with laser excitation. A transient aggregate formed *via* the photoejection of electrons is considered to be a precursor for complete fragmentation of the particle.[155]
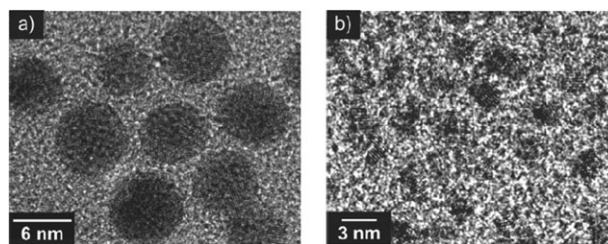

Fig. 18 Metal Au NPs synthesised by sputter deposition in the ILs (a) EMI.BF$_4$ and (b) NMe$_3$^{n}Pr.NTf$_2$. (Figure adapted from ref. 159).

of the material is removed in the form of nano- or micro-droplets consisting of intact IL. Approximately 1% is ejected as imidazole molecules (R$_1$R$_2$I) produced through the elimination of HCl, and about 0.1% of the material is ejected in the form of single salt molecules of [R$_1$R$_2$I]X.[157]

Gold NPs have been prepared by laser ablation of a gold plate in imidazolium-based ILs. The size and stability of gold NPs were dependent on the wavelength of the laser light and the alkyl chain length of the imidazolium-based cation.[158]

The extremely low vapour pressure of ILs has enabled vacuum deposition of solid materials onto ILs. This innovative synthesis is based on the sputter deposition technique where metal NPs are formed from a metal foil and then dispersed in the ILs. The main advantage of this process is that no additional stabilisers or reducing agents are needed. Torimoto and co-workers have described the preparation of soluble metal NPs in ILs by simple sputtering of a gold foil.[159] Indeed, highly dispersed [Au(0)]$_n$ NPs of 5.5 nm in diameter (Fig. 18) were obtained by sputter deposition in the IL 1-ethyl-3-methylimidazolium tetrafluoroborate (EMI.BF$_4$). Although a longer sputtering time increased the NP concentration in the IL, it did not significantly affect the particle size (entry 6, Table 5).

In sputter deposition, the bombardment of an Au foil surface with energetic gaseous ions causes the physical ejection of surface atoms and/or small Au clusters (Fig. 19).[160] Because of the low gas pressure, it is assumed there are no considerable gas-phase collisions of the sputtered species in the space between the Au foil and the IL medium. Their injection into the IL solution could produce an atom/cluster concentration high enough to coalesce with each other and result in the

formation of larger particles. In summary, sputtered Au species were injected into ILs without remarkable gas-phase collisions in the space between the target and IL solution, resulting in their coalescence with each other to form a dispersion of larger [Au(0)]$_n$ NPs with diameters of several nanometres.

Indeed, various irregular Au, Ag and Pt NPs have been prepared in some ILs (see entries 6–15, Table 5). The size of NPs depends apparently on the type of IL but not with the time of sputtering. For example, Au nanoparticles of 5.5 nm with a standard deviation of 0.86 nm were produced in EMI.BF$_4$, while sputter deposition onto NMe$_3$^{n}Pr·NTf$_2$ resulted in the formation of much smaller Au nanoparticles with 1.9 nm and standard deviation of 0.46 nm.[159] However, the size of NPs can be controlled by varying the discharge current. Indeed, sputter deposition of silver BMI.PF$_6$ produced Ag nanoparticles whose size increased from 5.7 to 11 nm by varying the discharge current from 10 to 40 mA.[164]

This method was extended for the generation of bimetallic NPs. The simultaneous sputter deposition of gold and silver onto ILs formed bimetallic alloy NPs. The sputter deposition produced spherical particles highly dispersed in the IL in which individual NPs were single crystals. By just varying the area ratio of the individual pure metal foils in the sputtering targets, the chemical composition and optical properties of the alloy NPs were easily controlled. These alloys exhibited composition-sensitive surface plasmon resonance with a red-shifted peak wavelength and an increased surface area of the sputtered gold foil targets.[161]

Table 5 Formation of metal NPs in ILs by laser ablation (pulse in nm) or sputtering of metal substrates

Entry	IL	Metal substrate	Bombardment	Size (nm)	Ref.
1	BMI.PF$_6$	[Rh(0)]$_n$ ($\sim$15 nm)	Laser 532	7.2	100
2	BMI.PF$_6$	[Pd(0)]$_n$ ($\sim$12 nm)	Laser 532	4.2	100
3	OMI.BF$_4$	Au plate	Laser 1064	13	158
4	OMI.BF$_4$	Au plate	Laser 532	4.2	158
5	BMI.BF$_4$	Au plate	Laser 532	3.6	158
6	EMI.BF$_4$	Au foil	Ar$^+$	5.5	159
7	BMI.PF$_6$	Au foil	Ar$^+$	2.6	161,162
8	BMI.PF$_6$	Ag foil	Ar$^+$	6.0	161
9	BMI.PF$_6$	Au and Ag foils^a	Ar$^+$	3.1	161
10	NMe$_3$^{n}Pr.NTf$_2$	Au foil	Ar$^+$	1.9–2.3	159,163
11	BMI.PF$_6$	Ag foil	Ar^{+b}	5.7	164
12	BMI.PF$_6$	Ag foil	Ar^{+c}	11	164
13	BMI.PF$_6$	Ag foil/HAuCl$_4$^{a}	Ar$^+$	6.4-6.9	164
14	NMe$_3$^{n}Pr.NTf$_2$	Pt foil	Ar$^+$	2.2	165
15	NMe$_3$^{n}Pr.NTf$_2$	Pt foil	N$_2$$^+$	3.3	165

^{a} Ag/Au alloy formed; ^{b} A discharge current of 10 mA was used; ^{c} A discharge current of 40 mA was used.

This journal is © The Royal Society of Chemistry 2010

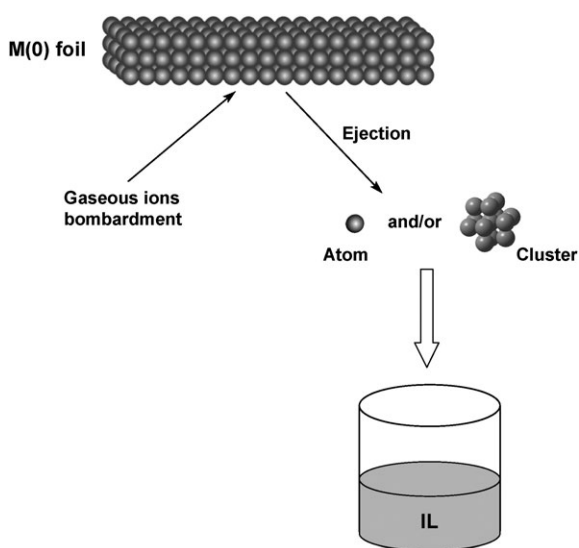*Chem. Soc. Rev.*, 2010, **39**, 1780–1804 | 1795

Fig. 19 Simplified model of metal NPs deposition in ILs by the sputtering method.

3.4 Synthesis of metal NPs in aqueous phase or organic solvents and transferred to the IL phase

Generally, the transfer of metal NPs from an aqueous phase to an organic phase is better attained in the presence of classical ligands, such as amines and thiols,[166] and the use of surfactants may act as phase transfer agents. Thus, capping the metal NPs with these ligands leads to increased NP solubility in the organic phase. Although the hydrophobicity of ILs can be modulated, it is possible to transfer metal NPs from the water or organic solvent to the IL. For example, metal gold NPs prepared in an aqueous solution of a thiol-functionalised IL were easily transferred from the water phase to a hydrophobic $BMI.PF_6$ IL.[85] Through an anion exchange of the water-miscible thiol-IL from Cl^- to PF_6^- using HPF_6, the $[Au(0)]_n$ NPs transferred quickly to the IL (1-*n*-hexyl-3-methylimidazolium hexafluorophosphate) phase. In this case, the HPF_6 acid acted as a phase transfer agent, allowing NP solubilisation in the organic phase (IL) due to the solubility change induced by anion exchange (Cl^- to PF_6^-) (entry 1, Table 6).

It was also reported that metal NPs prepared in water can be transferred to an IL phase without additional capping ligands (such as thiols).[167] The highly hydrophobic $BMI.PF_6$ IL was the best organic medium tested, as the $[Au(0)]_n$ NPs were practically completely transferred from the aqueous phase to the IL phase. For other classical organic solvents, such as benzene, hexane and chloroform, the gold NPs were poorly transferred. However, after phase separation, aggregation with further precipitation of the NPs was observed in the ILs. Therefore, tetradecyltrimethylammonium bromide (TTAB) was added to the aqueous phase for NP synthesis. The cationic surfactant TTAB is also transferred to the IL phase, thereby preventing NP aggregation (entry 2, Table 6).

Alternatively, poly(1-methyl-3-vinylbenzyl-imidazolium chloride) IL (ILP) was used to stabilise NP formation in water.[168] The reaction of an aqueous solution containing $[HAuCl_4]$, ILP and $NaBH_4$ rapidly afforded metal gold NPs.

Adding $BMI.PF_6$ to the aqueous solution, the $[Au(0)]_n$ NPs were reasonably transferred from the aqueous phase into the IL phase, although some NP aggregation was also observed in the IL. Interestingly, the ILP anion exchange from Cl^- to the same anion of the IL employed (in this case PF_6^-) improved the NP transfer to the IL phase. Using HPF_6 in the NP preparation and after addition of $BMI.PF_6$, the NPs were totally transferred to the IL phase without significant aggregation. The same result was observed employing $LiNTf_2$ during NP synthesis and further addition of $BMI.NTf_2$ to the aqueous phase. Again, the $[Au(0)]_n$ NPs were completely transferred from the aqueous phase to the IL phase (entry 3, Table 6 and Fig. 20). This method was successfully applied to other metal NPs, such as platinum and palladium.

The organic phase transfer was observed for surfactant-stabilised rhodium NPs previously synthesised in an aqueous solution of *N,N*-dimethyl-*N*-dodecyl-*N*-(2-hydroxyethyl) ammonium chloride (HEA12.Cl). The addition of $LiNTf_2$ to the aqueous suspension of Rh-HEA12.Cl transferred the hydrosol NPs to an IL phase (HEA12.NTf$_2$) (entry 4, Table 6).[169]

The novel application of gold and silver nanorods as irreversible thermochromic dyes in polymeric IL (PIL) nano-composites was recently reported. These materials have been synthesised by anion exchange of an imidazolium-based PIL in a solution that also contained gold nanorods. This resulted in the entrapment of the nano-objects within a solid polymer precipitate. In this work, the effect of the temperature was studied in relation to the change of shape and, consequently, colour of the gold or silver nanorods within the films. For the nanocomposites studied, a maximum of two visual thermochromic transitions was observed for gold nanorods, and up to three transitions were observed for silver nanorods.[170]

Carbon nanotubes, gold nanorods, and silver NPs can be transferred from water to organic solvents and back to water again by using PILs as vehicles. The PILs are able to trap several nano-objects during their anion-exchange-induced precipitation in water. This reversible process provides a PIL/nano-object composite that is fully re-dispersible in organic solvents.[171]

There is a single example in which metal NPs prepared in organic solvent were transferred to the IL (entry 5 in Table 6 and Scheme 9). In this process, the $[Pd(0)]_n$ NPs were prepared by reaction of a palladacycle with a large excess of dimethyl-allene in dichloromethane followed by transfer to $BMI.PF_6$.[98]

4. Characterisation of metal NPs in ILs

Although some ILs were reported to be vaporised with a very slow rate under high-vacuum and high-temperature conditions,[172] analyses conducted at ambient temperature did not detect any vaporisation of these fluids, even under high-vacuum conditions.[173] Therefore, ILs can be used in several vacuum techniques, including TEM,[141] XPS and SIMS.[174–178] Indeed, it was reported that ILs can be observed by TEM and thus the size and shape of NPs can be analysed *in situ*, such as with $[Pt(0)]_n$ NPs in $BMI·PF_6$ in this case.[141] After this report, *in situ* XPS analyses of metal NPs in ILs were performed.[43]

Table 6 Metal NPs synthesised in a non-IL medium and further transferred to an IL phase

Entry	Medium from/to	Preparation	Metal precursor	M(0) size (nm)[a]	Ref.
1	Water[b]/HMI.PF6	Reduction/NaBH4	[HAuCl4]	5.0	85
2	Water/BMI.PF6	Reduction/citrate	[HAuCl4]	48.1; 49.9[c]	167
3	Water[d]/BMI.PF6 or BMI.NTf2	Reduction/NaBH4	[HAuCl4]	2–10	168
4	Water[e]/HEA12.NTf2	Reduction/NaBH4	[RhCl3.3H2O]	2.4; 2.8[f]	169
5	CH2Cl2/BMI.PF6	Reductive elimination/allene	Palladacycle	1.7	98
6	Water/PIL[g]	Ascorbic acid	[HAuCl4]	Au nanorods	170
7	Water/PIL[g]	Ascorbic acid	[AgNO3]	Ag nanorods	170

[a] Determined by TEM; [b] In the presence of 3.3′-[disulfanyl*bis*(hexane-1,6-diyl)]-*bis*(1-methyl-1*H*-imidazol-3-ium)dichloride; [c] After transfer to the IL phase; [d] In the presence of poly(1-methyl-3-vinylbenzyl-imidazolium chloride); [e] In the presence of *N,N*-dimethyl-*N*-dodecyl-*N*-(2-hydroxy-ethyl) ammonium chloride (HEA12.Cl); [f] After transfer to the IL phase; [g] PIL = poly(1-ethyl-3-vinylimidiazolium *N-bis*(trifluoromethane-sulfonyl)imide). HMI = 1-*n*-hexyl-3-methylimidazolium.
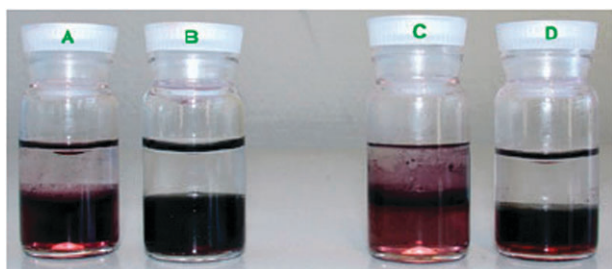
Fig. 20 (a) Gold NPs transferred from the aqueous phase to the BMI.PF6 phase (b) and in the presence of HPF6; (c) [Au(0)]n NPs transferred from water to BMI.NTf2 and (d) with LiNTf2. (Figure adapted from ref. 168).
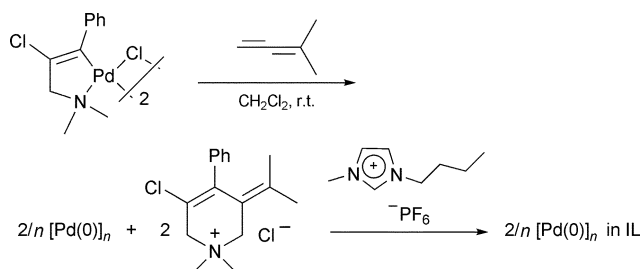
Scheme 9 Transfer of palladium metal NPs from an organic solvent to the IL phase.

Fig. 21 TEM micrographs and histograms showing the size distribution of [Pt(0)]n NPs (a) mixed in an epoxy resin and (b) dispersed in BMI.PF6 IL. (Copyright from ref. 141).

The structures of the metal NPs either dispersed in the ILs or after isolation have been studied by using various techniques, such as X-ray photoelectron spectroscopy (XPS),[40,41,43,100,144,179] X-ray absorption spectroscopy (EXAFS),[38,144] small-angle X-ray scattering (SAXS),[57,179] transmission electron microscopy (TEM)[38,40,41,57,61,76,96,98,100,141,144,145,179–181] and X-ray diffraction (XRD).[38,40,41,57,61,76,96,98,100,141,144,145,179–181] The mean diameters of these isolated materials have also been determined by TEM and usually are quite close to those obtained with the NPs dispersed in the ILs (Fig. 21).

The XRD data of the NPs isolated from the ILs have been used to check the crystalline nature of the material and to estimate the mean diameter by means of the Debye–Scherrer equation calculated from full width at half maximum (FWHM) of the crystalline planes obtained with Rietveld's refinements. The simulations of Bragg reflections and Rietveld's refinement were performed with a pseudo-Voigt

function using the FULLPROF code. It is worth pointing out that the use of full width at half maximum (FWHM) of a peak to estimate the size of crystalline grain by means of the Scherrer equation has serious limitations because it does not take into account the existence of a distribution of sizes and the presence of defects in the crystalline lattice. Therefore, the calculation of the diameter of grain from FWHM of the peak can overestimate the real value since the larger grains give a strong contribution to the intensity, while the smaller grains just enlarge the base of the peak.

Moreover, a significant amount of defects causes an additional enlargement of the diffraction line. Therefore, the obtained size can be smaller or larger than the real size of the grains. These problems can be minimised by using Rietveld's refinement method. Indeed, these discrepancies can be confirmed by values found for the average diameter of the NPs without structural refinement, which significantly differ from those found by means of Rietveld's refinement. The values obtained with Rietveld's refinement are invariably much closer to those determined by other techniques, such as TEM and SAXS (Table 7).[42] In the cases in which exposure to air of the isolated NPs may be problematic, such as with Ru, Co and Ni, the NPs form an oxide layer, and the analysis should be performed *in situ*.[96]

Sample	TEM	SAXS	XRD
$[Ir(0)]_n$ BMI.PF$_6$	2.0 ± 0.4	2.8 ± 0.4	2.1 ± 0.5
$[Ir(0)]_n$ BMI.CF$_3$SO$_3$	2.6 ± 0.6	2.4 ± 0.3	2.5 ± 0.3
$[Ir(0)]_n$ BMI.BF$_4$	2.9 ± 0.4	3.0 ± 0.3	2.6 ± 0.4
$[Pt(0)]_n$ BMI.BF$_4$	3.4 ± 0.3	3.4 ± 0.4	3.1 ± 0.4 (5.4 ± 0.7)[a]
$[Pt(0)]_n$ BMI.PF$_6$	2.3 ± 0.3	3.2 ± 0.4	2.6 ± 0.4 (3.8 ± 0.6)[a]

[a] Mean diameter obtained without Rietveld's refinement method in parentheses.

5. Applications of metal NPs in ILs

The use of metallic NPs in catalysis gives rise to a discussion on their catalytic nature. It is unclear if the catalyst behaves as a molecular species or, on the contrary, the metallic surface is directly involved in the reactivity. This dilemma is intrinsically associated with the kinetic stability of the nanoclusters, favouring their agglomeration, and also with the formation of molecular species by reaction of the atoms placed at low-coordination positions at the metallic surface (Fig. 22).

Soluble and stable transition-metal NPs embedded in ILs have been applied in several catalytic reactions. The first application of these nanomaterials was in C–C coupling reactions,[182] but the rapid hydrogenation of several substrates was described in most of the publications. Generally, transition-metal NPs prepared in ILs are used as colloidal catalysts for biphasic liquid–liquid reactions or as supported catalysts in solid materials. These multiphase systems allow for an easy product phase separation from the catalyst phase and the recycling of NPs without any significant loss of activity for a plethora of reactions.

Herein the catalytic properties of metal NPs immobilised in ILs will initially be discussed, and then the supported phase catalysts will be commented on briefly. Finally, the use of metal NPs in ILs for the construction of novel analytical

Fig. 22 Different types of interactions between metal NPs and functionalised arenes.

sensors will be introduced with a few examples described in more detail.

5.1 Transition-metal NPs dispersed in ILs as catalyst-phase

The main advantage of using metal NPs immobilised in ILs is the possibility of recovering the catalyst. As such, this system has been extensively applied as the catalyst phase in different reactions, such as hydrogenation and C–C coupling reactions.

For example, iridium NPs with a narrow size distribution ($\sim$2.0 ± 0.4 nm) prepared *in situ* from the reduction of [Ir(COD)Cl]$_2$ in BMI.PF$_6$ showed good activity in olefin,[15] arene[78] and ketone[79] hydrogenation. The hydrogenation of simple alkenes by $[Ir(0)]_n$ NPs dispersed in ILs depends on steric hindrance at the C=C double bond[75] and follows the same trend observed with classical iridium complexes in homogeneous conditions. The reaction follows the order: terminal > disubstituted > trisubstituted > tetrasubstituted.[183] Interestingly, the alkene hydrogenation process by the $[Ir(0)]_n$ NPs in BMI.PF$_6$ follows the classical monomolecular surface reaction mechanism $v = k_cK[S]/1 + K[S]$ (k_c = kinetic constant and K = adsorption constant). The reaction rate is a mass-controlled process at hydrogen pressure < 4 atm. The reaction at hydrogen pressures ≥ 4 atm is zero order with respect to hydrogen, and the reaction rate depends only on the olefin concentration in the IL phase.[75]

One of the most important aspects for using transition-metal NPs embedded in ILs is the possibility of tuning the selectivity of a reaction. The tunability is a consequence of the nature of multiphase catalytic systems, where the products can be extracted during the reaction, thereby modulating the selectivity. As an example, $[Pd(0)]_n$ NPs embedded in IL can selectively hydrogenate 1,3-butadiene to 1-butene when the diene solubility is (at least) four-times higher than that of the butenes in BMI.BF$_4$ (Fig. 23).[40]

The product 1-butene was obtained with a selectivity of 72% at 99% of 1,3-butadiene conversion and only small amounts of butane and *cis*-2-butene were detected. Similarly, the difference in solubility of benzene and cyclohexene (maximum of $\sim$1% cyclohexene concentration was attained with a $\sim$4% benzene concentration in BMI.PF$_6$) was used for the extraction of cyclohexene during the hydrogenation of benzene by $[Ru(0)]_n$ NPs in BMI.PF$_6$.[41] A cyclohexene selectivity of 39% could be obtained at very low benzene conversions.

Heck and Suzuki C–C coupling reactions are also promoted by Pd metal NPs in ILs. However, the $[Pd(0)]_n$ NPs are simple reservoirs of homogeneous metal catalytically active species in most cases, similar to those observed with phosphine-free palladium catalyst precursors,[184–186] such as simple Pd(II) compounds[187] or palladacycles.[188,189] It is highly probable that the Heck coupling reaction proceeds through the oxidative addition of the aryl halide on the NP surface in these cases, and the formed oxidised Pd species are detached from the surface and enter into the main catalytic cycle.[190] The Pd(0) formed in the main catalytic cycle, after β-hydride and reductive elimination steps, can either continue in the catalytic cycle or fall back to the nanoparticle reservoir.[98]

However, in terms of the structural and surface properties of these metal NPs, the hydrogenation of (functionalised) arenes
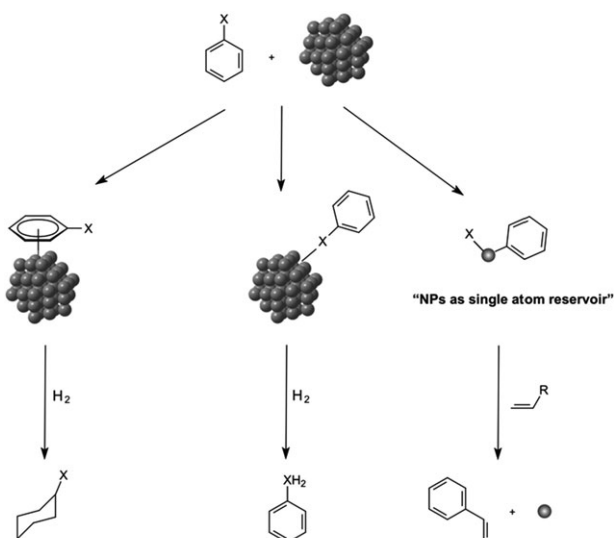
1798 | *Chem. Soc. Rev.*, 2010, **39**, 1780–1804

This journal is © The Royal Society of Chemistry 2010
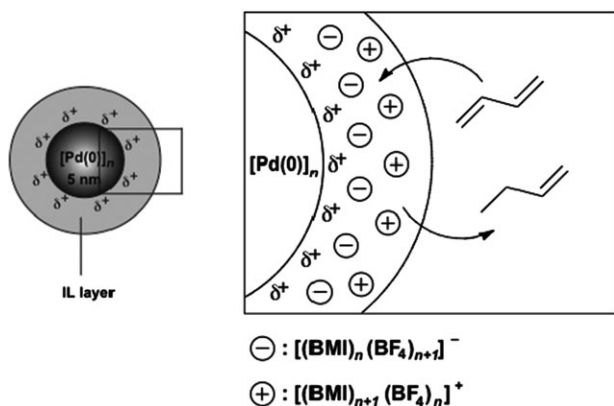
is of fundamental importance. It is generally accepted that metal homogeneous catalysts do not hydrogenate aromatic compounds, so arene hydrogenation has been used as a chemical probe for studying the surface properties of NPs and their interactions with stabiliser species. In this context, the use of imidazolium ILs for the synthesis of metal NPs and their application as the catalyst phase in arene hydrogenation was one of the first catalytic applications of metal NPs in ILs.[41,78,141]

The [Ir(0)]$_n$ and [Rh(0)]$_n$ NPs prepared in BMI.PF$_6$ were efficient catalysts for biphasic benzene hydrogenation, where the iridium NPs were superior in catalytic activity to their rhodium analogue.[78] Moreover, other arenes were also tested, such as toluene, anisole and *p*-xylene. Notably, hydrogenolysis products were detected during acetophenone and anisole hydrogenation under a solventless condition by [Ir(0)]$_n$ NPs. These results are diagnostic of surface metal catalysts (heterogeneous catalysts). The [Pt(0)]$_n$ and [Ru(0)]$_n$ NPs embedded in ILs were also suitable catalysts for benzene hydrogenation under biphasic conditions.[41,141] In the case of [Ru(0)]$_n$ NPs, as cited previously, selectivities up to 39% in cyclohexene could be detected for low benzene conversions, which is very unusual for metal NPs as catalysts.

5.2 Improving the catalytic performance of metal NPs in ILs with the presence of additional co-stabilisers

Usually, the system containing the catalyst and IL can be reused without any significant loss of activity in olefin hydrogenation, as observed for general metal nanocatalysts. Nevertheless, if more miscible compounds than alkenes in the ILs are hydrogenated, such as aromatic compounds or ketones, deactivation of the catalysts is eventually observed.[23] The aromatic or carbonyl and alcoholic compounds, which are partially soluble in the colloidal phase, are probably leaching out of the IL protective layer, leading to the nanoparticle agglomeration/aggregation process. This could eventually start a crystallite growth, generating bulk-like particles and consequent deactivation of the metal surface. To overcome this problem, additional co-stabilising agents, such as polymers, can be added to the IL solution during NP synthesis. In most cases, these NP/IL/co-stabiliser systems produce more homogeneous and dispersed NPs than those containing metal NPs only in the IL. Thus, improved catalytic activities can be achieved in different chemical processes using systems containing an additional co-stabiliser agent.

For example, the catalytic activity of [Rh(0)]$_n$ NPs for arene hydrogenation was increased several times compared with the "naked" particles prepared in pure ILs by adding an ionic copolymer in the IL at the reduction of the metallic precursor.[191] The co-stabilised particles were reused several times for hydrogenation reactions without any apparent loss of activity, whereas the naked particles were barely active at the reaction conditions. In addition, the ionic co-polymer/IL/ NP system was also used for selective hydrogenation of cinnamaldehyde[192] and nitro-functionalised compounds[193] using [Pt(0)]$_n$ NPs. Similarly, [Pd(0)]$_n$ NPs were prepared in nitrile-functionalised IL with poly-3-(4-vinylbenzyl)-1-methyl-imidazolium *N-bis*(trifluoromethanesulfonyl)imide as an extra stabiliser and applied in C–C cross-coupling reactions.[194] The obtained palladium metal NPs showed higher long-term stability during storage and increased reactivity during catalysis in comparison with those prepared in IL without the polymer. The [Rh(0)]$_n$ NPs immobilised in hydroxyl-functionalised ILs with poly(vinyl-pyrrolidone) (PVP) were used as the catalyst in the hydrogenation of several substrates.[195] The catalytic activity for styrene hydrogenation of the [Rh(0)]$_n$ NPs/hydroxyl IL/PVP system was significantly higher than that using non-functionalised IL. Moreover, this catalytic phase exhibited good activity for the hydrogenation of other typical unsaturated compounds. In the same context, stable catalysts for olefin hydrogenation based on Rh, Pt and Pd NPs and stabilised by PVP were prepared by simple ethanolic reduction of the corresponding halide salts and then immobilised in BMI.PF$_6$.[196]

Another interesting approach consists of using Lewis bases that bind in the metal surface, as in classical organometallic chemistry. For example, [Pd(0)]$_n$ NPs protected with phenanthroline in ILs are very active catalysts for selective hydrogenation of olefins, and these catalytic systems are reusable for several times without loss of activity.[106] In contrast, [Pd(0)]$_n$ NPs in pure "classical" ILs, such as BMI.PF$_6$, tend to agglomerate after hydrogenation reactions.[40]

In the same way, [Rh(0)]$_n$ NPs were co-stabilised by bipyridine compounds in several ILs and tested as catalysts for arene hydrogenation.[118] These systems showed notable colloidal stability when compared with simple rhodium NPs stabilised in IL, but their catalytic activities decreased by adding more than 0.75 equivalents of bipyridine compounds, probably by NP surface saturation. The protecting agents prevent the agglomeration/aggregation processes, but could also act simultaneously as a poison for the NP surface. Moreover, the influence of the bipyridine ligand coordination modes on [Rh(0)]$_n$ NPs was also discussed on arene hydrogenation to explain the differences observed in the catalytic activities.[49]

An elegant approach was showed by Dyson and co-workers on functionalised ILs,[197,198] such as imidazolium and pyridinium with the nitrile group attached to the alkyl side chain. In this work, the authors demonstrated the possibility of ILs acting as both the solvent and ligand for metal-catalysed reactions.[199]

In particular, $[Pd(0)]_n$ NPs immobilised in both N-butylpyridinium- and nitrile-functionalised ILs showed good catalytic activities for Stille coupling reactions.

Noteworthy, $[Ru(0)]_n$ NPs prepared in nitrile-functionalised ionic liquid **17** displayed unusual selectivity toward the hydrogenation of nitrile-containing aromatic compounds. In particular, a selective catalytic hydrogenative coupling of nitriles was observed (Scheme 10).[97] In this transformation, nitrile groups were exclusively hydrogenated in the presence of arenes, which are typically hydrogenated by ruthenium metal NPs in non-functionalised ILs.

5.3 Immobilisation of metal NPs in a solid support modified with ILs: supported ionic liquid phase catalysis

The combination of an IL with a solid-supported material is emerging as a new alternative for the immobilisation of transition-metal catalyst precursors.[200,201] This process, named Supported Ionic Liquid Phase (SILP) catalysis, is a concept that combines the advantages of ILs with those of heterogeneous supported materials. These materials are prepared by the covalent attachment of ILs to the support surface or by simply depositing the catalytically active species-containing IL phases on the surface of supports, which are usually silica- or polymeric-based materials. Similarly, supporting NPs prepared in ILs in inorganic supports prevent the deactivation of the nanostructures by agglomeration/aggregation and prevent some of the diffusion problems. For example, rhodium metal NPs were deposited on silica NPs prepared by a sol–gel method using IL BMI.BF$_4$ as the template.[202] This combination displayed an excellent synergistic effect that enhanced the activity and robustness of the Rh hydrogenation catalysts. All of the supported systems were more active than those constituted from isolated $[Rh(0)]_n$ NPs for the hydrogenation of alkenes. The silica-based systems prepared under acidic conditions were shown to be more active than commercial [Rh/C] (5%). In addition, palladium NPs were prepared in imidazolium salt modified carbon nanotubes, called ionic carbon nanotubes,[203] and then dispersed in hydrophobic ILs. These systems showed good activities for a series of alkene hydrogenations, and were able to be recycled as the catalyst for 50 runs.
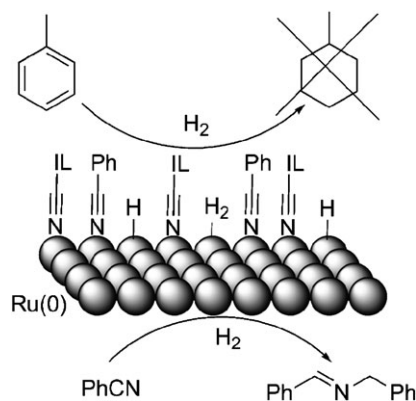
Hybrid materials based on multi-walled carbon nanotubes functionalised with ILs and containing $[Au(0)]_n$ NPs deposited on this modified support were developed by Niu and co-workers.[204] In this synthesis, the first step consists of the functionalisation of the carbon nanotubes with the IL containing an amine-attached group at the imidazolium cation. Then the chemical reaction between this modified material and an aqueous solution of [HAuCl$_4$] leads to the formation and further deposition of well-dispersed $[Au(0)]_n$ NPs on the carbon nanotubes/IL solid support. In addition, it was shown that the presence of an amine-IL and $[Au(0)]_n$ NPs have a positive effect by increasing dramatically the electrocatalytic activity in the oxygen reduction of the carbon nanotubes.

In a similar procedure, gold and platinum metal NPs were synthesised in carboxylic acid- and amino-functionalised imidazolium ILs and then supported on carbon nanotubes.[87] The ILs interact with the carbon nanotubes by π–π interactions between the imidazolium cation and the π-electronic nanotube surface. Moreover, the metal NPs interact with the functionalised moiety (–CO$_2$H or –NH$_2$) of the IL. In this case, the functionalised ILs act as a linker between the metal NPs and the carbon nanotubes (Fig. 24).

New hybrid membrane materials based on metal NPs/IL/cellulose were prepared by the combination of cellulose acetate, $[Rh(0)]_n$ or $[Pt(0)]_n$ NPs and BMI.NTf$_2$ in acetone.[205] The inclusion of IL led to an increased distance in between cellulose macromolecules, providing beneficial effects on the physico-chemical properties of the cellulose material. Most importantly, these hybrid materials are superior catalysts in cyclohexene hydrogenation and possess a higher stability when compared to the metal NPs embedded in the IL.

5.4 Sensor-based metal NPs in ILs

Recent advances in nanotechnology have led to the development of electrochemical sensors with rapid responses and high sensitivity and selectivity. Indeed, the use of nanodevices brings several new possibilities for biosensor construction and novel electrochemical bioassays.[206] In particular, the introduction of the metal NPs into the sensing interface to facilitate the electron transfer can significantly improve the sensitivity.[207] The NPs of noble metals with size control, chemical stability, high catalytic activity and surface tenability are advantageous for application in sensors. In this respect, the ILs are widely used to prepare modified electrodes and
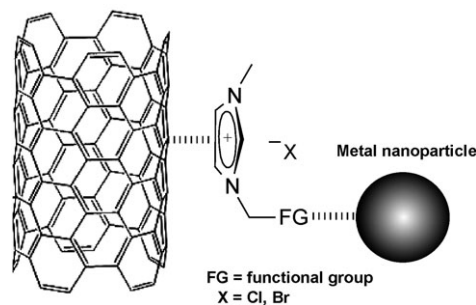

Scheme 10 Ru metal NPs dispersed in a nitrile-functionalised ILs, and selective hydrogenation of nitrile group. (Copyright from ref. 97).

Fig. 24 Proposed model for the interaction of the carbon nanotube/IL/NP system showing the functionalised IL as a linker between the C nanotubes and the metal NPs. (Figure adapted from ref. 87).

biosensors[208–212] and in preparation and stabilisation of nanomaterials and media for enzymatic processes.[213–216] Therefore, the IL-dispersed noble metal NPs may constitute an alternative material for the construction of novel biosensors. Indeed, a biosensor based on BMI.PF$_6$ IL containing dispersed iridium NPs and polyphenol oxidase was constructed.[217] The enzyme obtained from the sugar apple was immobilised in chitosan ionically cross-linked with oxalate. The biosensor was used for determination of chlorogenic acid by square-wave voltammetry. This biosensor exhibited simplicity, high sensitivity, fast response and good stability.[217]

Similarly, effective biosensors based on Ag or Au nanoparticles dispersed in BMI.PF$_6$ IL and laccase from *Aspergillus oryzae* immobilised in chitosan chemically cross-linked with cyanuric chloride were constructed. Laccase catalyses the oxidation of luteolin to the corresponding *o*-quinone, which is electrochemically reduced back to luteolin. These biosensors demonstrated high sensitivity, good repeatability and reproducibility, and long-term stability (13% decrease in response over 70 days).[218]

Platinum metal NPs dispersed in BMI.PF$_6$ were also successfully used in the construction of a novel biosensor for the determination of adrenaline in pharmaceutical formulations by square-wave voltammetry. Indeed, the inclusion of $[Pt(0)]_n$ NPs in IL to the biosensor led to an increase in sensitivity, probably because of the high conductivity of the IL combined with the electron transfer facilitated by the metal NPs. The proposed biosensor exhibited high sensitivity, rapid response, suitable selectivity, good reproducibility and stability. In addition, the low cost, simplicity and fast construction of the biosensor make it superior to other techniques used for catecholamine determination. Satisfactory results were obtained using this biosensor when compared with the official method, thus representing an alternative method to determine adrenaline in pharmaceutical formulations.[219]

6. Conclusions

The ILs offer a plethora of possibilities for the preparation, stabilisation and *in situ* investigations of the structural and surface properties of metal NPs. Indeed, soluble and stable transition-metal NPs with small sizes and narrow mean diameters can be prepared from metal precursors by different physical–chemical methods in the presence of ILs. Metal NPs can be prepared in ILs by reduction or decomposition of metal complexes, by bombardment (laser ablation or sputtering using energetic gaseous ions) of large metal clusters or metal foils and by simple extraction from previously prepared water- or organic solvent–soluble metal NPs. The non-functionalised ILs provide steric/electronic stabilisation of the "soluble" NPs by protective layers of discrete supramolecular $\{[(DAI)_x(X)_{x-n}]^{n+} \ [(DAI)_{x-n}(X)_x]^{n-}\}_m$ species through the loosely bound anionic moieties, non-polar imidazolium alkyl side chains and/or NHC species together with an oxide layer when present on the metal surface. Surface hydrogen species may be further elements of metal NP stability for those prepared under hydrogen reduction conditions. The introduction of moieties on the imidazolium side chain, such as N-, O- and S-containing groups, may provide extra stabilisation of the

metal NPs through coordination to the metal surface. However, in most cases, the surface-bound protective species are easily displaced by other substances present in the media and this is responsible for their catalytic activity and also explains their relatively low stability that leads to aggregation/agglomeration and eventually to the bulk metal. The stability and catalytic activity of transition-metal NPs in imidazolium ILs are also highly influenced by the coordinative strength of the aggregates with the metal surface and the type and nature of the substrates/products. The catalytic properties (activity and selectivity) of these soluble metal NPs indicate that they possess a pronounced surface-like (multi-site) rather than single-site-like catalytic properties. Indeed, most of the noble metal NPs in ILs are active catalysts for the hydrogenation of arenes, whereas they may serve as reservoirs of soluble mono-metallic catalysts for C–C coupling reactions, such as Heck and Suzuki. Moreover, the NPs can be used in conjunction with other stabilisers such as ligands, similar to classical coordination, chemistry or easily transferred to other organic and inorganic supports to generate more stable and active materials. The nanoparticle/IL/stabiliser combination usually exhibits an excellent synergistic effect that enhances the activity and durability of the material (chemical sensor or catalyst, for example). Although the use of ILs for the formation, stabilisation and applications of metal NPs is in its infancy, ILs have already proven to be some of the most versatile fluids for nanoscience and nanotechnology in "solution" and with many more applications certainly to come. The ILs are premiere "solutions" for the generation of tailor-made soluble nanomaterials.

Notes and references

1 O. A. Belyakova and Y. L. Slovokhotov, *Russ. Chem. Bull.*, 2003, **52**, 2299–2327.
2 J. Jortner, U. Even, A. Goldberg, I. Schek, T. Raz and R. D. Levine, *Surf. Rev. Lett.*, 1996, **3**, 263–280.
3 J. D. Aiken, Y. Lin and R. G. Finke, *J. Mol. Catal. A: Chem.*, 1996, **114**, 29–51.
4 R. G. Finke, *Transition-Metal Nanoclusters*, Marcel Dekker, New York, 2002.
5 C. Pan, K. Pelzer, K. Philippot, B. Chaudret, F. Dassenoy, P. Lecante and M. J. Casanove, *J. Am. Chem. Soc.*, 2001, **123**, 7584–7593.
6 J. L. Pellegatta, C. Blandy, V. Colliere, R. Choukroun, B. Chaudret, P. Cheng and K. Philippot, *J. Mol. Catal. A: Chem.*, 2002, **178**, 55–61.
7 J. Schulz, A. Roucoux and H. Patin, *Chem. Commun.*, 1999, 535–536.
8 M. T. Reetz and G. Lohmer, *Chem. Commun.*, 1996, 1921–1922.
9 J. D. Aiken and R. G. Finke, *J. Am. Chem. Soc.*, 1999, **121**, 8803–8810.
10 J. D. Aiken and R. G. Finke, *J. Am. Chem. Soc.*, 1998, **120**, 9545–9554.
11 A. Roucoux, J. Schulz and H. Patin, *Chem. Rev.*, 2002, **102**, 3757–3778.

This journal is © The Royal Society of Chemistry 2010

Chem. Soc. Rev., 2010, **39**, 1780–1804 | 1801

12 D. Astruc, F. Lu and J. R. Aranzaes, *Angew. Chem., Int. Ed.*, 2005, **44**, 7852–7872.

13 H. Bonnemann and R. M. Richards, *Eur. J. Inorg. Chem.*, 2001, 2455–2480.

14 Z. Ma, J. Yu and S. Dai, *Adv. Mater.*, 2010, **22**, 261–285.

15 J. Dupont, G. S. Fonseca, A. P. Umpierre, P. F. P. Fichtner and S. R. Teixeira, *J. Am. Chem. Soc.*, 2002, **124**, 4228–4229.

16 J. Dupont, R. F. de Souza and P. A. Z. Suarez, *Chem. Rev.*, 2002, **102**, 3667–3691.

17 S. Tsuzuki, H. Tokuda, K. Hayamizu and M. Watanabe, *J. Phys. Chem. B*, 2005, **109**, 16474–16481.

18 C. Hardacre, J. D. Holbrey, S. E. J. McMath, D. T. Bowron and A. K. Soper, *J. Chem. Phys.*, 2003, **118**, 273–278.

19 J. Dupont and P. A. Z. Suarez, *Phys. Chem. Chem. Phys.*, 2006, **8**, 2441–2452.

20 M. Antonietti, D. B. Kuang, B. Smarsly and Z. Yong, *Angew. Chem., Int. Ed.*, 2004, **43**, 4988–4992.

21 Y. Zhou, *Curr. Nanosci.*, 2005, **1**, 35–42.

22 A. Taubert and Z. Li, *Dalton Trans.*, 2007, 723–727.

23 P. Migowski and J. Dupont, *Chem.–Eur. J.*, 2007, **13**, 32–39.

24 F. Endres, *ChemPhysChem*, 2002, **3**, 144–154.

25 P. A. Z. Suarez, S. Einloft, J. E. L. Dullius, R. F. de Souza and J. Dupont, *J. Chim. Phys. Phys.-Chim. Biol.*, 1998, **95**, 1626–1639.

26 F. C. Gozzo, L. S. Santos, R. Augusti, C. S. Consorti, J. Dupont and M. N. Eberlin, *Chem.–Eur.J.*, 2004, **10**, 6187–6193.

27 B. A. D. Neto, L. S. Santos, F. M. Nachtigall, M. N. Eberlin and J. Dupont, *Angew. Chem., Int. Ed.*, 2006, **45**, 7251–7254.

28 J. Dupont, *J. Braz. Chem. Soc.*, 2004, **15**, 341–350.

29 J. Lopes and A. A. H. Padua, *J. Phys. Chem. B*, 2006, **110**, 3330–3335.

30 U. Schroder, J. D. Wadhawan, R. G. Compton, F. Marken, P. A. Z. Suarez, C. S. Consorti, R. F. de Souza and J. Dupont, *New J. Chem.*, 2000, **24**, 1009–1015.

31 J. L. Anderson and D. W. Armstrong, *Anal. Chem.*, 2003, **75**, 4851–4858.

32 A. Chaumont, R. Schurhammer and G. Wipff, *J. Phys. Chem. B*, 2005, **109**, 18964–18973.

33 A. Chaumont and G. Wipff, *Phys. Chem. Chem. Phys.*, 2005, **7**, 1926–1932.

34 N. Sieffert and G. Wipff, *J. Phys. Chem. B*, 2007, **111**, 4951–4962.

35 L. S. Ott and R. G. Finke, *Coord. Chem. Rev.*, 2007, **251**, 1075–1100.

36 B. W. Ninham, *Adv. Colloid Interface Sci.*, 1999, **83**, 1–17.

37 M. Bostrom, D. R. M. Williams and B. W. Ninham, *Phys. Rev. Lett.*, 2001, **87**, 168103.

38 G. S. Fonseca, G. Machado, S. R. Teixeira, G. H. Fecher, J. Morais, M. C. M. Alves and J. Dupont, *J. Colloid Interface Sci.*, 2006, **301**, 193–204.

39 L. S. Ott and R. G. Finke, *Inorg. Chem.*, 2006, **45**, 8382–8393.

40 A. P. Umpierre, G. Machado, G. H. Fecher, J. Morais and J. Dupont, *Adv. Synth. Catal.*, 2005, **347**, 1404–1412.

41 E. T. Silveira, A. P. Umpierre, L. M. Rossi, G. Machado, J. Morais, G. V. Soares, I. L. R. Baumvol, S. R. Teixeira, P. F. P. Fichtner and J. Dupont, *Chem.–Eur. J.*, 2004, **10**, 3734–3740.

42 C. W. Scheeren, G. Machado, S. R. Teixeira, J. Morais, J. B. Domingos and J. Dupont, *J. Phys. Chem. B*, 2006, **110**, 13011–13020.

43 F. Bernardi, J. D. Scholten, G. H. Fecher, J. Dupont and J. Morais, *Chem. Phys. Lett.*, 2009, **479**, 113–116.

44 J. D. Scholten, G. Ebeling and J. Dupont, *Dalton Trans.*, 2007, 5554–5560.

45 L. S. Ott, M. L. Cline, M. Deetlefs, K. R. Seddon and R. G. Finke, *J. Am. Chem. Soc.*, 2005, **127**, 5758–5759.

46 K. Pelzer, O. Vidoni, K. Philippot, B. Chaudret and V. Colliere, *Adv. Funct. Mater.*, 2003, **13**, 118.

47 J. Garcia-Anton, M. R. Axet, S. Jansat, K. Philippot, B. Chaudret, T. Pery, G. Buntkowsky and H. H. Limbach, *Angew. Chem., Int. Ed.*, 2008, **47**, 2074–2078.

48 T. Pery, K. Pelzer, G. Buntkowsky, K. Philippot, H. H. Limbach and B. Chaudret, *ChemPhysChem*, 2005, **6**, 605–607.

49 B. Leger, A. Denicourt-Nowicki, H. Olivier-Bourbigou and A. Roucoux, *Inorg. Chem.*, 2008, **47**, 9090–9096.

50 S. M. Zhang, C. L. Zhang, J. W. Zhang, Z. J. Zhang, H. X. Dang, Z. S. Wu and W. M. Liu, *Acta Phys. Chim. Sin.*, 2004, **20**, 554–556.

51 C. A. Stowell and B. A. Korgel, *Nano Lett.*, 2005, **5**, 1203–1207.

52 B. A. Korgel and D. Fitzmaurice, *Phys. Rev. B*, 1999, **59**, 14191–14201.

53 J. C. Liu, B. X. Han, H. L. Zhang, G. Z. Li, X. G. Zhang, J. Wang and B. Z. Dong, *Chem.–Eur. J.*, 2002, **8**, 1356–1360.

54 A. I. Frenkel, C. W. Hills and R. G. Nuzzo, *J. Phys. Chem. B*, 2001, **105**, 12689–12703.

55 B. G. Trewyn, C. M. Whitman and V. S. Y. Lin, *Nano Lett.*, 2004, **4**, 2139–2143.

56 Y. Zhou, J. H. Schattka and M. Antonietti, *Nano Lett.*, 2004, **4**, 477–481.

57 G. Machado, J. D. Scholten, T. de Vargas, S. R. Teixeira, L. H. Ronchi and J. Dupont, *Int. J. Nanotechnol.*, 2007, **4**, 541–563.

58 H. S. Schrekker, M. A. Gelesky, M. P. Stracke, C. M. L. Schrekker, G. Machado, S. R. Teixeira, J. C. Rubim and J. Dupont, *J. Colloid Interface Sci.*, 2007, **316**, 189–195.

59 R. A. Alvarez-Puebla, E. Arceo, P. J. G. Goulet, J. J. Garrido and R. F. Aroca, *J. Phys. Chem. B*, 2005, **109**, 3787–3792.

60 J. C. Rubim, F. A. Trindade, M. A. Gelesky, R. F. Aroca and J. Dupont, *J. Phys. Chem. C*, 2008, **112**, 19670–19675.

61 M. H. G. Prechtl, M. Scariot, J. D. Scholten, G. Machado, S. R. Teixeira and J. Dupont, *Inorg. Chem.*, 2008, **47**, 8995–9001.

62 Y. Gao, A. Voigt, M. Zhou and K. Sundmacher, *Eur. J. Inorg. Chem.*, 2008, 3769–3775.

63 Y. Qin, Y. Song, N. J. Sun, N. Zhao, M. X. Li and L. M. Qi, *Chem. Mater.*, 2008, **20**, 3965–3972.

64 T. Y. Kim, W. J. Kim, S. H. Hong, J. E. Kim and K. S. Suh, *Angew. Chem., Int. Ed.*, 2009, **48**, 3806–3809.

65 P. Migowski and J. Dupont, unpublished results.

66 H. J. Ryu, L. Sanchez, H. A. Keul, A. Raj and M. R. Bockstaller, *Angew. Chem., Int. Ed.*, 2008, **47**, 7639–7643.

67 E. Redel, R. Thomann and C. Janiak, *Inorg. Chem.*, 2008, **47**, 14–16.

68 P. Dash and R. W. J. Scott, *Chem. Commun.*, 2009, 812–814.

69 D. A. Carter, J. E. Pemberton and K. J. Woelfel, *J. Phys. Chem. B*, 1998, **102**, 9870–9880.

70 J. Dupont and J. Spencer, *Angew. Chem., Int. Ed.*, 2004, **43**, 5296–5297.

71 L. S. Ott, S. Campbell, K. R. Seddon and R. G. Finke, *Inorg. Chem.*, 2007, **46**, 10335–10344.

72 C. Besson, E. E. Finney and R. G. Finke, *J. Am. Chem. Soc.*, 2005, **127**, 8179–8184.

73 C. Besson, E. E. Finney and R. G. Finke, *Chem. Mater.*, 2005, **17**, 4925.

74 E. E. Finney and R. G. Finke, *Chem. Mater.*, 2008, **20**, 1956–1970.

75 G. S. Fonseca, J. B. Domingos, F. Nome and J. Dupont, *J. Mol. Catal. A: Chem.*, 2006, **248**, 10–16.

76 C. W. Scheeren, J. B. Domingos, G. Machado and J. Dupont, *J. Phys. Chem. C*, 2008, **112**, 16463–16469.

77 A. Chaumont and G. Wipff, *Inorg. Chem.*, 2004, **43**, 5891–5901.

78 G. S. Fonseca, A. P. Umpierre, P. F. P. Fichtner, S. R. Teixeira and J. Dupont, *Chem.–Eur. J.*, 2003, **9**, 3263–3269.

79 G. S. Fonseca, J. D. Scholten and J. Dupont, *Synlett*, 2004, 1525–1528.

80 J. M. Zhu, Y. H. Shen, A. J. Xie, L. G. Qiu, Q. Zhang and S. Y. Zhang, *J. Phys. Chem. C*, 2007, **111**, 7629–7633.

81 A. Imanishi, M. Tamura and S. Kuwabata, *Chem. Commun.*, 2009, 1775–1777.

82 T. Tsuda, S. Seino and S. Kuwabata, *Chem. Commun.*, 2009, 6792–6794.

83 L. Zhao, C. Y. Zhang, L. Zhuo, Y. G. Zhang and J. Y. Ying, *J. Am. Chem. Soc.*, 2008, **130**, 12586–12587.

84 K. S. Kim, D. Demberelnyamba and H. Lee, *Langmuir*, 2004, **20**, 556–560.

85 H. Itoh, K. Naka and Y. Chujo, *J. Am. Chem. Soc.*, 2004, **126**, 3026–3027.

86 R. Tatumi and H. Fujihara, *Chem. Commun.*, 2005, 83–85.

87 H. Zhang and H. Cui, *Langmuir*, 2009, **25**, 2604–2612.

88 R. Marcilla, D. Mecerreyes, I. Odriozola, J. A. Pomposo, J. Rodriguez, I. Zalakain and I. Mondragon, *Nano*, 2007, **2**, 169–173.

89 E. Dinda, S. Si, A. Kotal and T. K. Mandal, *Chem.–Eur. J.*, 2008, **14**, 5528–5537.

1802 | *Chem. Soc. Rev.,* 2010, **39**, 1780–1804

This journal is © The Royal Society of Chemistry 2010

90 Z. H. Li, Z. M. Liu, J. L. Zhang, B. X. Han, J. M. Du, Y. N. Gao and T. Jiang, *J. Phys. Chem. B*, 2005, **109**, 14445–14448.

91 W. R. Yang, J. Q. Liu, R. K. Zheng, Z. W. Liu, Y. Dai, G. N. Chen, S. Ringer and F. Braet, *Nanoscale Res. Lett.*, 2008, **3**, 468–472.

92 L. Y. Wang, X. Chen, Y. C. Chai and J. C. Hao, *Colloids Surf., A*, 2007, **293**, 95–100.

93 E. Redel, M. Walter, R. Thomann, C. Vollmer, L. Hussein, H. Scherer, M. Kruger and C. Janiak, *Chem.–Eur. J.*, 2009, **15**, 10047–10059.

94 H. J. Chen and S. J. Dong, *Langmuir*, 2007, **23**, 12503–12507.

95 Y. Wang and H. Yang, *Chem. Commun.*, 2006, 2545–2547.

96 L. M. Rossi, G. Machado, P. F. P. Fichtner, S. R. Teixeira and J. Dupont, *Catal. Lett.*, 2004, **92**, 149–155.

97 M. H. G. Prechtl, J. D. Scholten and J. Dupont, *J. Mol. Catal. A: Chem.*, 2009, **313**, 74–78.

98 C. C. Cassol, A. P. Umpierre, G. Machado, S. I. Wolke and J. Dupont, *J. Am. Chem. Soc.*, 2005, **127**, 3298–3299.

99 J. Durand, E. Teuma, F. Malbosc, Y. Kihn and M. Gomez, *Catal. Commun.*, 2008, **9**, 273–275.

100 M. A. Gelesky, A. P. Umpierre, G. Machado, R. R. B. Correia, W. C. Magno, J. Morais, G. Ebeling and J. Dupont, *J. Am. Chem. Soc.*, 2005, **127**, 4588–4589.

101 D. B. Zhao, Z. F. Fei, T. J. Geldbach, R. Scopelliti and P. J. Dyson, *J. Am. Chem. Soc.*, 2004, **126**, 15876–15882.

102 C. Dai, S. M. Zhang, J. Li, Z. S. Wu and Z. J. Zhang, *Chin. J. Inorg. Chem.*, 2007, **23**, 1653–1656.

103 S. M. Zhang, J. Li, C. L. Zhang, Z. S. Wu and Z. J. Zhang, *Chin. J. Inorg. Chem.*, 2007, **23**, 729–732.

104 Y. Hu, Y. Y. Yu, Z. S. Hou, H. Li, X. G. Zhao and B. Feng, *Adv. Synth. Catal.*, 2008, **350**, 2077–2085.

105 Y. Hua, H. Yang, Y. Zhang, Z. Hou, X. Wang, Y. Qiao, H. Li, B. Feng and Q. Huang, *Catal. Commun.*, 2009, in press.

106 J. Huang, T. Jiang, B. X. Han, H. X. Gao, Y. H. Chang, G. Y. Zhao and W. Z. Wu, *Chem. Commun.*, 2003, 1654–1655.

107 Y. Katayama, Y. Bando and T. Miura, *Trans. Inst. Met. Finish.*, 2008, **86**, 205–210.

108 R. R. Deshmukh, R. Rajagopal and K. V. Srinivasan, *Chem. Commun.*, 2001, 1544–1545.

109 N. A. Hamill, C. Hardacre and S. E. J. McMath, *Green Chem.*, 2002, **4**, 139–142.

110 M. Iida, C. Baba, M. Inoue, H. Yoshida, E. Taguchi and H. Furusho, *Chem.–Eur. J.*, 2008, **14**, 5047–5056.

111 S. Choi, K. S. Kim, S. H. Yeon, J. H. Cha, H. Lee, C. J. Kim and I. D. Yoo, *Korean J. Chem. Eng.*, 2007, **24**, 856–859.

112 S. Z. El Abedin and F. Endres, *Electrochim. Acta*, 2009, **54**, 5673–5677.

113 S. A. Meiss, M. Rohnke, L. Kienle, S. Z. El Abedin, F. Endres and J. Janek, *ChemPhysChem*, 2007, **8**, 50–53.

114 S. Z. El Abedin, M. Polleth, S. A. Meiss, J. Janek and F. Endres, *Green Chem.*, 2007, **9**, 549–553.

115 P. Roy, R. Lynch and P. Schmuki, *Electrochem. Commun.*, 2009, **11**, 1567–1570.

116 S. Harada, Y. Kimura, K. Saijo, T. Ogawa and S. Isoda, *J. Colloid Interface Sci.*, 2009, **339**, 373–381.

117 P. Singh, S. Kumar, A. Katyal, R. Kalra and R. Chandra, *Mater. Lett.*, 2008, **62**, 4164–4166.

118 B. Leger, A. Denicourt-Nowicki, A. Roucoux and H. Olivier-Bourbigou, *Adv. Synth. Catal.*, 2008, **350**, 153–159.

119 A. J. Bruss, M. A. Gelesky, G. Machado and J. Dupont, *J. Mol. Catal. A: Chem.*, 2006, **252**, 212–218.

120 L. Yu, H. Sun, J. He, D. Wang, X. Jin, M. Hu and G. Z. Chen, *Electrochem. Commun.*, 2007, **9**, 1374–1381.

121 M. Brettholle, O. Höfft, L. Klarhöfer, S. Mathes, W. Maus-Friedrichs, S. Z. E. Abedin, S. Krischok, J. Janek and F. Endres, *Phys. Chem. Chem. Phys.*, 2010, DOI: 10.1039/b906567a.

122 D. S. Jacob, I. Genish, L. Klein and A. Gedanken, *J. Phys. Chem. B*, 2006, **110**, 17711–17714.

123 Y. Wang and H. Yang, *J. Am. Chem. Soc.*, 2005, **127**, 5316–5317.

124 T. Osaka, T. Hachisu, A. Sugiyama, I. Kawakita, T. Nakanishi and H. Iida, *Chem. Lett.*, 2008, **37**, 1034–1035.

125 Y. Zhao, G. Cui, J. Wang and M. Fan, *Inorg. Chem.*, 2009, **48**, 10435–10441.

126 P. Migowski, *MsC Dissertation*, 2009, PPGQ-UFRGS.

127 T. Gutel, J. Garcia-Anton, K. Pelzer, K. Philippot, C. C. Santini, Y. Chauvin, B. Chaudret and J. M. Basset, *J. Mater. Chem.*, 2007, **17**, 3290–3292.

128 T. Gutel, C. C. Santini, K. Philippot, A. Padua, K. Pelzer, B. Chaudret, Y. Chauvin and J. M. Basset, *J. Mater. Chem.*, 2009, **19**, 3624–3631.

129 A. Manna, T. Imae, M. Iida and N. Hisamatsu, *Langmuir*, 2001, **17**, 6000–6004.

130 A. Berger, R. F. de Souza, M. R. Delgado and J. Dupont, *Tetrahedron: Asymmetry*, 2001, **12**, 1825–1828.

131 J. L. Anthony, E. J. Maginn and J. F. Brennecke, *J. Phys. Chem. B*, 2002, **106**, 7315–7320.

132 P. J. Dyson, G. Laurenczy, C. A. Ohlin, J. Vallance and T. Welton, *Chem. Commun.*, 2003, 2418–2419.

133 S. Arimotoa, H. Kageyama, T. Torimoto and S. Kuwabata, *Electrochem. Commun.*, 2008, **10**, 1901–1904.

134 K. R. Seddon, A. Stark and M. J. Torres, *Pure Appl. Chem.*, 2000, **72**, 2275–2287.

135 J. Dupont, S. M. Silva and R. F. de Souza, *Catal. Lett.*, 2001, **77**, 131–133.

136 G. S. Fonseca, A. P. Umpierre, P. F. P. Fichtner, S. R. Teixeira and J. Dupont, *Chem.–Eur. J.*, 2003, **9**, 3263–3269.

137 G. Schmid, M. Harms, J. O. Malm, J. O. Bovin, J. Vanruitenbeck, H. W. Zandbergen and W. T. Fu, *J. Am. Chem. Soc.*, 1993, **115**, 2046–2048.

138 G. Schmid, *Chem. Rev.*, 1992, **92**, 1709–1727.

139 B. Leger, A. Denicourt-Nowicki, H. Olivier-Bourbigou and A. Roucoux, *Tetrahedron Lett.*, 2009, 6531–6533.

140 I. Favier, S. Massou, E. Teuma, K. Philippot, B. Chaudret and M. Gomez, *Chem. Commun.*, 2008, 3296–3298.

141 C. W. Scheeren, G. Machado, J. Dupont, P. F. P. Fichtner and S. R. Texeira, *Inorg. Chem.*, 2003, **42**, 4738–4742.

142 O. Vidoni, K. Philippot, C. Amiens, B. Chaudret, O. Balmes, J. O. Malm, J. O. Bovin, F. Senocq and M. J. Casanove, *Angew. Chem., Int. Ed.*, 1999, **38**, 3736–3738.

143 K. Pelzer, O. Vidoni, K. Philippot, B. Chaudret and V. Colliere, *Adv. Funct. Mater.*, 2003, **13**, 118–126.

144 P. Migowski, G. Machado, S. R. Texeira, M. C. M. Alves, J. Morais, A. Traverse and J. Dupont, *Phys. Chem. Chem. Phys.*, 2007, **9**, 4814–4821.

145 P. Migowski, S. R. Teixeira, G. Machado, M. C. M. Alves, J. Geshev and J. Dupont, *J. Electron Spectrosc. Relat. Phenom.*, 2007, **156–158**, 195–199.

146 D. O. Silva, J. D. Scholten, M. A. Gelesky, S. R. Teixeira, A. C. B. Dos Santos, E. F. Souza-Aguiar and J. Dupont, *ChemSusChem*, 2008, **1**, 291–294.

147 M. Scariot, D. O. Silva, J. D. Scholten, G. Machado, S. R. Teixeira, M. A. Novak, G. Ebeling and J. Dupont, *Angew. Chem., Int. Ed.*, 2008, **47**, 9075–9078.

148 E. Redel, J. Kramer, R. Thomann and C. Janiak, *J. Organomet. Chem.*, 2009, **694**, 1069–1075.

149 E. Redel, R. Thomann and C. Janiak, *Chem. Commun.*, 2008, 1789–1791.

150 J. Kramer, E. Redel, R. Thomann and C. Janiak, *Organometallics*, 2008, **27**, 1976–1978.

151 Y. Wang, S. Maksimuk, R. Shen and H. Yang, *Green Chem.*, 2007, **9**, 1051.

152 Y. Wang and H. Yang, *Chem. Eng. J.*, 2009, **147**, 71–78.

153 R. C. Jin, Y. C. Cao, E. C. Hao, G. S. Metraux, G. C. Schatz and C. A. Mirkin, *Nature*, 2003, **425**, 487–490.

154 W. C. Bell and M. L. Myrick, *J. Colloid Interface Sci.*, 2001, **242**, 300–305.

155 P. V. Kamat, M. Flumiani and G. V. Hartland, *J. Phys. Chem. B*, 1998, **102**, 3123–3128.

156 C. B. Hwang, Y. S. Fu, Y. L. Lu, S. W. Jang, P. T. Chou, C. R. C. Wang and S. J. Yu, *J. Catal.*, 2000, **195**, 336.

157 Y. Dessiaterik, T. Baer and R. E. Miller, *J. Phys. Chem. A*, 2006, **110**, 1500–1505.

158 Y. Kimura, H. Takata, M. Terazima, T. Ogawa and S. Isoda, *Chem. Lett.*, 2007, **36**, 1130–1131.

159 T. Torimoto, K. Okazaki, T. Kiyama, K. Hirahara, N. Tanaka and S. Kuwabata, *Appl. Phys. Lett.*, 2006, **89**, 243117.

160 W. O. Hofer, in *Sputtering by Particle Bombardment III*, ed. R. Behrisch and K. Wittmaack, Springer, Berlin, 1991, p. 15.

This journal is © The Royal Society of Chemistry 2010

Chem. Soc. Rev., 2010, **39**, 1780–1804 | 1803

161 K. I. Okazaki, T. Kiyama, K. Hirahara, N. Tanaka, S. Kuwabata and T. Torimoto, *Chem. Commun.*, 2008, 691–693.

162 O. P. Khatri, K. Adachi, K. Murase, K. Okazaki, T. Torimoto, N. Tanaka, S. Kuwabata and H. Sugimura, *Langmuir*, 2008, **24**, 7785–7792.

163 K. Okazaki, T. Kiyama, T. Suzuki, S. Kuwabata and T. Torimoto, *Chem. Lett.*, 2009, **38**, 330–331.

164 T. Suzuki, K. Okazaki, T. Kiyama, S. Kuwabata and T. Torimoto, *Electrochemistry*, 2009, **77**, 636–638.

165 T. Tsuda, T. Kurihara, Y. Hoshino, T. Kiyama, K.-i. Okazaki, T. Torimoto and S. Kuwabata, *Electrochemistry*, 2009, **77**, 693–695.

166 W. Wang, S. Efrima and O. Regev, *Langmuir*, 1998, **14**, 602–610.

167 G. T. Wei, Z. S. Yang, C. Y. Lee, H. Y. Yang and C. R. C. Wang, *J. Am. Chem. Soc.*, 2004, **126**, 5036–5037.

168 D. B. Zhao, Z. F. Fei, W. H. Ang and P. J. Dyson, *Small*, 2006, **2**, 879–883.

169 V. Mevellec, B. Leger, M. Mauduit and A. Roucoux, *Chem. Commun.*, 2005, 2838–2839.

170 C. M. Tollan, R. Marcilla, J. A. Pomposo, J. Rodriguez, J. Aizpurua, J. Molina and D. Mecerreyes, *ACS Appl. Mater. Interfaces*, 2009, **1**, 348–352.

171 R. Marcilla, M. L. Curri, P. D. Cozzoli, M. T. Martinez, I. Loinaz, H. Grande, J. A. Pomposo and D. Mecerreyes, *Small*, 2006, **2**, 507–512.

172 M. J. Earle, J. Esperanca, M. A. Gilea, J. N. C. Lopes, L. P. N. Rebelo, J. W. Magee, K. R. Seddon and J. A. Widegren, *Nature*, 2006, **439**, 831–834.

173 J. P. Armstrong, C. Hurst, R. G. Jones, P. Licence, K. R. J. Lovelock, C. J. J. Satterley and I. J. Villar-Garcia, *Phys. Chem. Chem. Phys.*, 2007, **9**, 982–990.

174 O. Hofft, S. Bahr, M. Himmerlich, S. Krischok, J. A. Schaefer and V. Kempter, *Langmuir*, 2006, **22**, 7120–7123.

175 E. F. Smith, F. J. M. Rutten, I. J. Villar-Garcia, D. Briggs and P. Licence, *Langmuir*, 2006, **22**, 9386–9392.

176 E. F. Smith, I. J. V. Garcia, D. Briggs and P. Licence, *Chem. Commun.*, 2005, 5633–5635.

177 F. J. M. Rutten, H. Tadesse and P. Licence, *Angew. Chem., Int. Ed.*, 2007, **46**, 4163–4165.

178 F. Maier, J. M. Gottfried, J. Rossa, D. Gerhard, P. S. Schulz, W. Schwieger, P. Wasserscheid and H. P. Steinruck, *Angew. Chem., Int. Ed.*, 2006, **45**, 7778–7780.

179 C. W. Scheeren, G. Machado, S. R. Teixeira, J. Morais, J. B. Domingos and J. Dupont, *J. Phys. Chem. B*, 2006, **110**, 13011–13020.

180 M. Scariot, D. O. Silva, J. D. Scholten, G. Machado, S. R. Teixeira, M. A. Novak, G. Ebeling and J. Dupont, *Angew. Chem., Int. Ed.*, 2008, **47**, 9075–9078.

181 L. M. Rossi, J. Dupont, G. Machado, P. F. P. Fichtner, C. Radtke, I. J. R. Baumvol and S. R. Teixeira, *J. Braz. Chem. Soc.*, 2004, **15**, 904–910.

182 R. R. Deshmukh, R. Rajagopal and K. V. Srinivasan, *Chem. Commun.*, 2001, 1544–1545.

183 R. Crabtree, *Acc. Chem. Res.*, 1979, **12**, 331–338.

184 M. T. Reetz and J. G. de Vries, *Chem. Commun.*, 2004, 1559–1563.

185 A. H. M. de Vries, J. Mulders, J. H. M. Mommers, H. J. W. Henderickx and J. G. de Vries, *Org. Lett.*, 2003, **5**, 3285–3288.

186 A. Alimardanov, L. S. V. de Vondervoort, A. H. M. de Vries and J. G. de Vries, *Adv. Synth. Catal.*, 2004, **346**, 1812–1817.

187 A. S. Gruber, D. Pozebon, A. L. Monteiro and J. Dupont, *Tetrahedron Lett.*, 2001, **42**, 7345–7348.

188 C. S. Consorti, F. R. Flores and J. Dupont, *J. Am. Chem. Soc.*, 2005, **127**, 12054–12065.

189 C. S. Consorti, M. L. Zanini, S. Leal, G. Ebeling and J. Dupont, *Org. Lett.*, 2003, **5**, 983–986.

190 A. F. Schmidt, A. Al Halaiqa and V. V. Smirnov, *Synlett*, 2006, 2861–2878.

191 X. D. Mu, J. Q. Meng, Z. C. Li and Y. Kou, *J. Am. Chem. Soc.*, 2005, **127**, 9694–9695.

192 M. Zou, X. D. Mu, N. Yan and Y. Kou, *Chin. J. Catal.*, 2007, **28**, 389–391.

193 C. X. Mao, H. Z. Wang, X. D. Mu and Y. Kou, *J. Catal.*, 2007, **250**, 25–32.

194 X. Yang, Z. F. Fei, D. B. Zhao, W. H. Ang, Y. D. Li and P. J. Dyson, *Inorg. Chem.*, 2008, **47**, 3292–3297.

195 X. Yang, N. Yan, Z. F. Fei, R. M. Crespo-Quesada, G. Laurenczy, L. Kiwi-Minsker, Y. Kou, Y. D. Li and P. J. Dyson, *Inorg. Chem.*, 2008, **47**, 7444–7446.

196 F. R. Abreu, D. G. Lima, E. H. Hamu, C. Wolf and P. A. Z. Suarez, *J. Mol. Catal. A: Chem.*, 2004, **209**, 29–33.

197 J. H. Davis, *Chem. Lett.*, 2004, **33**, 1072–1077.

198 Z. F. Fei, T. J. Geldbach, D. B. Zhao and P. J. Dyson, *Chem.-Eur. J.*, 2006, **12**, 2123–2130.

199 D. B. Zhao, Z. F. Fei, R. Scopelliti and P. J. Dyson, *Inorg. Chem.*, 2004, **43**, 2197–2205.

200 C. P. Mehnert, *Chem.–Eur. J.*, 2004, **11**, 50–56.

201 A. Riisager, R. Fehrmann, M. Haumann and P. Wasserscheid, *Top. Catal.*, 2006, **40**, 91–102.

202 M. A. Gelesky, S. S. X. Chiaro, F. A. Pavan, J. H. Z. dos Santos and J. Dupont, *Dalton Trans.*, 2007, 5549–5553.

203 Y. S. Chun, J. Y. Shin, C. E. Song and S. G. Lee, *Chem. Commun.*, 2008, 942–944.

204 Z. J. Wang, Q. X. Zhang, D. Kuehner, X. Y. Xu, A. Ivaska and L. Niu, *Carbon*, 2008, **46**, 1687–1692.

205 M. A. Gelesky, C. W. Scheeren, L. Foppa, F. A. Pavan, S. L. P. Dias and J. Dupont, *Biomacromolecules*, 2009, **10**, 1888–1893.

206 M. Pumera, S. Sanchez, I. Ichinose and J. Tang, *Sens. Actuators, B*, 2007, **123**, 1195–1205.

207 Q. Kang, L. X. Yang and Q. Y. Cai, *Bioelectrochemistry*, 2008, **74**, 62–65.

208 D. V. Chernyshov, N. V. Shuedene, E. R. Antipova and I. V. Pletnev, *Anal. Chim. Acta*, 2008, **621**, 178–184.

209 M. Musameh and J. Wang, *Anal. Chim. Acta*, 2008, **606**, 45–49.

210 A. C. Franzoi, P. Migowski, J. Dupont and I. C. Vieira, *Anal. Chim. Acta*, 2009, **639**, 90–95.

211 D. Brondani, J. Dupont, A. Spinelli and I. C. Vieira, *Sens. Actuators, B*, 2009, **138**, 236–243.

212 A. C. Franzoi, J. Dupont, A. Spinelli and I. C. Vieira, *Talanta*, 2009, **77**, 1322–1327.

213 P. Lozano, T. de Diego, D. Carrie, M. Vaultier and J. L. Iborra, *Chem. Commun.*, 2002, 692.

214 P. Lozano, T. de Diego, D. Carrie, M. Vaultier and J. L. Iborra, *J. Mol. Catal. B: Enzym.*, 2003, **21**, 9.

215 R. A. Sheldon, R. M. Lau, M. J. Sorgedrager, F. van Rantwijk and K. R. Seddon, *Green Chem.*, 2002, **4**, 147–151.

216 M. Gamba, A. A. M. Lapis and J. Dupont, *Adv. Synth. Catal.*, 2008, **350**, 160–164.

217 S. C. Fernandes, S. K. Moccelini, C. W. Scheeren, P. Migowski, J. Dupont, M. Heller, G. A. Micke and I. C. Vieira, *Talanta*, 2009, **79**, 222–228.

218 A. C. Franzoi, I. C. Vieira, J. Dupont, C. W. Scheeren and L. F. d. Oliveira, *Analyst*, 2009, **134**, 2320–2328.

219 D. Brondani, C. W. Scheeren, J. Dupont and I. C. Vieira, *Sens. Actuators, B*, 2009, **140**, 252–259.

Artigo II

Tuning the Selectivity of Ruthenium Nanoscale Catalysts with Functionalised Ionic Liquids: Hydrogenation of Nitriles

Martin H. G. Prechtl, Jackson D. Scholten and Jairton Dupont

Tuning the selectivity of ruthenium nanoscale catalysts with functionalised ionic liquids: Hydrogenation of nitriles

Martin H.G. Prechtl, Jackson D. Scholten, Jairton Dupont*

Laboratory of Molecular Chemistry, Institute of Chemistry, Universidade Federal do Rio Grande do Sul, Av. Bento Gonçalves 9500, 91501-970 Porto Alegre, RS, Brazil

ARTICLE INFO

ABSTRACT

Ruthenium nanoparticles prepared in nitrile-functionalised ionic liquids (ILs) display unusual selectivities toward the hydrogenation of nitrile containing aromatic compounds. In particular, a selective catalytic hydrogenative coupling of nitriles was observed. In this transformation, nitrile groups are exclusively hydrogenated in the presence of arenes, which are typically hydrogenated by ruthenium nanoparticles in non-functionalised ILs. The catalyst material was characterised by means of TEM and EDS analysis. Furthermore, molecular species formed during the catalytic process were characterised by MS-analysis of the gaseous phase and the ionic liquid phase by ESI/MS Q-TOF.

© 2009 Elsevier B.V. All rights reserved.

1. Introduction

Catalytic hydrogenation and dehydrogenation reactions play an important role in both industrial processes and academic research [1]. In recent years, the progress in the catalytic hydrogenation of multiple carbon–carbon and carbon–heteroatom bonds by soluble metal nanoparticles (MNPs) has seen remarkable growth [2]. In most cases, these MNPs display typical surface-like (heterogeneous) catalytic properties rather than single site (homogeneous) catalytic properties [3,4]. For example, the hydrogenation of *O*-substituted arenes such as anisole by Ir(0) nanoparticles occurs with concomitant hydrogenolysis of the C–O bond. Hydrogenation of the aromatic ring takes place preferentially in ketone-containing aromatic compounds [5,6]. However, it is evident that the surface properties of soluble MNPs can be modulated by the addition of ligands akin to classical coordination catalysis, as is observed in enantioselective allylic alkylation catalysed by palladium nanoparticles modified with chiral xylofuranoside diphosphites. Under these reaction conditions, the catalysts provided different selectivity than typically observed for monometallic catalysts [7]. Herein, we report that the catalytic surface properties of ruthenium nanoparticles in ILs can be tuned by the use of nitrile containing ligand/substrates. In particular, a clean hydrogenative

coupling reaction of benzonitrile by aminolysis to provide (*E*)-*N*-benzylidene-1-phenylmethanamine takes place without arene hydrogenation [8].

For the present study, we chose nitrile-functionalised 1-butyronitrile-3-methylimidazolium bis(trifluoromethane-sulfonyl)-imidate ionic liquid **1** (Fig. 1), since it may stabilise the ruthenium nanoscale catalyst via nitrile binding without blocking the coordination of the substrates. Indeed, this ionic liquid was readily prepared and successfully applied by Dyson and co-workers for cross-coupling reactions by Pd nanoparticles [9,10].

2. Experimental

2.1. General methods: reagents, reactors and analyses techniques

All manipulations involving the ruthenium complexes were carried out under an argon atmosphere using Schlenk techniques. [Ru(COD)(2-methylallyl)₂] was obtained from Sigma–Aldrich and used without further purification. The IL (BCN)MI·NTf₂ was prepared according to known procedures [9,11], dried at 70 °C over night under reduced pressure, and stored under argon. Benzonitrile was degassed and stored under argon prior to use. All the other chemicals were purchased from commercial sources and used without further purification. NMR spectra were recorded on a Varian VNMR spectrometer (300 MHz). Mass spectra were obtained using an ESI/MS micromass Q-TOFmicro and HIDEN QIC-20 quadrupole mass spectrometer gas-analyser. Gas chromatogra-
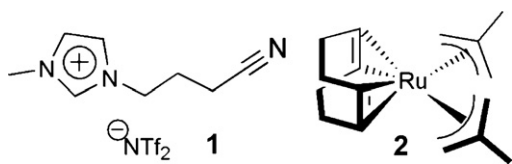
Fig. 1. Imidazolium IL **1** (BCN)MI·NTf$_2$ with a pendant nitrile functionality in the side-chain, which served as a stabilising group and a ruthenium precursor, **2**.

phy analyses were performed with a Hewlett–Packard-5890 gas chromatograph with an FID and a 30 m capillary column with a dimethylpolysiloxane stationary phase. Transmission electron microscopy (TEM) and EDS were performed on a JEOL–JEM 2010 operating at 200 kV with a magnification of 150 k. The nanoparticle formation and catalytic hydrogenation reactions were carried out in a modified stainless steel reactor (4–25 bar) or modified Fischer–Porter bottle (4 bar) with a glass insert immersed in a silicone oil bath and pressurised with hydrogen gas (4–25 bar). The substrates were added with a gas-tight precision syringe (2 mL). The temperature was maintained at 50 °C and 90 °C by a hot-stirring plate connected to a digital controller (ETS-D4 IKA). The catalyst/substrate ratios were calculated from the initial quantity of [Ru(COD)(2-methylallyl)$_2$] used.

2.2. Synthesis of ruthenium nanoparticle in ionic liquids

A stainless steel reactor was loaded with [Ru(COD)(2-methylallyl)$_2$] (45 mg, 141 μmol) under a flow of argon. Next,

(BCN)MI·NTf$_2$ (0.3 mL) was added via syringe under an argon flow. The mixture was stirred at room temperature for 60 min resulting in a turbid dispersion. The system was heated to 50 °C, and hydrogen (4 bar) was admitted to the system. After stirring for 18 h, a black suspension was obtained. The reactor was kept under reduced pressure to remove the formed cyclooctane and isobutane. The Ru nanoparticles embedded in the IL were analysed by TEM and used for subsequent catalytic experiments.

2.3. Catalytic hydrogenation of nitriles

Benzonitrile (2.0 mL, 19.4 mmol) was added to an ionic catalytic solution obtained as previously described, and the reactor was pressurised with 25 bar hydrogen gas at room temperature and heated to 90 °C (27 bar) for 22 h. Next, a gas sample was analysed with a MS quadrupole by connecting the reactor to the gas-analyser. The reactor was cooled to room temperature, pressure was released, and the reaction mixture was extracted with pentane (5× 2 mL). *CAUTION: The pressure should be released carefully in a well-ventilated fumehood because significant amounts of odorous and toxic ammonia is set free!* Samples of the organic layer were analysed by NMR and GC, with both methods indicating 70% conversion, and NMR confirmed this conversion by analysis of the crude reaction mixture. The Ru/IL-phase was analysed by ESI/MS and TEM. Catalysis with toluene was performed in a similar manner, but toluene was readily quantitatively isolated by condensation at reduced pressure into a cold-trap.
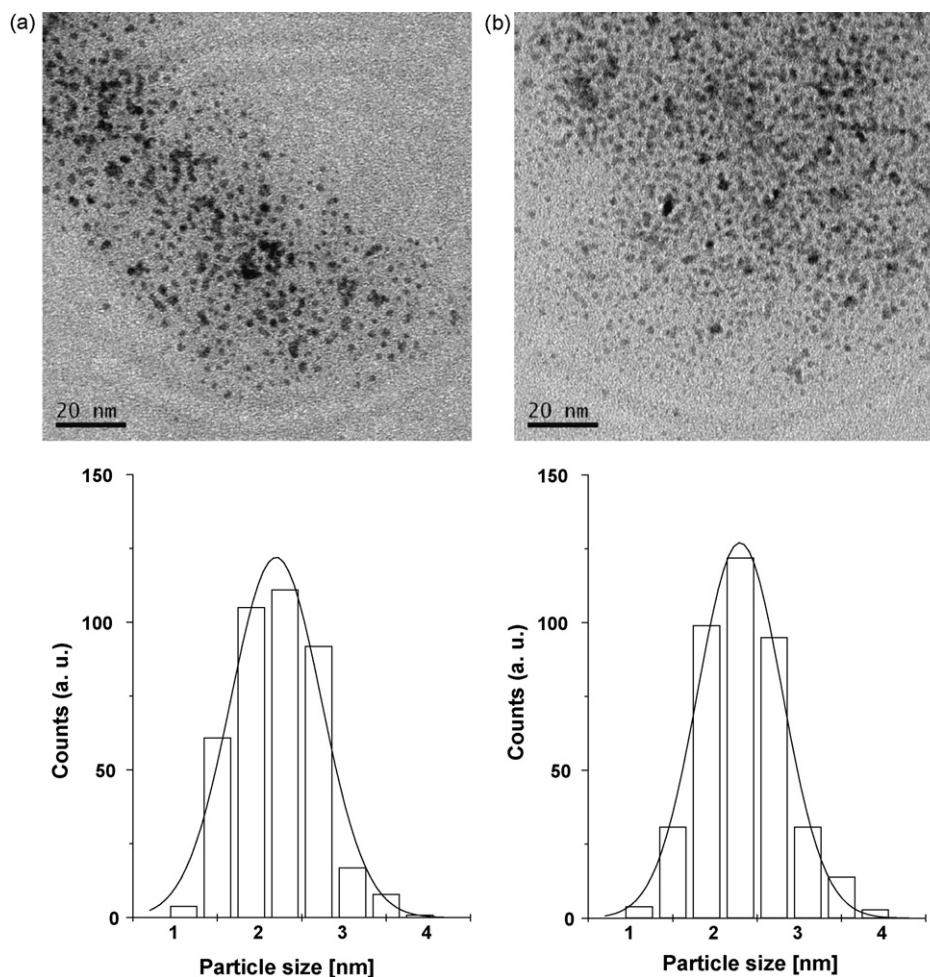
Fig. 2. Ru-NPs: (a) before catalysis (2.2 ± 0.5 nm) and (b) after catalysis (2.3 ± 0.5 nm) in IL (BCN)MI·NTf$_2$.

2.4. Sample preparation for TEM analysis

In order to perform TEM analysis, a drop of the suspension containing the Ru nanoparticles embedded in the IL was dispersed in isopropanol, and a small quantity of this dispersion was placed on a carbon-coated copper grid. Particle size distributions were determined from digital images. Nanoparticle diameters were estimated from ensembles of 200 particles (400 counts) chosen in arbitrary areas of the enlarged micrographs. The diameters of the particles in the micrographs were measured using Sigma Scan Pro 5.

3. Results and discussion

The treatment of [Ru(COD)(2-methylallyl)$_2$] **2** (COD = 1,5-cyclooctadiene) with hydrogen gas in (BCN)MI·NTf$_2$ **1** leads to the formation of stable and small-sized Ru-NPs (2.2 ± 0.5 nm, Fig. 2). The dimensions of the Ru-NPs in (BCN)MI·NTf$_2$ were comparable to those prepared in BMI·NTf$_2$ (2.1 nm; 1-*n*-butyl-3-methylimidazolium bis(trifluoromethane-sulfonyl)imidate) and DMI·NTf$_2$ (2.1 nm; 1-*n*-decyl-3-methylimidazolium bis(trifluoromethane-sulfonyl)imidate) [12]. This result highlights capability of (BCN)MI·NTf$_2$ to keep the Ru-NPs well dispersed and with low agglomeration. Although the nitrile group is maintained during the synthesis of the Ru-NPs (4 bar H$_2$, 50 °C, 18 h), it reacts after 5 days to provide primarily the reductive coupling product (see below). Most importantly, contrary to earlier observations of Ru-NPs dispersed in BMI·NTf$_2$ [12], these Ru-NPs are inactive toward the hydrogenation of aromatic compounds such as toluene, even under moderately forcing conditions (25 bar H$_2$ and 90 °C). However, under these reaction conditions, the reductive nitrile condensation product **6** was obtained in good yields (Scheme 1). Furthermore, the treatment of the Ru-NPs in (BCN)MI·NTf$_2$ in the presence of benzonitrile yields preferentially (*E*)-*N*-benzylidene-1-phenylmethanamine **5**. As indicated by the histograms in Fig. 2, the mean particle size (2.2–2.3 ± 0.5 nm) remained unchanged within the standard variation (0.5 nm) before (2.2 nm) and after catalysis (2.3 nm).

Analysis of the IL-phase by ESI(+)/MS and ^{13}C NMR confirmed the hydrogenative coupling of the nitrile group. Importantly, the ESI(+)/MS-analysis provided detailed insight into the overall reaction pathway of the nitrile hydrogenation of IL **1**, as well as into the catalytic hydrogenation of benzonitrile (Scheme 1). Analysis of a reaction sequence indicated the presence of unreacted IL **1**, with (m/z) M$^+$ 150.11 after 18 h at 50 °C and 4 bar H$_2$. Next, at 90 °C and 25 bar H$_2$, the ESI(+)/MS spectrogram showed four distinct species (Fig. 3): IL **1** (150.15, M$^+$), IL **3** (154.18, M$^+$; 77.59, M^{2+}, IL-amine), IL **7** (137.15, M$^+$, −NH$_3$), and IL **6** (145.66, M^{2+}; 97.44, M^{3+}, condensed dimer). This indicated that the Ru-NPs first catalysed the hydrogenation of the aliphatic nitrile to a primary amine (IL **3**), followed by subsequent aminolysis, resulting in the secondary imine IL **6** and in IL **7**.

The ESI(+)/MS of the catalytic hydrogenation of benzonitrile showed IL **1** (150.07, M$^+$), (*E*)-*N*-benzylidene-1-phenylmethanamine **5** (196.08, M$^+$) and the IL **4** (242.24). Most likely, (*E*)-*N*-benzylidene-1-phenylmethanamine **5** was detectable by ESI(+)/MS due to protonation from residual water content from the solvent (MeCN) used for this analysis. It is interesting to note that no benzylamine (protonated or not) was observed neither by ESI-MS or ^{1}H NMR indicating that such species are highly reactive undergoing rapidly coupling process to yield **5**. As such, the overall reaction pathway likely involves aminolysis, since ammonia was detected in the gaseous phase of the reactor during the benzonitrile hydrogenation by a MS Q-TOF gas-analyser (Fig. 4). The detected fragmentation of the sample is concurrent to the MS data listed in the literature (NIST). By time-resolved
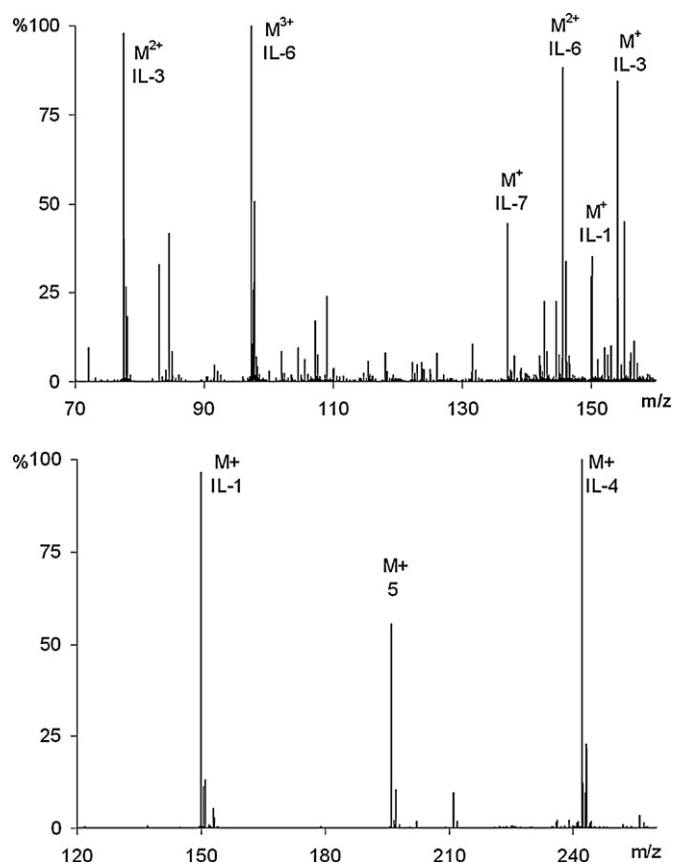
Fig. 3. ESI(+) spectrum of the hydrogenation of imidazolium IL **1** (BCN)MI·NTf$_2$ (top) and hydrogenation of benzonitrile forming (*E*)-*N*-benzylidene-1-phenylmethanamineand IL-**4** (bottom).
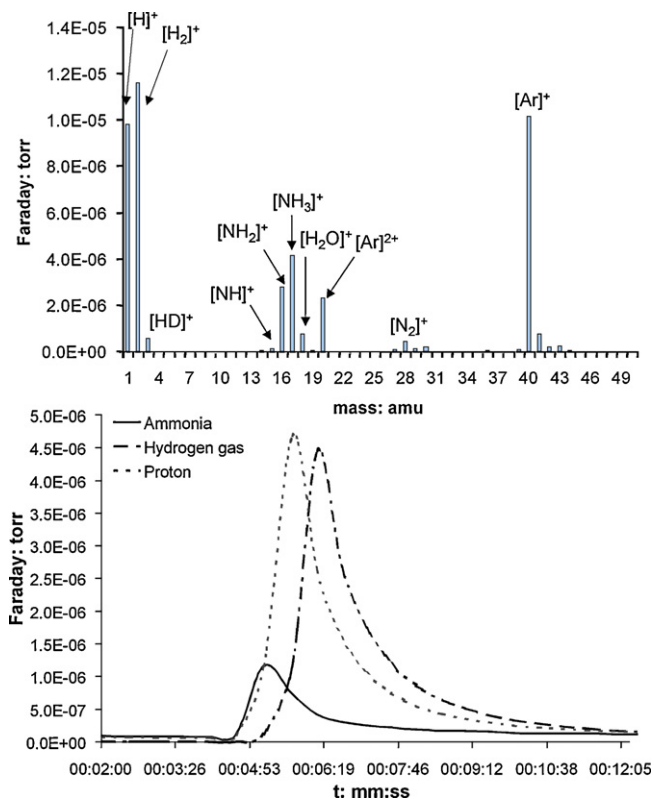
Fig. 4. MS spectrogram of the online analysis of the gaseous phase (top), and the time-resolved gas-injection monitoring of the M$^+$ of ammonia and hydrogen gas (bottom).
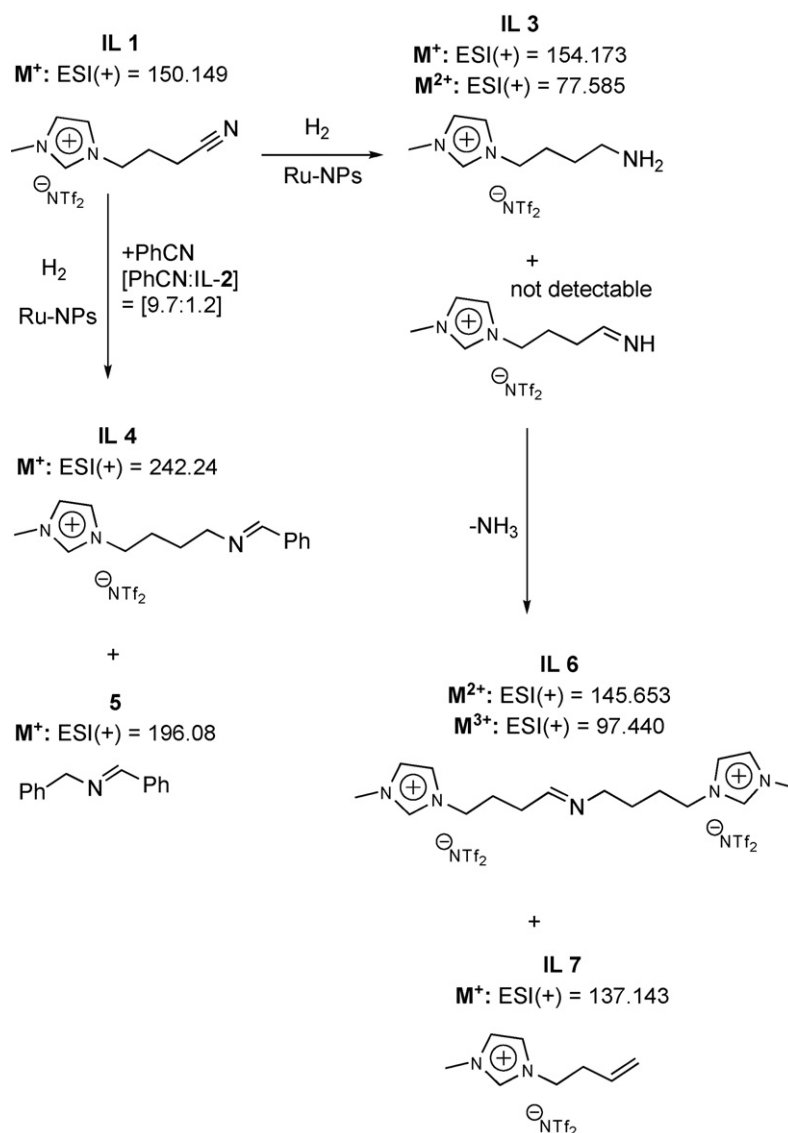
Scheme 1. Reaction pathways of the nitrile hydrogenation in the presence and in the absence of benzonitrile.

gas-injection monitoring of the M$^+$ of ammonia and hydrogen gas, it is clearly shown that a significant amount of ammonia is formed in relation to the excess hydrogen gas. Considering the described reaction pathway in Scheme 1 and the quantification of **5** by GC (70%; catalyst-system was recycled for three runs under identical conditions), the detection of ammonia by MS Q-TOF is related to a concentration of 6.8 mmol NH$_3$ extruded by aminolysis.

It is likely that in these systems the nitrile group is strongly coordinated to the ruthenium surface and is not easily displaced by the aromatic ring of toluene or benzonitrile. This selectivity is the opposite of that observed for the hydrogenation of aromatic ketones, in which the arene groups are preferentially hydrogenated [6]. In order to further confirm our hypothesis that the selectivity depends on the functional group of the IL **1** and not on the ruthenium nanoparticles, the arene hydrogenation catalyst-system Ru-NPs/BMI·NTf$_2$ **8** was tested for hydrogenation of benzonitrile under conditions identical to the Ru/(BCN)MI·NTf$_2$ system. System **8** catalyses the reaction of benzonitrile to (E)-N-benzylidene-1-phenylmethanamine **5** in 65% yield. This result indicates that the selectivity of the Ru-NPs/(BCN)MI·NTf$_2$ system likely depends on the IL support and not on the ruthenium nano-material.

It is possible that the true catalyst might be a molecular ruthenium species with IL-**1** acting as ligand, with the Ru-NPs simply acting as a reservoir for ruthenium atoms [13–15]. This might explain the exclusive hydrogenation of the nitrile, in which ruthenium polyhydride complexes are active for nitrile hydrogenation [16], while examples for molecular catalysts for arene hydrogenation are rare [17]. To provide support for this molecular pathway, we attempted to hydrogenate benzonitrile in the absence of IL under the reaction conditions in which the benzonitrile could only be hydrogenated by the molecular ruthenium precursor **2**; this reaction was unsuccessful. The present Ru-NPs do not show activity for arene hydrogenation, while other ILs Ru-NPs are active toward arene hydrogenation [12,18,19]. Additionally, the activation energy for toluene hydrogenation with ruthenium catalysts in IL is approximately 20% lower than the activation energy for hydrogenation of nitrile groups in ILs [8,12]. These results strongly indicate that the presence of the nitrile group in the IL side-chain influences the interaction between the Ru-NP surfaces and a corresponding substrate. The nitrile group of the IL coordinates as a ligand to the metal surface, forming an IL-layer and causing the surface to be blocked for coordination by arenes, since nitriles are known to strongly adsorb to solid metal catalysts [20,21]. Therefore, substrates bear-
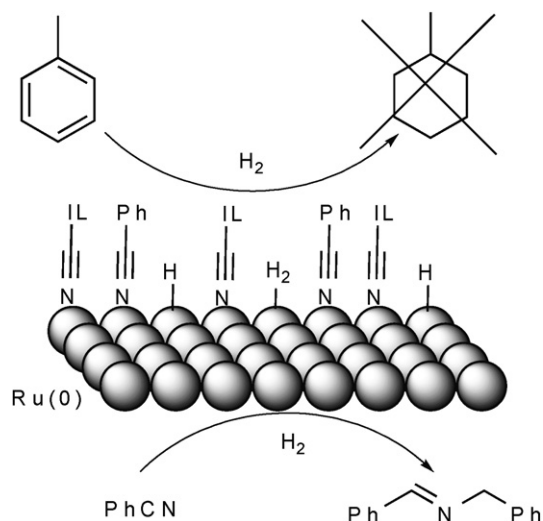
Fig. 5. Model depicting the Ru-NPs protected by a layer of (BCN)MI·NTf$_2$ and substrate nitriles, where nitriles are hydrogenated and arenes are not.

ing a nitrile group coordinated preferentially to the metal surface via ligand exchange, and arenes are unable to contact the catalyst (Fig. 5).

Moreover, it is well known that the hydrogenation of PhCN to benzylamine is catalysed by molecular complexes [22–24]. In the case of metal surfaces [20,21,25] the activated amine – benzylamine – is rapidly transformed into the benzylidene benzylamine via aminolysis and coupling although we were unable to detect neither benzylamine nor benzylimine by ESI-MS and NMR experiments. As already pointed out benzylamine undergoes exclusively aminolysis with solid catalysts, in contrast molecular catalysts give benzylamine as main product [22–24].

4. Conclusions

In conclusion, we have illustrated the influence of nitrile-functionalised ILs for the synthesis and application of ruthenium nanoscale catalysts, previously designed for arene hydrogenation in non-functionalised ILs. Both systems (Ru-NPs/(BCN)MI·NTf$_2$ and Ru-NPs/BMI·NTf$_2$) are active toward the hydrogenation of nitriles. Using IL **1**, the inherent functionality of the IL tunes the selectivity of the hydrogenation catalyst, preventing arene hydrogenation. However, nitriles remain competent substrates for hydrogenation. We propose that the selectivity for hydrogenation of other func-

tional groups can be influenced in a similar manner by this class of functionalised IL support. Our ongoing studies are aimed at improving the selectivity of hydrogenations of aliphatic nitriles to primary amines, and our results will be reported in due course.

References

[1] P.G. Jessop, R.H. Morris, Coord. Chem. Rev. 121 (1992) 155–284.
[2] D. Astruc, F. Lu, J.R. Aranzaes, Angew. Chem.-Int. Edit. 44 (2005) 7852–7872.
[3] A. Roucoux, J. Schulz, H. Patin, Chem. Rev. 102 (2002) 3757–3778.
[4] P. Migowski, J. Dupont, Chem.-Eur. J. 13 (2007) 32–39.
[5] G.S. Fonseca, A.P. Umpierre, P.F.P. Fichtner, S.R. Teixeira, J. Dupont, Chem.-Eur. J. 9 (2003) 3263–3269.
[6] G.S. Fonseca, J.D. Scholten, J. Dupont, Synlett (2004) 1525–1528.
[7] S. Jansat, M. Gomez, K. Philippot, G. Muller, E. Guiu, C. Claver, S. Castillon, B. Chaudret, J. Am. Chem. Soc. 126 (2004) 1592.
[8] For the hydrogenation of nitriles in ionic liquids see: K. Obert, D. Roth, M. Ehrig, A. Schönweiz, D. Assenbaum, H. Lange, P. Wasserscheid, Appl. Catal. A 356 (2009) 43–51.
[9] D.B. Zhao, Z.F. Fei, R. Scopelliti, P.J. Dyson, Inorg. Chem. 43 (2004) 2197–2205.
[10] Z.F. Fei, D.B. Zhao, D. Pieraccini, W.H. Ang, T.J. Geldbach, R. Scopelliti, C. Chiappe, P.J. Dyson, Organometallics 26 (2007) 1588–1598.
[11] C.C. Cassol, G. Ebeling, B. Ferrera, J. Dupont, Adv. Synth. Catal. 348 (2006) 243–248.
[12] M.H.G. Prechtl, M. Scariot, J.D. Scholten, G. Machado, S.R. Teixeira, J. Dupont, Inorg. Chem. 47 (2008) 8995–9001.
[13] M.T. Reetz, J.G. de Vries, Chem. Commun. (2004) 1559–1563.
[14] C.C. Cassol, A.P. Umpierre, G. Machado, S.I. Wolke, J. Dupont, J. Am. Chem. Soc. 127 (2005) 3298–3299.
[15] A.S. Gruber, D. Pozebon, A.L. Monteiro, J. Dupont, Tetrahedron Lett. 42 (2001) 7345–7348.
[16] R.P. Beaty, R.A. Paciello, WO9623802-A (1996).
[17] P.J. Dyson, Dalton Trans. (2003) 2964–2974.
[18] E.T. Silveira, A.P. Umpierre, L.M. Rossi, G. Machado, J. Morais, G.V. Soares, I.L.R. Baumvol, S.R. Teixeira, P.F.P. Fichtner, J. Dupont, Chem.-Eur. J. 10 (2004) 3734–3740.
[19] T. Gutel, J. Garcia-Anton, K. Pelzer, K. Philippot, C.C. Santini, Y. Chauvin, B. Chaudret, J.M. Basset, J. Mater. Chem. 17 (2007) 3290–3292.
[20] A. Chojecki, M. Veprek-Heijman, T.E. Muller, P. Scharringer, S. Veprek, J.A. Lercher, J. Catal. 245 (2007) 237–248.
[21] P. Scharringer, T.E. Muller, J.A. Lercher, J. Catal. 253 (2008) 167–179.
[22] S. Enthaler, D. Addis, K. Junge, G. Erre, M. Beller, Chem.-Eur. J. 14 (2008) 9491–9494.
[23] S. Enthaler, K. Junge, D. Addis, G. Erre, M. Beller, ChemSusChem 1 (2008) 1006–1010.
[24] D. Addis, S. Enthaler, K. Junge, B. Wendt, M. Beller, Tetrahedron Lett. 50 (2009) 3654–3656.
[25] P. Scharringer, T.E. Muller, A. Jentys, J.A. Lercher, J. Catal. 263 (2009) 34–41.

Artigo III

Imidazolium Ionic Liquids as Promoters and Stabilising Agents for the Preparation of Metal(0) Nanoparticles by Reduction and Decomposition of Organometallic Complexes

Martin H. G. Prechtl, Paul S. Campbell, Jackson D. Scholten, Georgina B. Fraser, Giovanna Machado, Catherine C. Santini, Jairton Dupont and Yves Chauvin

Imidazolium ionic liquids as promoters and stabilising agents for the preparation of metal(0) nanoparticles by reduction and decomposition of organometallic complexes

Martin H. G. Prechtl,†*[a] Paul S. Campbell,[b] Jackson D. Scholten,[a] Georgina B. Fraser,[b] Giovanna Machado,[c] Catherine C. Santini,*[b] Jairton Dupont*[a] and Yves Chauvin[b]

The organometallic complexes ([Ru(COD)(2-methylallyl)$_2$] and [Ni(COD)$_2$] (COD = 1,5-cyclooctadiene) dissolved in imidazolium ionic liquids (ILs) undergo reduction and decomposition, respectively, to afford stable ruthenium and nickel metal(0) nanoparticles (Ru(0)-NPs and Ni(0)-NPs) in the absence of classical reducing agents. Depending on the case, the reduction/auto-decomposition is promoted by either the cation and/or anion of the neat imidazolium ILs.

Introduction

In recent years, ILs have proven their versatility in synthetic and catalytic applications, provoking ever-growing interest in both academic and industrial research. One particularly intriguing field is the synthesis of nanoscale metal catalysts of controlled size and shape, namely metal(0) nanoparticles (M-NPs).[1–4] ILs have unique and tuneable properties useful in the synthesis of M-NPs *via* chemical routes. This can be controlled simply by incorporating coordinating groups,[5–7] varying the coordination strength of the anion,[8,9] or changing the length of the alkyl-chain in the cation.[10–15] In general, appropriate metal complexes or metal salts are dispersed/dissolved in the IL and subsequently reduced to the corresponding M-NPs, in the ubiquitous presence of reducing reagents such as molecular hydrogen gas, complex hydrides (NaBH$_4$ and LiAlH$_4$), hydrazine,[1–4] alcohols,[16] and thiols.[17] In some cases, the IL itself can carry the reducing agent, *e.g.* hydroxylated imidazolium salts,[18,19] and depending on the redox potential of the metal precursor, the imidazolium cation may even undergo oxidation. For example, in the case of Au(III), the imidazolium cation itself can act as a reducing agent to yield prismatic gold particles in BMI·PF$_6$.[20]

The preparation of M-NPs in ILs by simple decomposition of organometallic compounds in their formal zero oxidation states is invariably performed in the presence of hydrogen[11,21,22] or under thermal[8,15,23] or photolytic[9] conditions.

In this work, we report a novel approach for the synthesis of Ru(0)- and Ni(0)-NPs in imidazolium ILs, which act as incommensurably mild reducing/decomposing reagents for the organometallic complexes [Ru(COD)(2-methylallyl)$_2$]

(COD = 1,5-cyclooctadiene) and [Ni(COD)$_2$] under very mild conditions. In these studies the role of both anion and cation is addressed and reaction pathways for the reduction/decomposition processes are proposed.

Results and discussion

The formation of Ru(0)-NPs using standard protocol with [Ru(COD)(2-methylallyl)$_2$] in IL (*i.e.* under 4 bar hydrogen at 50 °C)[7,14] was accompanied by the evolution of small amounts of odorous by-products (characteristic of ammonia/amines). This odour was particularly intense in the ILs BMI·NTf$_2$ and HM$_2$I·NTf$_2$ (Fig. 1).

The volatiles were thus analysed online in the gas phase with a mass gas-analyser. Indeed, compounds were detected with masses that could be assigned to small molecules formed due to the fragmentation of the imidazolium ring, such as acetonitrile/isocyanomethane (M$^+$ = 41), methylamine (M$^+$ = 29, MeN), ethylene (M$^+$ = 28) and hydrogen cyanide (M$^+$ = 27). Moreover, the observed C$_4$-fragment signals (M$^+$ = 56–58) provide strong evidence for the decomposition of the ruthenium complex [Ru(COD)(2-methylallyl)$_2$] involving the formation of isobutene/isobutane from the 2-methylallyl-ligand in the Ru(II) complex. Interestingly, the fragmentation of the IL seems to occur only during the reduction of Ru complex, but it is not promoted by the Ru(0)-NPs. The gaseous by-products were exclusively detected during the NP synthesis, but not when Ru(0)-NPs were stirred in BMI·NTf$_2$ and HM$_2$I·NTf$_2$ for a prolonged duration (several days) under identical conditions. A similar observation for the imidazolium ring fragmentation has previously been made, during the ultrasonic irradiation of imidazolium chloride

[a]Laboratory of Molecular Catalysis, Institute of Chemistry, Universidade Federal do Rio Grande do Sul, Av. Bento Gonçalves 9500, 91501-970 Porto Alegre, RS, Brazil. E-mail: jairton.dupont@ufrgs.br; Fax: +55 51 33087304; Tel: +55 51 33086321
[b]Université de Lyon, Institut de Chimie de Lyon, C2P2, UMR 5265 CNRS—ESCPE Lyon, 43 bd du 11 Novembre 1918, F-69626 Villeurbanne Cedex, France. E-mail: santini@cpe.fr
[c]Centro de Tecnologias Estratégicas do Nordeste—CETENE, 50740-540 Recife, PE, Brazil
† Present address: Humboldt University Berlin, Brook-Taylor-Strasse 2, 12489 Berlin, Germany. E-mail: . E-mail: martin.prechtl@hu-berlin.de
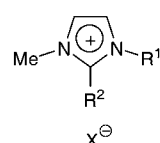
BMI.NTf$_2$, R^1= ^{n}Bu, R^2= H, X= N(SO$_2$CF$_3$)$_2$
HM$_2$I.NTf$_2$, R^1= ^{n}Hex, R^2= Me, X= N(SO$_2$CF$_3$)$_2$
BMI.BF$_4$, R^1= ^{n}Bu, R^2= H, X= BF$_4$
EMI.B(CN)$_4$, R^1= Et, R^2= H, X= B(CN)$_4$
BMI.N(CN)$_2$, R^1= ^{n}Bu, R^2= H, X= N(CN)$_2$
EMI.NTf$_2$, R^1= Et, R^2= H, X= N(SO$_2$CF$_3$)$_2$
BM$_2$I.NTf$_2$, R^1= ^{n}Bu, R^2= Me, X= N(SO$_2$CF$_3$)$_2$

Fig. 1 Structure of the ILs used in this study.

at 135 °C, causing degradation of ILs.[24–26] However, herein the observed decomposition of the imidazolium ring is not clearly understood.

More interestingly, further investigations of the Ru(II)/IL reaction system revealed a more important result: the presence of hydrogen gas as a reducing reagent for the Ru complex seems to be obsolete. Stirring a mixture of the complex in $HM_2I \cdot NTf_2$ under argon atmosphere at 50 °C for a prolonged period (2 days) resulted in a dark brown/black colloidal solution. Samples for TEM analysis were prepared by placing a small amount of the Ru(0)-NPs dispersed in $HM_2I \cdot NTf_2$ onto a holey carbon film supported by a copper grid. The diameters of the particles in the micrographs were measured using the software Sigma Scan Pro 5. Size distribution histograms of the NPs were obtained by measuring the diameter of randomly selected particles, resulting in the particle size of 2.0 ± 0.3 nm (see Fig. 2) with a monomodal distribution.

The crystalline structure of the particles was confirmed by HR-TEM micrographs, analysed using *Gatan Digital Micrograph Software*. By means of HR-TEM measurements it was possible to obtain the Fourier transform images from which lattice spacings of 2.04 Å and 2.13 Å were measured. These lattice spacings correspond to the interplanar distances (1 0 1) and (0 0 2), respectively, of hcp Ru(0). Isolation of the Ru(0)-NPs for analysis by XRD was not possible, corroborating previous reports.[14,22] The size and size distribution of the ruthenium NPs were similar to those of Ru(0)-NPs previously generated using hydrogen gas as a reducing agent for the reduction of [Ru(COD)(2-methylallyl)$_2$] or decomposition of [Ru(COD)(COT)] (COT = 1,3,5-cyclooctatriene).[7,11,14,22]
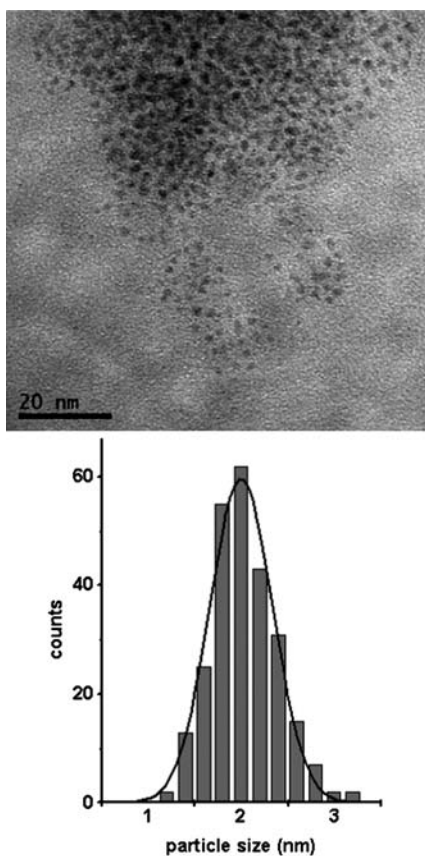
The Ru(0)-NP formation led us to propose a reaction pathway in which the imidazolium ILs $BMI \cdot NTf_2$ and $HM_2I \cdot NTf_2$ might act as reducing agents for [Ru(COD)(2-methylallyl)$_2$]. Here the NTf_2 anion would act as a nucleophile[27,28] and attack the allylic-ligand of the complex (Schemes 1 and 2).

This stoichiometric reaction would cause the concomitant reduction of the Ru(II) complex and subsequent decomposition of the IL. Consequently, the ruthenium would lose its ligand-sphere and be reduced to ruthenium(0) atoms that coalesce generating the Ru(0)-NPs. It is proposed that during the reduction process of the Ru(II) complex, the first step involves a ligand exchange between the COD and a stronger coordinating ligand, occurring readily under the given reaction conditions.[29] A stronger coordinating ligand is easily provided in *neat* imidazolium ionic liquid as solvent, where classical and abnormal *N*-heterocyclic carbenes (NHCs) formed *in situ* might act as a ligand.[30,31] As a consequence, the NTf_2 anion would "lose" its counterion, thus enhancing its nucleophilicity. And this would favour its subsequent attack on the allylic species of the Ru(II) complex. The resulting ruthenium(0) metal atoms in the IL go on to generate the M-NPs. The isobutene by-product was detected by MS analysis of the gas phase (see above). However, attempts to detect the hypothesised by-product *N*-isobutene *N*-triflate in the liquid-phase by NMR were unsuccessful, presumably due to the very low concentration.

Fig. 2 Selected TEM image of Ru(0)-NPs (2.0 ± 0.3 nm) in $HM_2I \cdot NTf_2$ and the histogram of the NPs size distribution.
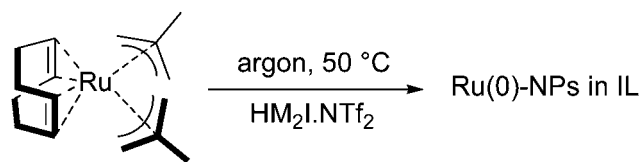
Scheme 1 Formation of Ru(0)-NPs in $HM_2I \cdot NTf_2$.
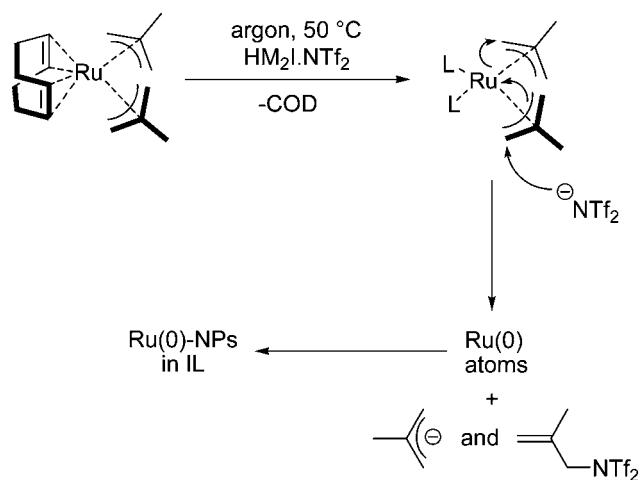
Scheme 2 Proposed reductive elimination of the allyl-ligand induced by the NTf_2 anion (L = ligand/solvent-IL).

To prove this pathway, the anion-effect in different imidazolium ILs was therefore investigated. When using the IL BMI·BF$_4$ (BF$_4$ = tetrafluoroborate), for example, a green suspension that showed no indication of IL decomposition or Ru(0)-NPs formation was obtained. Also, using EMI·B(CN)$_4$ and BMI·N(CN)$_2$, the strongly coordinating nature of the anions prevented the reduction of the Ru(II) complex and the reaction solution remained clear and colourless, even when subjected to a longer reaction time (5 days). Furthermore, the typical catalytic properties of nanoscale ruthenium catalysts in arene hydrogenation were tested with these Ru/IL-systems.[14] Indeed, the Ru(0)-NPs produced in HM$_2$I·NTf$_2$ showed the highest activity in toluene hydrogenation, resulting in conversions above 95% (4 bar H$_2$ at 75 °C, 18 h), similar to results previously reported.[14] The Ru(0)-NPs in BMI·NTf$_2$ were also active in toluene hydrogenation, but with a poorer conversion (55%) under the same conditions. In addition, the systems using the ILs BMI·BF$_4$, EMI·B(CN)$_4$ and BMI·N(CN)$_2$ were subjected to identical conditions, to gauge whether Ru(0)-NPs would form *in situ* during toluene hydrogenation. Indeed, the green suspension in BMI·BF$_4$ turned dark brown and the toluene was hydrogenated, albeit with low conversion (<20%), indicating the formation of Ru(0)-NPs. In contrast, the clear solutions in EMI·B(CN)$_4$ and BMI·N(CN)$_2$ turned slightly yellow, but no hydrogenation of toluene was observed.

The stability of [Ni(COD)$_2$] in imidazolium ILs was also investigated. This complex can be easily decomposed affording Ni(0)-NPs under hydrogen in organic solvents such as THF, in the presence of hexadecylamine (HDA) as the stabilising ligand or polyvinylpyrrolidone (PVP) as the polymer support.[32,33] In this case, cyclooctane is produced as a side product. Moreover, Ni(0)-NPs from the decomposition of [Ni(COD)$_2$] under hydrogen in imidazolium-based ILs have also been reported.[12,34] However, it is worth noting that in this previous work a substantial amount of benzene was used to aid the dissolution of [Ni(COD)$_2$] (6 mL of benzene for 2 mL of IL), and although effort was made to remove the volatiles before decomposition, it is not possible to be sure of the complete removal of benzene and therefore the media in which the decomposition actually occurred.[12,34]

In this work, spontaneous decomposition of [Ni(COD)$_2$] occurred upon dissolution at 25 °C, in both EMI·NTf$_2$ and BMI·NTf$_2$, in the absence of hydrogen. TEM was performed on the resulting black solutions and revealed in each case a mixture of Ni(0)-NPs (<10 nm) and sponge-like agglomerates of larger particles (Fig. 3). It can be seen from the TEM image that these sponge-like structures clearly consist of agglomerates of individual particles. This is completely different from previous findings, highlighting the important role of co-solvents.[12,34]

Notably ^{1}H NMR spectroscopy and gas chromatography performed on the resulting solution showed only a trace of cyclooctane, resulting from the hydrogenation of 1,5-COD ligand, the by-product of decomposition reported in the literature.[32,33] Instead, the presence of both 1,5-COD and its isomer 1,3-cyclooctadiene (1,3-COD) was detected by both gas chromatography and ^{1}H/^{13}C NMR spectroscopy. 1,3-COD must be a result of the isomerisation of 1,5-COD, which could only take place at a metal centre in the presence of Ni–H bond (Scheme 3).
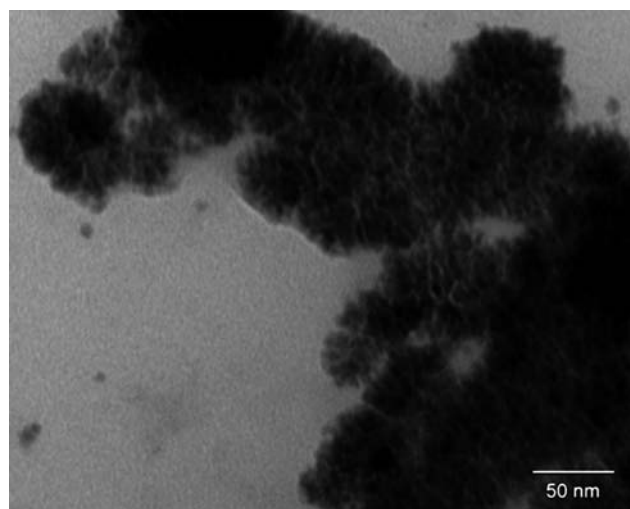
Fig. 3 Sponge-like agglomerates of Ni(0)-NPs formed by auto-decomposition of [Ni(COD)$_2$] in BMI·NTf$_2$.
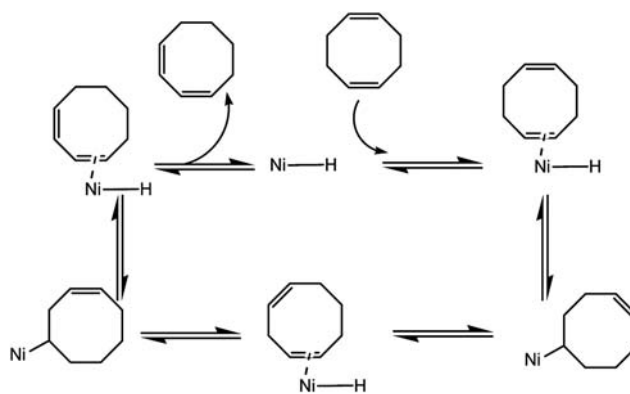
Scheme 3 Mechanism for the isomerisation of COD necessitating a Ni–H specie.

With Ru(0)-NPs, the presence of surface hydrides has been proven by hydrogenation of ethylene without the addition of H$_2$ by a solution of Ru(0)-NPs in IL.[35] This experiment was repeated for the Ni(0)-NPs formed by auto-decomposition of [Ni(COD)$_2$] in BMI·NTf$_2$. After treatment under ethylene atmosphere (4 bars, 100 °C, 24 h) no ethane was detected by GC as a result of ethylene hydrogenation, however, significant amounts of butenes and hexenes were detected, probably a result of oligomerisation of the ethylene. Interestingly, the formation of an ethyl substituted IL BMEI·NTf$_2$ (BMEI = 1-*n*-butyl-2-ethyl-3-methylimidazolium) was also observed by NMR spectroscopies (COSY, HETCOR and DOSY) and confirmed by electrospray mass spectrometry where cations at m/z = 139 and 167 were observed with similar abundances, corresponding to [BMI]$^+$ and [BMEI]$^+$, respectively. A small amount of the cation [B$_2$MI]$^+$ (B$_2$MI = 1,2-di-*n*-butyl-3-methylimidazolium) was also observed by mass spectrometry, m/z = 195, probably a result of oligomerisation of ethylene to 1-butene before reaction with the imidazolium cycle. The evidence gathered suggests that the observed decomposition could be due to the cleavage of the very acidic C2–H bond and the consequent *in situ* generation of NHC

species, as already reported in the case of Ir(0)-NP preparation in ILs,[36–40] and with homogeneous complexes of Ni,[41] Pd,[42–44] Rh,[30,45] and Ir.[45] Cavell and co-workers have proposed a mechanism for the possible catalytic cycle for the imidazolium/alkene coupling reaction where the organometallic starting material was [Ni(OAc)$_2$].[46] The same phenomenon has also been observed in work by Lecocq and Olivier-Bourbigou who were investigating the oligomerisation behaviour of Ni in imidazolium ILs.[41] At this point it is impossible to determine whether the observed reactions (isomerisation of COD and formation of BMEI·NTf$_2$) occur on molecular or colloidal species. However, these results do prove that the cleavage of the C2–H bond occurs during the spontaneous decomposition on dissolution. The proposed mechanism of the reaction of imidazolium salts with low valent M(0) (M = Pd and Ni) hypothesises the formation of a molecular carbene–M–H species, as also proposed in the catalytic cycle for oligomerisation and formation of trialkylimidazolium species.[47,48] The presence of bis(imidazolylidene)nickel complexes [(NHC)$_2$NiH]$^+$ was also detected by mass spectrometry, implying that a molecular intermediate is in fact present as proposed. This may act as a transient species and could be the active species for the above mentioned reactions. Similar bis-carbene iodide nickel complexes have already been prepared in imidazolium ILs and isolated by Wasserscheid's group.[46] These were indeed found to be active in the dimerisation of butene carried out in ILs, although no production of Ni(0)-NPs was noted here, perhaps due to the presence of the strongly coordinating iodides. Although the exact mechanism remains unclear, from our investigations it is certain that the spontaneous decomposition of [Ni(COD)$_2$] on dissolution into the ILs with short alkyl chains involves attack on the acidic C2–H (Scheme 4).

To achieve the controlled generation of small-size Ni(0)-NPs, we must find a way of inhibiting this auto-decomposition in imidazolium ILs with short alkyl chains. Another strategy attempted in order to circumvent the problem was to use an IL which does not contain the most acidic C2–H proton such as BM$_2$I·NTf$_2$. Surprisingly, the [Ni(COD)$_2$] still decomposed on stirring, but this time afforded well dispersed Ni(0)-NPs (7.0 ± 2.0 nm, Fig. 4). This can only be explained by attack on the two less acidic protons C4–H, C5–H of the imidazolium ring and generation of transient non-classical NHC ligands.[31]

In another attempt to avoid auto-decomposition the NTf$_2$-anion was exchanged for the more strongly coordinating BF$_4$-anion, yielding important results. In this case, similarly to
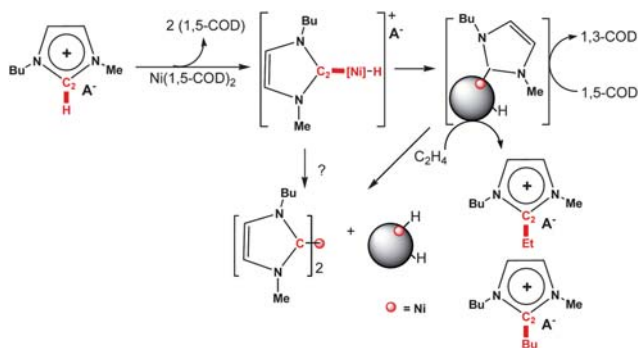
Scheme 4 Reactions occurring during the auto-decomposition of [Ni(COD)$_2$] in imidazolium ILs.
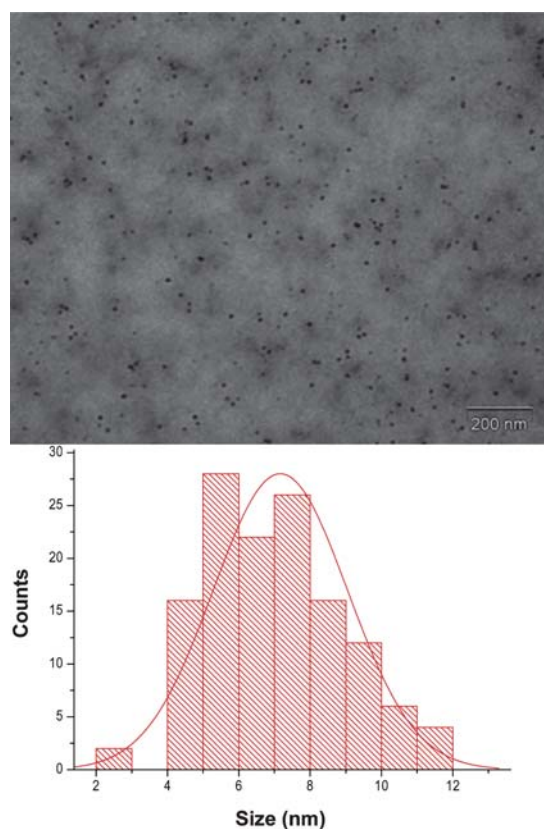
Fig. 4 TEM image of Ni(0)-NPs (7.0 ± 2.0 nm) formed by auto-decomposition of [Ni(COD)$_2$] in BM$_2$I·NTf$_2$ and size distribution histogram.

the case of [Ru(COD)(2-methylallyl)$_2$] the decomposition of [Ni(COD)$_2$] in BMI·BF$_4$ occurred not spontaneously but very slowly at 25 °C only under 4 bar of H$_2$, once again highlighting the importance of the NTf$_2$-anion. Therefore, as the auto-decomposition of [Ni(COD)$_2$] to Ni(0)-NPs was also observed uniquely in NTf$_2$-ILs, it is possible that the NTf$_2$ anion intervenes in the Ni(0)-NP formation through interaction with the COD ligands, similarly to the case of the Ru(II) complex.

Conclusions

In summary, IL decomposition and simultaneous Ru(0)-NP formation are limited to imidazolium salts containing the NTf$_2$ anion. These results may explain how the Ru(0)-NPs formation is induced by imidazolium N-triflate ILs, but cannot explain the exact mechanism for the imidazolium ring fragmentation in small quantities. Most importantly, the formation of small-sized active ruthenium nanoscale hydrogenation catalysts is possible at low temperature and atmospheric pressure in the absence of classical and potentially dangerous reducing agents such as hydrogen gas (under elevated pressure), pyrophoric LiAlH$_4$ or hazardous hydrazine. Moreover, an unexpected spontaneous decomposition of [Ni(COD)$_2$] occurred without the addition of hydrogen for imidazolium ILs with short alkyl chains: ILs BMI·NTf$_2$, EMI·NTf$_2$ and BM$_2$I·NTf$_2$. In the case of ILs BMI·NTf$_2$ and EMI·NTf$_2$, TEM micrographs showed that Ni(0)-NPs of fairly large diameter were formed as well as sponge-like super

agglomerates. However, for IL $BM_2I \cdot NTf_2$ well dispersed Ni(0)-NPs are formed. An explanation for the activation of the acidic protons on the imidazolium ring and the subsequent NHC formation that led to a rapid decomposition of the complex has been proposed. The additional interaction between the NTf_2 anion and the COD ligands on the Ni complex, which also may support the Ni(0)-NPs formation, cannot be excluded nonetheless. It is conceivable that this novel approach may be extended as a general access to M-NPs in imidazolium NTf_2-ILs, starting from organometallic complexes bearing only COD, allylic and/or olefinic ligands, such as $[Co(COD)_2]$, $[Ru(COD)(COT)]$, $[Rh(allyl)_3]$, $[Pd(COD)_2]$, $[Pt(COD)_2]$ or $[Pt(norbornene)_3]$.

Experimental

General

All manipulations were carried out under argon atmosphere. The organometallic complexes $[Ru(COD)(2\text{-methylallyl})_2]$ and $[Ni(COD)_2]$ were purchased from Sigma-Aldrich and Strem Chemicals, respectively. For the ruthenium experiments, a Hiden QIC20 MS-QTOF gas-analyser was used for the gas phase analysis after the synthesis of Ru(0)-NPs. TEM analyses were performed in a JEOL-JEM 2010 microscope operating at 200 kV (*UFRGS-CME*, Brazil) and EDS, and used for catalytic experiments as previously described.[14] The HR-TEM was performed at the *"Centro de Tecnologias Estratégicas do Nordeste" (CETENE)*, Recife/Brazil. The ILs were synthesised as previously reported,[49] and ILs $EMI \cdot B(CN)_4$ and $BMI \cdot N(CN)_2$ were purchased from *Merck KGaA*, Germany.

In the case of nickel experiments, conventional TEM micrographs were obtained at the *"Centre Technologique des Microstructures"*, France, using a Philips 120 CX electron microscope operating at 120 kV. Size distribution histograms were constructed from the measurement of at least 200 different NPs assuming a near spherical shape and random orientation. Solution NMR spectra were recorded on Bruker Avance 300 MHz spectrometer for ^{1}H and ^{13}C. DRX 500 MHz for ^{2}H. Gas phase ^{1}H NMR spectra were obtained on a Bruker DRX 500 instrument at 298 K (nominal). Mass spectra were acquired on a ThermoFinnigan LCQ Advantage ion trap instrument, detecting positive (+) and negative (−) ions in the ESI mode. Samples (1 to 10 µg mL^{-1} in acetonitrile) were infused directly into the source (5 µL min^{-1}) using a syringe pump. The following source parameters were applied: spray voltage 3.0–3.5 kV, nitrogen sheath gas flow 5–20 arbitrary units. The heated capillary was held at 200 °C. MS spectra were obtained by applying a relative collision energy of 25 to 40% of the instrumental maximum. The products were quantitatively analysed by gas chromatography on a P6890 chromatograph equipped with a flame ionisation detector (FID) and an Al_2O_3/KCl column (*L*: 50 m, diameter: 0.32 mm, and film thickness: 5 µm). The injector and detector temperature was 230 °C, and the injection volume was 1 µL. The temperature was fixed at 190 °C. The synthesis of ILs was carried out as previously reported.[43]

Synthesis of Ru(0)-NPs

In a typical experiment, a Fischer–Porter bottle was loaded with $[Ru(COD)(2\text{-methylallyl})_2]$ (30 mg, 0.094 mmol) under argon.

Then, the IL $HM_2I \cdot NTf_2$ (1.5 mL) was added *via* syringe under an argon flow. The mixture was stirred at room temperature for 60 min, resulting in a turbid dispersion. The system was heated to 50 °C, and stirred under argon for two days resulting in a black suspension. The Fischer–Porter bottle was connected to a mass gas-analyser in order to evaluate the gas phase. After analysis the Fischer–Porter bottle was then kept under reduced pressure to eliminate the organic volatiles formed. An aliquot of the Ru(0)-NPs embedded in the IL was analysed by TEM.

Synthesis of Ni(0)-NPs

$[Ni(COD)_2]$ (50 mg, 0.14 mmol) was stirred under argon in the ILs $BMI \cdot NTf_2$, $EMI \cdot NTf_2$ and $BM_2I \cdot NTf_2$ (10 mL) producing a pale yellow solution at 25 °C. After 1 h the solution had turned green and after a further hour a black solution resulted. Samples for TEM observations were prepared by placing a thin film of the Ni(0)-NPs dispersed in ILs on a copper grid coated with holey carbon film.

Oligomerisation of ethylene by Ni(0)-NPs in IL

A 2 mL sample of the Ni(0)-NPs solution in the IL was introduced under argon into a Schlenk of known volume. The sample was treated under flow of argon for 18 h. The argon atmosphere was replaced with a known pressure of ethylene using a vacuum line and the system was stirred. A decrease of the internal pressure was observed, and the composition of the gas phase was monitored by gas chromatography. After 12 h, the atmosphere was replaced by a H_2 atmosphere and the system was heated and stirred for 12 h. The composition of the gas phase was again monitored by gas chromatography.

References

1 J. Dupont and J. D. Scholten, *Chem. Soc. Rev.*, 2010, **39**, 1780–1804.
2 P. Migowski and J. Dupont, *Chem.–Eur. J.*, 2007, **13**, 32–39.
3 H. Boennemann and K. S. Nagabhushana, *Nanoclusters in Catalysis and Materials Science: the Issue of Size Control*, ed. B. Corain, G. Schmid and N. Toshima, Elsevier B.V., Amsterdam, 2008, pp. 21–48.
4 H. Boennemann, K. S. Nagabhushana and R. M. Richards, *Nanoparticles and Catalysis*, Wiley-VCH, Weinheim, 2008.
5 Y. G. Cui, I. Biondi, M. Chaubey, X. Yang, Z. F. Fei, R. Scopelliti, C. G. Hartinger, Y. D. Li, C. Chiappe and P. J. Dyson, *Phys. Chem. Chem. Phys.*, 2010, **12**, 1834–1841.
6 Z. F. Fei, D. B. Zhao, D. Pieraccini, W. H. Ang, T. J. Geldbach, R. Scopelliti, C. Chiappe and P. J. Dyson, *Organometallics*, 2007, **26**, 1588–1598.
7 M. H. G. Prechtl, J. D. Scholten and J. Dupont, *J. Mol. Catal. A: Chem.*, 2009, **313**, 74–78.
8 E. Redel, R. Thomann and C. Janiak, *Inorg. Chem.*, 2008, **47**, 14–16.
9 E. Redel, R. Thomann and C. Janiak, *Chem. Commun.*, 2008, 1789–1791.

10 P. S. Campbell, C. C. Santini, F. Bayard, Y. Chauvin, V. Collière, A. Podgorsek, M. F. Costa Gomes and J. Sá, *J. Catal.*, 2010, **257**, 99–107.
11 T. Gutel, C. C. Santini, K. Philippot, A. Padua, K. Pelzer, B. Chaudret, Y. Chauvin and J. M. Basset, *J. Mater. Chem.*, 2009, **19**, 3624–3631.
12 P. Migowski, G. Machado, S. R. Texeira, M. C. M. Alves, J. Morais, A. Traverse and J. Dupont, *Phys. Chem. Chem. Phys.*, 2007, **9**, 4814–4821.
13 P. Migowski, D. Zanchet, G. Machado, M. A. Gelesky, S. R. Teixeira and J. Dupont, *Phys. Chem. Chem. Phys.*, 2010, **12**, 6826–6833.
14 M. H. G. Prechtl, M. Scariot, J. D. Scholten, G. Machado, S. R. Teixeira and J. Dupont, *Inorg. Chem.*, 2008, **47**, 8995–9001.
15 M. Scariot, D. O. Silva, J. D. Scholten, G. Machado, S. R. Teixeira, M. A. Novak, G. Ebeling and J. Dupont, *Angew. Chem., Int. Ed.*, 2008, **47**, 9075–9078.
16 H. J. Ryu, L. Sanchez, H. A. Keul, A. Raj and M. R. Bockstaller, *Angew. Chem., Int. Ed.*, 2008, **47**, 7639–7643.
17 L. Zhao, C. Y. Zhang, L. Zhuo, Y. G. Zhang and J. Y. Ying, *J. Am. Chem. Soc.*, 2008, **130**, 12586–12587.
18 S. Choi, K. S. Kim, S. H. Yeon, J. H. Cha, H. Lee, C. J. Kim and I. D. Yoo, *Korean J. Chem. Eng.*, 2007, **24**, 856–859.
19 K. S. Kim, S. Choi, J. H. Cha, S. H. Yeon and H. Lee, *J. Mater. Chem.*, 2006, **16**, 1315–1317.
20 Y. Gao, A. Voigt, M. Zhou and K. Sundmacher, *Eur. J. Inorg. Chem.*, 2008, 3769–3775.
21 E. T. Silveira, A. P. Umpierre, L. M. Rossi, G. Machado, J. Morais, G. V. Soares, I. L. R. Baumvol, S. R. Teixeira, P. F. P. Fichtner and J. Dupont, *Chem.–Eur. J.*, 2004, **10**, 3734–3740.
22 T. Gutel, J. Garcia-Anton, K. Pelzer, K. Philippot, C. C. Santini, Y. Chauvin, B. Chaudret and J. M. Basset, *J. Mater. Chem.*, 2007, **17**, 3290–3292.
23 D. O. Silva, J. D. Scholten, M. A. Gelesky, S. R. Teixeira, A. C. B. Dos Santos, E. F. Souza-Aguiar and J. Dupont, *ChemSusChem*, 2008, **1**, 291–294.
24 D. J. Flannigan, S. D. Hopkins and K. S. Suslick, *J. Organomet. Chem.*, 2005, **690**, 3513–3517.
25 J. D. Oxley, T. Prozorov and K. S. Suslick, *J. Am. Chem. Soc.*, 2003, **125**, 11138–11139.
26 S. Sowmiah, V. Srinivasadesikan, M. C. Tseng and Y. H. Chu, *Molecules*, 2009, **14**, 3780–3813.
27 S. Chowdhury, R. S. Mohan and J. L. Scott, *Tetrahedron*, 2007, **63**, 2363–2389.
28 R. Bini, C. Chiappe, E. Marmugi and D. Pieraccini, *Chem. Commun.*, 2006, 897–899.
29 J. P. Genet, S. Mallart, C. Pinel, S. Juge and J. A. Laffitte, *Tetrahedron: Asymmetry*, 1991, **2**, 43–46.
30 J. D. Scholten and J. Dupont, *Organometallics*, 2008, **27**, 4439–4442.
31 S. Grundemann, A. Kovacevic, M. Albrecht, J. W. Faller and R. H. Crabtree, *Chem. Commun.*, 2001, 2274–2275.
32 N. Cordente, C. Amiens, B. Chaudret, M. Respaud, F. Senocq and M. J. Casanove, *J. Appl. Phys.*, 2003, **94**, 6358–6365.
33 N. Cordente, M. Respaud, F. Senocq, M. J. Casanove, C. Amiens and B. Chaudret, *Nano Lett.*, 2001, **1**, 565–568.
34 P. Migowski, S. R. Teixeira, G. Machado, M. C. M. Alves, J. Geshev and J. Dupont, *J. Electron Spectrosc. Relat. Phenom.*, 2007, **156**, 195–199.
35 P. S. Campbell, C. C. Santini, D. Bouchu, B. Fenet, K. Philippot, B. Chaudret, A. A. H. Padua and Y. Chauvin, *Phys. Chem. Chem. Phys.*, 2010, **12**, 4217–4223.
36 L. S. Ott, S. Campbell, K. R. Seddon and R. G. Finke, *Inorg. Chem.*, 2007, **46**, 10335–10344.
37 L. S. Ott, M. L. Cline, M. Deetlefs, K. R. Seddon and R. G. Finke, *J. Am. Chem. Soc.*, 2005, **127**, 5758–5759.
38 L. S. Ott and R. G. Finke, *Inorg. Chem.*, 2006, **45**, 8382–8393.
39 J. D. Scholten, G. Ebeling and J. Dupont, *Dalton Trans.*, 2007, 5554–5560.
40 J. D. Scholten and J. Dupont, in *Iridium Complexes in Organic Synthesis*, ed. L. A. Oro and C. Claver, Wiley-VCH Verlag GmbH & Co. KGaA, Weinheim, 2009, pp. 369–389.
41 V. Lecocq and H. Olivier-Bourbigou, *Oil Gas Sci. Technol.*, 2007, **62**, 761–773.
42 C. M. Crudden and D. P. Allen, *Coord. Chem. Rev.*, 2004, **248**, 2247–2273.
43 L. Magna, Y. Chauvin, G. P. Niccolai and J. M. Basset, *Organometallics*, 2003, **22**, 4418–4425.
44 M. H. G. Prechtl, J. D. Scholten and J. Dupont, *Molecules*, 2010, **15**, 3441–3461.
45 U. Hintermair, T. Gutel, A. M. Z. Slawin, D. J. Cole-Hamilton, C. C. Santini and Y. Chauvin, *J. Organomet. Chem.*, 2008, **693**, 2407–2414.
46 D. S. McGuinness, W. Mueller, P. Wasserscheid, K. J. Cavell, B. W. Skelton, A. H. White and U. Englert, *Organometallics*, 2002, **21**, 175–181.
47 N. D. Clement, K. J. Cavell, C. Jones and C. J. Elsevier, *Angew. Chem., Int. Ed.*, 2004, **43**, 1277–1279.
48 D. C. Graham, K. J. Cavell and B. F. Yates, *Dalton Trans.*, 2007, 4650–4658.
49 C. C. Cassol, G. Ebeling, B. Ferrera and J. Dupont, *Adv. Synth. Catal.*, 2006, **348**, 243–248.

Artigo IV

Probing the Chemical Interaction Between Iridium Nanoparticles and Ionic Liquid by XPS Analysis

Fabiano Bernardi, Jackson D. Scholten, Gerhard H. Fecher, Jairton Dupont and Jonder Morais

Probing the chemical interaction between iridium nanoparticles and ionic liquid by XPS analysis

F. Bernardi [a], J.D. Scholten [b,1], G.H. Fecher [c], J. Dupont [b,1], J. Morais [a,*]

[a] *Instituto de Física – UFRGS, P.O. Box 15051, 91501-970 Porto Alegre, RS, Brazil*
[b] *Laboratory of Molecular Catalysis, Instituto de Química – UFRGS, P.O. Box 15003, 91501-970 Porto Alegre, RS, Brazil*
[c] *Institut für Anorganische und Analytische Chemie – Johannes Gutenberg Universität, 55099 Mainz, Germany*

ABSTRACT

In situ X-ray photoelectron spectroscopy analysis of Ir(0) nanoparticles (1.6 ± 0.3 nm) dispersed in imidazolium ionic liquid (EMI.EtSO$_4$) shows evidences of the effective interaction between the metallic clusters and the surrounding liquid. By monitoring the C 1s signal of the ionic liquid one observes a change of the binding energy in one of its components (C2) when in the presence of Ir nanoparticles. This result was corroborated by isotope labeling experiments.

© 2009 Elsevier B.V. All rights reserved.

1. Introduction

The surface properties of soluble-metal nanoparticles depend not only on the relative abundance of different types of active sites (such as diameter, shape and size distribution) but also on the concentration and type of stabilizers present in the medium [1–4]. Therefore the type and nature of the interaction between the nanoparticles and the stabilizer plays an important role on the metal-surface properties such as in catalysis [5]. Quaternary ammonium salts are among the most popular and used metal nanoparticles stabilizers [1–4], and it is assumed that stabilization in these cases is due to the positive charge on the metal surface, which is ultimately induced by the adsorption of the anions onto the coordinative unsaturated, electron-deficient, and initially neutral metal surface [6,7]. More recently, ionic liquids and in particular imidazolium based salts have been used as stabilizers for the formation of 'soluble' transition-metal nanoparticles [8–26]. These fluids are per-definition quaternary ammonium salts but their interaction with the metal-surface is apparently some-how different especially due to their particular structural organization [15,27–29]. It has been recently proposed that together with the electrostatic stabilization provided by the intrinsic high charge of the ionic liquid, there is a steric type stabilization due to the presence of anionic and cationic supramolecular aggregates of the type $[(BMI)_x(X)_{x-n}]^{n+}[(BMI)_{x-n}(X)_x]^{n-}$ (BMI is the 1-*n*-butyl-3-methylimidazolium cation and X is the anion) [11,30,31]. Moreover, strong evidences obtained by H/D and D/H exchange experiments

indicated that the stabilization may also involve surface attached *N*-heterocyclic carbenes (NHC), at least as transient species [32,33].

Among the various techniques used, X-ray photoelectron spectroscopy (XPS) is one that may give more detailed indications concerning the type and nature of the interactions existent in the metal surfaces [34]. Although the surface XPS analysis, that have been already performed with isolated transition-metal nanoparticles prepared in ionic liquids, showed the presence of an oxide layer [30,35] together with of residual fluid on their surfaces [12,30,35], no direct evidence of the interaction between the metal nanoparticles dispersed in the ionic liquid has been observed. It is worth to mention that due to their very low vapor pressure [36–38], high vacuum techniques may be used for the investigation of process occurring in the imidazolium ionic liquids [19]. Transmission electron microscopy (TEM) has been used for monitoring the evolution of size and shape of palladium nanoparticles [39], dissolved in ionic liquids during the Heck coupling reaction [40]. Moreover, XPS technique has been successfully used for the investigation of various imidazolium ionic liquids [41–44], such as 1-ethyl-3-methylimidazolium ethylsulfate (EMI.EtSO$_4$) [42]. These investigations have shown that ILs are stable during X-ray exposure and the 1s atomic emissions of these ionic liquids displayed well resolved features. The chemical composition, calculated from the peak areas, is close to the stoichiometric one and the preferential orientation of the *N*-alkyl imidazolium chain is away from the liquid surface. Moreover, XPS was used to reveal the composition of the surface layer [45,46], the chemical state of the atoms and for purity analysis of ionic liquids [47]. For example, it was demonstrated the top most layer of 1-ethyl-3-methylimidazolium ethylsulfate with dissolved [Pt(NH$_3$)$_4$]Cl$_2$ is enriched with the platinum complex [48]. Therefore XPS can constitute an interesting tool to investigate the surface properties of metal nanoparticles

---

* Corresponding author. Fax: +55 51 3308 6510.
  E-mail address: jonder@if.ufrgs.br (J. Morais).
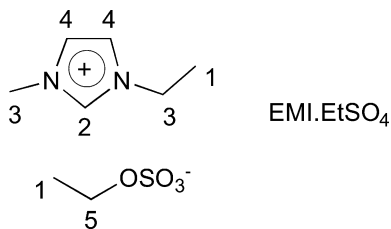[1] Fax: +55 51 3308 7304.

Fig. 1. Chemical structure of the IL EMI.EtSO$_4$ with their respective carbon components.

dispersed in ionic liquids. In this work we disclose our recent findings on the interaction of Ir(0) nanoparticles surface with ionic species of the EMI.EtSO$_4$ (Fig. 1) obtained from X-ray photoelectron spectroscopy experiments.

2. Experimental

2.1. General

The reactions involving Ir compounds were carried out under an argon atmosphere in oven dried Schlenk tubes. The IL purity was checked by ^{1}H NMR spectra using the intensity of the ^{13}C satellites of the imidazolium N-methyl group as an internal standard [49]. All other chemicals were purchased from commercial sources.

2.2. Nanoparticles formation and isolation

In a typical experiment, a Fischer–Porter bottle containing an orange solution of [Ir(COD)Cl]$_2$ (COD = 1,5-cyclooctadiene) (0.02 g, 0.03 mmol) in dichloromethane (2.0 mL) was added to the respective ionic liquid (1.0 mL) and stirred at room temperature for 15 min. The volatiles were then removed under reduced pressure. The system was kept at 75 °C and molecular hydrogen (4 atm) was admitted to the system. The solution turn into black after stirring for 24 h. Acetone (5.0 mL) was added to the black suspension and the black powder was separated by centrifugation (3000 rpm for 5 min). The acetone washing was repeated five times (5 × 5.0 mL). Then, Ir nanoparticles were dried under reduced pressure for 5 h. The isolated Ir nanoparticles (0.01 g) prepared in EMI.EtSO$_4$ were re-dissolved in the same ionic liquid (0.5 mL). The sample of the solution containing Ir nanoparticles and IL (C = 10 mg Ir(0)/0.5 mL IL) were analyzed by XPS.

2.3. TEM analysis of the iridium nanoparticles

TEM micrographs were taken on a JEOL-JEM 2010 operating at an acceleration voltage of 200 kV. In order to perform the TEM analysis, a droplet of the black suspensions containing the [Ir(0)]$_n$ nanoparticles embedded in the IL was dispersed in isopropanol and a slight amount of this dispersion was placed on a carbon coated copper grid. The nanoparticles diameter was estimated from ensembles of 400 particles (800 counts) chosen in arbitrary areas of the enlarged micrographs. The diameters of the particles in the micrographs were measured using the software Sigma scan pro 5.

2.4. XPS measurements

The photoemission studies were performed using a VG ESCALAB MkII, equipped with 150 mm hemispherical analyzer and Al Kα anode X-ray source. The analyzer was set with pass energy of 20 eV, the energy step was 0.1 eV, with acquisition time of 500 ms/point. The overall resolution was 200 meV. The detection angle of the

photoelectrons was 45° with respect to the sample surface. The measurements were performed for the EMI.EtSO$_4$ IL and Ir nanoparticles dispersed in this liquid. Prior to analysis, in the case of IL with Ir nanoparticles, the samples were submitted to an ultrasonic agitation for 1 h 15 min in order to homogenize the sample and avoid precipitation of the nanoparticles during measurements. The samples were presented for analysis using standard stubs. Since IL is electrically conducting, none of the problems associated with differential charging are encountered and charge neutralization is not required. No IL decomposition was observed during exposure to the X-ray source. The XPSPEAK 4.1 software was used to fit the XPS results. Shirley type background was used and for all components a Gaussian–Lorentzian product function with 30% Lorentzian was used to model the peak shape with the fwhm's constrained to ~1.5 eV [42]. We have also considered that there is no change in the FWHM value of a given carbon component after insertion of Ir nanoparticles.

2.5. Isotope labeling experiments

The deuterated ionic liquid [EMI]-d_3.EtSO$_4$ was synthesized under argon atmosphere in dried glassware using standard Schlenk techniques as previously described [33]. ^{1}H NMR spectrum indicates a deuterium content of, respectively, 89% at C$_2$, 85% at C$_4$ and 82% at C$_5$ positions of the imidazolium ring. ^{1}H and ^{13}C NMR spectra were recorded on a Varian VNMRS 300 MHz spectrometer in acetone-d_6. Chemical shifts are reported relative to TMS standard. For ^{1}H NMR studies the following spectral parameters were used: pulse, 45°; acquisition time, 2.049 s; relaxation delay, 10.0 s; scan repetitions, 128; and total acquisition time, 26 min 7 s. The D/H exchange reaction was monitored during the cyclohexene hydrogenation with the iridium nanoparticles.

3. Results and discussion

The sample containing a solution of the Ir(0) nanoparticles synthesized in EMI.EtSO$_4$ was analyzed by TEM showing a monomodal size distribution with a mean diameter of 1.6 ± 0.3 nm (Fig. 2) and the iridium content was confirmed by EDS analysis.

Fig. 3 displays the XPS overall scans of the pure EMI.EtSO$_4$ IL and of the same IL containing dispersed Ir nanoparticles. The spectra showed the presence of carbon, nitrogen, oxygen and sulphur. Possible contaminations (e.g. silicones) were not observed.

An analysis of the C 1s region can provide the electronic structure of the five chemical states of carbon present in the IL, numbered 1 to 5 in Fig. 1. In this work, the C 1s spectrum was adjusted with five components of C with distinct binding energies, in accordance with the literature [41]. The binding energy positions of the components relative to each other were fixed [41], such that (C2–C4) = 0.43, (C2–C3) = 1.17 eV and (C2–C1) = 2.4 eV. The ratio of peak areas for the C1–C5 components was restricted to 1:0.4:1:0.8:0.5, where the losses due to shake-up/off process (from the aromatic ring carbons C2 and C4) were considered. The C1 was assigned as aliphatic carbon and charge corrected to 285 eV accordingly [42]. The best fitting results was chosen considering the least deviation to the experimental data.

Fig. 4 shows the C 1s photoemission spectra and fitting results for the EMI.EtSO$_4$ IL before and after insertion of the Ir nanoparticles. The carbon bonds numbered in Fig. 1 are identified with the components in the fitted peaks.

Table 1 shows the binding energy of the C 1s chemical components before and after insertion of Ir nanoparticles. The best fitting was obtained with the C2 component shifted 0.3 eV to lower binding energy value in the presence of the Ir nanoparticles. Therefore, it can be assumed that the carbon (C2) is turning into a more pro-
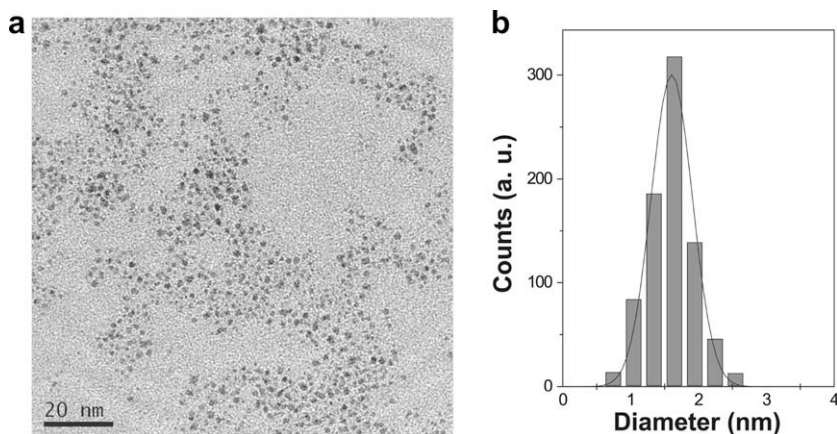
Fig. 2. (a) Selected TEM micrograph of the iridium nanoparticles prepared in EMI.EtSO$_4$ and (b) the histogram showing the size distribution.
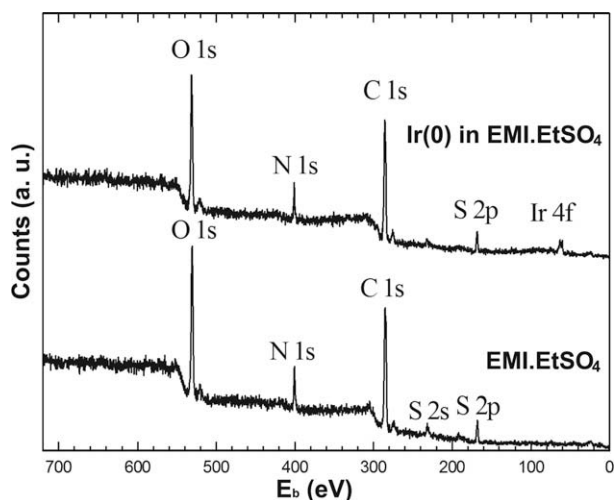

Fig. 3. XPS overall scans of the pure EMI.EtSO$_4$ IL and the mixture containing Ir(0) nanoparticles and the IL.
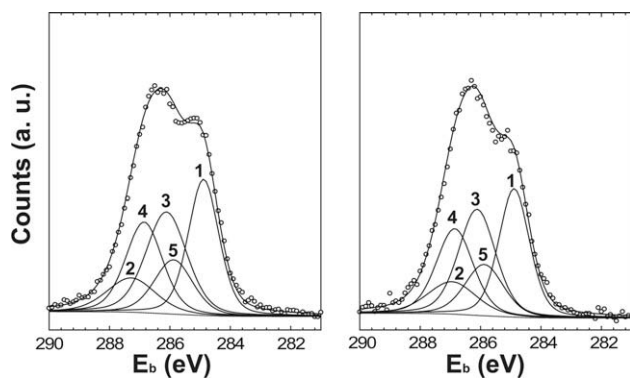
Table 1
Binding energies (eV) of the different carbon chemical states for pure EMI.EtSO$_4$ and with Ir(0) re-dispersed in this IL. The symbols C1–C5 correspond to the carbons identified in Fig. 1.

Carbon	Pure EMI.EtSO$_4$	Ir(0) in EMI.EtSO$_4$
C1	285.0	285.0
C2	287.4	287.1
C3	286.2	286.2
C4	287.0	287.0
C5	286.0	286.0

hydrogen (namely C2 position in Fig. 1) at imidazolium cation and the anion. This strong interaction between C2–H and EtSO$_4^-$ can result in a very fast polarization of the C–H bond sufficiently to lead the formation of transient NHC species in the presence of metal. Due to its electronic configuration, these NHCs are strong σ electron-donor ligand and then, they could interact with the electrophilic surface of the Ir nanoparticles explaining the shift observed for the C2 component in XPS analysis.

Ir 4f signal of Ir nanoparticles dispersed in EMI.EtSO$_4$ is shown in Fig. 5. One notices a component corresponding to Ir^0 metallic at 60.7 eV (dashed curve) and an Ir–O (dotted curve) contribution at 62.0 eV. The peak area analysis gives a contribution of 78% Ir^0 and 22% Ir–O. It can be observed that the nanoparticles in the IL present a large contribution from the Ir–Ir component character. The small Ir–O component observed in the sample is probably orig-

Fig. 4. X-ray photoelectron spectra showing the C 1s region with the fitting results for the pure IL EMI.EtSO$_4$ (left) and with dispersed Ir(0) nanoparticles (right).

nounced nucleophilic character. In other words, *N*-heterocyclic carbene (NHC) species derived from imidazolium cation could be presented in the medium. Particularly for the EMI.EtSO$_4$ IL, it is possible to suggest a basic behavior for the EtSO$_4$ anion. This comportment could be explained by the high coordination ability of the EtSO$_4$ anion in the 3D IL network where generally it is well known that the more pronounced interaction is between the most acidic

Fig. 5. X-ray photoelectron spectra of the Ir 4f region for Ir dispersed in EMI.EtSO$_4$ IL. The Ir doublet presents two components corresponding to Ir^0 (dashed curve) and Ir–O (dotted curve) bonds.
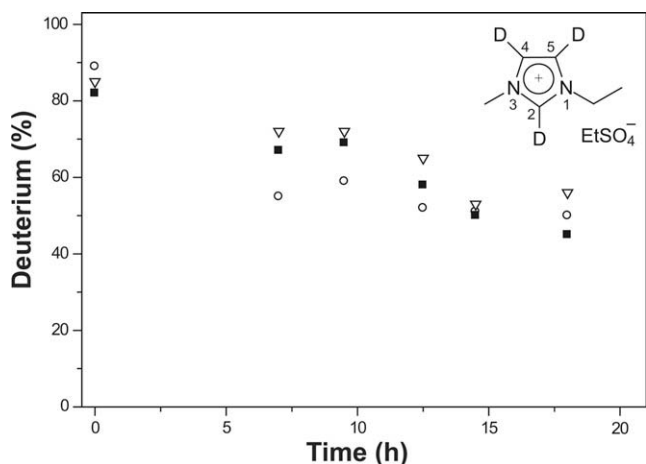
Fig. 6. D/H exchange reaction on the imidazolium cation in [EMI]-d_3.EtSO$_4$ IL catalyzed by Ir(0) nanoparticles at 75 °C under 5 atm of H$_2$. (○) C$_2$, (▽) C$_4$ and (■) C$_5$ [33].

inated from the brief air exposure occurred between isolation and dispersion of the nanoparticles. The N 1s region was adjusted and no shift in the binding energy was observed after dispersion of Ir nanoparticles. The same was true for the S 2p and O 1s in EMI.EtSO$_4$.

Moreover, this result obtained by XPS analysis for EMI.EtSO$_4$/Ir(0) is in agreement with those observed by D/H labeling experiments in a previous published work [33]. There, it was related that NHC species are involved in reactions employing imidazolium ILs and Ir(0) nanoparticles. For all deuterated ILs tested, D/H exchange reactions were detected at the three imidazolium C–D moieties (namely C$_2$, C$_4$ and C$_5$ in Fig. 6). Unexpectedly, in the most cases, the D/H exchange processes occur at the least acidic positions of the imidazolium cation (C$_4$ and C$_5$), suggesting that ILs interact with the metal preferentially as aggregates of the type $\{[(DAI)_x(X)_{x-n}]^{n+}[(DAI)_{x-n}(X)_x]^{n-}\}_n$ (where DAI is the 1,3-dialkylimidazolium cation and X the anion) rather than isolated ions.

However, only for the [EMI]-d_3.EtSO$_4$ IL, it was observed an anomalous comportment of D/H exchange reaction. In particular, the D/H exchange rate is higher at the most acidic position (C$_2$) at the beginning of reaction (Fig. 6). Therefore, it can be assumed that the EtSO$_4$ anion could be acting as a 'base' interacting with the most acidic hydrogen at imidazolium cation in 3D IL arrangement leading the C$_2$-D moiety more susceptible to D/H reaction (NHCs formation).

Additional attempts to determinate the interaction between the Ir(0) nanoparticles and the EMI.EtSO4 IL by infrared measurements were unsuccessful. It was not possible to observe significant modification on the vibrational modes of the IL induced by the presence of Ir nanoparticles.

4. Conclusion

In conclusion, the observed changes on the binding energy of the C 1s component, namely C2, after dispersion of Ir nanoparticles in EMI.EtSO$_4$ IL are a strong indication of the effective interaction of the ionic species to the nanoparticles surface. In addition, it cannot be excluded the possibility of the EtSO$_4$ anion acts as a 'base' in EMI.EtSO$_4$/Ir(0) system due to experimental evidences obtained by XPS analysis and D/H exchange measurements.

Therefore, Ir nanoparticles in EMI.EtSO$_4$ IL are much probably stabilized by protective layers via the loosely bond anionic moieties of the ionic liquid and/or NHC transient species. These loosely surface-bonded protective species are in one hand, responsible in some extend for their catalytic activity but in other hand to their relatively low stability that leads to aggregation/agglomeration and eventually to the bulk metal.

References

[1] J.D. Aiken, R.G. Finke, J. Mol. Catal. A: Chem. 145 (1999) 1.
[2] A. Roucoux, J. Schulz, H. Patin, Chem. Rev. 102 (2002) 3757.
[3] D. Astruc, F. Lu, J.R. Aranzaes, Angew. Chem., Int. Ed. 44 (2005) 7852.
[4] M. Moreno-Manas, R. Pleixats, Acc. Chem. Res. 36 (2003) 638.
[5] A. Roucoux, J. Schulz, H. Patin, Adv. Synth. Catal. 345 (2003) 222.
[6] S. Ozkar, R.G. Finke, J. Am. Chem. Soc. 124 (2002) 5796.
[7] L.S. Ott, R.G. Finke, Coord. Chem. Rev. 251 (2007) 1075.
[8] D.B. Zhao, Z.F. Fei, W.H. Ang, P.J. Dyson, Small 2 (2006) 879.
[9] D. Zhao, Z. Fei, J. Geldbach Tilmann, R. Scopelliti, P.J. Dyson, J. Am. Chem. Soc. 126 (2004) 15876.
[10] A.J. Bruss, M.A. Gelesky, G. Machado, J. Dupont, J. Mol. Catal. A: Chem. 252 (2006) 212.
[11] G.S. Fonseca, J.B. Domingos, F. Nome, J. Dupont, J. Mol. Catal. A: Chem. 248 (2006) 10.
[12] A.P. Umpierre, G. Machado, G.H. Fecher, J. Morais, J. Dupont, Adv. Synth. Catal. 347 (2005) 1404.
[13] M.A. Gelesky et al., J. Am. Chem. Soc. 127 (2005) 4588.
[14] L.M. Rossi, J. Dupont, G. Machado, P.F.P. Fichtner, C. Radtke, I.J.R. Baumvol, S.R. Teixeira, J. Braz. Chem. Soc. 15 (2004) 904.
[15] E.T. Silveira et al., Chem. Eur. J. 10 (2004) 3734.
[16] G.S. Fonseca, J.D. Scholten, J. Dupont, Synlett (2004) 1525.
[17] L.M. Rossi, G. Machado, P.F.P. Fichtner, S.R. Teixeira, J. Dupont, Catal. Lett. 92 (2004) 149.
[18] G.S. Fonseca, A.P. Umpierre, P.F.P. Fichtner, S.R. Teixeira, J. Dupont, Chem. Eur. J. 9 (2003) 3263.
[19] C.W. Scheeren, G. Machado, J. Dupont, P.F.P. Fichtner, S.R. Texeira, Inorg. Chem. 42 (2003) 4738.
[20] K. Anderson, S. Cortinas Fernandez, C. Hardacre, P.C. Marr, Inorg. Chem. Commun. 7 (2003) 73.
[21] S.M. Chen, Y.D. Liu, G.Z. Wu, Nanotechnology 16 (2005) 2360.
[22] S.Y. Gao, H.J. Zhang, X.M. Wang, W.P. Mai, C.Y. Peng, L.H. Ge, Nanotechnology 16 (2005) 1234.
[23] J. Huang, T. Jiang, B.X. Han, H.X. Gao, Y.H. Chang, G.Y. Zhao, W.Z. Wu, Chem. Commun. (2003) 1654.
[24] P. Migowski, J. Dupont, Chem. Eur. J. 13 (2007) 32.
[25] Y. Wang, H. Yang, Chem. Commun. (2006) 2545.
[26] Y. Wang, H. Yang, J. Am. Chem. Soc. 127 (2005) 5316.
[27] J. Dupont, P.A.Z. Suarez, Phys. Chem. Chem. Phys. 8 (2006) 2441.
[28] J. Dupont, J. Braz. Chem. Soc. 15 (2004) 341.
[29] M. Antonietti, D.B. Kuang, B. Smarsly, Z. Yong, Angew. Chem., Int. Ed. 43 (2004) 4988.
[30] C.W. Scheeren, G. Machado, S.R. Teixeira, J. Morais, J.B. Domingos, J. Dupont, J. Phys. Chem. B 110 (2006) 13011.
[31] C.S. Consorti et al., J. Phys. Chem. B 109 (2005) 4341.
[32] L.S. Ott, M.L. Cline, M. Deetlefs, K.R. Seddon, R.G. Finke, J. Am. Chem. Soc. 127 (2005) 5758.
[33] J.D. Scholten, G. Ebeling, J. Dupont, Dalton Trans. (2007) 5554.
[34] J.W. Niemantsverdriet, Spectroscopy in Catalysis, VCH, Weinheim, 1995.
[35] G.S. Fonseca, G. Machado, S.R. Teixeira, G.H. Fecher, J. Morais, M.C.M. Alves, J. Dupont, J. Colloid Interf. Sci. 301 (2006) 193.
[36] M.J. Earle et al., Nature 439 (2006) 831.
[37] P. Wasserscheid, Nature 439 (2006) 797.
[38] B.A.D. Neto, L.S. Santos, F.M. Nachtigall, M.N. Eberlin, J. Dupont, Angew. Chem., Int. Ed. Engl. 45 (2006) 7251.
[39] C.C. Cassol, A.P. Umpierre, G. Machado, S.I. Wolke, J. Dupont, J. Am. Chem. Soc. 127 (2005) 3298.
[40] C.S. Consorti, M.L. Zanini, S. Leal, G. Ebeling, J. Dupont, Org. Lett. 5 (2003) 983.
[41] E.F. Smith, F.J.M. Rutten, I.J. Villar-Garcia, D. Briggs, P. Licence, Langmuir 22 (2006) 9386.
[42] E.F. Smith, I.J.V. Garcia, D. Briggs, P. Licence, Chem. Commun. 45 (2005) 5633.
[43] V. Lockett, R. Sedev, C. Bassell, J. Ralston, Phys. Chem. Chem. Phys. 10 (2008) 1330.
[44] C. Aliaga, C.S. Santos, S. Baldelli, Phys. Chem. Chem. Phys. 9 (2007) 3683.
[45] K.R.J. Lovelock, E.F. Smith, A. Deyko, I.J. Villar-Garcia, P. Licence, R.G. Jones, Chem. Commun. 46 (2007) 4866.
[46] J.H. Kwon, S.W. Youn, Y.C. Kang, Bull. Korean Chem. Soc. 27 (2006) 1851.
[47] D.S. Silvester, T.L. Broder, L. Aldous, C. Hardacre, A. Crossleyc, R.G. Compton, The Analyst 132 (2007) 196.
[48] F. Maier et al., Angew. Chem., Int. Ed. Engl. 45 (2006) 7778.
[49] C.C. Cassol, G. Ebeling, B. Ferrera, J. Dupont, Adv. Synth. Catal. 348 (2006) 243.

Artigo V

Alkene Hydroformylation Catalyzed by Rhodium Complexes in Ionic Liquids: Detection of Transient Carbene Species

Jackson D. Scholten and Jairton Dupont

Alkene Hydroformylation Catalyzed by Rhodium Complexes in Ionic Liquids: Detection of Transient Carbene Species

Jackson D. Scholten and Jairton Dupont*

Laboratory of Molecular Catalysis, Institute of Chemistry-UFRGS, Avenida Bento Gonçalves, 9500 P.O. Box 15003, 91501-970 Porto Alegre-RS, Brazil

D/H exchange reactions at the imidazolium cation of an ionic liquid were observed in hydroformylation reactions of 1-octene catalyzed by [Rh(acac)(CO)$_2$](phosphine ligand) dissolved in 1-*n*-butyl-3-methylimidazolium-*d*$_3$ *N*-bis(trifluoromethanesulfonyl)imidate at 75 °C under 5 atm (constant pressure) of CO/H$_2$ (1:1). This D/H exchange occurs preferentially at the C2 position and occurs essentially in the presence of the phosphine ligand and the rhodium precursors, and it is more pronounced in the presence of bases, even a very weak one such as methanol. The presence of phosphine is also essential for the hydroformylation reaction. This result suggests the formation of *N*-heterocyclic carbenes (NHCs) in the biphasic hydroformylation reactions promoted by Rh complexes in imidazolium ionic liquids. These carbene species are easily displaced by the other species present in the ionic liquid, and they do not cause any significant changes in the catalytic activity or selectivity of the hydroformylation reaction.

Introduction

The hydroformylation reaction is one of the most investigated procedures in the field of catalysis.[1,2] Discovered by Roelen in 1938,[3] this reaction is an important industrial homogeneous catalytic process, as it is a powerful method to functionalize C=C bonds to provide aldehyde compounds.[4]

The common metal catalysts used in hydroformylation of general olefins are rhodium,[5−8] cobalt,[9,10] and platinum.[11] Supported metal catalysts also have been employed in an attempt to combine the practical advantages of a heterogeneous system with the efficiency of a homogeneous catalyst.[12,13] Also, different reaction media have been used for hydroformylation such as organic solvents,[14,15] aqueous media,[16] supercritical CO$_2$,[17] and ionic liquids,[18] in addition to solventless conditions.[19] In particular, ionic liquids (ILs) have demonstrated various advantages as immobilizing agents for catalytic biphasic hydroformylation reactions. Among the various advantages, it is worth mentioning catalyst stabilization and recycling, product separation (distillation, decantation, extraction with supercritical carbon dioxide, and continuous-flow processes, for example), selectivity controlled through ionic reaction pathways, and the possibility of using long-chain alkenes.[20−24]

However, as is well-known, the C2 deprotonation of 1,3-dialkylimidazolium ILs using relatively weak bases produces *N*-heterocyclic carbenes[25−27] derived from the imidazolium cation.[28] Moreover, imidazolium cations can oxidatively add to low-valent and electron-rich Ni(0), Pd(0), and Pt(0) complexes to form carbene complexes via C−H activation.[29−33] It

* To whom correspondence should be addressed. E-mail: dupont@iq.ufrgs.br.

(1) Ungvary, F. *Coord. Chem. Rev.* **2007**, *251*, 2087.
(2) Ungvary, F. *Coord. Chem. Rev.* **2007**, *251*, 2072.
(3) Roelen, O. Ger. Offen. 849,548, 1938.
(4) Claver, C., van Leeuwen, P. W. N. M., Eds. *Rhodium Catalyzed Hydroformylation*; Kluwer Academic: Dordrecht, The Netherlands, 2000; Vol. 1.
(5) Yan, Y. J.; Zhang, X. W.; Zhang, X. M. *J. Am. Chem. Soc.* **2006**, *128*, 16058.
(6) Peixoto, A. F.; Pereira, M. M.; Silva, A. M. S.; Foca, C. M.; Bayon, J. C.; Moreno, M.; Beja, A. M.; Paixao, J. A.; Silva, M. R. *J. Mol. Catal. A: Chem.* **2007**, *275*, 121.
(7) Praetorius, J. M.; Kotyk, M. W.; Webb, J. D.; Wang, R. Y.; Crudden, C. M. *Organometallics* **2007**, *26*, 1057.
(8) Kuil, M.; Soltner, T.; van Leeuwen, P.; Reek, J. N. H. *J. Am. Chem. Soc.* **2006**, *128*, 11344.
(9) Bungu, P. N.; Otto, S. *Dalton Trans.* **2007**, *2876*.
(10) Klingler, R. J.; Chen, M. J.; Rathke, J. W.; Kramarz, K. W. *Organometallics* **2007**, *26*, 352.
(11) van Duren, R.; van der Vlugt, J. I.; Kooijman, H.; Spek, A. L.; Vogt, D. *Dalton Trans.* **2007**, 1053.
(12) Peng, Q. R.; He, D. H. *Catal. Lett.* **2007**, *115*, 19.
(13) Bourque, S. C.; Alper, H.; Manzer, L. E.; Arya, P. *J. Am. Chem. Soc.* **2000**, *122*, 956.
(14) Clarke, M. L.; Roff, G. J. *Green Chem.* **2007**, *9*, 792.
(15) Barros, H. J. V.; Guimaraes, C. C.; dos Santos, E. N.; Gusevskaya, E. V. *Catal. Commun.* **2007**, *8*, 747.
(16) Paganelli, S.; Marchetti, M.; Bianchin, M.; Bertucci, C. *J. Mol. Catal. A: Chem.* **2007**, *269*, 234.

(17) Ke, J.; Han, B. X.; George, M. W.; Yan, H. K.; Poliakoff, M. *J. Am. Chem. Soc.* **2001**, *123*, 3661.
(18) Haumann, M.; Riisager, A. *Chem. Rev.* **2008**, *108*, 1474.
(19) Bruss, A. J.; Gelesky, M. A.; Machado, G.; Dupont, J. *J. Mol. Catal. A: Chem.* **2006**, *252*, 212.
(20) Chauvin, Y.; Mussmann, L.; Olivier, H. *Angew. Chem., Int. Ed. Engl.* **1996**, *34*, 2698.
(21) Wasserscheid, P.; Waffenschmidt, H.; Machnitzki, P.; Kottsieper, K. W.; Stelzer, O. *Chem. Commun.* **2001**, 451.
(22) Favre, F.; Olivier-Bourbigou, H.; Commereuc, D.; Saussine, L. *Chem. Commun.* **2001**, 1360.
(23) Brasse, C. C.; Englert, U.; Salzer, A.; Waffenschmidt, H.; Wasserscheid, P. *Organometallics* **2000**, *19*, 3818.
(24) Dupont, J.; Silva, S. M.; de Souza, R. F. *Catal. Lett.* **2001**, *77*, 131.
(25) Mathews, C. J.; Smith, P. J.; Welton, T.; White, A. J. P.; Williams, D. J. *Organometallics* **2001**, *20*, 3848.
(26) McLachlan, F.; Mathews, C. J.; Smith, P. J.; Welton, T. *Organometallics* **2003**, *22*, 5350.
(27) Xu, L.; Chen, W.; Xiao, J. *Organometallics* **2000**, *19*, 1123.
(28) Dupont, J.; Spencer, J. *Angew. Chem., Int. Ed.* **2004**, *43*, 5296.
(29) Bacciu, D.; Kingsley, R.; Cavell, K.; Fallis, I. A.; Ooi, L.-L. *Angew. Chem., Int. Ed.* **2005**, *44*, 5282.
(30) Clement, N. D.; Cavell, K. J. *Angew. Chem., Int. Ed.* **2004**, *43*, 3845.
(31) Clement, N. D.; Cavell, K. J.; Jones, C.; Elsevier, C. J. *Angew. Chem., Int. Ed.* **2004**, *43*, 1277.
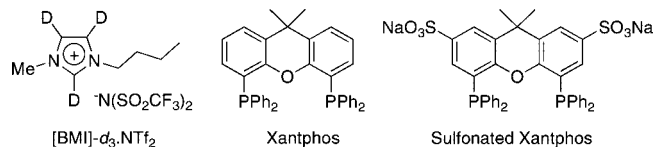(32) Duin, M. A.; Clement, N. D.; Cavell, K. J.; Elsevier, C. J. *Chem. Commun.* **2003**, 400.

Figure 1. Structures of the deuterated ionic liquid and phosphines used.

is assumed that these processes are much likely to occur *in situ* when coordinatively unsaturated low-valent metal species (particularly ones bearing strong σ-donor ligands) are present or are formed during reactions in imidazolium ILs. It has been recently demonstrated, via labeling experiments, the involvement of carbenes in hydrogenation reactions catalyzed by iridium nanoparticles in imidazolium ionic liquids.[34] Interestingly, in these hydrogenations the D/H exchange occurs mainly at the least acidic positions (C4 and C5) on the imidazolium cation.[35] Herein we have demonstrated, via labeling experiments, that carbenes are also formed during the hydroformylation of 1-octene by [Rh(acac)(CO)$_2$] (phosphine) (acac = acetylacetonate) in [BMI]-$d_3 \cdot$NTf$_2$ (Figure 1) and, in particular, in the presence of weak bases such as methanol.

Results and Discussion

The hydroformylation of 1-octene was performed in the presence of the precursor [Rh(acac)(CO)$_2$](phosphine ligand) (substrate/Rh = 250) in [BMI]-$d_3 \cdot$NTf$_2$ at 75 °C and 5 atm (constant pressure) of a CO/H$_2$ (1/1) gas mixture (Scheme 1).

Table 1 summarizes the obtained results for the hydroformylation of 1-octene as well as the control experiments performed.

The hydroformylation in the presence of the phosphine sulfonated Xantphos (molar ratio L/Rh = 4) gives 73% conversion after 21 h with a selectivity of 69% in aldehydes (l/b = 20), 23% octene isomers, and 8% octane (entry 1, Table 1). Most importantly, there was 80% of D/H exchange at the C2 position of the imidazolium cation and only 4% at the least acidic positions (C4 + C5), suggesting the formation of NHC species in the reaction medium. The reaction performed using Xantphos as ligand (molar ratio L/Rh = 1) in the hydroformylation of 1-octene gave similar results: 90% conversion after 1.5 h with a selectivity of 70% in aldehydes (l/b = 21), 28% octene isomers, and 2% octane (entry 3, Table 1). A high percentage of D/H exchange was verified at the C2 position (86%), but none at C4 and C5. The 1-octene hydroformylation performed without the addition of phosphine ligands, i.e. using only the precursor [Rh(acac)(CO)$_2$], gave almost complete olefin conversion after 21 h of reaction (entry 5, Table 1). However, in this case the products are constituted mainly of olefin isomers, octane, and traces of aldehydes. More interestingly, there was *no* detectable D/H exchange in any of the three imidazolium positions. The same result, i.e. no D/H exchange, was observed in the control experiment of [Rh(acac)(CO)$_2$] in [BMI]-$d_3 \cdot$NTf$_2$ at 75 °C and under 5 atm (constant pressure) of CO/H$_2$ without 1-octene after 21 h (entry 7, Table 1). This result indicates that the phosphine-free organometallic precursor is not responsible for the isotopic exchange (see Figure 2). It is also important to note that no significant D/H exchange reaction is attained in the reaction performed in the presence of the phosphine

Xantphos without the metal catalyst precursor after 21 h under the same reaction conditions. Notably, in the experiment using [Rh(acac)(CO)$_2$] dispersed in [BMI]-$d_3 \cdot$NTf$_2$ at 75 °C and 5 atm (constant pressure) of CO/H$_2$ in the presence of Xantphos ligand (molar ratio L/Rh = 1), 85% of D/H exchange at the C2 position and just 1% at the least acidic positions (C4 + C5) were observed (entry 8, Table 1) (Figure 2). However, it is important to note that these D/H exchange reactions are more pronounced when the catalyst precursor and phosphine ligands were immobilized in the IL using methanol than when dichloromethane was used (compare entries 1 and 3 with entries 2 and 4, respectively). This result clearly indicates that even the presence of trace amounts of weak bases, such as methanol, increases the D/H exchange via dedeuteration/protonation reactions. Indeed, a relatively fast H/D exchange process was observed at C2 by the simple dissolution of BMI·NTf$_2$ (0.018 g) in CD$_3$OD (0.5 mL) (66% after 1.5 h at 25 °C) but no reaction was observed in CDCl$_3$. Therefore, carbenes are quite probably formed when the reactions are performed in imidazolium ionic liquids, even in the presence of weak bases.

It is quite plausible to assume that this D/H exchange process occurs through the oxidative addition of the imidazolium ring to the metal center, generating Rh-containing carbene species, similar to those recently isolated from the mixture of Rh(I) dimeric species dissolved in imidazolium ionic liquids.[36] The presence of the phosphine is apparently necessary to increase the complex electron density, thus favoring the C−D addition process and/or acting as a base. Moreover, the formation of the carbene is also observed from the simple deprotonation of the C2 of the imidazolium ring by methanol. Therefore, the basicity of the methanol increased when dissolved in the ionic liquid akin to the basicity of water when dissolved in ILs.[37] No deuterated alkene, alkane, or aldehydes were detected by NMR, IR, or MS analysis of the organic phase isolated after the catalytic reactions. Therefore, the deuterium is much probably incorporated in the acid−base reaction and/or by exchange of the Rh−D intermediate with molecular hydrogen. It is also clear that the catalytic species contains the phosphine ligands, since the selectivity (l/b = 20) is typical of complexes containing Xantphos type ligands.[8,38]

The formation of NHC carbenes during the hydroformylation reaction in ILs is also evident, but these species are easily displaced by the other compounds present in the media and/or are transient species, since they do not inhibit the reaction rates or significantly change the selectivity (l/b). Indeed, no hydroformylation, hydrogenation, or isomerization products were detected in the reaction performed in the presence of a base (*t*-BuOK) and in the absence of a phosphine ligand (entry 6, Table 1). Moreover, the D/H exchange occurred in modest yield at the C2 position (19%), indicating that both the hydroformylation and the D/H exchange reactions are catalyzed essentially by the Rh−phosphine complex in the IL.

Interestingly, the system employing Xantphos as ligand shows a higher catalytic activity in 1-octene hydroformylation as compared to that of the sulfonated Xantphos phosphine (Figure 3).

The same behavior was observed in the hydroformylation of heavy olefins by Rh−phosphines in 1-*n*-butyl-3-methylimida-

(33) McGuinness, D. S.; Cavell, K. J.; Yates, B. F. *Chem. Commun.* **2001**, 355.

(34) Ott, L. S.; Cline, M. L.; Deetlefs, M.; Seddon, K. R.; Finke, R. G. *J. Am. Chem. Soc.* **2005**, *127*, 5758.

(35) Scholten, J. D.; Ebeling, G.; Dupont, J. *Dalton Trans.* **2007**, 5554.

(36) Hintermair, U.; Gutel, T.; Slawin, A. M. Z.; Cole-Hamilton, D. J.; Santini, C. C.; Chauvin, Y. *J. Organomet. Chem.* **2008**, *693*, 2407.

(37) Thornazeau, C.; Olivier-Bourbigou, H.; Magna, L.; Luts, S.; Gilbert, B. *J. Am. Chem. Soc.* **2003**, *125*, 5264.

(38) Bronger, R. P. J.; Silva, S. M.; Kamer, P. C. J.; van Leeuwen, P. *Chem. Commun.* **2002**, 3044.
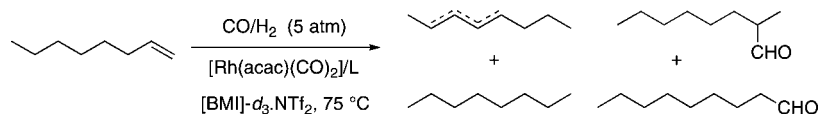
Scheme 1. Biphasic Hydroformylation of 1-Octene Catalyzed by [Rh(acac)(CO)$_2$](phosphine) Complexes in [BMI]-d_3·NTf$_2$

Table 1. Hydroformylation of 1-Octene in [BMI]-d_3·NTf$_2$^{a} at 75 °C and 5 atm (Constant Pressure) of CO/H$_2$ (1/1) with the Precursor [Rh(acac)(CO)$_2$] (1-Octene/Rh = 250) and Control Experiments

entry	system	time (h)	alkene conversn (%)	D/H exchange at C2 (%)	D/H exchange at C4 + C5 (%)
1	1-octene + [Rh(acac)(CO)$_2$](sulfonated Xantphos) (L/Rh = 4)^g	21.0	73^b	80	4
2	1-octene + [Rh(acac)(CO)$_2$](sulfonated Xantphos) (L/Rh = 1)^h	21.0	30^c	1	9
3	1-octene + [Rh(acac)(CO)$_2$](Xantphos) (L/Rh = 1)^g	1.5	90^d	86	
4	1-octene + [Rh(acac)(CO)$_2$](Xantphos (L/Rh = 1)^h	1.5	62^e	6	7
5	1-octene + [Rh(acac)(CO)$_2$]^g	21.0	99^f		
6	1-octene + [Rh(acac)(CO)$_2$](t-BuOK) (base/Rh = 2)^g	21.0		19	2
7	[Rh(acac)(CO)$_2$]^g	21.0			
8	[Rh(acac)(CO)$_2$](Xantphos) (L/Rh = 1)^g	20.0		85	1
9	[Rh(acac)(CO)$_2$](Xantphos) (L/Rh = 1)^h	21.0		6 (100)^i	8 (16)^i

^{a} 93% D at C2 and 90% at C4 + C5 (88% C4, 92% C5). ^{b} 69% aldehydes (l/b = 20), 23% octene isomers, 8% octane. ^{c} 43% aldehydes (l/b = 7), 54% octene isomers, 3% octane. ^{d} 70% aldehydes (l/b = 21), 28% octene isomers, 2% octane. ^{e} 67% aldehydes (l/b = 20), 29% octene isomers, 4% octane. ^{f} traces of aldehydes, 83% octene isomers, 17% octane. ^{g} IL and catalyst previously dissolved in MeOH. ^{h} IL and catalyst previously dissolved in CH$_2$Cl$_2$. ^{i} The values in parentheses were obtained after the addition of MeOH (0.5 mL) and the reaction was conduced for 2 h at 25 °C.
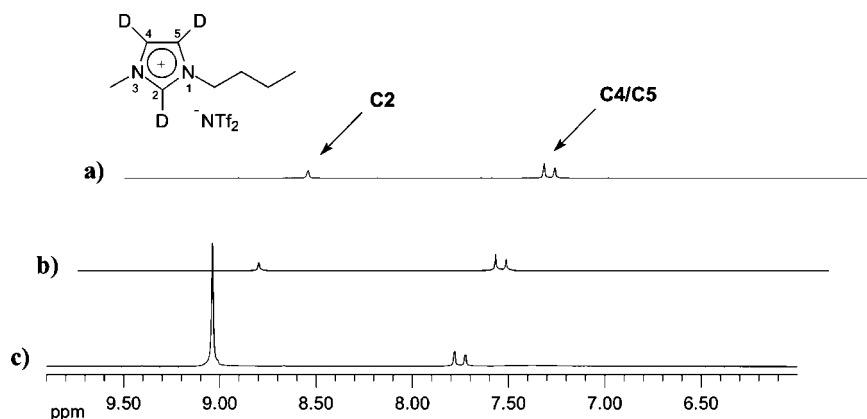
Figure 2. Parts of the ^{1}H NMR spectra (a) of the pure [BMI]-d_3·NTf$_2$ ionic liquid containing 93% D at C2, 88% D at C4, and 92% D at the C5 position of the imidazolium ring, (b) after the control experiment using [Rh(acac)(CO)$_2$] in [BMI]-d_3·NTf$_2$ without 1-octene (entry 7 in Table 1), and (c) after the control experiment using the same catalytic system but with the presence of Xantphos (entry 8 in Table 1).

zolium hexafluorophosphate ionic liquid.[24] The considerable difference in the catalytic activity observed for both hydroformylation systems is probably related to the different kinds of interactions between the phosphine ligand in the modified catalyst and the IL. Indeed, it was recently reported that the sulfonated phosphine TPPMS (TPPMS = triphenylphosphine-monosulfonated) interacts with the IL mainly through C−H···X$^-$ hydrogen bonding with the sulfonate group (where the IL is an anion receptor), while for the neutral phosphine TPP (TPP = triphenylphosphine), supramolecular structures[39,40] are formed by π-stacking interactions.[41] It is quite possible that the reactions performed with the nonionic phosphines[42] occurs in both phases (organic and in the ionic liquid), whereas those performed with the sulfonated ligands occur preferentially in the ionic phase (typical under multiphase conditions).

Conclusions

There is almost no doubt that there is involvement of NHC species during the hydroformylation of 1-octene by the complex [Rh(acac)(CO)$_2$] in the presence of phosphine ligands dispersed in a deuterated imidazolium-based ionic liquid. Most importantly, the phosphine ligands in the presence of methanol play an essential role in the occurrence of D/H exchange reactions. Therefore, *N*-heterocyclic carbenes derived from imidazolium cations are probably present, even in typical hydroformylation reactions in ionic liquids promoted by metal complexes without strong σ-donor ligands. Also of great importance, the probability for the formation of these carbene species is increased in the presence of weak bases such as an IL dissolved in methanol.

Experimental Section

General Considerations. The synthesis of deuterated ionic liquids was performed under an argon atmosphere using Schlenk tubes. The hydroformylation reactions were performed on a modified Fischer−Porter bottle immersed in a silicon oil bath and connected to a gas reservoir. The system temperature was kept at 75 °C with constant stirring (400 rpm). The fall in the gas pressure

(39) Migowski, P.; Dupont, J. *Chem. Eur. J.* **2007**, *13*, 32.
(40) Dupont, J. *J. Braz. Chem. Soc.* **2004**, *15*, 341.
(41) Leclercq, L.; Suisse, I.; Agbossou-Niedercorn, F. *Chem. Commun.* **2008**, 311.
(42) Consorti, C. S.; Aydos, G. L. P.; Ebeling, G.; Dupont, J. *Org. Lett.* **2008**, *10*, 237.
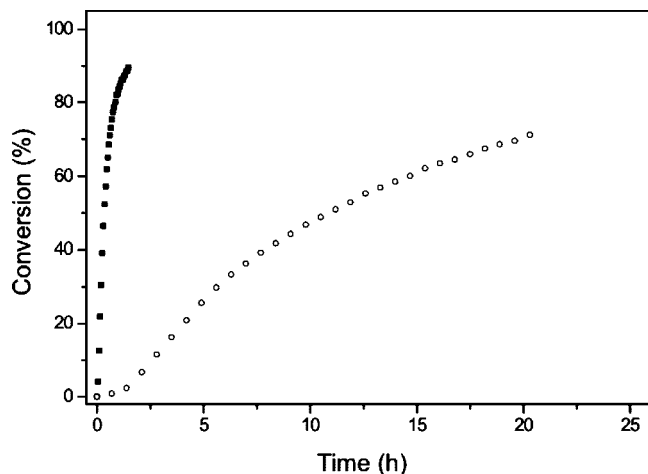
Figure 3. Biphasic hydroformylation of 1-octene in [BMI]-$d_3 \cdot$NTf$_2$ at 75 °C and 5 atm of CO/H$_2$ (constant pressure) with the precursor [Rh(acac)(CO)$_2$] (substrate/Rh = 250) in the presence of (■) Xantphos and (○) sulfonated Xantphos.

in the reservoir was monitored with a pressure transducer interfaced through a Novus converter to a PC, and the data were worked up via Microcal Origin 7.0. The total pressure of gas (∼5 atm) in hydroformylation reactions was estimated by considering that before the catalytic reaction the Fischer−Porter bottle was placed under vacuum (3.0−5.0 mmHg) for 5 s in order to remove the argon atmosphere and then 4 atm of the gas mixture was added to the reactor. NMR spectra were recorded on a Varian VNMRS 300 MHz instrument. For ^{1}H NMR studies the following spectral parameters were used: pulse, 45°; acquisition time, 2.049 s; relaxation delay, 10.0 s; scan repetitions, 128; total acquisition time, 26 min 7 s. Mass spectra were obtained using a GC-MS Shimadzu QP-5050

spectrometer (EI, 70 eV). Gas chromatography analyses were performed with a Hewlett-Packard 5890 gas chromatograph with a FID and 30 m capillary column with a polyphenylmethylsiloxane stationary phase. Reagents were purchased from commercial sources (Strem Chemicals, Acros, Aldrich) and used without further purification. The deuterated ionic liquid [BMI]-$d_3 \cdot$NTf$_2$ was synthesized as previously reported[35] from the methanesulfonate imidazolium salt.[43] Analysis of ^{1}H NMR indicates a deuterium content of 93% at C2, 88% at C4, and 92% at the C5 position of the imidazolium ring.

Procedure for 1-Octene Hydroformylation. In a Fischer−Porter bottle reactor, [Rh(acac)(CO)$_2$] (0.0134 g; 0.052 mmol) and sulfonated Xantphos (0.163 g, 0.208 mmol) or Xantphos (0.0301 g, 0.052 mmol) was dissolved in methanol (2.0 mL) or dichloromethane (2.0 mL) and then the d_3 ionic liquid (1.0 mL) was added with stirring at room temperature. The volatiles were evaporated under reduced pressure at 50 °C (methanol) or 25 °C (CH$_2$Cl$_2$) for 1 h. In sequence, 1-octene (1.46 g, 13.0 mmol, substrate/catalyst adjusted for a molar ratio of 250) was added, CO/H$_2$ (1/1 mixture; 5 atm of constant pressure) was admitted to the reactor, and the mixture was heated to 75 °C. The products were analyzed by GC-MS.

Supporting Information Available: Figures giving ^{1}H and ^{13}C NMR spectra of the ILs before and after hydroformylation reactions. This material is available free of charge via the Internet at http://pubs.acs.org.

(43) Cassol, C. C.; Ebeling, G.; Ferrera, B.; Dupont, J. *Adv. Synth. Catal.* **2006**, *348*, 243.

Alkenes Hydroformylation Catalyzed by Rhodium Complexes in Ionic Liquids: Detection of Transient Carbene Species

Jackson D. Scholten and Jairton Dupont[*]

Laboratory of Molecular Catalysis, Institute of Chemistry - UFRGS, Avenida Bento Gonçalves, 9500 P.O. Box 15003, 91501-970, Porto Alegre, RS Brazil.

E-mail:dupont@iq.ufrgs.br – Fax: 55 51 3308 7304
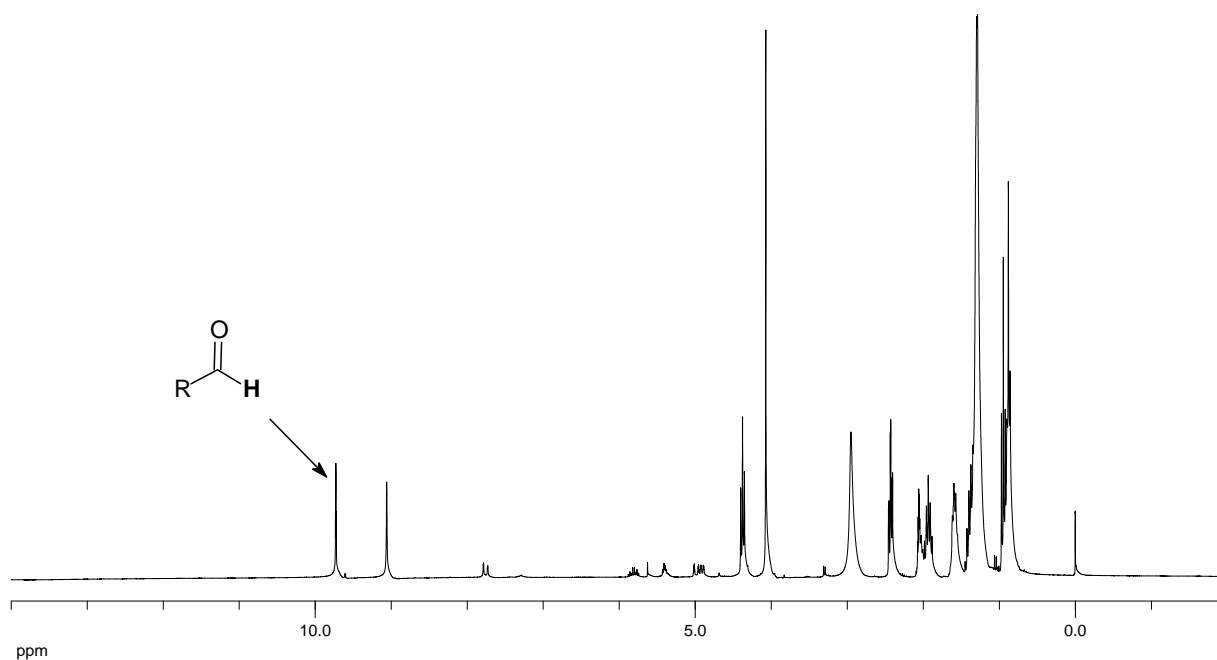
Figure S1. ^{1}H NMR spectrum of the [BMI]-d_3.NTf$_2$ after 1-octene hydroformylation at 75 ºC and 5 atm of CO/H$_2$ (1:1) catalyzed by [Rh(acac)(CO)$_2$]/Sulfonated Xantphos (MeOH was used as previously solvent).
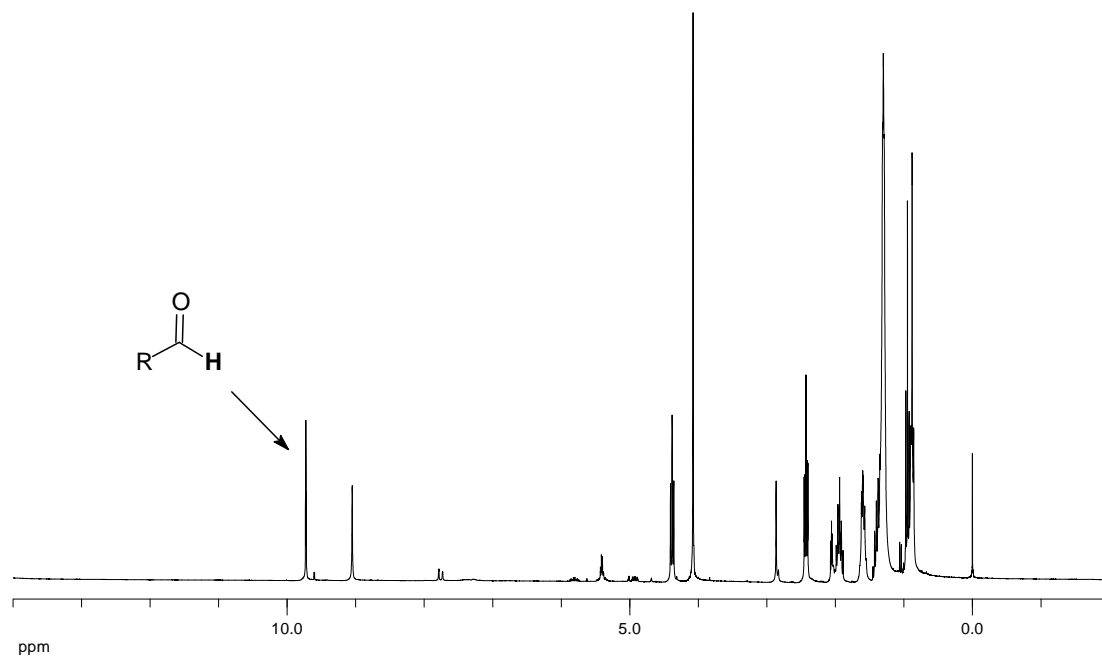
Figure S2. ^{1}H NMR spectrum of the [BMI]-d_3.NTf$_2$ after 1-octene hydroformylation at 75 °C and 5 atm of CO/H$_2$ (1:1) catalyzed by [Rh(acac)(CO)$_2$]/Xantphos (MeOH was used as previously solvent).
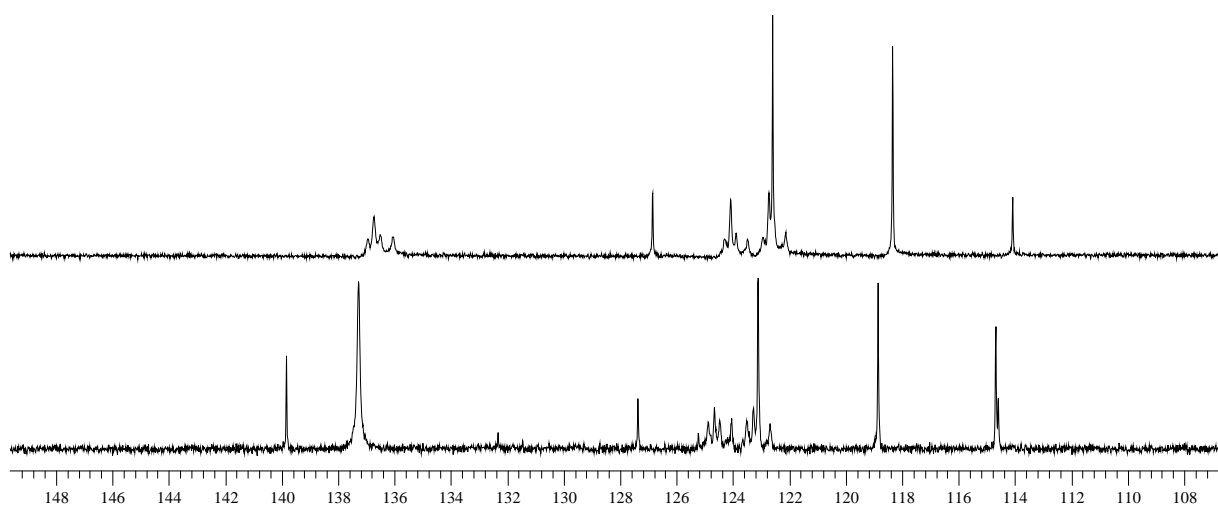
Figure S3. Part of ^{13}C NMR spectrum of the pure [BMI]-d_3.NTf$_2$ (top) and after hydroformylation reaction catalyzed by [Rh(acac)(CO)$_2$]/Xantphos (bottom) showing the region of imidazolium carbons (C2, C4 and C5).
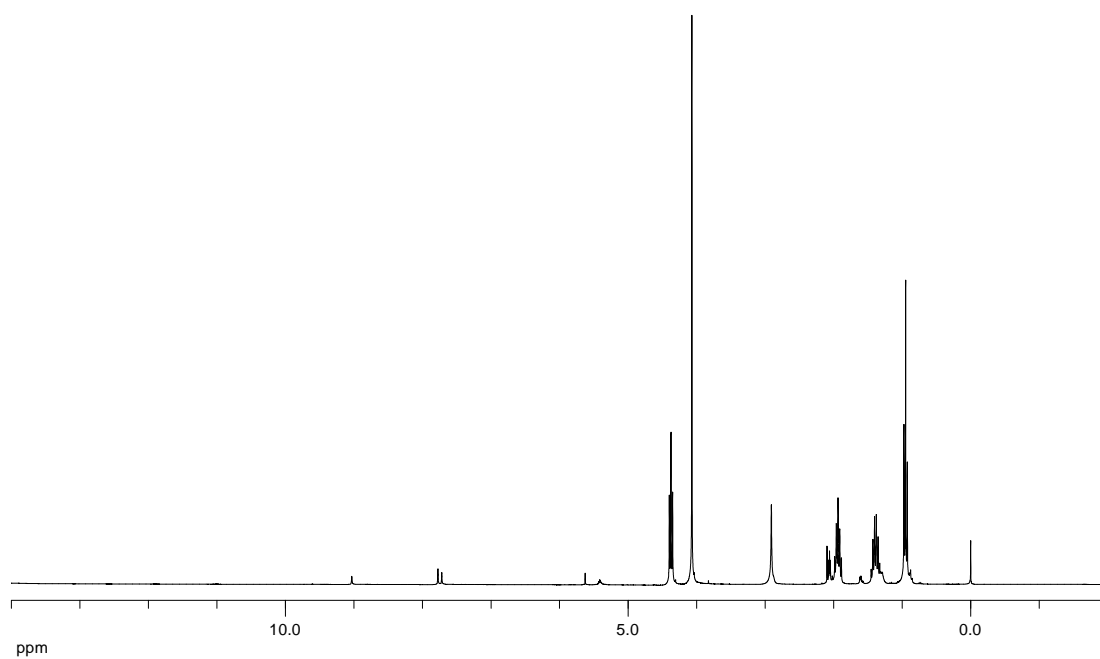
Figure S4. ^{1}H NMR spectrum of the [BMI]-d_3.NTf$_2$ after 1-octene hydroformylation at 75 ºC and 5 atm of CO/H$_2$ (1:1) catalyzed by [Rh(acac)(CO)$_2$] (MeOH was used as previously solvent).
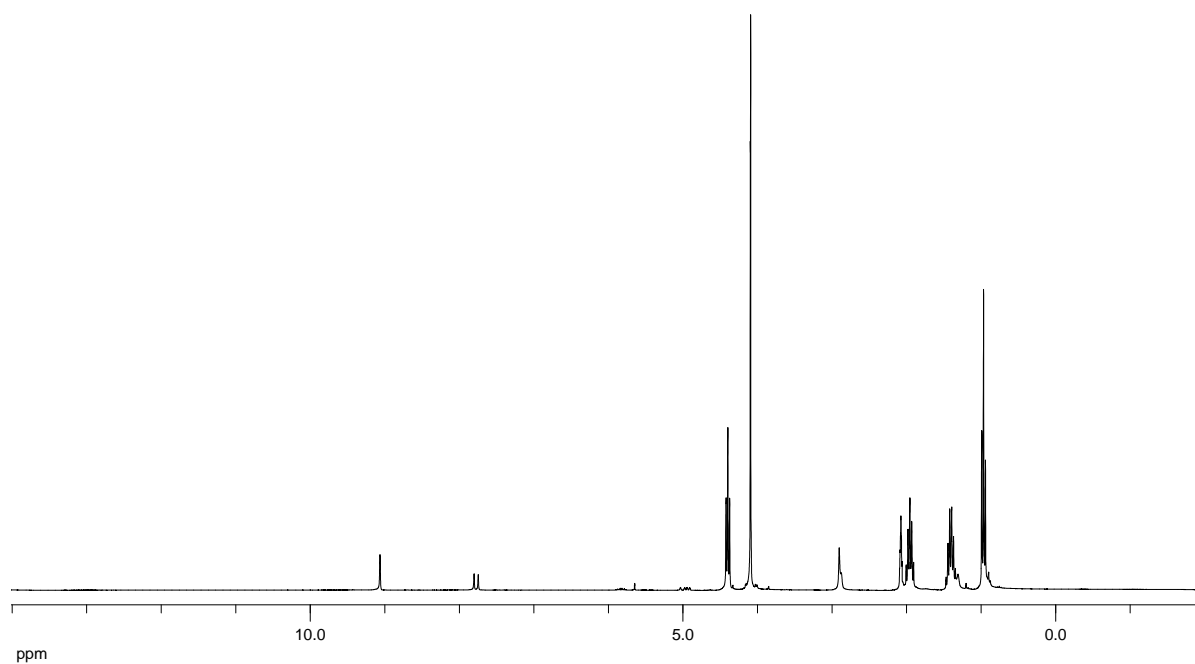
Figure S5. ^{1}H NMR spectrum of the [BMI]-d_3.NTf$_2$ after 1-octene hydroformylation at 75 ºC and 5 atm of CO/H$_2$ (1:1) catalyzed by [Rh(acac)(CO)$_2$] in the presence of t-BuOK (in this reaction MeOH was not used as previously solvent).
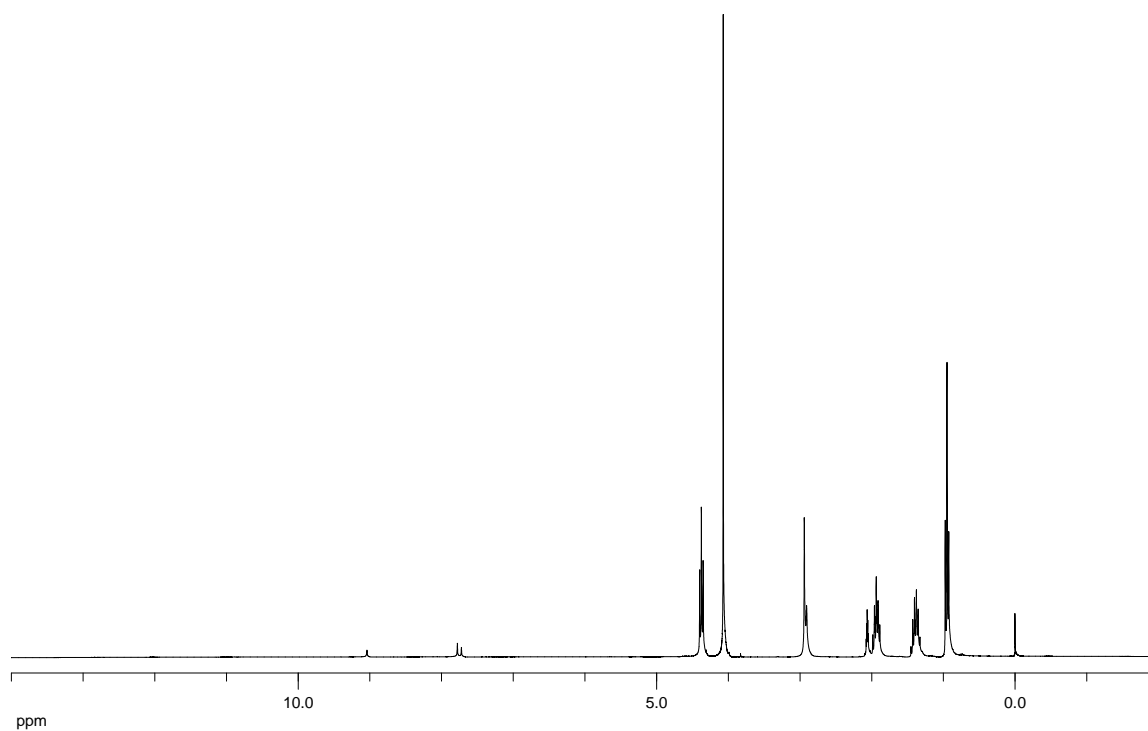
Figure S6. ^{1}H NMR spectrum of the [BMI]-d_3.NTf$_2$ after the control experiment at 75 ºC and 5 atm of CO/H$_2$ (1:1) in the presence of [Rh(acac)(CO)$_2$] without 1-octene (MeOH was used as previously solvent).
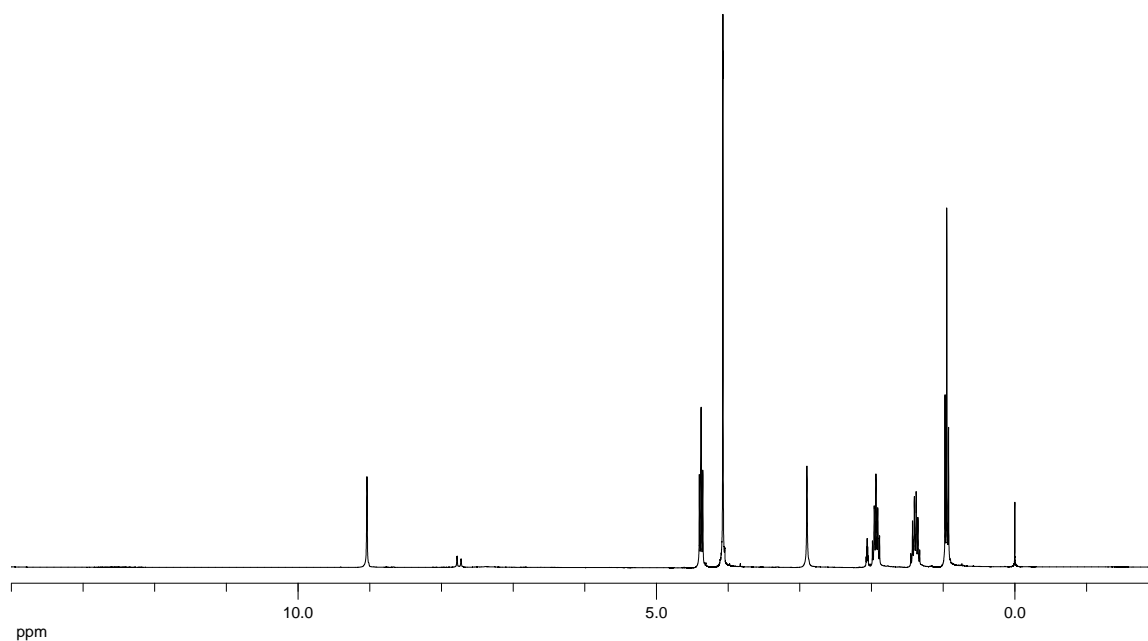
Figure S7. ¹H NMR spectrum of the [BMI]-*d₃*.NTf₂ after the control experiment at 75 ºC and 5 atm of CO/H₂ (1:1) in the presence of [Rh(acac)(CO)₂]/Xantphos without 1-octene (MeOH was used as previously solvent).
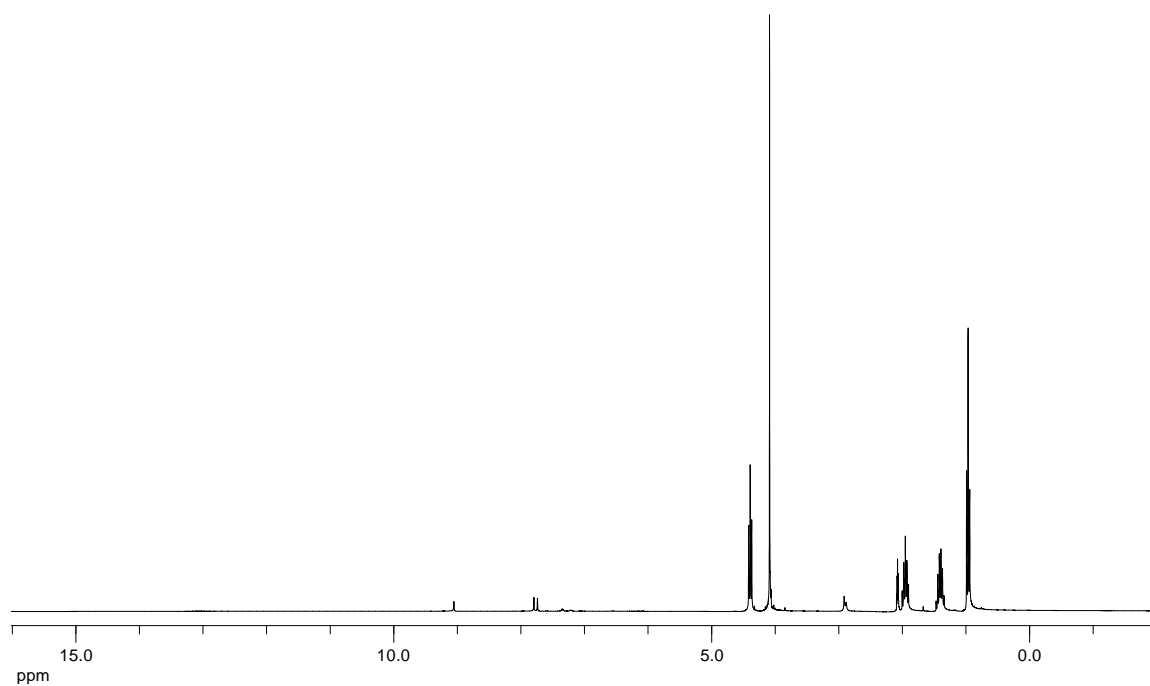
Figure S8. ^{1}H NMR spectrum of the [BMI]-d_3.NTf$_2$ after the control experiment at 75 ℃ and 5 atm of CO/H$_2$ (1:1) in the presence of Xantphos without the metal catalyst (in this reaction MeOH was not used as previously solvent).

Artigo VI

Decomposition of Formic Acid Catalyzed by a Phosphine-Free Ruthenium Complex in a Task-Specific Ionic Liquid

Jackson D. Scholten, Martin H. G. Prechtl and Jairton Dupont

Decomposition of Formic Acid Catalyzed by a Phosphine-Free Ruthenium Complex in a Task-Specific Ionic Liquid

Jackson D. Scholten, Martin H. G. Prechtl, and Jairton Dupont*[a]

The dehydrogenation of formic acid is effectively catalyzed by the Ru complex [{RuCl$_2$(p-cymene)}$_2$] dissolved in the ionic liquid (IL) 1-(2-(diethylamino)ethyl)-3-methylimidazolium chloride at 80 °C without additional bases. This catalytic system gives TOF values of up to 1540 h^{-1}. Preliminary kinetic insights show formal reaction orders of 0.70($\pm$0.15), 0.78($\pm$0.03) and 2.00($\pm$0.17) for the Ru catalyst, IL **1**, and formic acid, respectively. The apparent activation energy of this process is estimated to be (69.1$\pm$7.6) kJ mol^{-1}. In addition, dimeric Ru hydride ionic species involved in the reaction, such as [{Ru(p-cymene)}$_2${(H)μ-(H)-μ-(HCO$_2$)}]$^+$ and [{Ru(p-cymene)}$_2${(H)μ-(Cl)μ-(HCO$_2$)}]$^+$, are identified by mass spectrometry. The presence of water in large amounts inhibits higher conversions. Finally, a remarkable catalytic activity is observed during recycles, indicating this system's potential for hydrogen gas production.

Introduction

Currently, there is a strong interest in hydrogen storage to serve an advanced hydrogen-based energy system.[1–4] In this context, one of the most significant challenges of hydrogen-based energy generation is the storage of large quantities of hydrogen at safe pressures.[1] In particular for portable applications, the use of liquid hydrogen has several disadvantages due to its continuous evaporation. Among various storage materials and methods currently under investigation, molecular hydrogen adsorption on materials of large surface area[5–8] and clathrate hydrates,[9] the use of bonded hydrogen atoms in hydrocarbons,[10] metal hydrides[11,12] or formic acid (FA)[13–17] show considerable promise.

The decomposition of FA as a formate–amine adduct, such as the azeotropic mixture comprising HCO$_2$H and NEt$_3$ (5:2 molar ratio), is usually the method of choice for hydrogen generation.[18–22] FA decomposition to hydrogen and carbon dioxide can easily be catalyzed by several homogeneous[14,16,18–23] and heterogeneous catalysts.[24] In particular, Ru phosphine complexes in the presence of a base, such as triethylamine or sodium formate, in water are quite effective catalysts for this transformation. However, these systems use volatile amines and/or water that should be removed before application in fuel cell devices. Very recently, Deng and co-workers indicated that FA decomposition can be catalyzed by [{RuCl$_2$(p-cymene)}$_2$] **2** in amine-functionalized ILs in the presence of

sodium formate with turnover numbers of up to 627 in one hour at 60 °C.[25] Herein, we report our findings on the decomposition of FA by the phosphine-free [{RuCl$_2$(p-cymene)}$_2$] **2** in functionalized IL[26,27] **1** (Figure 1) in the absence of base, with discussion of kinetic and mechanistic aspects, and identification of the ionic organometallic species involved in this transformation.

Results and Discussion

The functionalized IL **1** was chosen for study not only because of its basicity and very low vapor pressure, but also because Ru catalyst precursor **2** and the other components (FA and water) are highly soluble in this liquid, whereas the main product is almost insoluble. Therefore, the catalytic system could be considered as one-phase, and the kinetic and mechanistic aspects were investigated using classical homogeneous catalytic models.

Investigation of the catalyst system **1/2** showed activities with initial turnover frequencies (TOFs) of up to 1540 h^{-1} without additional solvents or bases. The TOFs were determined from the normalized slopes obtained by online pressure monitoring and calibration by ^{1}H NMR spectroscopy. Preliminary experiments showed that it was crucial to slightly heat (T = 40 °C, 80 °C) the reaction mixture of FA (17.6 mmol), IL **1** (7.0 mmol) and complex **2** (6.5 μmol; Table 1, entries 1 and 2). There was no significant reaction at 25 °C, probably due to a lack of for-
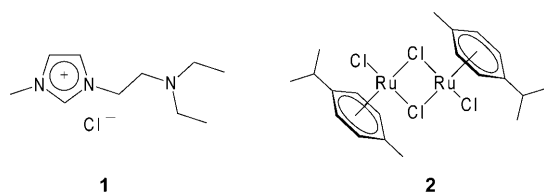

Figure 1. Cocatalyst IL **1** and ruthenium precursor **2**.

[a] J. D. Scholten, Dr. M. H. G. Prechtl, Prof. Dr. J. Dupont
INCT-Catal., Laboratory of Molecular Catalysis, Institute of Chemistry
Universidade Federal do Rio Grande do Sul (UFRGS)
Av. Bento Gonçalves 9500, Porto Alegre, RS, Brazil, CEP 90710-501 (Brazil)
Fax: (+55) 51-3308-7304
E-mail: jairton.dupont@ufrgs.br

Table 1. Ruthenium **2**-catalyzed FA decomposition using IL **1** as a co-catalyst.

Entry	IL [mmol]	FA [mmol]	Ru [μmol]	T [°C]	t [h]	Conv. [%][a]	TOF [h^{-1}][b]
1	7.0	17.6	6.5	40	45	31	N.D.
2	7.0	17.6	6.5	80	7	91[c]	1540
3[d]	7.0	17.6	6.5	80	24	41	280
4[e]	7.0	17.6	6.5	80	22	86	1684
5	2.3	17.6	6.5	80	5	92[f]	738
6	2.3	17.6	13.1	80	3	97	472
7	7.0	17.6	19.6	80	6	90[g]	664
8	2.3	17.6	19.6	80	3	99	366
9	0.9	17.6	19.6	80	4	91[h]	206
10	2.3	26.5	19.6	80	5	>99	352
11	2.3	8.8	19.6	80	2	>99	374
12	2.3	17.6	19.6	40	24	87	26
13	2.3	17.6	19.6	50	24	91	38
14	2.3	17.6	19.6	60	8	99	180
15	2.3	17.6	19.6	70	7	98	220
16	2.3	17.6	19.6	95	2	99	460

[a] Formic acid decomposition to H_2 and CO_2 (1:1); [b] TOF = (mol$_{product}$)/(mol$_{Ru\ dimer}$ × t) (at 20% conversion); [c] conversion > 99% after 17 h; [d] in the presence of water (1.0 mL); [e] in the presence of toluene (1.0 mL); [f] conversion = 99% after 20 h; [g] conversion = 98% after 20 h; [h] conversion > 99% after 20 h. N.D. = not determined.

mation of catalytically active species, which apparently only occurs at higher temperatures. Indeed, at $T = 40$ °C (Table 1, entry 1) conversion was quite low (31%) at a prolonged reaction time (45 h). However, at 80 °C, the conversion was over 90% within 7 h and was practically complete (>99%) within 17 h (Table 1, entry 2). It is worth noting that the obtained catalytic activities (TOFs of up to 1540 h^{-1}) reported herein are superior to those recently reported using a *i*Pr$_2$NEMimCl/**2** at 60 °C in the presence of sodium formate (TOF up to 627 h^{-1}).[25] These differences are probably related to the use of strong base, which is known to form *N*-heterocyclic carbenes by imidazolium deprotonation[28] and/or decompose imidazolium ILs in the presence of water by Hoffman elimination.[29] Water plays an important role in this catalytic reaction; the addition of 1 mL of water had a detrimental effect (Table 1, entry 3), in contrast to Laurenczy's system, which operates in water.[16] In our system, excess water gave lower conversions, and after 24 h, only 41% of the FA was dehydrogenated at 80 °C, which corroborates a recent report using the same catalytic system in the presence of an extra base.[25] In this case, the excess of water may make difficult the formation of catalytic active species in the medium, probably as a result of solvation or coordination processes that have a negative effect on the reaction. However, traces of residual water did not drastically influence the catalysis, as all reactions were prepared without the exclusion of humidity. Furthermore, another run was set up with the addition of toluene (1 mL) to check whether a lower viscosity of the catalyst system (owing to the presence of a cosolvent) supported faster conversion (Table 1, entry 4). Surprisingly, the conversion was slightly lower (86% after 22 h).

More importantly, in our investigations we found that high quantities of IL may slow down the catalytic reaction, and that even small amounts are sufficient to make the FA capable of dehydrogenation. Although high amounts of IL make the dehydrogenation faster up to 20% conversion, the overall reaction is slower when compared to that with low concentrations of the IL (Table 1, entries 2 and 5, 7 and 8), which may be related to the a high viscosity of the medium being attained with a high IL concentration and/or the amine moiety of the IL blocking the active sites of the ruthenium complex. Although no transition species containing the IL–amine as a ligand were detected by electrospray ionization mass spectrometry (ESI–MS) analysis (see later), the second (site-blocking) aspect is in agreement with previous observations, where excess ligands such as phosphine blocked the catalyst active site and drastically lowered the conversion.[16] Moreover, the addition of phosphine ligands to our system completely inhibited the catalytic decomposition of FA. In other words, the active sites of the ruthenium species are blocked by strongly coordinating phosphine ligands. Consequently, we ran a phosphine-free system and tested lower base concentrations in the FA decomposition reaction. Initially, decreasing the IL amount from 7.0 to 2.3 mmol led to a drop in the reaction time under the same conditions (Table 1, entries 7 and 8). However, using 0.9 mmol of the IL did not significantly improve FA decomposition (Table 1, entry 9). Therefore, it was assumed that the best reaction conditions consisted of the use of 2.3 mmol of IL **1** and 19.6 μmol of **2** at 80 °C. As expected, increasing the FA concentration (to 26.5 mmol) increased the reaction time, whereas with a lower quantity (8.8 mmol), the reaction was practically complete in less time and a high conversion was reached after a few hours (Table 1, entries 8, 10, and 11). The stability of the catalyst system was tested by performing recycling experiments using the standard conditions (2.3 mmol IL **1**, 19.6 μmol **2**, 17.6 mmol FA, $T = 80$ °C). Although a slight decrease in the catalytic activity was observed after the first run, the system proved robust even after five recycles (Figure 2). In all cases, gas-phase analyses of the FA dehydrogenation reactions by mass spectrometry indicated the formation of H_2 and CO_2 in a 1:1 ratio. Moreover, carbon monoxide was detected in
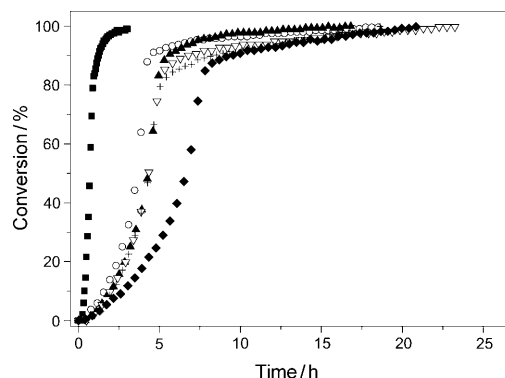

Figure 2. Reaction profiles for FA (0.81 g; 17.6 mmol) decomposition catalyzed by Ru complex **2** (0.012 g; 19.6 μmol) in IL **1** (0.5 g; 2.3 mmol) at 80 °C for 6 cycles: ■ 1st; ○ 2nd; ▲ 3rd; ▽ 4th; ◆ 5th; + 6th cycle.

trace amounts in the gas-phase of the reactions by infrared analysis (Figure 3).

It is important to note that no CO was detected by gas chromatography (GC) analysis indicating that the CO concentration
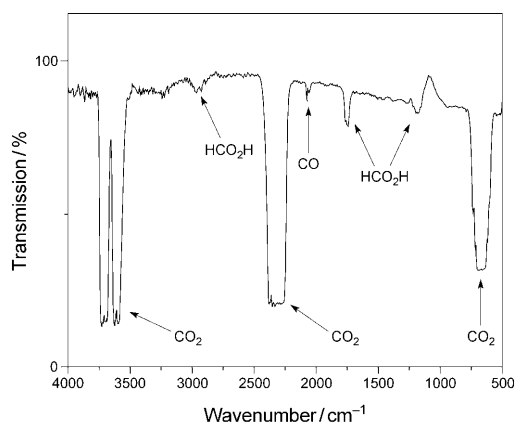

Figure 3. Infrared spectrum of the gas-phase after FA decomposition catalyzed by Ru complex **2** in IL **1** at 80 °C. Conditions as for Figure 2.

is below the detection limit of the detector (TCD, 10 ppm). This result is similar to those reported previously by Beller and co-workers.[21] However, a week CO stretching was detected by IR spectroscopy indicating its concentration was in the range 1–10 ppm in the gas-phase. Since CO generation implies water formation (dehydration of FA), the water content was also monitored by mass spectrometry (MS). In fact, no water was detected in the gas-phase by MS, again indicating a CO production less than 10 ppm[30] (see the Supporting Information). Although the time for complete conversion on the recharges was slightly higher than the first run, the presence of traces of CO did not significantly influence the catalytic activity of the system. The reaction parameters of this homogeneous system at different temperatures (40–95 °C), catalyst loadings (6.5–19.6 μmol), substrate loadings (8.8–26.5 mmol) and base amounts (0.9–7.0 mmol) are summarized in Table 1.

Using the determined initial rate constants of the selected curves at low conversions (< 20 %), it was possible to estimate the formal reaction order for this catalytic system (see the Supporting Information). From a double logarithmic plot of the initial rates, a formal "broken" reaction order (0.70 ± 0.15) was deduced for catalyst **2** (constant IL and FA amounts of 2.3 and 17.6 mmol, respectively; Table 1, entries 5, 6 and 8). The reaction order with respect to IL **1** was also checked by variation of its concentration at a constant catalyst loading of 19.6 μmol of **2** and 17.6 mmol of FA at 80 °C (Table 1, entries 7–9), and showed a similar order (0.78 ± 0.03). Broken reaction orders are usually related to the formation of the active species. In this case, it is probable that not all of the Ru precursor gives Ru hydrides, but also gives other Ru species (neutral complexes, for example) that could not be identified by ESI analysis (see further). This entire process was possibly supported by the IL **1**. Furthermore, a formal reaction order for the FA substrate was determined in a similar manner, which showed a second-order

dependence (2.00 ± 0.17; Table 1, entries 8, 10 and 11). Thus, this preliminary result suggests that FA is present in its dimeric form during the catalytic reaction. The influence of the reaction temperature was investigated with the standard system (19.6 μmol **2**, 2.3 mmol IL **1**, 17.6 mmol FA) in the range of 40–95 °C (Table 1, entries 8 and 12–16; Figure 4). The slope of the
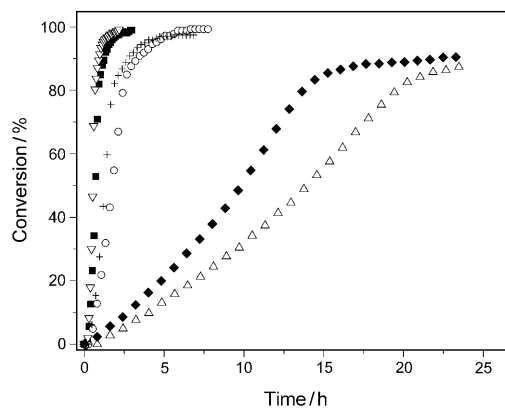

Figure 4. FA decomposition catalyzed by Ru complex **2** in IL **1** at different temperatures: $\triangledown$ 95 °C; $\blacksquare$ 80 °C; + 70 °C; $\bigcirc$ 60 °C; $\blacklozenge$ 50 °C; $\triangle$ 40 °C. Amounts as for Figure 2.

line up to 20 % conversion (initial rate) was used to determine the apparent activation energy of the process. From the Arrhenius plot (Figure 5), the activation energy was derived as $E_a = 69.1 ± 7.6$ kJ mol^{-1}. This activation energy fits in the range of the most active catalyst systems previously reported for the dehydrogenation of FA.[24] In general, heterogeneous catalysts have activation energies higher than 100 kJ mol^{-1}.[31]

Moreover, the standard catalytic system was investigated by means of ESI-MS techniques for the detection of ruthenium complexes during the catalysis. For the detection of intermediates and organometallic complexes in dilute homogeneous solutions, especially in IL systems, ESI-MS spectrometry is the most powerful and convenient tool, and is best known as ion fishing.[32–38] An aliquot of the reaction mixture was taken after 45 min (ca. 50 % conversion), and the sample was analyzed in
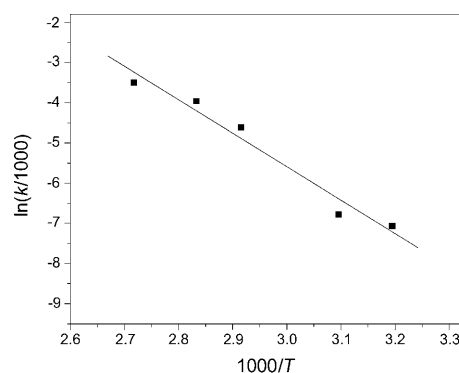

Figure 5. Arrhenius plot for the determination of the apparent activation energy of the process ($E_a = 69.1 ± 7.6$ kJ mol^{-1}). Reaction conditions: Amounts as for Figure 2; $T = 40$–95 °C.

water. The ESI(+)-MS spectrogram (Figure 6) showed the IL ($m/z = 182.07$) and two ruthenium species with signal sets at around 518.81 and 552.76. Both signal sets had the typical iso-
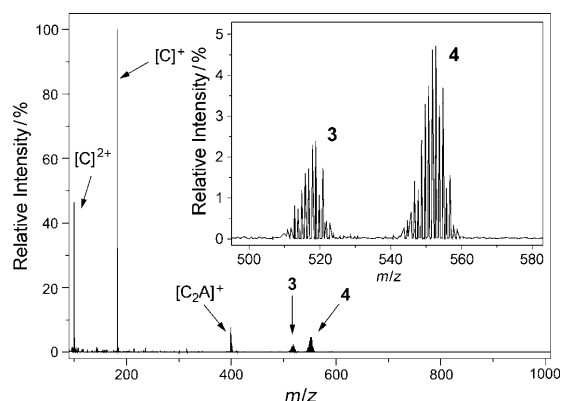

Figure 6. ESI(+)-MS analysis of FA dehydrogenation catalyzed by Ru complex **2** in IL **1**, analyzed at 50% of conversion. Conditions as for Figure 2. The inset shows the signals of intermediary ruthenium species **3** ($m/z = 518.81$) and **4** ($m/z = 552.76$). [C]$^+$ corresponds to the cation of IL **1**, [C]$^{2+}$ is the protonated dicationic IL **1** and [C$_2$A]$^+$ is one cluster where A is the anion.

topic distribution for ruthenium. Considering the dimeric ruthenium precursor **2** with a chloride bridge, we observed some evidence of dimeric ruthenium complexes **3** and **4**, with a formate–hydride bridge and formate–chloride bridge, respectively (Figure 7). Formate-bridged ruthenium dimers have been previously reported for the ruthenium-catalyzed dehydrogenation of FA,[22] where a simple ligand exchange between halide and formate is likely to occur and can be easily understood in presence of excess FA. The analysis of both main signals ($m/z = 518.81$ and 552.76) with higher energies (50 V) in the ESI(+)-MS/MS experiments showed the loss of the formate bridge ligand, with the ruthenium fragments rearranged. In the case of Ru complex **3**, a formerly terminal hydride acts as a hydride bridge in proposed ruthenium dimer **5** ($m/z = 473.84$), and chloride-bridged ruthenium dimer **6** ($m/z = 507.78$) is formed after the fragmentation of Ru complex **4** (Figure 7). The ESI(+)-MS/MS experiments also showed that the formate ligand in the stable dimers **3** and **4** can be eliminated more easily and with reasonably low energies in the gas-phase, rather than a hydride or chloride being eliminated under these conditions. Additionally, for the proposed complexes (**3** and **4**), the theoretical isotope modeling fit well with the experimental data, which strengthens the assumed presence of the catalytic species in a dimeric form. Consequently, the calculated TOFs are based on ruthenium dimers and not ruthenium monomers.

Attempts to characterize the related ruthenium species in situ by ^{1}H and ^{13}C NMR spectroscopy failed, probably due to the very low Ru concentration becoming difficult to obtain NMR spectra from the crude reaction mixture.

To prove the high potential of our in situ-formed catalytic system **1/2**, we considered the use of the corresponding solid hydrochloride of the amine-functionalized IL (soluble in FA),
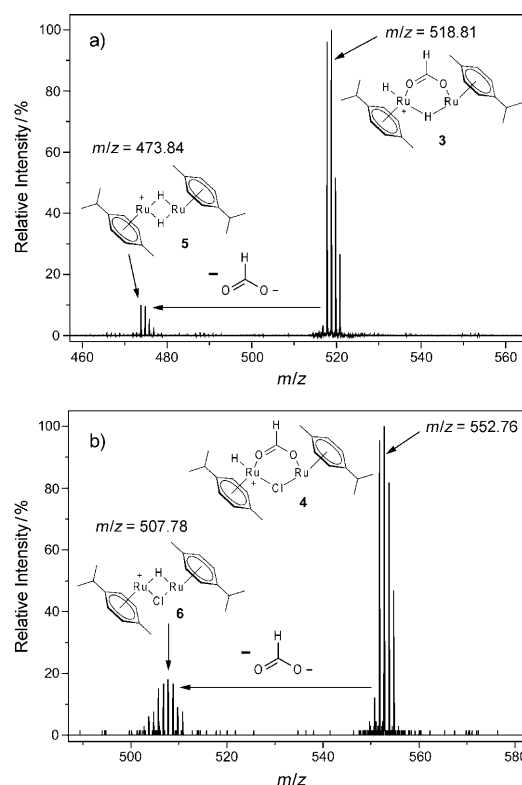

Figure 7. ESI(+)-MS/MS analysis of the signals in Figure 6: a) $m/z = 518.81$ (**3**); b) $m/z = 552.76$ (**4**). Capillary voltage = 3050 V; Sample cone voltage = 50 V.

IL **1**·HCl, which renders the last synthetic step with IL **1** (deprotonation) unnecessary. Indeed, the formation of a catalytically active ruthenium species and the deprotonation (in equilibrium) of FA with the IL **1**·HCl was possible under identical reaction conditions, and resulted in a moderate conversion of 60% after 25 h (50% after 9 h; see the Supporting Information). Such a long reaction time compared to that performed in IL **1** is a probable consequence of IL **1**·HCl crystallization during the course of the reaction. Notably, the conversions were estimated here by fitting the pressure curves using the previously calibrated and normalized conversion curves. This was crucial because at high conversions of FA, the IL **1**·HCl started to crystallize from the FA/formate solution; thus, IL **1**·HCl backbone signals could not be used as an internal standard for quantification by ^{1}H NMR spectroscopy. Interestingly, a very low concentration of IL **1**·HCl (39.2 μmol; 1 equivalent with respect to Ru) still produced a conversion of 30% after 20 h (see the Supporting Information).

Conclusions

In conclusion, we have demonstrated the easy conversion of FA into dihydrogen and carbon dioxide gas using phosphine-free ruthenium complex [{RuCl$_2$(*p*-cymene)}$_2$] **2** in a task-specific IL. The task-specific IL **1** stabilizes the active catalyst species and the immobilized amine group acts as crucial promoter for the dehydrogenation of FA. High conversions (TOF values of up to 1540 h^{-1}) of FA dehydrogenation could be obtained in a

few hours under mild conditions. Kinetic measurements indicated formal broken reaction orders of 0.70 ± 0.15 and 0.78 ± 0.03 for catalyst **2** and IL **1**, respectively, whereas the reaction order was estimated as 2.00 ± 0.17 for FA, suggesting that FA is present in its dimeric form during the catalytic reaction. The apparent activation energy of this process was estimated to be 69.1 ± 7.6 kJ mol^{-1}, which is in the range of the most common catalytic systems used for FA dehydrogenation. Moreover, ESI(+)-MS analyses showed ionic dimeric Ru complexes (**3** and **4**) as probable catalytic species involved in the FA decomposition. The stability to air and humidity and potential for catalyst recycling suggests that the catalyst system is quite robust and easy to handle, indicating it as a potential system for hydrogen gas production. Interestingly, the reaction was also possible with IL **1**·HCl as a promoting agent.

Experimental Section

General

All manipulations were performed in air. Ruthenium complex **2** (di-μ-chlorobis[(p-cymene)chlororuthenium(II)]) was purchased from STREM and used as received. The FA (88%, Labsynth) was distilled and used without further purification. ^{1}H NMR spectra were recorded on a Varian Inova 300 MHz instrument using [D$_6$]DMSO as the solvent. Mass spectra were obtained using a QIC-20 Hiden Analytical gas analyzer. An aliquot of the gas-phase was introduced to a pre-reservoir and then this sample was injected into the mass analyzer. Electrospray ionization mass spectrometry (ESI(+)-MS) analyses were performed on a Waters micromass Q-Tof microTM instrument operating at 2750 V of capillary voltage and 13 V of sample cone voltage. For ESI analysis, 5 mg of the reaction mixture was first diluted in 1 mL of water. Thereafter, one drop of this solution was diluted again in 1 mL water and then the sample was analyzed. Infrared analyses of the gas-phase were obtained using a Bomem FTLA 2000 equipped with a DRIFT cell (Harrick Praying Mantis reaction chamber). At the end of the reaction, the DRIFT cell was pressurized with the gas contained in the reactor (ca. 2 MPa) and the gas phase was analyzed at 25 °C. Gas chromatography analyses were carried out in Agilent Technologies equipment using a TCD detector. Analysis condition: column = Supelco-Molecular Sieves 5 A; column temperature = 100 °C; detector temperature = 150 °C; time for analysis = 20 min; carrier gas = He.

Synthesis of IL 1

IL **1** was prepared using a similar method to that previously reported.[39] First, IL **1**·HCl was prepared from the reaction of 1-methylimidazole (19.1 g; 232.4 mmol) and 2-chloro-*N,N*-diethylethylamine hydrochloride (40.0 g; 232.4 mmol) in acetonitrile (200 mL) under reflux conditions. After 4–5 days of reaction, a white solid was separated by filtration and washed with a 1:1 v/v mixture of ethyl ether and acetonitrile (3×80 mL). The resultant white solid was dried under reduced pressure to afford IL **1**·HCl in 90% yield. Further, deprotonation of IL **1**·HCl (15.0 g; 58.9 mmol) with NaOH (2.4 g; 58.9 mmol) in water (150 mL) was carried out for 2 h. Water was then removed under reduced pressure and the liquid residue was extracted with dichloromethane (100 mL). The organic phase was dried over MgSO$_4$ and filtered through celite/neutral alumina. The solvent was removed under reduced pressure to afford the de-

sired IL **1** in good yields (76–98%). Finally, IL **1** was dried under vacuum for 5 h at 50 °C.

Formic acid dehydrogenation

In a typical FA decomposition experiment, IL **1** (0.5 g; 2.3 mmol) was mixed with FA (0.81 g; 17.6 mmol) in a glass reaction vessel. Afterwards, the mixture was stirred until it became a homogeneous solution, and then Ru complex **2** (0.012 g; 19.6 μmol) was added. The vessel containing the solution was placed into a high-pressure Parr reactor. The system was then immersed in a silicon oil bath at 80 °C under stirring. A sample was analyzed by ^{1}H NMR before and after reaction, where signals of IL **1** were used as the internal standard to determine the conversion based on FA/IL **1** integral ratios. For recharges, at the end of each cycle, more FA (0.81 g; 17.6 mmol) was added to the system and the reaction was restarted. The increase in the gas pressure in the reactor was monitored with a pressure transducer interfaced through a Novus converter to a PC, and the data was worked up via Microcal Origin 7.0.

[1] L. Schlapbach, A. Zuttel, *Nature* **2001**, *414*, 353–358.
[2] S. Enthaler, *ChemSusChem* **2008**, *1*, 801–804.
[3] F. Joó, *ChemSusChem* **2008**, *1*, 805–808.
[4] P. Makowski, A. Thomas, P. Kuhn, F. Goettmann, *Energy Environ. Sci.* **2009**, *2*, 480–490.
[5] P. Chen, X. Wu, J. Lin, K. L. Tan, *Science* **1999**, *285*, 91–93.
[6] C. Liu, Y. Y. Fan, M. Liu, H. T. Cong, H. M. Cheng, M. S. Dresselhaus, *Science* **1999**, *286*, 1127–1129.
[7] G. Mpourmpakis, G. E. Froudakis, G. P. Lithoxoos, J. Samios, *Nano Lett.* **2006**, *6*, 1581–1583.
[8] S. Meng, E. Kaxiras, Z. Y. Zhang, *Nano Lett.* **2007**, *7*, 663–667.
[9] H. Lee, J. W. Lee, D. Y. Kim, J. Park, Y. T. Seo, H. Zeng, I. L. Moudrakovski, C. I. Ratcliffe, J. A. Ripmeester, *Nature* **2005**, *434*, 743–746.
[10] Y. G. Wang, N. Shah, G. P. Huffman, *Energy Fuels* **2004**, *18*, 1429–1433.
[11] J. Yang, A. Sudik, D. J. Siegel, D. Halliday, A. Drews, R. O. Carter, C. Wolverton, G. J. Lewis, J. W. A. Sachtler, J. J. Low, S. A. Faheem, D. A. Lesch, V. Ozolins, *Angew. Chem.* **2008**, *120*, 896–901; *Angew. Chem. Int. Ed.* **2008**, *47*, 882–887.
[12] V. Ozolins, E. H. Majzoub, C. Wolverton, *J. Am. Chem. Soc.* **2009**, *131*, 230–237.
[13] P. Mars, J. J. F. Scholten, P. Zwietering, *Adv. Catal.* **1963**, *14*, 35–113.
[14] C. Fellay, P. J. Dyson, G. Laurenczy, *Angew. Chem.* **2008**, *120*, 4030–4032; *Angew. Chem. Int. Ed.* **2008**, *47*, 3966–3968.
[15] S. Fukuzumi, T. Kobayashi, T. Suenobu, *ChemSusChem* **2008**, *1*, 827–834.
[16] C. Fellay, N. Yan, P. J. Dyson, G. Laurenczy, *Chem. Eur. J.* **2009**, *15*, 3752–3760.
[17] G. N. Khairallah, R. A. J. O'Hair, *Int. J. Mass Spectrom.* **2006**, *254*, 145–151.
[18] B. Loges, A. Boddien, H. Junge, M. Beller, *Angew. Chem.* **2008**, *120*, 4026–4029; *Angew. Chem. Int. Ed.* **2008**, *47*, 3962–3965.
[19] A. Boddien, B. Loges, H. Junge, M. Beller, *ChemSusChem* **2008**, *1*, 751–758.
[20] B. Loges, A. Boddien, H. Junge, J. R. Noyes, W. Baumann, M. Beller, *Chem. Commun.* **2009**, 4185–4187.

[21] H. Junge, A. Boddien, F. Capitta, B. Loges, J. R. Noyes, S. Gladiali, M. Beller, *Tetrahedron Lett.* **2009**, *50*, 1603–1606.

[22] D. J. Morris, G. J. Clarkson, M. Wills, *Organometallics* **2009**, *28*, 4133–4140.

[23] S. Fukuzumi, T. Kobayashi, T. Suenobu, *J. Am. Chem. Soc.* **2010**, *132*, 1496–1497.

[24] M. Ojeda, E. Iglesia, *Angew. Chem.* **2009**, *121*, 4894–4897; *Angew. Chem. Int. Ed.* **2009**, *48*, 4800–4803.

[25] X. Li, X. Ma, F. Shi, Y. Deng, *ChemSusChem* **2010**, *3*, 71–74.

[26] Z. F. Fei, T. J. Geldbach, D. B. Zhao, P. J. Dyson, *Chem. Eur. J.* **2006**, *12*, 2123–2130.

[27] J. H. Davis, *Chem. Lett.* **2004**, *33*, 1072–1077.

[28] J. D. Scholten, J. Dupont, *Organometallics* **2008**, *27*, 4439–4442.

[29] J. E. L. Dullius, P. A. Z. Suarez, S. Einloft, R. F. de Souza, J. Dupont, J. Fischer, A. De Cian, *Organometallics* **1998**, *17*, 815–819.

[30] The relative component content of a sample is classified as follows: Major = 1–100%; minor = 0.01–1%; trace < 0.01%; ultra-trace ≤ 1 ppb. J. F. Rubinson, K. A. Rubinson, *Contemporary Chemical Analysis*, Prentice Hall, Upper Saddle River, NJ, **1998**, Chap. 5, pp. 141–143.

[31] R. Larsson, M. H. Jamroz, M. A. Borowiak, *J. Mol. Catal. A: Chem.* **1998**, *129*, 41–51.

[32] L. S. Santos, C. H. Pavam, W. P. Almeida, F. Coelho, M. N. Eberlin, *Angew. Chem.* **2004**, *116*, 4430–4433; *Angew. Chem. Int. Ed.* **2004**, *43*, 4330–4333.

[33] F. C. Gozzo, L. S. Santos, R. Augusti, C. S. Consorti, J. Dupont, M. N. Eberlin, *Chem. Eur. J.* **2004**, *10*, 6187–6193.

[34] A. A. M. Lapis, B. A. D. Neto, J. D. Scholten, F. M. Nachtigall, M. N. Eberlin, J. Dupont, *Tetrahedron Lett.* **2006**, *47*, 6775–6779.

[35] M. H. G. Prechtl, J. D. Scholten, J. Dupont, *J. Mol. Catal. A: Chem.* **2009**, *313*, 74–78.

[36] M. N. Eberlin, *Eur. J. Mass Spectrom.* **2007**, *13*, 19–28.

[37] C. Daguenet, R. Scopelliti, P. J. Dyson, *Organometallics* **2004**, *23*, 4849–4857.

[38] C. Daguenet, P. J. Dyson, *Organometallics* **2004**, *23*, 6080–6083.

[39] M. V. Jiménez, J. J. Perez-Torrente, M. I. Bartolome, V. Gierz, F. J. Lahoz, L. A. Oro, *Organometallics* **2008**, *27*, 224–234.

Supporting Information

Decomposition of Formic Acid Catalyzed by a Phosphine-Free Ruthenium Complex in a Task-Specific Ionic Liquid

Jackson D. Scholten, Martin H. G. Prechtl, and Jairton Dupont*[a]
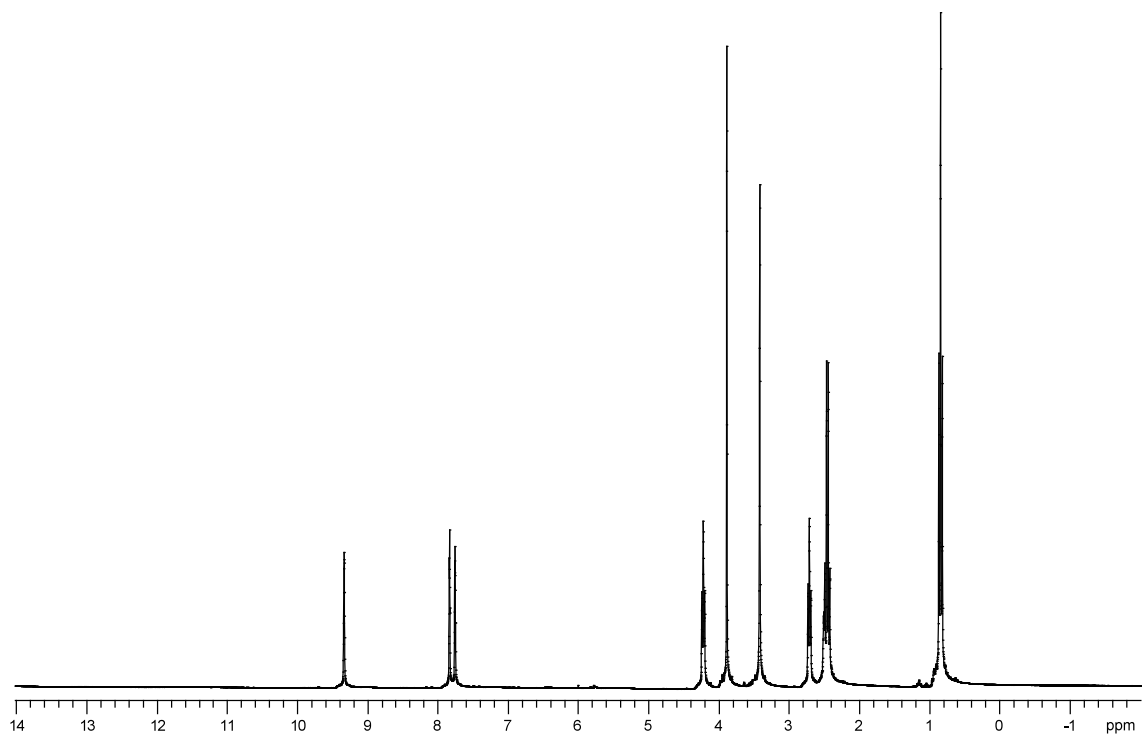
cctc_201000119_sm_miscellaneous_information.pdf

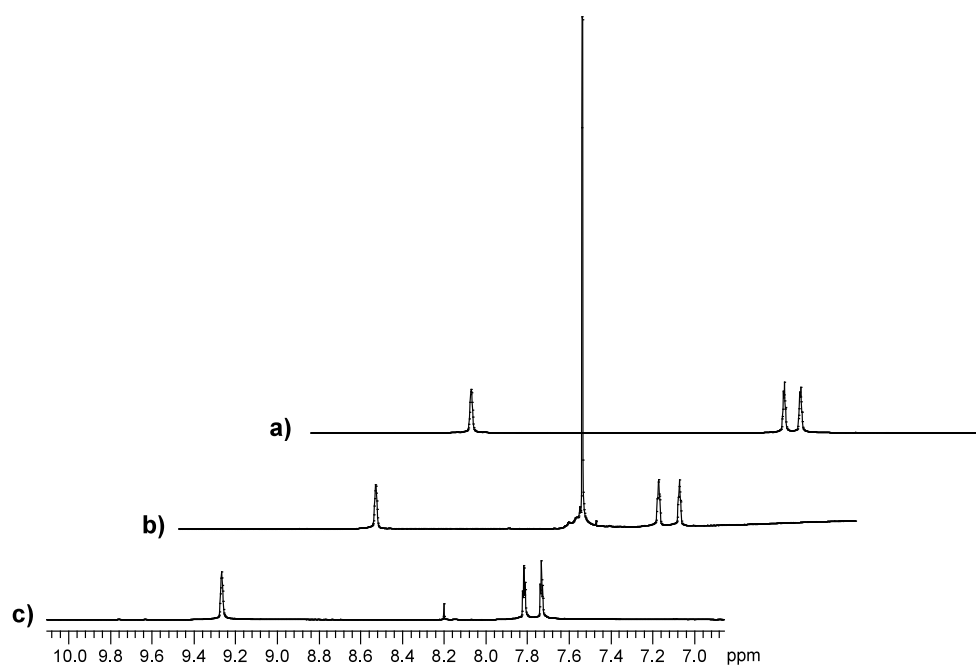**Fig. S1** [1]H **N**MR (300 MHz, DMSO-d_6) spectrum of the pure IL **1**.

Fig. S2 Comparison of the ^{1}H **NMR** (300 MHz, DMSO-d_6) analyses of **a)** the pure IL **1**, **b)** in the presence of formic acid (FA:IL **1** = 7.65) before and **c)** after reaction. The singlet at 9.27 ppm and the doublet at 7.77 ppm correspond to C_2-H and C_4-H/C_5-H of the imidazolium ring of IL, respectively; singlet at 8.20 ppm is due to the formic acid.
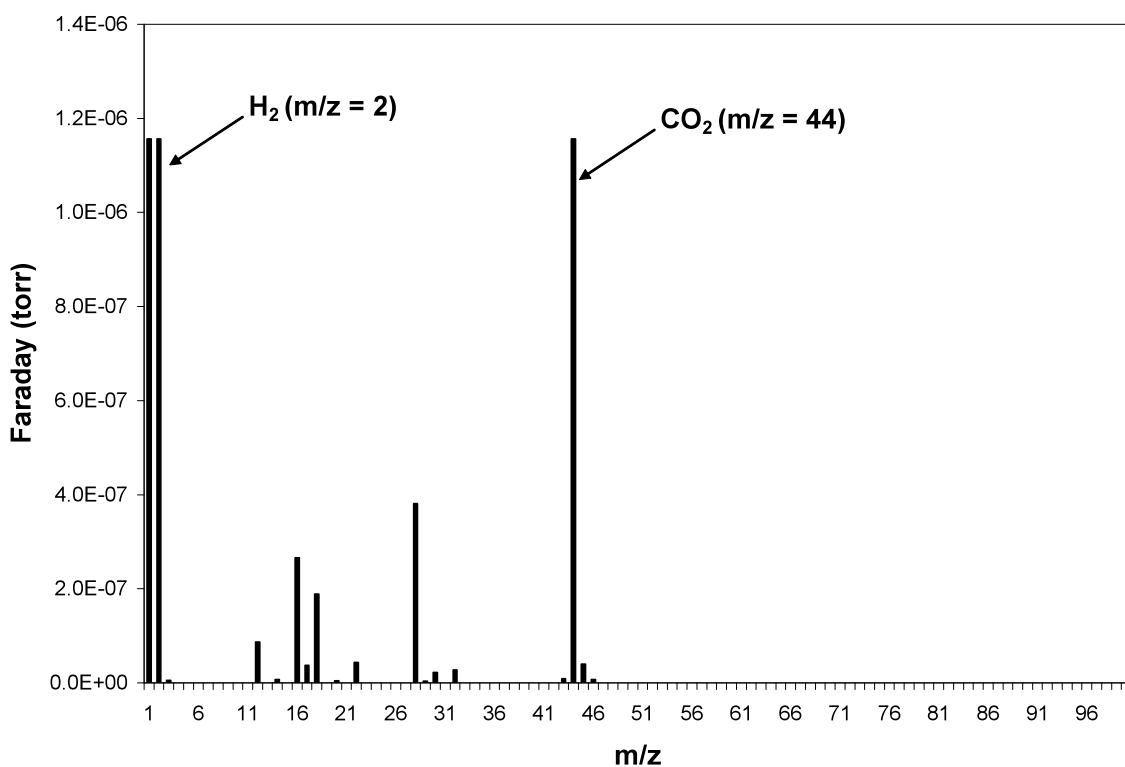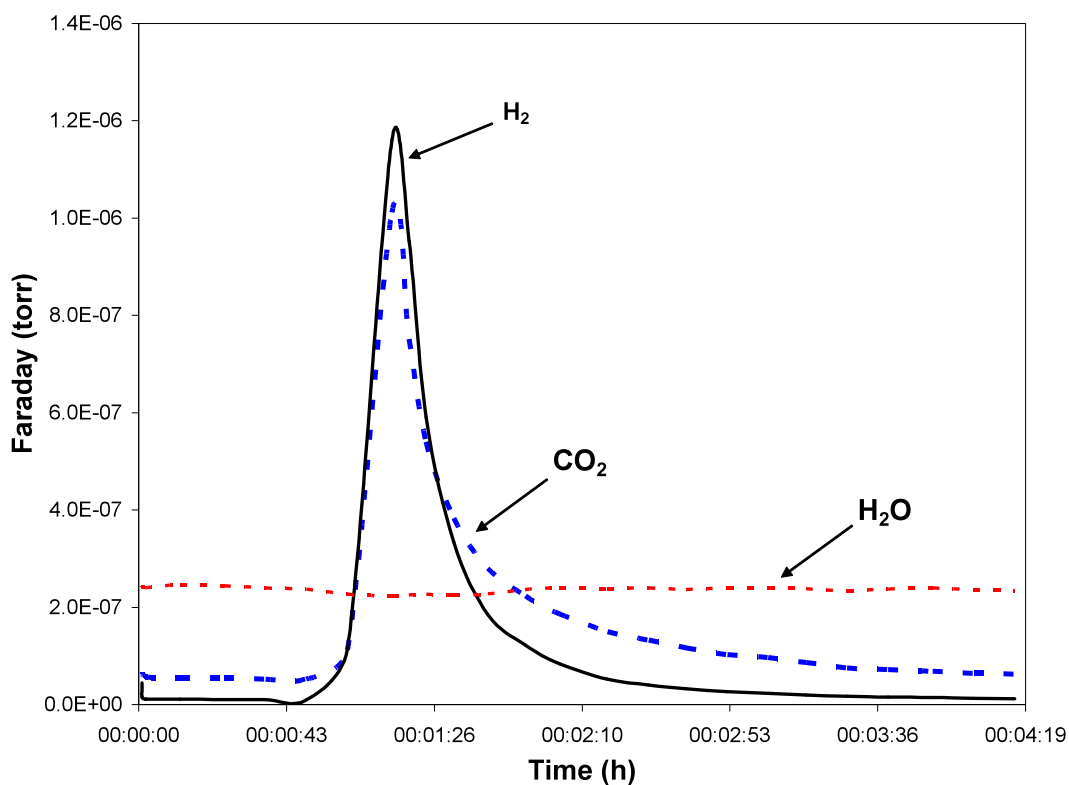
Fig. S3 Mass analysis of the gas-phase after the formic acid (0.81 g; 17.6 mmol) decomposition catalysed by the Ru **2** complex (0.012 g; 19.6 μmol) in IL **1** (0.5 g; 2.3 mmol) at 80 ºC. The water signal in the bar mode (below) corresponds to the same value before the sample analysis.
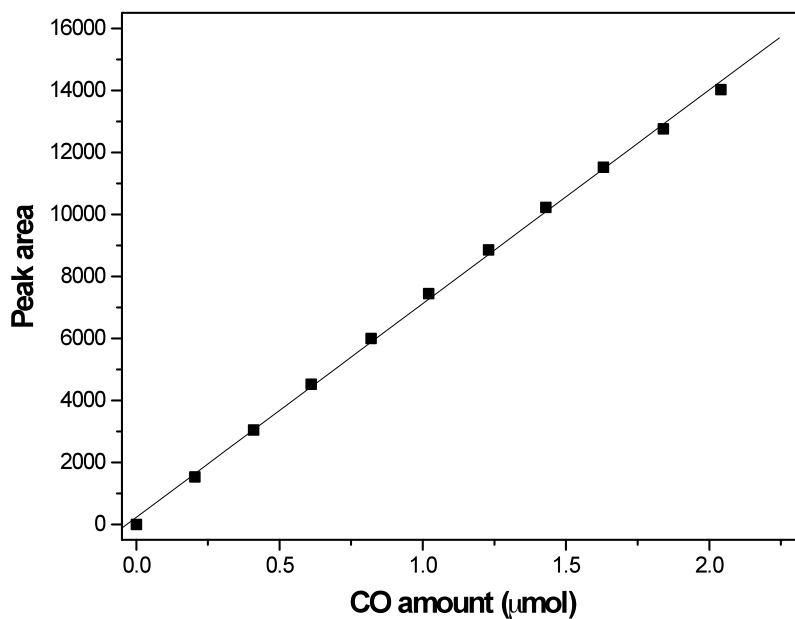
Fig. S4 Calibration curve made using a standard gas containing 5 mol% of CO in He. Analysis condition: Column = Supelco − Molecular Sieves 5A; column temperature = 100 ℃; detector = 150 ℃; time for analysis = 20 min; carrier gas = He.
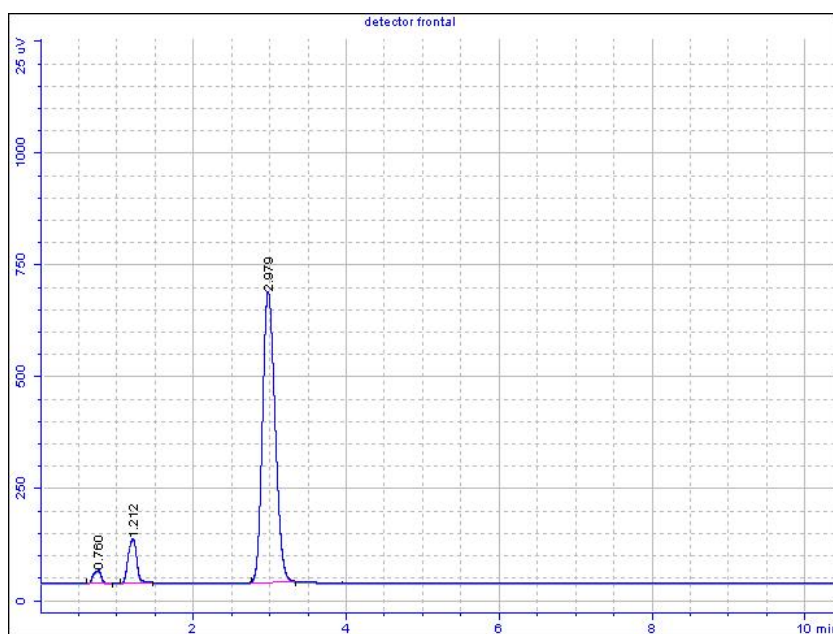
Fig. S5 Typical GC analysis of the standard 5 mol% CO in He for an injection of 500 μL of gas sample. Retention times of 0.760 and 1.212 min correspond to oxygen and nitrogen impurities from air, respectively.
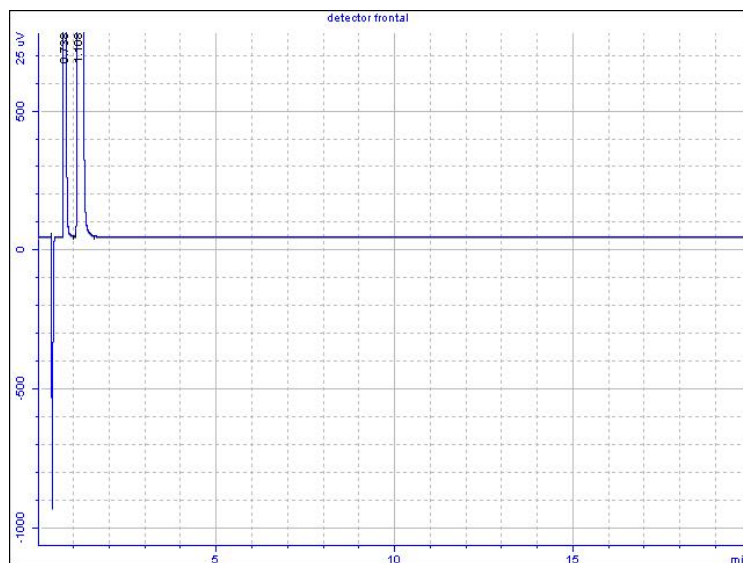
Fig. S6 GC analysis of the gas-phase (800 μL) after the FA (0.81 g; 17.6 mmol) decomposition catalysed by the Ru **2** complex (0.012 g; 19.6 μmol) in IL **1** (0.5 g; 2.3 mmol) at 80 ºC. The negative signal corresponds to hydrogen gas. Signals at 0.738 and 1.108 min correspond to oxygen and nitrogen impurities from air, respectively.
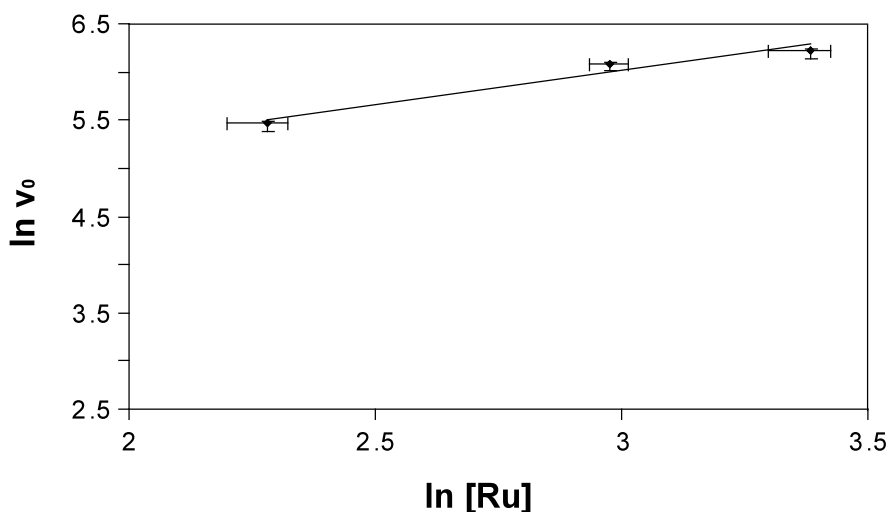
Fig. S7 Data for the determination of the formal reaction order deduced for the catalyst **2** (reaction conditions: 6.5-19.6 μmol of Ru **2**, 2.3 mmol of IL **1** and 17.6 mmol of formic acid at 80 ℃). Equation obtained from the linear fit: y = 3.900 + 0.704 (± 0.147)x; formal "broken" order = 0.70 ± 0.15 (Correlation = 0.98). On graphic, v_0 is the initial rate.
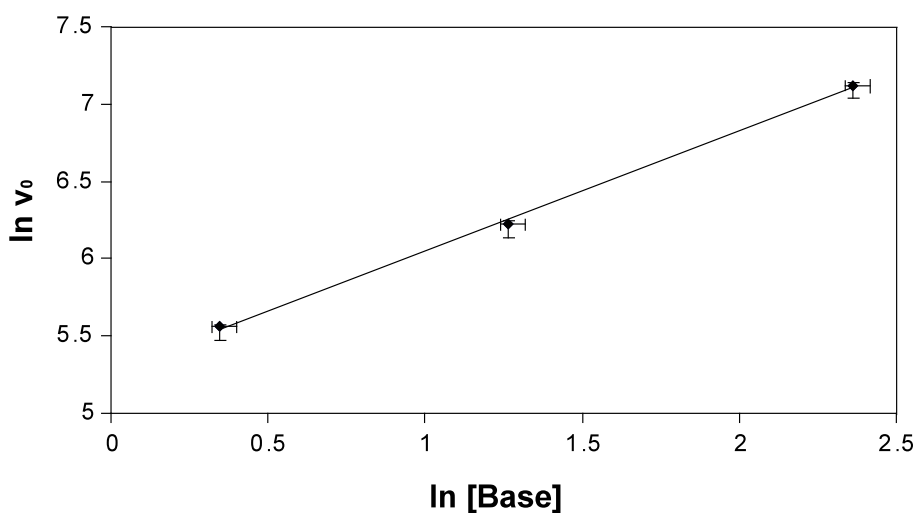
Fig. S8 Data for the determination of the formal reaction order deduced for the IL **1** (base) (reaction conditions: 0.9-7.0 mmol of IL **1**, 19.6 μmol of Ru **2** and 17.6 mmol of formic acid at 80 ℃). Equation obtained from the linear fit: y = 5.276 + 0.776 (± 0.026)x; formal "broken" order = 0.78 ± 0.03 (Correlation = 0.99). On graphic, v_0 is the initial rate.
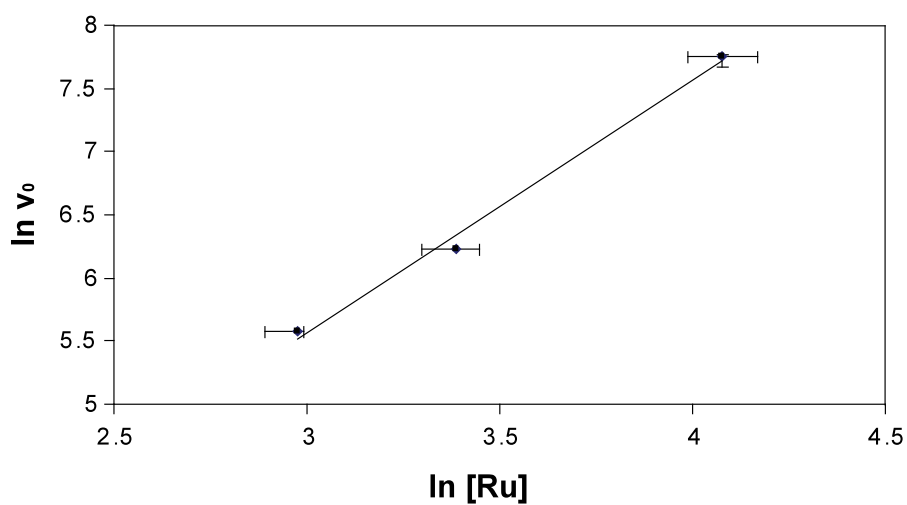
Fig. S9 Data for the determination of the formal reaction order deduced for formic acid (reaction conditions: 8.8-26.5 mmol of formic acid, 2.3 mmol of IL **1** and 19.6 μmol of Ru **2** at 80 ºC). Equation obtained from the linear fit: y = -0.433 + 1.998 (± 0.165)x; formal order = 2.00 ± 0.17 (Correlation = 0.99). On graphic, v_0 is the initial rate.
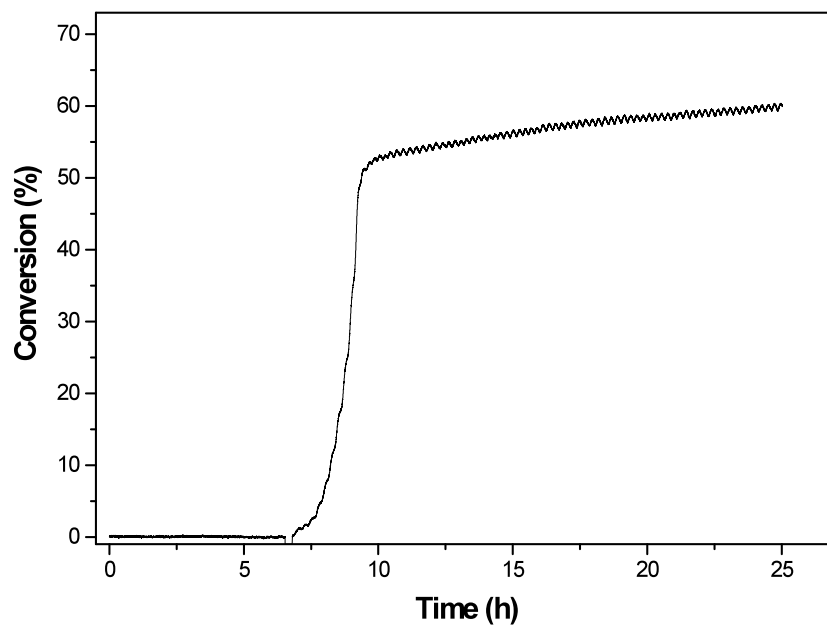
Fig. S10 Formic acid (0.81 g; 17.6 mmol) decomposition catalysed by Ru **2** complex (0.012 g; 19.6 µmol) in the IL **1**•HCl (0.58 g; 2.3 mmol) at 80 °C.
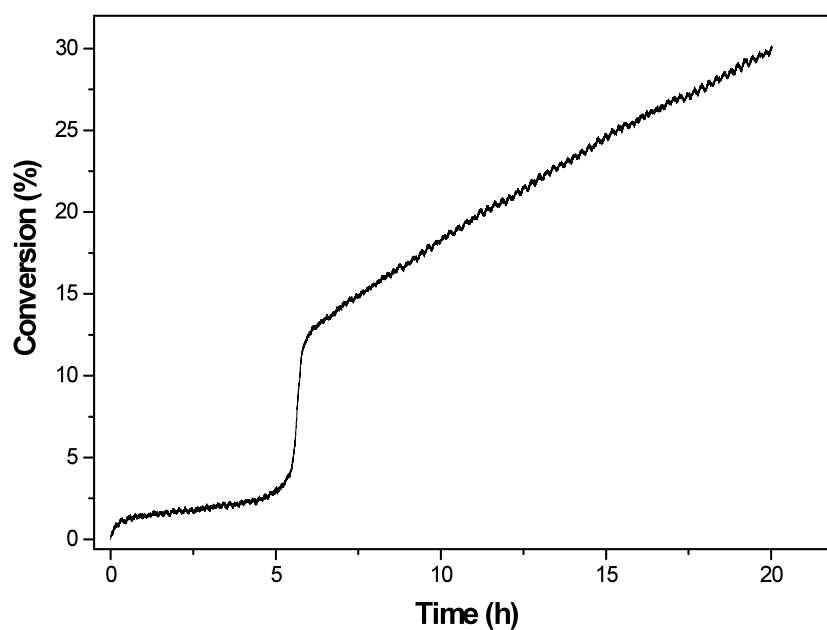

Fig. S11 Formic acid (0.81 g; 17.6 mmol) decomposition catalysed by Ru **2** complex (0.012 g; 19.6 µmol) in the IL **1**•HCl (0.0099 g; 39.2 µmol; 1 eq. per Ru atom) at 80 °C.

Notas de Correção dos Artigos

Artigo I

i) Página 1796, linha 11 (esquerda): o LI correto é HMI.PF$_6$ e não BMI.PF$_6$ como descrito.

Artigo II

i) Página 76, figura 4: o sinal em m/z = 3 é referente à espécie [H$_3$]$^+$ e não [HD]$^+$ como mostrado.

ii) Página 77, esquema 1: a relação [PhCN:IL-**2**] deve ser corrigida para [PhCN:IL **1**].

Artigo V

i) Página 4441, tabela 1, entrada 6: neste caso não houve adição prévia de metanol ao sistema. Portanto, o índice *g* deve ser desconsiderado.

Artigo VI

i) Página 1268, figura 7: uma análise detalhada das espécies envolvidas sugere que a fragmentação mais provável das espécies **3** e **4** seja a perda de um ligante HCO$_2$ radical e não aniônico (formiato) como mostrado, gerando os cátions radicais **5** e **6**.
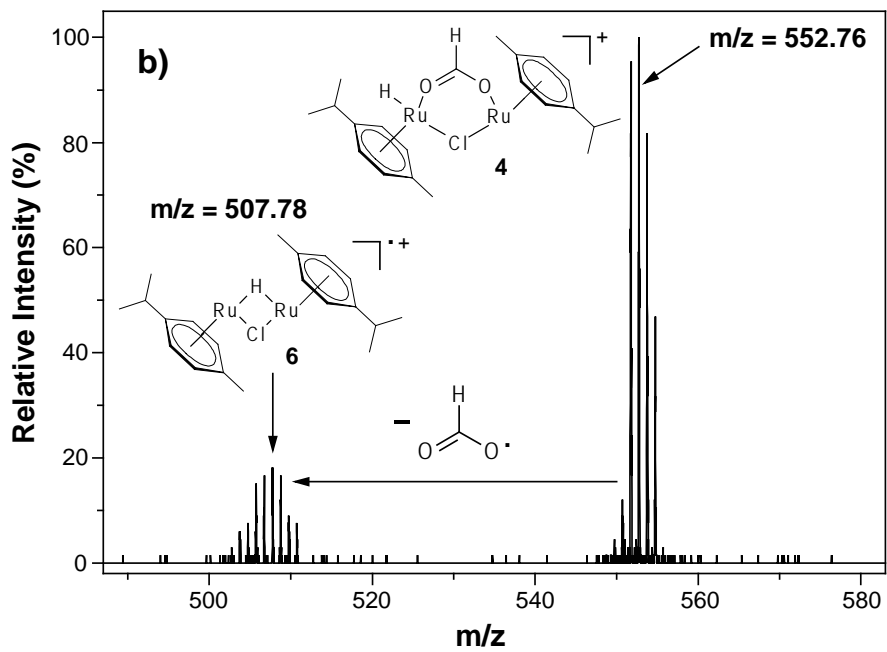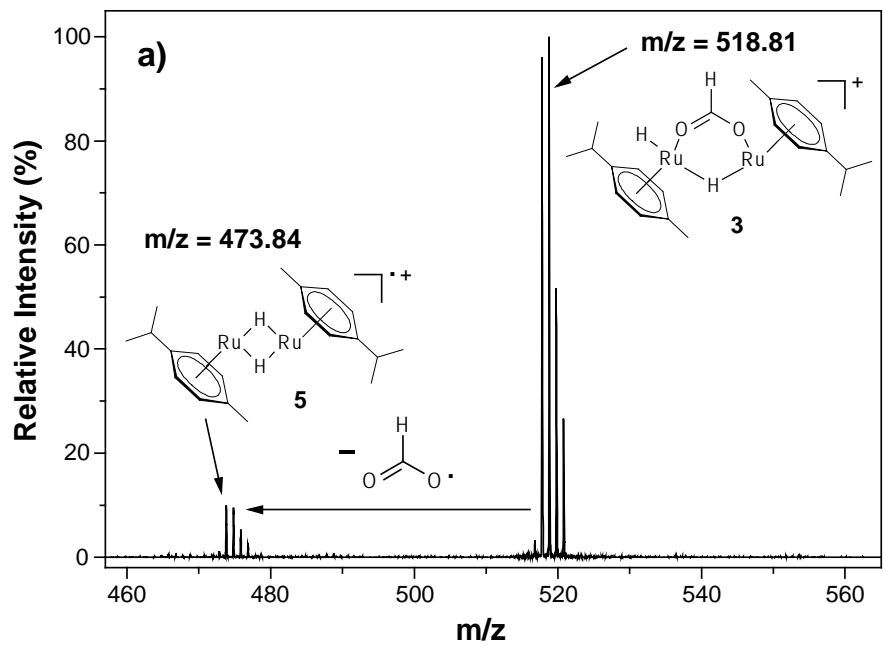
Figura 7 corrigida (Artigo VI).